JOURNAL OF SCIENCE
SAKARYA UNIVERSITY

Sakarya University Journal of Science



SAKARYA UNIVERSITY
e-issn: 2147-835X

VOLUME: 24
ISSUE: 2
APRIL 2020

Sakarya University Journal of Science
Volume: 24 Issue: 2 April 2020

Editorial Boards

Editor-in-Chief

Editors

Editorial Board

SAKARYA UNIVERSITY JOURNAL OF SCIENCE

CONTENTS

Volume: 24 - Issue: 2 (APRIL 2020)

RESEARCH ARTICLES

JOURNAL OF SCIENCE
SAKARYA UNIVERSITY

Sakarya University Journal of Science

ISSN 1301-4048 | e-ISSN 2147-835X | Period Bimonthly | Founded: 1997 | Publisher Sakarya University
http://www.saujs.sakarya.edu.tr/en/

Title: Effects of Plant Growth Promoting Rhizobacteria (PGPR) on Physiological Parameters Against Salinity in Apple Cultivar “Fuji”

Authors: Şeyma Arıkan, Lütfi Pırlak
Recieved: 2018-10-11 14:42:16

Accepted: 2019-10-08 12:36:55

Article Type: Research Article
Volume: 24
Issue: 2
Month: April
Year: 2020
Pages: 281-286

How to cite
Şeyma Arıkan, Lütfi Pırlak ; (2020), Effects of Plant Growth Promoting Rhizobacteria (PGPR) on Physiological Parameters Against Salinity in Apple Cultivar “Fuji”. Sakarya University Journal of Science, 24(2), 281-286, DOI: https://doi.org/10.16984/saufenbilder.469522
Access link
http://www.saujs.sakarya.edu.tr/tr/issue/52471/469522

Sakarya University Journal of Science 24(2), 281-286, 2020

Effects of Plant Growth Promoting Rhizobacteria (PGPR) on Physiological Parameters Against Salinity in Apple Cultivar "Fuji"

Şeyma ARIKAN*[1], Lütfi PIRLAK[2]

Abstract

The present study was conducted with the cultivar 'Fuji' grafted on M9 rootstock in both 2014 and 2016 years. The effect of PGPR (*Bacillus subtilis* EY2, *Bacillus atrophaeus* EY6, *Bacillus spharicus GC subgroup B* EY30, *Staphylococcus kloosii* EY37 and *Kocuria erythromyxa* EY43) were investigated under salt stress conditions. PGPR's effects were tested on leaf relative water content (LRWC), membrane permeability, stomatal conductivity, photosynthetic activity and chlorophyll content (by SPAD-502). The saplings were grown in pots filled 2:1:1 peat: perlite: sand. Salinity was obtained by NaCl: Na_2SO_4: $CaCl_2$: $MgSO_4$ (7:9:3:1) solution. The solution was applied twice a week with irrigation during the growing period. When the salinity reached 2.5-3.0 $dScm^{-1}$, the solution application was ended. All bacteria treatments significantly reduced the physiological damage of leaves compared with the salt treatment in both two years. The LRWC range from 13.33 % (salt treatment) to 26.76 % (control). The best result of bacteria treatment was measured in EY43 with 23.93 % LRWC. The highest rate of membrane permeability was found in salt treatment (30.35 %). The stomatal conductivity was decreased in the salt application (154.35 mmol $m^{-2}s^{-1}$) unlike EY43 treatment (234.44 mmol $m^{-2}s^{-1}$). Similarly, EY43 treatment significantly increased photosynthetic activity (15.24 µmol CO_2 $m^{-2}s^{-1}$) compared with the salt treatment (8.22 µmol CO_2 $m^{-2}s^{-1}$). As a result, bacteria strains had been ameliorative of the deleterious effects under salt stress on "Fuji".

Keywords: Apple, Fuji, PGPR, Salt Stress

1. INTRODUCTION

Soil salinity that is the most important abiotic stress factor after drought in world agriculture, limits yield and plant growth especially in arid and semi-arid regions, In such areas, long periods of drought coincide with high temperatures [1]. However, salinity occurs quickly in these regions with irrigation. Salt in the upper layers of soil transported to by capillary during the irrigation and evaporation and accumulates in the rhizosphere. The wrong applications of irrigation, the presence of high soluble salts level in the water, lack of

*Corresponding Author
[1]The University of Selçuk, Faculty of Agriculture, Department of Horticulture, Konya, TURKEY, arikan@selcuk.edu.tr ,ORCID ID: 0000-0002-4328-0263
[2]The University of Selçuk, Faculty of Agriculture, Department of Horticulture, Konya, TURKEY, pirlak@selcuk.edu.tr , ORCID ID: 0000-0003-3630-3591

drainage and are among other causes of salinity. Salinity is one of the major problems in the agricultural area of Turkey. Agricultural fields, about 1.500.000ha, are faced with salinity problem in Turkey [2]. Salinity is one of the most effective factors which limited yield and soil fertility in production areas. Salt stress causes increasing of respiration rate, ion toxicity, changes in plant growth, mineral disorders, damaging of membrane permeability, decreasing of photosynthetic activity. In addition, soil salinity has negative impacts on nitrogen and carbon metabolism. The salinity tolerances of different species or cultivars differ by their different stages of growth and different soil and environmental conditions. The reactions of fruit species to salinity were examined [3] and observed that many fruit species were very sensitive to salinity. (Table-1).

Table-1. The response of fruit species against salinity [3]

Tolerant	Moderately Sensitive	Too Sensitive
Pheoneix dactylifera	*Ficus carica*	*Citrus paradisi*
	Punica granatum	*Citrus limon*
	Olea europea	*Citrus reticulata*
		Citrus sinensis
		Prunus amgydalus
		Prunus armeniaca
		Prunus avium
		Malus communis

In order to improve soil salinity, it needs lots of time and more expense. Therefore, these methods cannot be applied to prevalent countries. Many studies focused on chemical treatments and suitable rootstocks against for saline soil but nowadays, biological treatments with plant growth-promoting rhizobacteria (PGPR) have been started to use for solving this problem [4, 5].

PGPR are free-living microorganisms as colonizing in the rhizosphere of plants [5]. These bacteria which increased root growth and plant pathogens kept under the control have great importance in sustainable agriculture. Such as bio-control of plant disease, plant growth-promoting, bio-fertilizers and growth regulator substances production have been functioning [6]. PGPR affects plants a-symbiotically notwithstanding plant species. PGPR can have beneficial effects on plant growth and yield by two main mechanisms. These are direct and indirect mechanisms. There are different ways in the direct effect mechanism. Direct mechanisms may act on the plant itself and auxins, cytokinin's, and gibberellins or lowering of the ethylene in the plant, solubilization of inorganic phosphate and mineralization of organic phosphate, a-symbiotic fixation of atmospheric nitrogen, and stimulation of disease-resistance mechanisms [6, 7]. In the indirect mechanism; PGPR acts like biocontrol agents reducing disease or stimulate other beneficial symbioses or protect the plant [8]. Additionally, PGPR improves the plant's tolerance to stresses, such as drought, high salinity, metal toxicity, and pesticide load [9].

In this study, we aimed at determining effect of PGPR strains (*Bacillus subtilis* EY2, *Bacillus atrophaeus* EY6, *Bacillus spharicus* GC subgroup B EY30, *Staphylococcus kloosii* EY37, *Kocuria erythromyxa* EY43) which were identified positive effects on vegetables, apple, cherry and crops on leaf relative water content (LRWC), membrane permeability, stomatal conductivity, photosynthetic activity and chlorophyll content of cv. Fuji apple saplings.

2. MATERIALS AND METHOD

2.1. Material

This study was carried out under controlled greenhouse conditions at Selçuk University Department of Horticulture in Turkey. The "Fuji" apple cultivar grafted on M9 rootstock was used as plant materials and saplings were planted to 12-liter pots in March 2014. The pots contained 2:1:1 peat: perlite: sand mixture.

The strains of bacteria, EY2, EY6, EY30, EY37, EY43 were obtained from the University of Iğdır in Turkey (Assos. Prof. Dr. M. Figen Dönmez). These bacteria have been the ability to grow in a saline culture medium [10% sodium chloride (NaCl)] [10].

2.2. Method

2.2.1. Bacterial treatments

All bacteria were inoculated into the roots before planting. Roots were held in bacterial suspensions of the concentration of 10^9 CFU mL^{-1} for 30 minutes. After planting saplings were watered with bacterial suspensions once in a month.

2.2.2. Salinity treatments

Bacteria inoculated saplings started to be irrigated once

a week with NaCl: Na2SO4: CaCl2: the MgSO4 solution in a ratio of 7: 9: 3: 1 one month after planting and this application have continued during the growth period. When the EC of soil reached 2.5-3.0 $dScm^{-1}$, solutions application was ended.

2.2.3. Analysis of physiological features

Physiological effects of bacterial treatments were evaluated by leaf relative water content (LRWC), membrane permeability, stomatal conductivity, photosynthetic activity and chlorophyll content (by SPAD-502).

2.2.4. Statistical analysis

Experiment divided into seven application groups each including nine saplings with three replicates in a completely randomized design. The collected data were analyzed statistically using the SPSS 23. All data in the present study were subjected to analysis of variance (ANOVA) and means were separated by Duncan's Multiple Range Tests at 5% level of significance.

3. RESULTS

The highest chlorophyll content was obtained from control saplings (52.95 SPAD unit) while the lowest chlorophyll content value was measured in salt treatment (39.28 SPAD unit). All bacteria applications were increased chlorophyll contents of leaves as compared to salt treatment. But the highest increase occurred the EY43 bacteria strain with 49.58 SPAD unit of chlorophyll reading the value in comparison to salt treatment.

All bacteria applications decreased membrane damaged increased by the salt treatment in leaves. The EY37 and EY43 bacteria strains were the most effective against the reduction of membrane damage. The membrane permeability rate of salt treatment was measured as 30.35%, which was the highest, in salt treatment (Table-2.). The lowest membrane permeability rate was found in the control (18.05%) followed EY43 treatment with 19.21%.

The leaves of the control saplings had the highest LRWC with 26.76 %, while the lowest LRWC was found in the salt treatment with 13.33 %. All bacteria strains have enhanced significantly LRWC as compared to the salt applications, EY43 and EY37 were the highest bacteria applications that increased LRWC ratio by 23.92 % and 21.93% respectively, compared to the salt application (Table-2.).

The stomatal conductivity was found lower in salt treatment than other applications. Although the highest stomatal conductivity was measured in control (275.13 $mmolm^{-2}s^{-1}$), EY43, EY37, and EY2 bacteria applications were increased significantly with 234.44 $mmolm^{-2}s^{-1}$, 215.03 $mmolm^{-2}s^{-1}$ and 208.40 $mmolm^{-2}s^{-1}$ stomatal conductivity values respectively, compared to the salt application (Table-2.).

The photosynthetic activity was increased all bacteria applications in comparison with the salt application. The lowest activity was found in salt treatment with 8.22 µmol CO_2 $m^{-2}s^{-1}$. The highest photosynthetic activity was obtained from EY43 bacteria strain with 15.24 µmol CO_2 $m^{-2}s^{-1}$ followed the control (17.01 µmol CO_2 $m^{-2}s^{-1}$) group.

Table-2. Effect of bacterial applications and solution treatments on physiological parameters of Fuji saplings

	C. C.	M. P.	LRWC	S. C.	P. A.
Control	52.95 a	18.05 d	26.76 a	275.13 a	17.01 a
Salt	39.28 f	30.35 a	13.33 f	154.35 e	8.22 f
EY2+Salt	44.57 e	23.54 b	18.57 d	208.40 c	12.08 e
EY6+Salt	45.01 e	22.81 b	15.85 e	190.13 d	13.57 d
EY30+Salt	46.03 d	22.18 bc	19.16 d	189.62 d	14.42 c
EY37+Salt	47.36 c	19.81 cd	21.93 c	215.03 c	14.68 bc
EY43+Salt	49.58 b	19.21 d	23.92 b	234.44 b	15.24 b

*** Difference between averages in the same column with different lower case letters are significant (P <0.05).**

C.C: Chlorophyll Content (SPAD Unit); **M.P:** Membrane Permeability (%); **LRWC:** Leaf Relative Water Content (%); **S.C:** Stomatal Conductance ($mmolm^{-2}s^{-1}$); **P.A**: Photosynthetic Activity (µmol CO_2 $m^{-2}s^{-1}$)

4. DISCUSSION

In our study, all bacteria strains significantly increased chlorophyll values in comparison with the salt application. Moreover, Bashan, et al. [11] reported that the quantity of photosynthetic pigments significantly increased by *Azospirillum brasilense* inoculation in wheat.

Salinity has an adverse effect on photosynthesis by affecting different parameters on plants. Indeed, many researchers have reported that photosynthetic activity was decreased in salt stress [12-15]. However, it has been determined that the PGPR applications can inhibit this decrease in photosynthesis caused by salt stress in our experiment. Thus, EY43 (15.24 µmol CO_2 $m^{-2}s^{-1}$) bacteria strain, except the control group had the highest photosynthetic activity while lowest activity had in salt treatment with 8.22 µmol CO_2 $m^{-2}s^{-1}$. Similarly,

Kumari, et al. [16], reported that *Pseudomonas sp.* and *Bacillus sp.* species increased photosynthesis in soybean under the salt stress conditions.

Net photosynthesis rate, transpiration rate, and stomatal conductivity decrease while the stoma resistance increases with salt stress. Thus, it limits the availability of CO_2 which is responsible for carbon metabolism with a decrease in the rate of photosynthesis, leading to a reduced in stoma conductance [17]. The lowest values in stomatal conductivity measurements were obtained from the salt applications where no bacterial application was observed. This reduction in stomatal conductivity caused by the salt stress was tolerated in bacteria applications and the highest increase was obtained from EY43 bacteria strain with 234.44 mmol m^2s^{-1}. Studies carried out under salinity stress reported that *Serratia sp*. and *Rhizobium sp*. species in lettuce [18], *Pseudomonades sp.* and *Bacillus lentus* species in basil [19], *Bacillus megaterium* species in tomato [20] and *Enterobacter cloacae* and *Bacillus drentensis* species in mung beans [21] have been shown to improve stomatal conductivity.

Bacterial inoculation can restrict Na and Cl uptake and enhance the uptake of other nutrients, especially K and NO_3. Thus, it can provide membrane stability in cells [5]. In addition, PGPR reduces electrolyte leakage by protecting plant cell membrane integrity in tissues [22]. In our study supports this information such that the EY37 and EY43 bacteria strains were the most effective against to membrane damage. Karlidag, et al. [5] and Karlidag, et al. [10], EY6, EY30, EY37 bacteria strains in strawberry, Arikan, et al. [23] EY2, EY43 bacteria strains in citrus rootstocks reported that reduce membrane permeability under salt stress. The LRWC result of our study is supposed by Karlidag, et al. [5] in strawberry. They determined LRWC decreased by salt treatment, but all bacteria inoculations were increased LRWC. EY43 bacteria treatment having the best result was found to increased LRWC rate of 23.92%.

The results of this study show that the PGPR applications could be ameliorative of the deleterious effects of salt stress on cv. Fuji apple saplings. This positive effect arose with increasing chlorophyll content, relative water content and reduced membrane injury.

5. CONCLUSIONS

The results of the present study showed that used bacteria strains had been ameliorative of the deleterious effects under salt stress in apple plants. This study was observed to improved physiological parameters and reduced membrane injury with bacterial applications. The highest chlorophyll contents were obtained in the control group but EY43 (49.58 SPAD Unit) bacteria strain had the best effect with compared other bacteria applications.

In stomatal conductivity, control group (275.13 $mmolm^{-2}s^{-1}$) was found the best result, while salt treatment (154.35 $mmolm^{-2}s^{-1}$) was found the lowest result in Fuji saplings. Furthermore, EY43 (234.44 $mmolm^{-2}s^{-1}$) bacteria strains significantly increased stomatal conductivity with compared salt applications. The photosynthetic activity has increased with EY43 (15.24 µmol CO_2 $m^{-2}s^{-1}$) bacteria strain in comparison with the salt application.

The maximum LRWC was obtained from control plants (26.76%) in the study. In addition, EY43 (23.92%) bacteria strain was provided with an increase with respect to the salt application in LRWC. The salt application increased membrane permeability in apple leaves. The highest membrane damage was obtained from the salt application (30.35%), while the control (18.05%) and EY43(19.21%), EY37 (19.81%), bacteria strains had the lowest damage.

It is reported that the use of bacteria that promote ACC deaminase-producing plant growth under stress conditions can be stimulated to plant growth. Even if bacteria do not provide a great benefit to the plant in the bacterial-root association, beneficial effects are observed by reducing ethylene levels. In addition to bacteria exhibiting effective ACC deaminase activity in the future, intensive research should be carried out on the possibilities of increasing the resistance of plants to salinity, low temperature and drought stress so that appropriate and effective bacterial-plant combinations should be demonstrated. In this study, it is foreseen that the identification of beneficial bacteria that can affect the perennial fruit species grown in salty soil conditions may increase the possibility of fruit cultivation in some areas where salinity problems are encountered in our country.

ACKNOWLEDGMENTS

This research was supported by a grant from Selçuk University, Scientific Research Projects Institute-Turkey (Project No: 14101013).

REFERENCES

[1] A. Alizadeh, X. Xlilova, and A. Eivazi, "Biochemical Response of Apple Dwarf Rootstock to Salinity Stress," *Tech. J. Eng. Appl. Sci.,* vol. 1, pp. 118-124, 2011.

[2] Anonymous, "www.fao.org Access date: 2016," 2008.

[3] E. V. Maas and G. Hoffman, "Crop salt tolerance\-current assessment," *Journal of the irrigation and drainage division,* vol. 103, no. 2, pp. 115-134, 1977.

[4] M. Ashraf, S. Hasnain, O. Berge, and T. Mahmood, "Inoculating wheat seedlings with exopolysaccharide-producing bacteria restricts sodium uptake and stimulates plant growth under salt stress," *Biology and Fertility of Soils,* vol. 40, no. 3, pp. 157-162, 2004.

[5] H. Karlidag, A. Esitken, E. Yildirim, M. F. Donmez, and M. Turan, "Effects of plant growth promoting bacteria on yield, growth, leaf water content, membrane permeability, and ionic composition of strawberry under saline conditions," *Journal of plant nutrition,* vol. 34, no. 1, pp. 34-45, 2011.

[6] H. Antoun and D. Prévost, "Ecology of plant growth promoting rhizobacteria," in *PGPR: Biocontrol and biofertilization*: Springer, 2005, pp. 1-38.

[7] Z. A. Zahir, M. Arshad, and W. T. Frankenberger, "Plant growth promoting rhizobacteria: applications and perspectives in agriculture," *Advances in Agronomy,* vol. 81, pp. 97-168, 2003.

[8] C. S. Jacobsen, "Plant protection and rhizosphere colonization of barley by seed inoculated herbicide degrading *Burkholderia (Pseudomonas) cepacia* DBO1 (pRO101) in 2, 4-D contaminated soil," *Plant and Soil,* vol. 189, no. 1, pp. 139-144, 1997.

[9] Y. Bashan and L. de Bashan, "Plant growth-promoting," *Encyclopedia of soils in the environment,* vol. 1, pp. 103-115, 2005.

[10] H. Karlidag, E. Yildirim, M. Turan, M. Pehluvan, and F. Donmez, "Plant growth-promoting rhizobacteria mitigate deleterious effects of salt stress on strawberry plants (*Fragaria× ananassa*)," *HortScience,* vol. 48, no. 5, pp. 563-567, 2013.

[11] Y. Bashan, M. Moreno, and E. Troyo, "Growth promotion of the seawater-irrigated oilseed halophyte *Salicornia bigelovii* inoculated with mangrove rhizosphere bacteria and halotolerant *Azospirillum spp.*," *Biology and Fertility of Soils,* vol. 32, no. 4, pp. 265-272, 2000.

[12] P. M. Hasegawa, R. A. Bressan, J.-K. Zhu, and H. J. Bohnert, "Plant cellular and molecular responses to high salinity," *Annual review of plant biology,* vol. 51, no. 1, pp. 463-499, 2000.

[13] R. Munns, "Comparative physiology of salt and water stress," *Plant, cell & environment,* vol. 25, no. 2, pp. 239-250, 2002.

[14] W.-Y. Kao, T.-T. Tsai, and C.-N. Shih, "Photosynthetic gas exchange and chlorophyll a fluorescence of three wild soybean species in response to NaCl treatments," *Photosynthetica,* vol. 41, no. 3, pp. 415-419, 2003.

[15] M. Ashraf and M. Shahbaz, "Assessment of genotypic variation in salt tolerance of early CIMMYT hexaploid wheat germplasm using photosynthetic capacity and water relations as selection criteria," *Photosynthetica,* vol. 41, no. 2, pp. 273-280, 2003.

[16] S. Kumari, A. Vaishnav, S. Jain, A. Varma, and D. K. Choudhary, "Bacterial-mediated induction of systemic tolerance to salinity with expression of stress alleviating enzymes in soybean (*Glycine max* L. Merrill)," *Journal of Plant Growth Regulation,* vol. 34, no. 3, pp. 558-573, 2015.

[17] E. Brugnoli and O. Björkman, "Growth of cotton under continuous salinity stress: influence on allocation pattern, stomatal and non-stomatal components of photosynthesis and dissipation of excess light energy," *Planta,* vol. 187, no. 3, pp. 335-347, 1992.

[18] H. Han and K. Lee, "Plant growth promoting rhizobacteria effect on antioxidant status, photosynthesis, mineral uptake and growth of lettuce under soil salinity," *Res J Agric Biol Sci,* vol. 1, no. 3, pp. 210-215, 2005.

[19] A. Golpayegani and H. G. Tilebeni, "Effect of biological fertilizers on biochemical and physiological parameters of basil (*Ociumum basilicm* L.) medicine plant," *Am Eurasian J Agric Environ Sci,* vol. 11, pp. 411-416, 2011.

[20] R. Porcel, Á. M. Zamarreño, J. M. García-Mina, and R. Aroca, "Involvement of plant endogenous ABA in *Bacillus megaterium* PGPR activity in tomato plants," *BMC plant biology,* vol. 14, no. 36, pp. 1-12, 2014.

[21] S. Mahmood *et al.*, "Plant Growth Promoting Rhizobacteria and Silicon Synergistically Enhance Salinity Tolerance of Mung Bean," *Frontiers in Plant Science,* vol. 7, p. 876, 2016.

[22] P. S. Shukla, P. K. Agarwal, and B. Jha, "Improved salinity tolerance of *Arachis hypogaea* (L.) by the interaction of halotolerant plant-growth-promoting rhizobacteria," *Journal of plant growth regulation,* vol. 31, no. 2, pp. 195-206, 2012.

[23] Ş. Arikan, M. İpek, and L. Pirlak, "Effect Of Some Plant Growth Promoting Rhizobacteria (PGPR) On Growth, Leaf Water Content And Membrane Permeability Of Two Citrus Rootstock Under Salt Stress Condition," presented at the VII International Scientific Agriculture Symposium, Jahorina, Bosnia and Herzegovina, October 06 - 09, 2016 2016.

JOURNAL OF SCIENCE
SAKARYA UNIVERSITY

Sakarya University Journal of Science

ISSN 1301-4048 | e-ISSN 2147-835X | Period Bimonthly | Founded: 1997 | Publisher Sakarya University
http://www.saujs.sakarya.edu.tr/en/

Title: Parametric Analysis of a Plain-Fin Compact Heat Exchanger for a Small-Scale Gas Turbine

Authors: Princely Kolle Epie, Can Haşimoğlu, Göhkan Coşkun, Hakan Serhad Soyhan
Recieved: 2019-08-08 13:13:37

Accepted: 2019-10-22 14:54:50

Article Type: Research Article
Volume: 24
Issue: 2
Month: April
Year: 2020
Pages: 287-300

How to cite
Princely Kolle Epie, Can Haşimoğlu, Göhkan Coşkun, Hakan Serhad Soyhan; (2020), Parametric Analysis of a Plain-Fin Compact Heat Exchanger for a Small-Scale Gas Turbine. Sakarya University Journal of Science, 24(2), 287-300, DOI: https://doi.org/10.16984/saufenbilder.603756
Access link
http://www.saujs.sakarya.edu.tr/tr/issue/52471/603756

Sakarya University Journal of Science 24(2), 287-300, 2020

Parametric Analysis of a Plain-Fin Compact Heat Exchanger for a Small-Scale Gas Turbine

Princely Kolle EPIE*[1], Can HAŞİMOĞLU[2], Göhkan COŞKUN[3], Hakan Serhad SOYHAN[4]

ABSTRACT

The influence of the thermal parameters of a Plain-Fin Compact Heat Exchanger on its performance is examined in this paper. The objective of this work is to analyse the effect of the different flow and geometric parameters on the output performance of a plain fin compact heat exchanger (PFCHE) designed to be used on a small-scale gas turbine and how these parameters can be used for the optimisation of PFCHEs.

In this work, we examined the effects of the variation of input parameters of a plain-fin compact heat exchanger (fin length, fin height, fin thickness, mass flow rate of air and turbine exhaust gas) on the output performance of the heat exchanger (Overall heat exchanger efficiency, fin heat transfer efficiency and the outlet temperatures). The analytical expressions for the outlet temperatures and heat exchanger efficiencies were derived and analysed. Then the derived model was designed and simulated using CFD codes. Also, from the derived expressions, the performance model of the heat exchanger was programmed for analysis. From the results, it shows that the effectiveness (e-value), fin length, fin height and mass flow rates of the gases influence performance of a plain-fin compact heat exchanger. A 50% reduction in fin height can cause as much as an 18% increase in the fin efficiency of the heat exchanger. While a 50% increase in the effectiveness value can cause as much as a 40% increase in the outlet temperature.

Keywords: Heat exchanger, compact heat exchanger, gas turbine, fin efficiency, overall efficiency, mass flow rate, PFCHE, fin length, fin height, fin thickness.

*Corresponding Author: princely.epie@ogr.sakarya.edu.tr
[1] Sakarya University, Sakarya, Turkey. ORCID: 0000-0001-6970-3423
[2] Sakarya University of Applied Sciences, Sakarya, Turkey, ORCID: 0000-0002-5313-1229
[3] Sakarya University, Sakarya, Turkey, ORCID: 0000-0003-1485-4325
[4] Sakarya University, Sakarya, Turkey, ORCID: 0000-0003-3723-9640

1. INTRODUCTION

A gas turbine is a type of continuous internal combustion engine. Small scale gas turbines are gas turbines with an output of up to 500KW. These internal combustion engines unlike the traditional Otto and Diesel engines, work following the Brayton cycle. For these engines to achieve efficiencies values of about 50% [1], with an electrical efficiency of about 35%, they need to be run with a recuperated energy cycle of varying configurations. Due to the need for lightweight, space-saving, and economic factors, the Compact Heat Exchanger has been used in wide variety of applications of gas turbines. Typical among these are gas turbines used in automobiles, cryogenics, aircraft and spacecraft, ocean power plants, and small-scale or micro gas turbines. With the use of a compact heat exchanger, the turbine's overall efficiency can be improved up to 90%. [2–5].

Different studies have been carried out to investigate the effects of the different hydraulic and geometric features of a heat exchanger on its performance. For example, the effects of parameters like the heat transfer, effectiveness, heat transfer coefficient, etc. on the performance of heat exchanger and how they could be used to reduce the size of the heat exchanger have been carried out by Thakre et al, 2016 and Rahul et al 2018 [6,7]. But their studies were limited to CH4 and rectangular offset strip fin compact heat exchangers. Also, they considered just liquid as working fluid. Experimental analysis of the cold inlet temperature on the thermal performance of a heat exchanger have also been carried out [8]. But their study was limited on a two mini channel flat-tube with a multi-louvered fin compact heat exchanger. However, the working fluid was a mixture of a liquid and a gas. Also, effects of the mass flow rate on the pressure drop and heat transfer and the heat exchanger effectiveness value have been studied [9,10]. But these effects were not studied against the outlet temperatures of the fluids. Also, the fluids used were liquids.

The effects of the fin length, fin height and fin thickness on the performance of compact heat exchangers have not been given much attention and the available literature is limited to fin-and-tube heat exchangers. Furthermore, most of the studies are limited to the evaluation of one parameter at a time. There are no analyses on the variation of more than two input parameters. Lastly, most of the studies are limited to liquids as the working fluid or using a combination of a liquid through one path and a gas through the other. The purpose of this work is then to analyse and study how the fin length, height, thickness of a heat exchanger with gases as working medium affects its performance and how these features can be used to alter the size of the heat exchanger. Also, to study the effect of the mass flow rate and effectiveness value on the outlet temperatures with respect to the heat exchanger's performance. The type of heat exchanger used in this study is the plain-fin compact heat exchanger with rectangular fins and a crossflow arrangement as shown in figure 3.

2. MATHEMATICAL MODELLING OF THE COMPACT HEAT EXCHANGER (PFCHE)

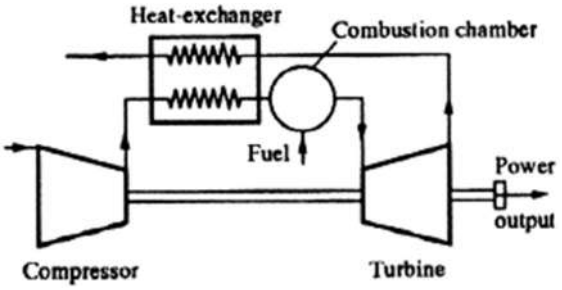

Figure 1 a. Gas turbine with heat exchanger

2.1. Thermodynamic Analysis of a Recuperated Heat Exchanger

Let's consider the figure 2 below [5] which describes the thermodynamic cycle of a gas turbine.

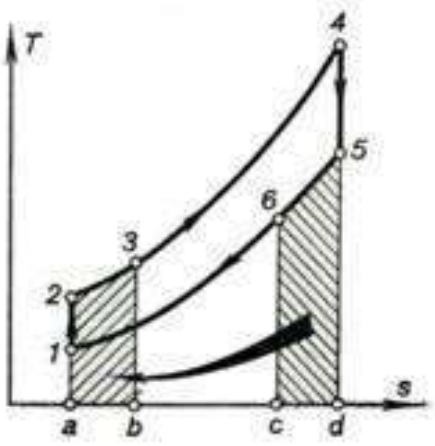

Figure 1 b. Constant pressure gas turbine with adiabatic air compression

The added heat is

$$q_1 = c_p(T_4 - T_3) \qquad (1)$$

The rejected heat is

$$q_2 = c_p(T_6 - T_1) = c_p(T_5 - T_1) - c_p(T_5 - T_6) \qquad (2)$$

But

$$c_p(T_5 - T_6) = c_p(T_3 - T_2) \qquad (3)$$

Which implies

$$q_2 = c_p(T_5 - T_1) - c_p(T_3 - T_2) \qquad (4)$$

The thermal efficiency of the cycle will then be

$$\eta_{Brayton,regen} = 1 - \frac{c_p(T_5 - T_1) - c_p(T_3 - T_2)}{c_p(T_4 - T_3)} \qquad (5)$$

The maximum possible degree of regeneration or regeneration fraction occurs at $T_3 = T_5$, i.e. at $\gamma_{max} = T_5/T_2$. In this case we have [5]

$$\eta_{Brayt,regen,max} = 1 - \frac{T_1}{T_5} \qquad (6)$$

Thus, the thermal efficiency of a constant-pressure gas-turbine operating with maximum regeneration and adiabatic compression depends only on the temperature of the gas at the end of adiabatic expansion, T_5. So, to improve on the efficiency and performance of the gas turbine, there is a need to increase these temperatures while adjusting the other operating parameters of the recuperator.

2.2. Heat Transfer and Hydraulic Flow Analysis

Assuming the same heat capacity for both the hot and cold streams of air, we have [4], for the hot gas outlet temperature

$$T_{h,o} = T_{h,i} - \varepsilon\left(T_{h,i} - T_{c,i}\right) \qquad (7)$$

And for the cold air we have,

$$T_{c,o} = T_{c,i} + \varepsilon\frac{\dot{m}_h}{\dot{m}_c}\left(T_{h,i} - T_{c,i}\right) \qquad (8)$$

But taking into account the heat capacity of the gases, we have the corrected outlet temperature of the cold air stream as follows

$$T_{c,o} = T_{c,i} + \varepsilon\left(\frac{\dot{m}_h c_{p,h}}{\dot{m}_c c_{p,c}}\right)\left(T_{h,i} - T_{c,i}\right) \qquad (9)$$

- Refined value of Cold stream AMT

$$T_{c,m} = \frac{T_{c,o} + T_{c,i}}{2} \qquad (10)$$

From the above fluid property values, the NTU can be gotten.

- The Core mass velocities of the fluids (G)

The value of G is expressed as follows

$$G_i = \left[\frac{2g_c}{\left(\frac{1}{\rho}\right)_m P_r^{2/3}}\frac{\eta_0 \Delta P}{NTU} j/f\right]_i^{1/2} \qquad (11)$$

Where, $i = h, c$ for the hot gas and cold air respectively.

- The Reynolds Number and the j and f factors

The Reynolds number is expressed as

$$Re_i = \left(\frac{GD_h}{\mu}\right)_i \quad (12)$$

For plane rectangular PFHE and laminar flow [11], we have

$$f_i = 12.892 Re_i^{-1.229} \left(\frac{b}{n}\right)_i^{0.452} \left(\frac{\delta_w}{n}\right)_i^{-0.198} \quad (13)$$

and

$$j_i = 0.454 Re_i^{-0.977} \left(\frac{b}{n}\right)_i^{0.455} \left(\frac{\delta_w}{n}\right)_i^{-0.277} \quad (14)$$

- The heat transfer coefficient (h)

The heat transfer coefficient can be calculated from the expression below

$$h_i = \left(\frac{jGC_p}{P_r^{2/3}}\right)_i \quad (15)$$

- Fin Efficiency (η_f)

The fin efficiency is expressed as follows

$$\eta_{f,i} = \left(\frac{\tanh(ml)}{ml}\right)_i \quad (16)$$

Where,

$$m_i = \left[\frac{2h}{k_f \delta}\left(1 + \frac{\delta}{l_s}\right)\right]_i^{1/2} \quad (17)$$

and

$$l_c = l_h = \frac{b}{2} - \delta \quad (18)$$

- Overall Surface Efficiency (η_o)

We have

$$\eta_o = 1 - (1 - \eta_f)\frac{A_f}{A} \quad (19)$$

- Overall Heat Transfer Coefficient

The overall heat transfer coefficient is evaluated as follows

$$\frac{1}{U} = \frac{1}{(\eta_o h)_h} + \frac{\alpha_h/\alpha_c}{(\eta_o h)_c} \quad (20)$$

Where,

$$\alpha_i = \frac{(b\beta)_i}{b_c + b_h + 2\delta_w} \quad (21)$$

And,

$$\frac{A_c}{A_h} = \frac{\alpha_c}{\alpha_h} = 1.0 \quad (22)$$

- Total Surface Area (A)

For the hot air stream, we have

$$A_h = NTU \frac{C_h}{U_h} \quad (23)$$

- Heat Transfer between Fluids

The effectiveness $\boldsymbol{\varepsilon}$ is defined as the ratio of the actual heat transfer rate and the maximum heat transfer rate. This is expressed as follows [12]

$$\varepsilon = \frac{Q}{Q_{max}} \quad (24)$$

The maximum heat transfer rate, Q_{max}, between the fluids can be determined from Equation 2.7 [13] as expressed below

$$Q_{max} = U_h A(T_{h,i} - T_{h,o}) \quad (25)$$

Thus, the actual heat transfer between the fluids is

$$Q = \varepsilon Q_{max} \quad (26)$$

2.3. Numerical Application

Design specifications**:** Due to the operating fluids all being gases, low cost, low space requirements, manufacturability, and operating temperatures and pressures, a regenerator of Plate-Fin Compact Heat Exchanger (PFCHE) type with Rectangular fins and a crossflow arrangement was chosen.

- Required Effectiveness: $\varepsilon = 0.8381$
- Fin height: $b_h = b_c = 15mm$
- Fin thickness: $\delta_w = 1mm$, $\delta_h = \delta_c = \delta_w$
- Heat transfer surface area density: $\beta_c = \beta_h = 2000m^2/m^3$
- Fin area/total area ratio: $\left(\frac{A_f}{A}\right)_h = \left(\frac{A_f}{A}\right)_c = 0.785$
- Hydraulic diameter: $D_{h,h} = D_{h,c} = 1.6mm$
- Fluid mass flow rates: $\dot{m}_h = 1.66kg/s$, $\dot{m}_c = 2.0kg/s$
- Pressure drop : $\Delta P_h = 9.0kPa$, $\Delta P_c = 8.79kPa$
- Plate Thermal heat transfer (Both plates are made of steel): $k_w = 33W/mK$
- Inlet Temperatures of gases: $T_{h,i} = 798K$, $T_{c,i} = 317K$

Outlet temperatures $T_{h,o}$and $T_{c,o}$

$$T_{h,o} = 798 - 0.8381(798 - 317) = 394.87\ K \quad (27)$$

$$T_{c,o} = 317 + 0.8381\left(\frac{1.66}{2}\right)(798 - 317) = 651.59\ K \quad (28)$$

Corrected value of cold stream outlet temperature

$$T_{c,o} = 317 + 0.8381\left(\frac{1.66 \times 1.051}{2 \times 1.030}\right)(798 - 317) = 658.42\ K \quad (29)$$

Refined value of outlet temperatures

$$T_{h,o} = \frac{798 + 394.87}{2} = 596.44\ K \quad (30)$$

$$T_{c,o} = \frac{317 + 658.42}{2} = 487.71\ K \quad (31)$$

- The Core mass velocities of the fluids (G)

$$G_h = \left(\frac{2 \times 1 \times 0.8 \times 9.05 \times 10^3 \times 0.25}{(1/0.5804) \times 0.777 \times 10.790}\right)^{1} = 6.3047\ kg/m^2s \quad (32)$$

$$G_c = \left(\frac{2 \times 1 \times 0.8 \times 8.79 \times 10^3 \times 0.25}{(1/0.6964) \times 0.776 \times 9.139}\right)^{1/2} = 7.0153\ kg/m^2s \quad (33)$$

- The Reynolds Number and the j and f factors

$$Re_h = \frac{6.3047 \times 0.0016}{305.8 \times 10^{-7}} = 329 \quad (34)$$

$$Re_c = \frac{7.0153 \times 0.0016}{270.1 \times 10^{-7}} = 415.57 \quad (35)$$

- The heat transfer coefficient (h)

$$h_h = \frac{0.00358 \times 6.3047 \times 1.051 \times 10^3}{0.777} = 30.53\ W/m^3K \quad (36)$$

$$h_c = \frac{0.002856 \times 7.0153 \times 1.030 \times 10^3}{0.776} = 26.59\ W/m^3K \quad (37)$$

- Fin Efficiency (η_f)

$$\eta_{f,c} = \frac{\tanh(40.184 \times 0.0065)}{40.184 \times 0.0065} = 0.9779 \quad (38)$$

$$\eta_{f,c} = \frac{\tanh(43.008 \times 0.0065)}{43.008 \times 0.0065} = 0.9747 \quad (39)$$

- Overall Surface Efficiency (η_o)

$$\eta_{o,h} = 1 - (1 - 0.9747) \times 0.785 = 0.980 \quad (40)$$

$$\eta_{o,c} = 1 - (1 - 0.9779) \times 0.785 = 0.983 \quad (41)$$

- Overall Heat Transfer Coefficient

$$\frac{1}{U_h} = \frac{1}{0.98 \times 30.53} + \frac{1}{0.983 \times 26.59} \quad (42)$$

$$U = 13.95\ W/m^2K \quad (43)$$

- Total Surface Area (A)

$$A = \frac{5.395 \times 1.745 \times 10^3}{13.95} = 674.86\ m^2 \quad (44)$$

- Heat Transfer between Fluids ($\dot{q}$)

$$\dot{q} = 0.8381 \times 3785.2 \times 10^3 = 3180.8\ kW \quad (45)$$

Tables 1 and 2 present a summary of the coefficients and geometric properties of the HE

Table 1. Heat Exchanger Coefficients and Fluid Properties

Coefficient/Property	**Value**	
	Cold Air Stream	**Hot Gas Stream**
Outlet Temperature $T_{i,o}$	685.42 K	394.87 K
NTU	9.139	9.139
Core Velocity G_i	7.0153 kg/m^{2}s	6.3047 kg/m^{2}s
Reynolds Number Re_i	415.57	329.84
j-factor j_i	0.002856	0.00358
f-factor f_i	0.014777	0.01963
Heat transfer Coefficient h_i	30.53 W/m^{2}K	26.59 W/m^{2}K
Fin Efficiency $\eta_{f,i}$	0.9779	0.9747
Overall Surface Efficiency η_o	0.983	0.980
Overall Heat Transfer Coefficient U	13.95	-
Maximum Heat transfer between Fluids Q_{max}	3795.2 kW	-
Heat transfer between Fluids Q	3180.8 kW	-

Table 2. Heat Exchanger Geometric features

Feature	Calculated Value		Rounded Value
	Cold Air Stream	Hot Air Stream	
Total Surface Area A (m^2)	674.86	674.86	-
Minimum free flow area A_o (m^2)	0.2851	0.2635	-
Frontal Area A_{fr} (m^2)	0.6740	0.6229	-
Air Flow Length (m)			
Lc	0.947	-	1.0
Lh	-	1.024	1.0
L_3 (Height)	0.648		0.5

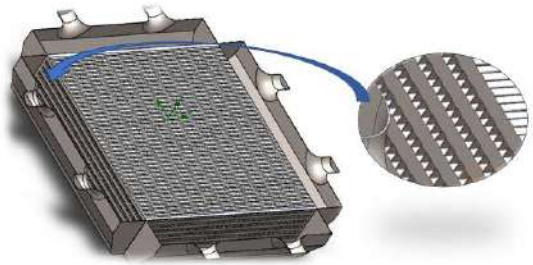

(a)

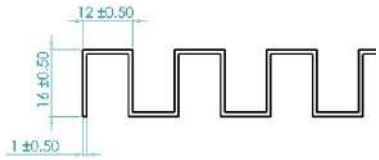

(b)

Figure 2. (a) Cross section of plain-fin compact heat exchanger. (b) Fin geometry (rectangular fins)

RESULTS AND DISCUSSIONS

2.4. Boundary Conditions

The boundary conditions for the CFD analysis were as specified above in input data. The CFD analyses were carried with the assumptions of ideal operating states. A full adaptive and automatic meshing structure was used in the simulation. The figure 3a shows the meshed structure. In the final optimised structure (figure 3a), we used a minimum length and an adaptive mesh structure. This was appropriate for the simulation of our heat exchanger since it permits for an increased computational and storage savings, it accommodates the complexity of our structure and it is proper for our physical system since it makes the simulation independent of the mesh size.

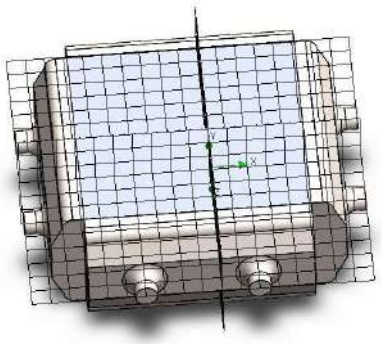

Figure 3a: Meshed Heat exchanger

A fluid flow simulation was performed using SOLIDWORKS Flow Simulation. During the simulations we applied a finite volume method (FVM) for simulation algorithm. The results of the CFD study were as follows.

2.5. Heat distribution profile within the Heat Exchanger

During the simulation, the heat distribution profile was in the HE was recorded. Figure 3b below shows the temperature variation within the HE. After 116 iterations, the HE attained a

convergence point and reached maximum operating state.

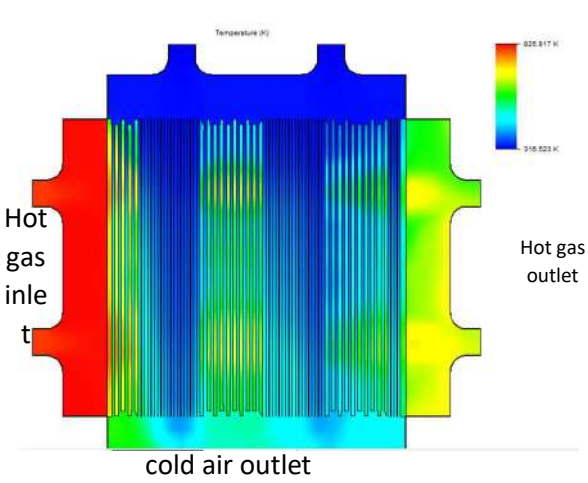

Figure 3b. Heat distribution in Heat Exchanger

2.6. Effects of fin length

The figure 4 presents the relation between the heat exchanger fin efficiency versus the fin length at different values of fin height. It can be seen that the fin length has no effect on the fin efficiency. But as the fin height increases, there is an increase in the Fin Efficiency. As shown by figure 4, fin length does not have any effect on the Overall Surface Efficiency of the heat exchanger. An increase in fin height causes an increase on the Overall Surface Efficiency.

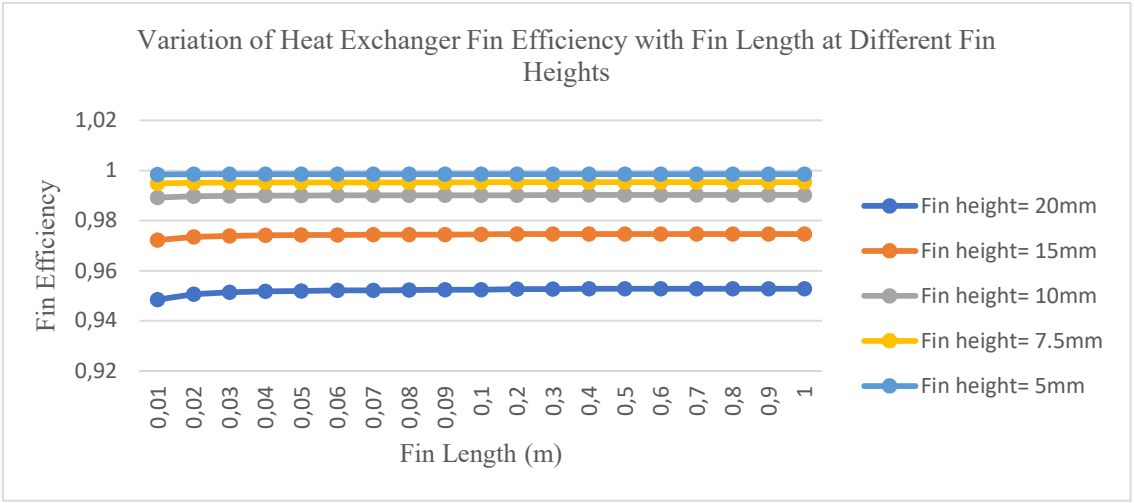

(a) Fin Efficiency

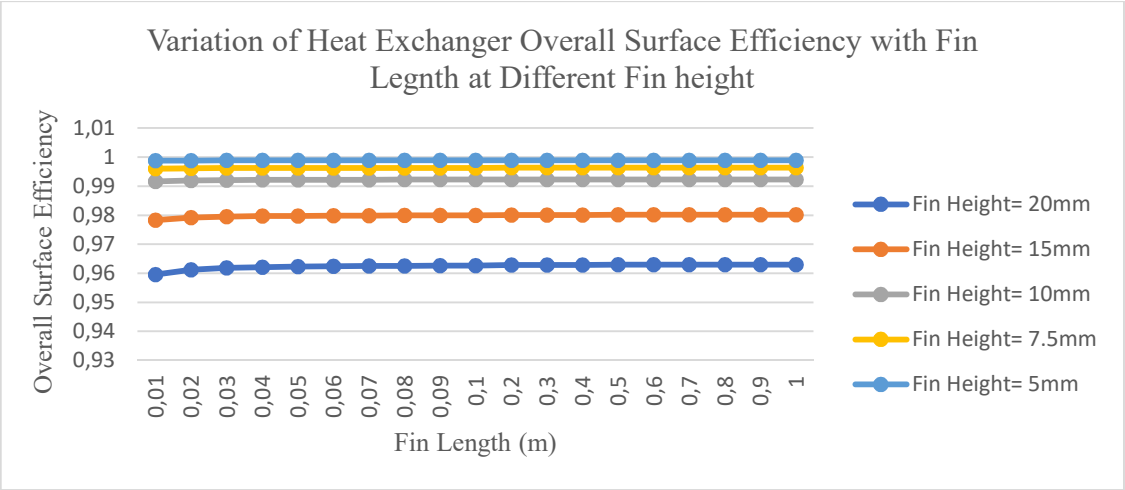

(b) Overall Surface Efficiency

Figure 4. Variation of Heat Exchanger Fin Efficiency and Overall Surface Efficiency versus Fin Length at different values of fin height

2.7. Effects of fin thickness

As presented in figure 5, the relationship between the heat exchanger fin efficiency and overall surface efficiency versus the fin thickness can be seen. The figure 5 also shows the effects of the fin height on these relations. As we can see on figure 5a, the fin thickness has a significant effect on the fin efficiency. As the fin thickness increases, the fin efficiency increases as well. This continues until it reaches a peak value after which it stays constant. Thus, there is an optimum fin thickness where the fin efficiency is maximum and an increase in fin thickness causes no change on the efficiency. Also, as the fin height increases, this optimum fin thickness also shifts to the right. But it can be seen that, the increase in fin height has a negative effect on the fin efficiency. Furthermore, at lower values of fin thickness, a change in fin height has more effect on the heat exchanger efficiency.

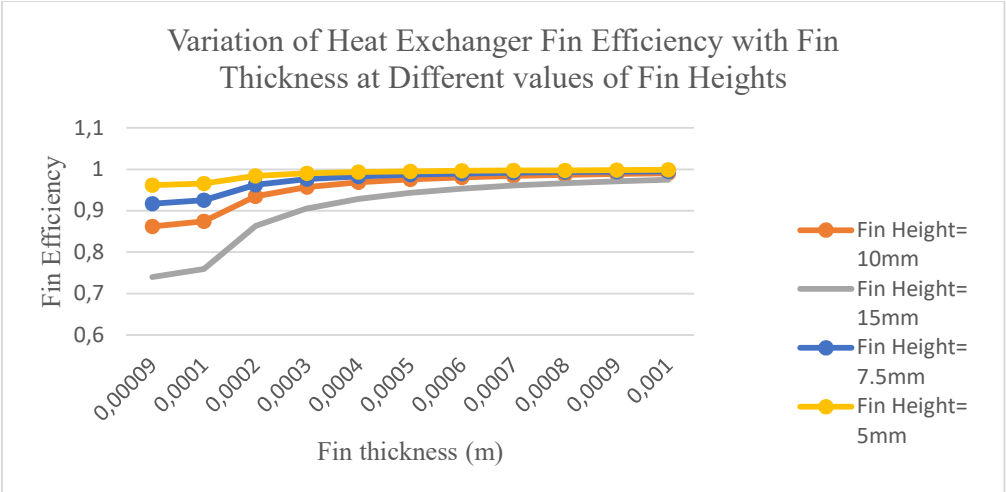

(a) Fin efficiency

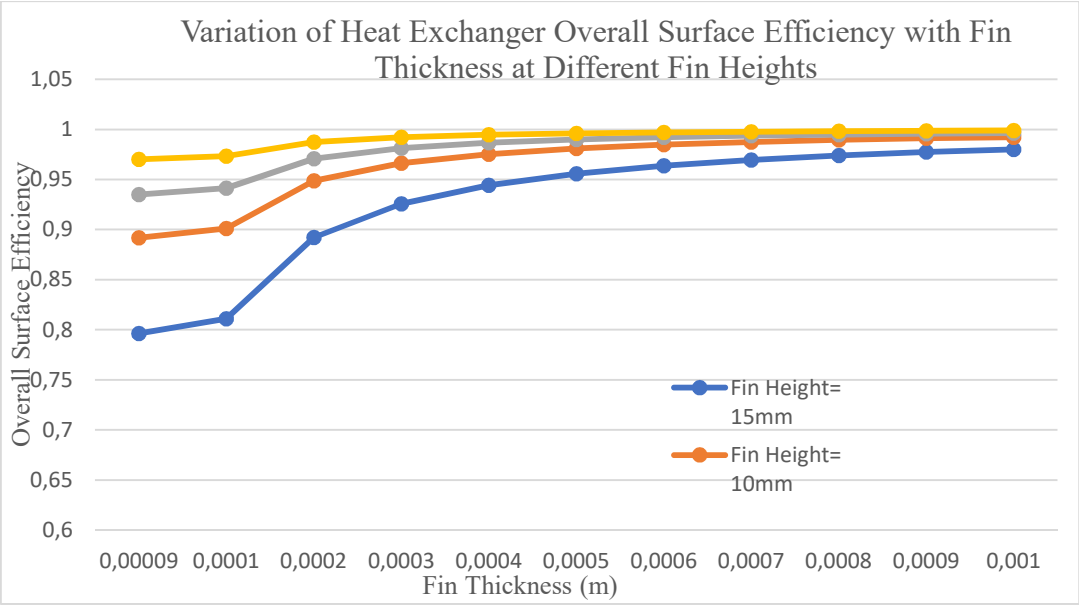

(b) Overall surface Efficiency

Figure 5. Variation of Heat Exchanger Fin Efficiency and Overall surface Efficiency with Fin Thickness at different fin heights (other parameters are constant as stated in the design specifications)

The figure 5b, presents the relationship between the overall surface efficiency versus the fin thickness. It can be observed that the overall surface efficiency has a positive relationship with the fin thickness. This positive relation continues until a maximum value is reached. As the fin height increases, there is a decrease in the overall surface efficiency. Finally, we observe that at lower values of fin thickness, an increase in fin height has more effect on the efficiency of the heat exchanger. The Same observations were made by Kourosh et al, 2018 in their experimental study of the effects of fin height, fin-tube contact thickness compact of a heat exchanger [14].

2.8. Effects of hot gas stream mass flow rate

Figure 6 presents the relation between the outlet temperatures of the two streams versus the gas mass flow and this study was done based on ideal conditions. It is observed that the gas mass flow rate has no effect on the hot gas stream. But it has a positive effect on the cold air stream.

The figure 7 presents the relationship between the hot gas stream mass flow rate and the cold air stream outlet temperature (the air from the compressor). This relationship is examined at different values of the Effectiveness Value, the cold air stream inlet temperature, and the hot gas stream inlet temperature. It can be observed that the hot gas flow rate has a positive

effect on the cold air stream outlet temperature. The graphs show an increasing linear relationship between the two variables. From figure 7a and 7b, an increase in effectiveness value positively affects the cold air stream outlet temperature. These observations were also made by Panthee, 2017 and Thakre et al, 2016 in their experimental observations of the effect of the mass flow rate over the effectiveness value [6,10]. Also, at lower mass flow rates, there little effect of effectiveness value over the outlet temperature. But as the mass flow rate increases, the effect becomes more important.

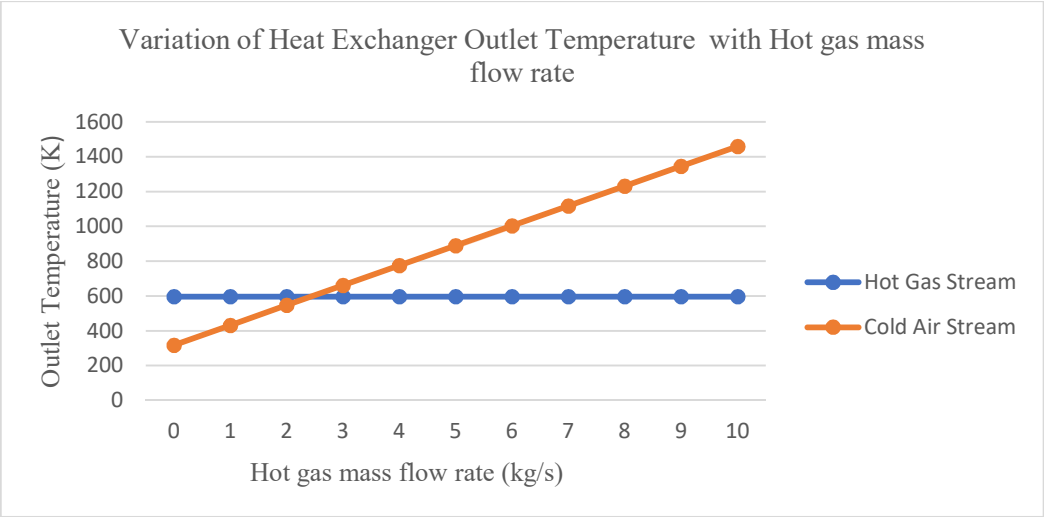

Figure 6. Cold air stream and Hot gas stream outlet temperatures versus hot gas mass flow rate

The increase in cold air stream inlet temperature has a converging effect on the cold air stream outlet temperature at lower mass flow rates (figure 7c). This happens until it reaches the convergence point. From this point, as the cold air stream inlet temperature increases, the cold air outlet temperature decreases. This point of convergence is the when the cold air stream inlet temperatures equals the hot gas stream inlet temperatures. So, after this point, the direction of heat flow interchanges.

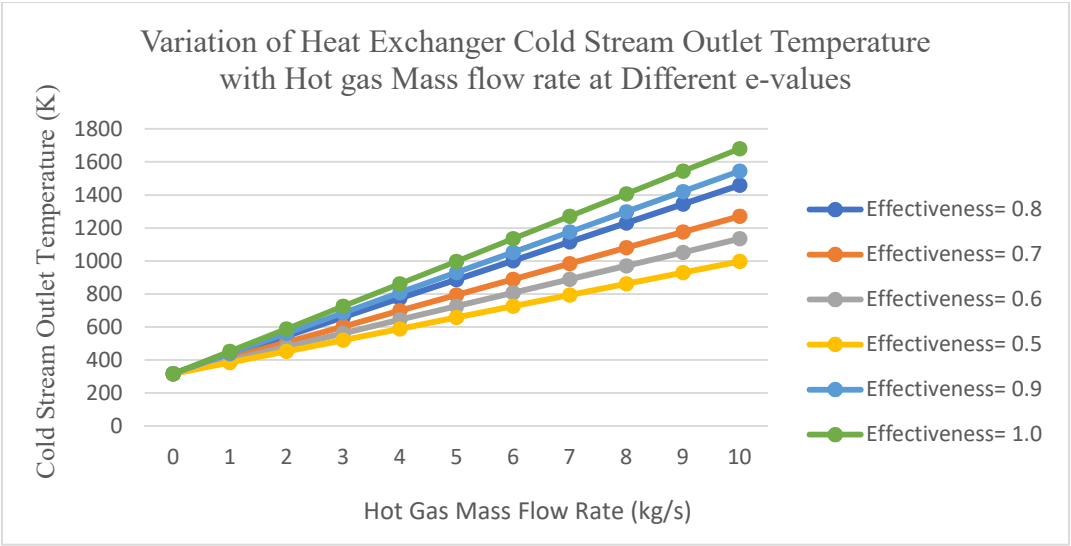

(a) Effectiveness value (e)

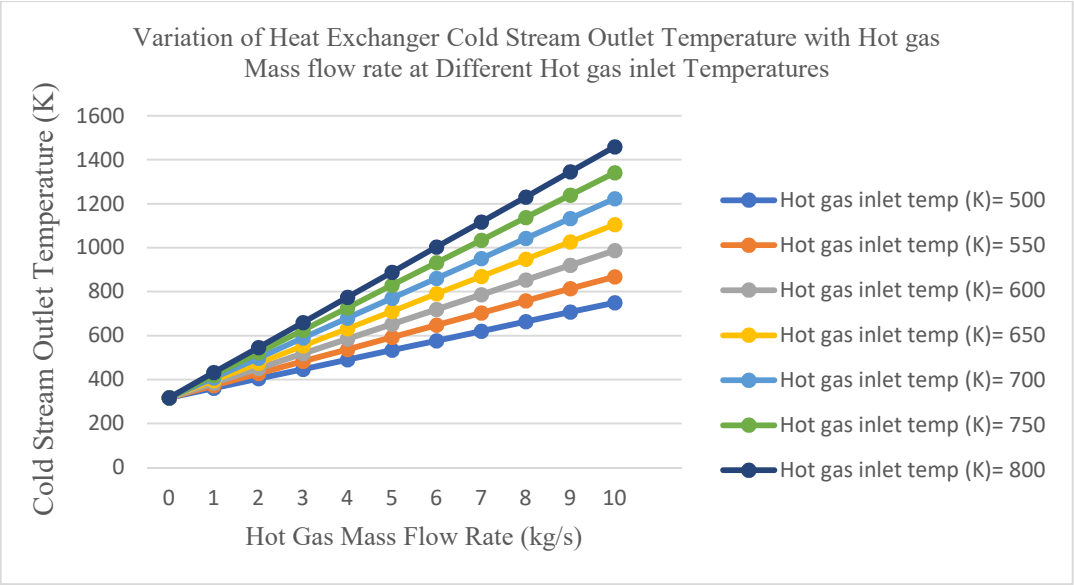

(b) Hot gas stream inlet temperature

2.9. Discussions

The fin efficiency, overall surface efficiency and outlet temperatures of a PFCHE depends on the operating conditions (mass flow rates and inlet temperatures of fluids), and the heat exchanger geometric features (fin length, fin height, fin thickness and the effectiveness value).

From figures 4 and 5, it can be seen that; using thinner and shorter fins will produce efficient and more compact plain fin compact heat exchangers. A 50% reduction in fin height can cause as much as an 18% increase in the fin efficiency of the heat exchanger. This can be considered when there is a problem of space. But this will also require advanced manufacturing techniques and thus incurring more cost.

From the figures 6 and 7, it can be seen that plain fin compact heat exchangers with higher effectiveness values attain higher outlet temperatures. For example, a 50% increase in the effectiveness value can cause as much as a 40% increase in the outlet temperature. Furthermore, as the fluid flow rate increases, this effect of the e-value on the outlet temperature also increases (with values of 15% at 1 kg/s, 34% at 5 kg/s and 40.1% at 10 kg/s). Also, to obtain higher outlet temperatures on the cold stream, the hot gas flow rate (flow velocity) can be increased. These results were obtained based on ideal conditions but experimental works done by other researchers obtained similar results. For example in Panthee's work, for plate heat exchangers he registered a 20 % increase in e-value and a 9 % increase in outlet temperature for a 50% change in mass flow rate of hot gas [10].

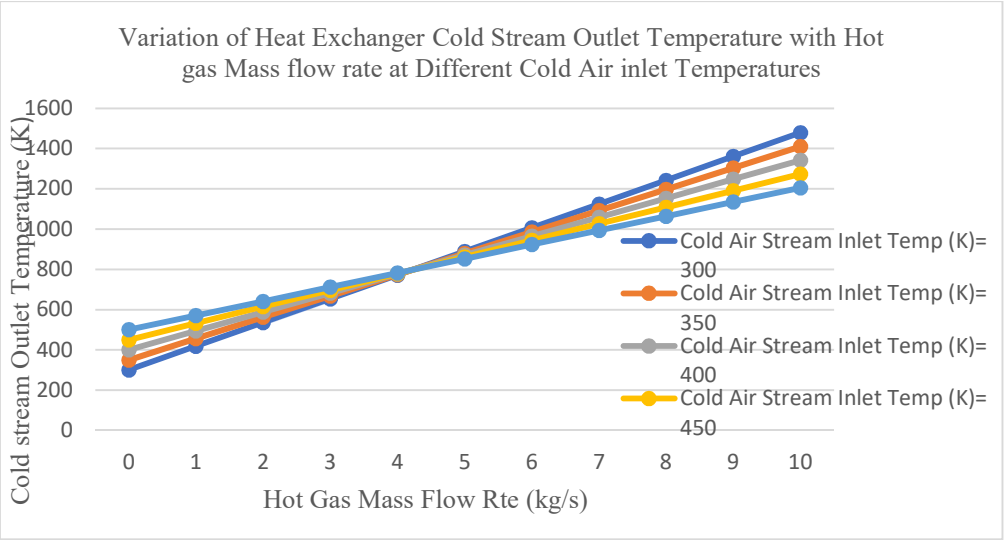

(c) Cold air stream inlet temperature

Figure 7. Variation of Heat Exchanger Outlet Temperatures with Hot gas Mass flow rate (other parameters are constant as stated in the design specifications)

3. CONCLUSIONS

In this study the parametric analysis of the PFCHE was carried out. The different flow and geometric parameters of the heat exchanger were studied to evaluate their influence on the performance of the heat exchanger. The results of the simulation from the modelling of the influence of heat exchanger parameters showed that the hot gas mass flow rate, effectiveness value, fin height, fin thickness and the inlet temperatures of the fluids have effect on the performance of the PFCHE. The summary of these results are as follows:

- Increasing the fin thickness and fin height reduces the fin efficiency and thus the overall efficiency of PFCHEs
- There is an optimum fin thickness after which increasing the fin thickness no longer influences the fin and overall surface efficiencies.
- The fin length has little effect on the fin and overall surface efficiencies of the PFCHE.
- Increasing the effectiveness value and the hot gas flow rate also increases the cold stream outlet temperature of the PFCHE.
- After the convergence point, the performance of the heat exchanger inverses due to change in heat flow direction.

4. REFERENCES

[1] Medicine NA of SE and. Commercial Aircraft Propulsion and Energy Systems Research. 2016. doi:10.17226/23490.

[2] Mcdonald CF, Massardo AF, Rodgers C, Stone A, Mcdonald CF, Rodgers C, et al. Recuperated gas turbine aeroengines . Part III : engine concepts for reduced emissions , lower fuel consumption , and noise abatement 2008. doi:10.1108/00022660810882773.

[3] Thulukkanam K. Heat exchanger design handbook 2nd Edition. 2013.

[4] Ramesh K. Shah, Dušan P. Sekulic. Fundamentals of Heat Exchanger Design.

2003.

[5] Spakovsky) ZS. Thermodynamics and Propulsion. n.d.

[6] Thakre PB, Pachghare PR. Performance Analysis on Compact Heat Exchanger. Mater Today Proc 2017;4:8447–53. doi:10.1016/j.matpr.2017.07.190.

[7] Vr R, R AK. Parametric Study of Heat Transfer and Pressure Drop Characteristics of a Rectangular Offset Strip Fin Compact Heat Exchanger 2018;71:1381–6. doi:10.3303/CET1871231.

[8] Doğan B. EXPERIMENTAL ANALYSIS OF THE EFFECT OF COLD FLUID INLET TEMPERATURE ON THE THERMAL PERFORMANCE OF A HEAT EXCHANGER 2016;2:583–92.

[9] Asadi M, Khoshkhoo RH. Effects of mass flow rate in terms of pressure drop and heat transfer characteristics 2013;1:5–11.

[10] Panthee P. Testing and Characterising the Performance of Heat Exchangers 2017.

[11] Dewatwal J. DESIGN OF COMPACT PLATE FIN HEAT EXCHANGER. National Institute of Technology Rourkela, 2009.

[12] Aral MC, Ho M, Suhermanto M. Heat Transfer Modelling of a Parallel Flow Micro Channel / Louvered Fin Condenser Using Refrigerants R134a and R1234yf n.d.:1–11.

[13] Kakaç, Sadik; Liu, Hongtan; Pramuanjaroenkij A. HEAT EXCHANGERS 3rd Edition. CRC Press, Taylor & Francis Group; 2012.

[14] Javaherdeh K, Vaisi A, Moosavi R. The effects of fin height , fin-tube contact thickness and louver length on the performance of a compact fin-and-tube heat exchanger 2018;36:825–34.

JOURNAL OF SCIENCE
SAKARYA UNIVERSITY

Sakarya University Journal of Science

ISSN 1301-4048 | e-ISSN 2147-835X | Period Bimonthly | Founded: 1997 | Publisher Sakarya University
http://www.saujs.sakarya.edu.tr/en/

Title: Determining the Binding Capacities of Cr (VI) and Zn (II) Ions of Oscillatoria sp.

Authors: Gülşan Sezgin, Şükran Yıldız, Tuğba Şentürk
Recieved: 2019-03-11 12:54:11

Accepted: 2019-12-30 16:54:12

Article Type: Research Article
Volume: 24
Issue: 2
Month: April
Year: 2020
Pages: 301-311

How to cite
Gülşan Sezgin, Şükran Yıldız, Tuğba Şentürk; (2020), Determining the Binding Capacities of Cr (VI) and Zn (II) Ions of Oscillatoria sp.. Sakarya University Journal of Science, 24(2), 301-311, DOI:
https://doi.org/10.16984/saufenbilder.538117
Access link
http://www.saujs.sakarya.edu.tr/tr/issue/52471/538117

Sakarya University Journal of Science 24(2), 301-311, 2020

Determining the Binding Capacities of Cr (VI) and Zn (II) Ions of *Oscillatoria* sp.

Gülşan SEZGİN[1], Şükran YILDIZ[2], Tuğba ŞENTÜRK*[3]

Abstract

This study aimed to determine the removal capacity for Cr (VI) and Zn (II) ions from high concentration of aqueous solutions by using *Oscillatoria* microalgae. In the biosorption process, live and dead *Oscillatoria* cells were exposed for 24 hours to Cr and Zn metals of different concentrations (2.5, 5 and 10 mg/L). In addition, chlorophyll-a analysis have been made to examine the effects on cell metabolism of chromium and zinc metals. The best metal removal percentages was obtained; of chromium ion is 46.74% with dead cells and for zinc ion 82.53% with living cells. Chlorophyll-a analysis shows that when the metals separately applied on *Oscillatoria* cells, chlorophyll-a content of organism increase but when metals together applied decrease of chlorophyll-a content was observed. For this study, Freundlich model best fitted the data for two metal ions with 1/n value <1. This study revealed that *Oscillatoria* cells were an effective adsorbent for removal of the two heavy metals, especially Zn ions from aqueous solutions due to its high efficiency of Zn adsorption. It shows that it is a kind of potential for this heavy metal removal operations.

Keywords: *Oscillatoria*, bioremediation, heavy metal removal, Cr (VI), Zn (II)

1. INTRODUCTION

In recent years, environmental pollution has been increasing steadily due to the increase in consumption by utilizing technologically [1]. At the top of this environmental pollution problem is the pollution of the water with vital importance for the living things by various factors. Industrial activities constitute the biggest share in water pollution. The amount of heavy metals released as a result of industrial activities is rapidly

[1]Manisa Celal Bayar University, Science and Art Faculty, Biology Department, Manisa, Turkey, https://orcid.org/000-0002-3856-2178
[2]Manisa Celal Bayar University, Science and Art Faculty, Biology Department, Manisa, Turkey, https://orcid.org/0000-0003-3195-2269
*Corresponding Author.
[3]Manisa Celal Bayar University, Science and Art Faculty, Biology Department, Manisa, Turkey, https://orcid.org/0000-0002-9882-0079, e-mail: tugba_sen34@hotmail.com

increasing every day [2]. Heavy metals are naturally occurring compounds in ground shells and they do not deteriorate and can not be destroyed [3]. Some of these metals are important as kofactor of enzymatic reactions in trace amounts. However, high amounts of these metals can be extremely toxic to living organisms or slow down metabolic reactions [1]. These heavy metals are a serious threat to human and environmental health because of the toxic effect, remain intact in nature for an indefinite period of time, travel through the food chain and accumulate [3]. For this reason, the heavy metal contents of the wastewater must be purified and reduced below the permissible values according to various water quality standards before being given to the environment [4-5]. The remediation of heavy metal pollution are used some methods such as chemical precipitation, coagulation, flocculation, ion exchange, extraction, complex separation, biological processes, electrochemical processes, membrane processes, adsorption [6-8]. With these traditional methods, the metals in the environment can not be completely removed. However, these techniques have some disadvantages like expensive equipment and monitoring systems, the need for excessive chemical and energy, toxic sludge and other waste products [9, 10]. Due to the above reasons, new technologies are being studied on removal of metal ions from aqueous media and different technologies are being developed. One of the methods developed in this regard is the biosorption method. The use of microbial biomass in the removal of toxic heavy metals from water and wastewater is a new low cost alternative metods. The most important advantages of biosorption technology are the use of economical biosorbent materials [11, 12], which are capable of reducing the concentrations of heavy metals in wastewater to very low levels and are easily produced in abundant quantities. In addition, this method effectively removes pollutants even from very dilute water [13], allowing in situ application in polluted areas, bioprocessing technologies are also environmentally, which means that they do not cause a second pollution, high efficiency, no need for supplementary nutrients and the possibility of recovering the metal [14,15]. The living organisms used in this process are microorganisms such as algae, fungi and bacteria [16]. Compared to microbial biomass such as fungi and yeast, the heavy metal biosorption capacity of algae was higher. This is due to the high metal binding capacity of functional groups such as amino, hydroxyl, carboxyl and sulfate found in cell contents of algae. These organism can be used dead or alive in the biosorption process. There are some advantages to using dead biomass compared to living biomass. Dead cells can be stored at room temperature for extended periods, are not affected by metal toxicity, and do not require nutrients [17-19]. In this study, the biosorption capacity of Cr (VI) and Zn (II) ions on dead and live blue-green algae *Oscillatoria* sp. was investigated. At the same time, the effect of heavy metals on chlorophyll-a was investigated and biosorption capacities were determined with Freundlich and Langmuir isotherm models. *Oscillatoria* species are preferred because of their easy availability in nature and their high adsorption capacity.

2. MATERIAL AND METHODS

2.1 Organism and culture condition

Oscillatoria cells were obtained from CicCartuja Instituto de Bioquímica Vegetal Y Fotosíntesis Laboratory (Seville, Spain). The alga was grown in 250 mL flasks containing 100 mL BG-11 [20] medium and incubated in an illuminated incubator at 28°C and irradiance at 36 μmol m^{-2} sec^{-1} and magnetic stirring (110 rpm), provided by cool white fluorescent lamps (20 E m^{-2} s^{-1} ± 20%) set on 16:8 h photoperiod. The pH value was adjusted to 6–7 using 1 M NaOH and 1 M HCI. The growth of algae and biomass concentration was monitored by measuring optical density at a wavelength of 660 nm and 730 nm for 30 days. Cells were harvested from the culture by centrifugation. The biomass pellets collected were then washed with distilled water and centrifuged again for the removal of medium.

2.2 Heavy metal concentrations

Stock solutions of the heavy metals K_2CrO_4 and $Zn(NO_3)_2.6H_2O$ were prepared, from which concentrations 2.5, 5 and 10 mg/L of heavy metals

was used. All experiments were repeated three times.

2.3 Biosorption studies

Oscillatoria cells were used in the experiment of heavy metal removal using the algal concentrations 2 g. The metal concentration used was 15 mL and the exposure time was 24 h. pH was adjusted to 5 for Cr (VI) and 7 for Zn (II) and incubation was performed at the previous mentioned conditions. After centrifugation at 4000 rpm to separate the biomass, the samples were analysed by ICP-MS (Inductively Coupled Plasma– Mass Spectrometer-Agilent 7700) [21]. The metal uptake loading capacity qe (mg of metal per g of adsorbent) and removal efficiency (RE %) for each sorption system was determined using Eq. 1 and Eq. 2:

$$q = \frac{V(Ci - Ct)}{m} (Eq. 1)$$

$$RE\ \% = \frac{100*(Ci-Ce)}{Ce} (Eg. 2)$$

Where q is the metal uptake (mg/g of biomass); Ci and Ce are the metal concentrations before and after adsorption (mg/mL), respectively; m is the mass of biosorbent used (g) and V is the volume of solution (mL).

2.4 Determinations of chlorophyll-a content

Chlorophyll-a content were estimated in acetone extract according to Parsons and Strickland (1963). For determination of pigment concentrations, 10 mL of culture was filtered using GF/C filters. An aliquot of the sample was centrifuged at 12000 rpm for 5 min and supernatant discarded. The pellet was suspended in 10 mL of boiling acetone at 4°C and stored in dark for 24 h. Pigment content in the filtered extract were determined by the absorbance at 630, 645, 665 and 750 nm in a 1cm quartz cell against a blank of 90% aqueous acetone [22].

2.5 Determination of dry weight

A definite volume (20 g) of algal suspension was filtered through weighted glass fiber (Whatman GF/C). The cells, after being precipitated on the filter study, were washed twice with distilled water and dried overnight in an oven at 105°C. Data were given as mg/mL algal suspension.

2.6 Statistics

All experiments were performed in 3 replicates. The amount of metal ions adsorbed by used biosorbent was obtained by using Langmuir model and Freundlich models [23-25]. The adsorption equilibrium isotherms were evaluated in terms of maximum sorption capacity and sorption affinity. Among the several isotherm equations, two isotherms (Langmuir and Freundlich adsorption isotherms) were investigated, which are widely used to analyses data for water and wastewater treatment applications [26]. Freundlich isotherm model is derived for describing singlecomponent adsorption equilibria on heterogeneous surfaces. Langmuir isotherm represents a single layer and uniform adsorbent without interactions between adsorbed molecules. In the current study, the Freundlich (Eq. 3) and Langmuir (Eq. 4) models were used to determine the concentration of the adsorbed material. If 1/n= 0, the adsorption process is irreversible. If 1< 1/n<0, it is desired. If 1/n>0, it is undesirable [23, 24].

$$\log q_e = \log K_F + \left(\frac{1}{n}\right)\log C_e \quad (Eq. 3)$$

q_e: the amount of metal adsorbed (mg/g).

K_F: Adsorption capacity at unit concentration (L/g).

1/n: Intensity of adsorption (L/g).

C_e: the equilibrium concentration of metal ion (mg/L).

In the Langmuir model, q_m and b are Langmuir parameters, which are the maximum adsorption capacity and associated energy, respectively. The equilibrium parameter (R_L) is the basis of the Langmuir isotherm, which is defined by equation, $R_L=1/(1+bC_0)$ [23]. In this equation, C_0 is the initial concentration and R_L is the type of isotherms. $1<R_L<0$ is favourable adsorption, $R_L>1$ is for undesirable adsorption, $R_L=1$ shows

linear adsorption and R_L=0 demonstrates irreversible adsorption [25]. The R_L value was calculated at 50 mg/L of initial metal concentration.

$$\frac{Ce}{qe} = \frac{1}{qmb} + \frac{Ce}{qm} \qquad \text{(Eq.4)}$$

q_m: Langmuir maximum adsorption capacity (mg/g). b: the constant related to free energy of adsorption (L/mg).

3. RESULTS

3.1 Analysis results of the heavy metal uptake (mg/g) and efficiency (%) Cr (VI) uptake (mg/g) and efficiency (%)

The effects of Cr (VI) on *Oscillatoria* sp. was investigated using increasing concentration of chromium from 2.5 to 10 mg/L (Table 1). The metal adsorption capacity by both live and dead algae increased significantly with an increasing initial metal concentration. The metal adsorption value was 5.69, 17.52 and 17.89 mg/g for dead and 0.36, 0.75 and 1.77 mg/g for live algae, when Cr (VI) concentration was 2.5, 5 ve 10 mg/L, respectively. The adsorption efficiency of dead algae was found to be slightly higher (40 %) and significantly different than that of live algae (2 %) using an initial cadmium concentration of 5 mg/L.

Table 1. Cr (VI) adsorption capacity and efficiency by live and dead *Oscillatoria* sp. Data are means (triplicates).

	Live cells		Dead cells	
Cons. (mg/L)	**Adsorption capacity (mg/g)**	**Adsorption efficiency (%)**	**Adsorption capacity (mg/g)**	**Adsorption efficiency (%)**
2.5	0.36	1.96%	5.69	30.36%
5	0.75	2.06%	17.52	46.74%
10	1.77	2.46%	17.89	23.85%

3.2 Zn (II) uptake (mg/g) and efficiency (%)

The efficiency of Zn (II) removal at 2.5, 5 and 10 mg/L concentrations was reported 14.28, 29.81 and 54.20 mg/g by live *Oscillatoria* sp. cells, and 11.27, 14.53 and 12.83 mg/g by dead *Oscillatoria* sp. cells, respectively (Table 2). The maximum Zn removal was 82.53% and 54.18% by live and dead *Oscillatoria* sp. cells at 2.5 mg/L concentration, respectively. The Zn removal decreased at 5 and 10 mg/L concentrations in the two algae.

Table 2. Zn (II) adsorption capacity and efficiency by live and dead *Oscillatoria* sp. Data are means (triplicates).

	Live cells		Dead cells	
Cons. (mg/L)	**Adsorption capacity (mg/g)**	**Adsorption efficiency (%)**	**Adsorption capacity (mg/g)**	**Adsorption efficiency (%)**
2.5	14.28	82.53%	11.27	54.18%
5	29.81	80.96%	14.53	40.07%
10	54.20	74.98%	12.83	17.07%

3.3 Chlorophll-a contents

The effects of chromium and zinc on concentration of chlorophyll derivatives are seen in the Table 3. Chlorophylla concentration was recorded to be decreased simultaneously from an initial value of 1.440 µg/L to 0.0338 µg/L and 0.02 µg/L at the end of the application of chromium and zinc separately and together on live *Oscillatoria* cells, respectively. Zn (II) and Cr (VI) showed a strong inhibition of chlorophyll-a biosynthesis even at the lower concentrations (2.5–5mg/L) on *Oscillatoria* biomass.

Table 3. Effect of heavy metals (Zn and Cr) on the chlorophyll-a content in *Oscillatoria* cultures (μg/L).

	Separate application		Together application	
Control	1.4404 μg/L			
Cons. (mg/L)	**Cr**	**Zn**	**Cr**	**Zn**
2.5	0.0368	0.0410	0.0001	0.0003
5	0.0305	0.0464	0.0009	0.0029
10	0.0334	0.0438	0.0050	0.0047
Mean	0.034	0.044	0.002	0.003

3.4 Adsorption isotherms study

The results of Langmuir and Freundlich isotherms are presented in Table 4. We concluded that maximum adsorption capacity (q_m) of chromium and zinc calculated from Langmuir isotherm was around 5.6939 (dead cells) and 14.2907 (live cells) mg/g on *Oscillatoria* sp. cells, respectively. According to the correlation coefficient obtained (R^2= 0.99), the adsorption process of *Oscillatoria* sp. algae follows the Langmuir model. K_L in the range between 2 and 6 indicates the undesired chromium and zinc adsorption by the dead and live *Oscillatoria* sp. algae [27]. For live and dead *Oscillatoria* cells, 1/n value was determined between 0.3418-0.8557 and 0.1585-0.1681, respectively. According to Kadirvelu and Namasivayam (2000) [28], n values between 1 and 10 indicate a useful adsorption representative. For a good adsorbent, 0.2<1/n<0.8 and a smaller value of 1/n indicates better adsorption and formation of rather strong bond between the adsorbate and adsorbent [28] Freundlich isotherm coefficient indicated that the adsorption process does follow this model (Figure 1-4).

Table 4. Compliance of live and dead *Oscillatoria* sp. cells equilibrium data via Langmuir and Freundlich models.

	Langmuir			*Freundlich*		
Adsorbent	**q_m (mg/g)**	**K_L (L/mg)**	**R^2**	**1/n (L/g)**	**K_F (L/g)**	**R^2**
Live	0.360	2.777	0.987	0.855	1.168	0.365
Dead	5.693	6.309	0.999	0.158	0.175	0.754
Live	14.290	2.069	0.994	0.341	2.925	0.008
Dead	11.275	2.925	5.948	0.168	0.088	0.035

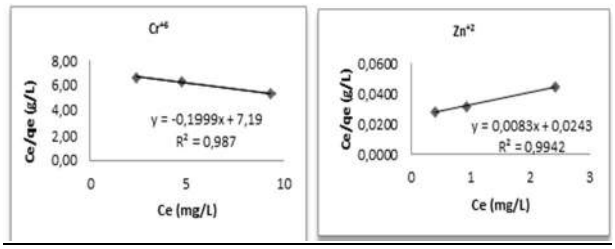

Figure 1. Langmuir adsorption isotherm of live *Oscillatoria* sp. cells.

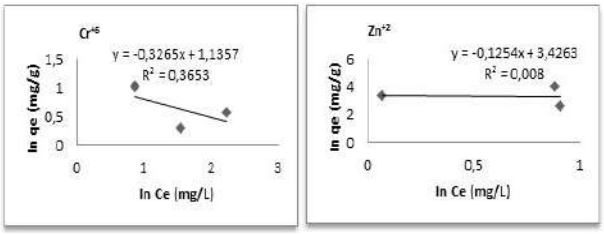

Figure 2. Freundlich adsorption isotherm of live *Oscillatoria* sp. cells.

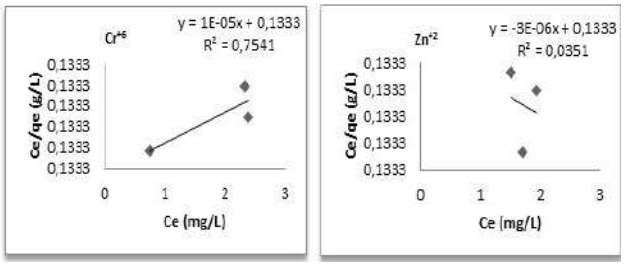

Figure 3. Langmuir adsorption isotherm of dead *Oscillatoria* sp. cells.

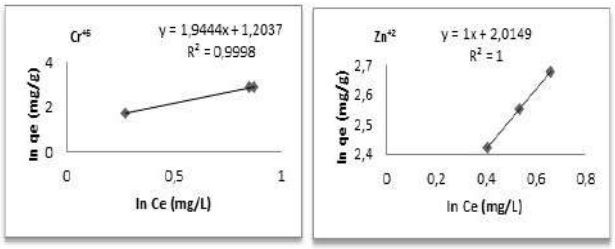

Figure 4. Freundlich adsorption isotherm of dead *Oscillatoria* sp. cells.

4. DISCUSSION

Many studies have emphasized that biosorption is a lowcost technology and that the use of microalgae for the treatment of metal-bearing wastes is more effective [28-2936]. Bhatnagar and et al. [30] pointed out that microalgae has many mechanisms and some of them unknown what their function is still developing bioremediation technology has emphasized that necessity of re-imaged and modified urgently according to needs and to create a new biological form.

In this study, samples were used both live and dead in order to provide a better comparison in heavy metal removal processes. Studies show that when the same metal is treated with both living and dead cells of the same organism, different findings can be obtained. In example the study with *Oscillatoria* sp. cells Katırcıoğlu and et al. [31], get better removal of Cd (II) with live cells, while Azizi et al. [32] obtained best results with dead cells in their work with the same organism and metal. Das [33], noted that the initial ion concentration plays an important role in determining the adsorption capacity. These two metals are abundant amounts in waste waters. Although the Cr (VI) ion must be found to be very low amount in the water but the Zn (II) ion may be present in small quantities in the water as it is one of the essential metal for living things. Concentration values used in the study have been taken into consideration. As a result of the findings obtained that when the concentration increased, the removal of metals are also increased. These findings are in parallel with other studies [31-33].

Given the previous work, it was reported that the adsorption was completed within a few hours [30,33]. Singh [34], found that absorption of zinc was very rapid in the first 10 minutes of study. Shukla et al. [35] reported that the adsorption for the Cr (VI) ion started within 15 min and the metal was removed up to 96% within 210 min. For this reason, the *Oscillatoria* sp. microalgae exposure to metals was kept constant for 24 hours.

As a result of this study, the best removal for Cr (VI) ion was found with dead cells, increasing the solution concentration gives increasing metal removal. The maximum removal capacity was 17.89 mg/g and the maximum removal percentage was found to be 46.74%. Findings have also been supported by other studies [31-35]. The best removal for the Zn (II) ion was achieved with live cells and the work done with these cells showed that the concentration of zinc was increased by increasing the concentration, and no such correlation was observed in dead cells. The study with dead cells was also found at the highest concentration of 10 mg/L, while the metal removal capacities were close to each other in three concentrations. The maximum removal capacity was found to be 54.20 mg/g, with a maximum removal rate of 82.53%. The data obtained in the bivalent zinc ion correspond to other studies. The environmental factors and the environment in which it is cultivated have been determined by studies that affect the chemical composition of microalgae and which change in the adsorption capacity of heavy metals by changing the chemical composition. Looking at all these, there is a difference in the data obtained in systems where any organism is involved. Factors such as the structure of the organism, content, defense mechanisms for living cells can give different findings even in the same study. As a result of the study, in the removal of Cr ions with live *Oscillatoria* cells, different results obtained with the study of Shukla et al. [35] but similar values were obtained with the study of Jayashree ve et al. [35,40].

In the removal of bivalent zinc, high values were obtained in both with dead cells and live cells. Comparisons within the entire study showed that optimal removal occurred in living cells treated with Zn (II) ions. This can be explained by the fact that the Zn (II) ion is a more elaborate metal in terms of the organism's metabolic needs than the Cr (VI) ion.

When the effect of the application of the metals separately and together is examined on the chlorophylla content of the living organism, the metals are applied individually, there is an increase in the amount of chlorophyll-a in all metal doses, whereas a decrease in the amount of chlorophyll-a is observed when the metals are applied together. When previous studies were examined, Brahmbhatt et al. [36] reported that metal toxicity was considered to be a biomarker and that there was an increase in the amount of alginate chlorophyll exposed to metal compared to the stress-free area. In the same way, Shankar et al. [37] reported an increase in chlorophyll-a in their work with *Oscillatoria* annae cyanobacterium. On the other hand, co-application of metals is thought to have more effect on the cell content of living organisms, which explains the decrease in chlorophyll content. It supports the findings obtained in previous studies [38-39].

When the effect of environmental factors on the study was examined, Shankar et al. [37] reported that the best growth of *Oscillatoria* microalgae was achieved at an optimum temperature of 29 ± 2°C, at approximately 7 pH. In this study, the same values were applied to the samples taken from the culture.

It has been observed in previous studies that the increase in temperature during the biosorption process affects the adsorption capacity positively [32]. For this reason, the temperature was determined to be 29 ± 2°C during the adsorption process. It is supported by this study data that the determined temperature is suitable for adsorption capacity.

One of the important factors in adsorption processes is the pH range. Several studies have shown that mild acidic pH values are more suitable for metal adsorption [31-36]. The dependence of metal uptake on pH is related to the competition between protons and metal cations on the surface of the absorption medium. These different chemical interactions between cell surfaces and metal can result in different retention capacities for metal ions at various pHs [7]. Dabbagh et al. [38] reported that the optimum pH for strontium metal was 9 ± 0.3 while the previous studies evaluated, the pH ranges for chromium and zinc metals were determined to be 5.0 and 7.0, respectively. When the adsorption capacities are evaluated, the chromium (VI) ion is less biosorbent than the zinc (II) ion can be attributed to the working pH values. At lower pH, the cell surface charge is positive and H_3O^+ ions show a rate-reducing effect by competing with positive metal cations to bind to the cell. At pH values on the isoelectric points of the cells, the cell surface has a net negative charge. The ionic state of ligands such as carboxyl, phosphate, imidazole and amino groups accelerate the binding of metal cations to biomass [7].

Langmuir and Freundlich biosorption isotherms were used in the evaluation of the study findings. These isotherms used to describe biosorption have previously been used in many studies [31, 39]. According to Nakiboğlu [39] regarding the evaluation of isotherms, it has been reported that in some cases this adsorption can not be explained by Langmuir isotherm, even though C_e coefficient value increases. In such cases, more Freundlich isotherm coefficient values are used to define the adsorbance. For Freundlich isotherms, the lower the value of 1/n, the more absorbance bonds are formed. When the findings obtained are evaluated, it is seen that the study is better explained by Freundlich isotherm.

5. CONCLUSION

The goal of this work was to explore the potential use of *Oscillatoria* sp. biomass as a low-cost sorbent for the removal of Cr (VI) and Zn (II) heavy metal ions from aqueous solutions. Batch experiments showed that the dead and live

Oscillatoria sp. cells have a remarkable ability to take up Cr (VI) and Zn (II) heavy metal ions, respectively. Only 2.6 % of the world's water reserves are composed of fresh water. A large part of this is found in glaciers in the polar regions, only 0.02% of which form lakes and rivers. The limited amount of water resources that can be contained is polluted by various pollutants from day to day. The heavy metals from industrial wastes come at the expense of the polluting water resources. Biologically available heavy metals accumulate in tissues, causing different levels of negativity in living organisms. The heavy metal accumulation in the aquatic ecosystem continues from the first ring of the nutrient chain to the upper steps of the nutrient chain. For this reason, microalgae in the first part of the food chain are widely used for the assessment of heavy metal toxicity. In this study, different concentrations of chromium and zinc metals, which are quite common in wastewater, are classified as a microalgae, *Oscillatoria* sp. has been investigated, significant contributions have been made to the findings literature. It is once again seen that pH is an important parameter as a result of this study. When previous studies examined, it is known that different pHs affect the removal capacity when applied to live or dead samples of the same metals. Accordingly, it may be advisable to evaluate pH over a wide range during subsequent studies for the same organism and metals. It is also known that the initial ion concentration plays an important role in determining the adsorption capacity. The metals used in the study were selected by looking at the parameters that should be found in the clean waters. The chromium (VI) ion is toxic to living organisms even at very low levels in the water, while the zinc (II) ion, another metal, is a metal that enters organisms in vigorous quantities. For this reason, it is suggested to extend the construction intervals for further studies.

This study with *Oscillatoria* sp. microalgae has shown that chromium (VI) and zinc (II) ions are effective biosorbents in removing water from water under the determined conditions. However, the *Oscillatoria* sp. is a kind of microalgae that requires more care than other types of algae to cultivate and maintain the culture. It is advisable to consider this for other studies. As a result of this and similar studies in the literature, it has been shown that the biosorption method can be an effective method of removing heavy metal ions from water and wastewater environments. Many organisms are used in the biosorption process, but studies show that microalgae have more removal capacity in these processes. Microalgae are found more easily than other biosorbents and are easily cultured in inexpensive environments. At the same time, much biomass removal can be achieved with these biosorbents. With these organisms, it is possible to develop more effective and cheap treatment systems and to protect existing water resources.

Acknowledgments

The authors wish to express their gratitude to the Celal Bayar University Scientific Investigation Project for the funding of this work (Project No. FEF 2014–089).

6. REFERENCES

[1]T. Olmez, I. Kabdatly and O. Tunay, “Tekstil endüstrisi reaktif boya banyolarında ozon ile renk giderimine etki eden faktörlerin belirlenmesi”, 8. Endüstriyel Kirlenme Kontrolu Sempozyumu, 18-20 Eylul, 2002, İstanbul, Türkiye (Bildiri Özetleri Kitabı, s 191-197).

[2]Ü. Yetiş, F.B. Dilek, G. Özcengiz, A. Dölek, N. Ergen and A. Erbay, “Ağır metallerin *P. chrysosporium* ve *C. versicolor* ile biyosorpsiyonu–atık çamurun biyosorbent olarak kullanılması”, TÜBİTAK YDABÇAG-203, Orta Doğu Teknik Üniversitesi, Çevre Mühendisliği Bölümü, Ankara, 1998, 1.1-1.3, 4.26, 4.48-4.57.

[3]Anonymous. http://www.food-info.net/tr/metal/intro.htm

[4]J.R. Lloyd, “Bioremediation of metals; the application of microorganisms that make and break minerals”, Microbiology Today, vol. 29, no. 2, pp. 67-69, 2002.

[5]S. Ilhan, M.N. Nourbakhsh, S. Kılıcarslan, and H. Ozdag, “Removal of chromium, lead and

copper ions from industrial waste waters by *Staphylococcus saprophyticus*", Turkish Electronic Journal of Biotechnology, vol. 2, no. 2, pp 50-57, 2004.

[6]N. Ahalya, T.V. Ramachandra and R.D. Kanamadi, "Biosorption of heavy metals", Research Jorunal of Chemistry Environment, vol. 7, no. 4, pp. 71-79, 2003.

[7]J.T. Matheickal and Q. Yu, "Biosorption of lead (II) and copper (II) from aqueous solutions by pre-treated biomass of Australian marine algae", Bioresource Technology, vol. 69, no. 3, pp. 223-229, 1999.

[8]P. Kaewsarn, "Biosorption of Copper (II) from aqueous solutions by pre-treated biomass of marine algae *Padina* sp.", Chemosphere, vol. 47, no. 10, pp. 1081-1085, 2002.

[9]H. Hussein, S.F. Ibrahim and K. Kandeel, "Biosorption of heavy metals from waste water using *Pseudomonas* sp.", Electronic Journal of Biotechnology, vol. 1, no. 7, pp. 38-46, 2004.

[10]M.J. Horsfall, A.A. Abıa and A.I Spıff, "Removal of Cu (II) and Zn (II) ions from wastewater by cassava (Manihot esculenta Cranz) waste biomass", African Journal of Biotechnology, vol. 2, no. 3, pp. 360-364, 2003.

[11]G. Bayramoglu, G. Celik and E. Yalcın, "Modification of surface properties of Lentinus sajor-caju mycelia by physical and chemical methods: evaluation of their Cr^{6+} removal efficiencies from aqueous medium", Journal of Hazardous Materials, vol. 119, no. 1-3, pp. 219-29, 2005.

[12]C.L. Stanley, L.K. Ogden, "Biosorption of copper (II) from chemical mechanical planarization wastewater", Journal of Environmetal Managemant, vol. 69, no. 2, pp. 289-297, 2003.

[13]N. Tewari, P. Vasudevan, B.K. Guha, "Study on biosorption of Cr (VI) by Mucor hiemalis", Biochemical Engineering Journal, vol. 23, no. 1, pp. 185–192, 2005.

[14]D. Kratochvil and B. Volesky, "Advances in the biosorption of heavy metals", TIBTECH, vol. 16, no. 2, pp. 291–300, 1998.

[15]K. Vijayaraghavan and Y.S. Yun, "Bacterial biosorbents and biosorption", Biotechnology Advances, vol. 26, no. 3, pp. 266–291, 2008.

[16]N.M. Figueira, B. Volesky B, V.S.T Ciminelli, A. Felicity and A. Roddick, "Biosorption of metals in brown seaweed biomass", Water Research, vol. 34, no. 1, pp. 196-204, 2000.

[17]R.H. Crist, K. Oberholser, K. Shank and M. Nguyen, "Nature of bonding between metallic ions and algal cell walls", Environmental Science Technology, vol. 15, no. 4, pp. 1212-1217, 1981.

[18]. T.A. Oyedepo, " Biosorption of lead (II) and copper (II) metal ions on *Calotropis procera* (Ait.)", Science Journal of Purel and Applied Chemistry, vol. 12, no. 2, pp. 1-7, 2011.

[19]P. Lodeiro, B. Cordero, J.L. Barriada, R. Herrero and M.E. Sastre de Vicente, "Biosorption of cadmium by biomass of brown marine macroalgae", Bioresource Technology, vol. 96, no. 16, pp. 1796-1803, 2005.

[20]R.Y. Stanier, R. Kunisawa, M. Mandel and G. Cohen-Bazire, "Purification and properties of unicellular blue-green algae (order Chroococcales", Bacteriol Reviewer, vol. 35, no. 2, pp. 171–205, 1971.

[21]V. Cucarella and G. Renman, "Phosphorus sorption capacity of filter materials used for on-site wastewater treatment determined in batch experiments-a comparative study", Journal of Environmental Quality, vol. 38, no. 2, pp. 381-392, 2009.

[22]T.R. Parsons and J.D.H. Strickland, "Discussion of pectrophotometric determination of marine plant pigments, with revised equations for ascertaining chlophylls and carotenoids", Journal of Marine Research, vol. 21, no. 2, 115-163, 1963.

[23]A. Sari, A and M. Tuzen, "Biosorption of Pb (II) andCd (II) from aqueous solution using green alga (UIva lactuca) biomass", Journal of Hazardous Materiales, vol. 152, no. 1, pp. 302-308, 2008.

[24]S. Khorramfar, N. Mahmoodi and M. Arami, "Dye removal from colored textile wastewater using tamarindusindica hull: Adsorption isotherm and kinetics study", Journal of Color Science Technology, vol. 3, no. 1, pp. 81-88, 2009.

[25]P. Molazadeh, N. Khanjani, M.Z. Rahimi and A. Nasiri, "Adsorption of lead by microalgae *Chaetoceros* sp. and *Chlorella* sp. from aqueous solution", Journal of Community Health Research, vol. 4, no. 2, pp. 114-127, 2015.

[26]H. Freundlich, "Uber die adsorption in Losungen", Physical Chemistry, vol. 57, no. 2, pp. 385-470, 1907.

[27]M. Bansal, D. Singh, V.K. Garg and P. Rose, "Use of agricultural waste for the removal of nickel ions from aqueous solutions: equilibrium and kinetics studies", International Journal of Environmental Science and Engineering, vol. 1, no. 2, pp. 108-114, 2009.

[28]K. Kadirvelu and C. Namasivayam, "Agricutural by-product as metal adsorbent: sorption of lead (II) from aqueous solution onto coirpith carbon", Environmental Technology vol. 21, no. 10, pp. 1091–1097, 2000.

[29]S. Basha, D. Keane, A. Morrissey, K. Nolan, M. Oelgemöller and J. Tobin, "Studies on the adsorption and kinetics of photodegradation of pharmaceutical compound, indomethacin using novel photocatalytic adsorbents (IPCAs)", Industrial and Engineering Chemistry Research, vol. 49, no. 2, pp. 11302– 11309, 2010.

[30]S. Bhatnagar and R. Kumari, "Bioremediation: A sustainable tool for environmental management – a review", Annual Review and Research in Biology, vol. 3, no. 4, pp. 974-993, 2013.

[31]H. Katırcıoğlu, B. Aslım, A.R. Türker, T. Atıcı and Y. Beyatlı, "Removal of cadmium(II) ion from aqueous system by dry biomass, immobilized live and heat-inactivated *Oscillatoria* sp. H1 isolated from freshwater (Mogan Lake)", Bioresource Technology, vol. 99, no. 10, pp. 4185-4191, 2008.

[32]S.N. Azizi, A.H. Colagar and S.M. Hafeziyan, "Removal of Cd(II) from aquatic system using *Oscillatoria* sp. biosorbent", The Scientific World Journal, vol. 12, no. 2, pp. 7-21, 2012.

[33]S. Das, "Biosorption of chromium and nickel by dried biomass of cyanobacterium *Oscillatoria laete-virens*", International Journal of Environmental Sciences, vol. 3, no.1, pp. 426-442, 2012.

[34]D. Singh, "Removal of Ni (II) from aqueous solution by biosorption using two green algal species *Oscillatoria* sp. and *Spirogyra* sp.", In 5th Wseas Int. Conf. on Environment, Ecosystems and Development, pp. 310-314, 2007.

[35]D. Shukla, P.S. Vankar, S.K and Srivastava, "Bioremediation of hexavalent chromium by a cyanobacterial mat", Applied Water Science, vol. 2, no.1, pp. 245-251, 2012.

[36]N. Brahmbhatt, R. Patel and R.T. Jasrai, "Heavy metal accumulation in *Oscillatoria* sp. induced biochemical response", Advances in Applied Science Research, vol. 4, no. 3, pp. 182-185, 2013.

[37]M. Shankar, A.S. Henciya and P. Malliga, "Bioremediation of tannery effluent using fresh water cyanobacterium *Oscillatoria annae* with coir pith", International Journal of Environmental Sciences, vol. 3, no. 6, pp. 1881-1890, 2013.

[38]R. Dabbagh, H. Ghafourian, A. Baghvand, G.R. Nabi, H. Riahi and M.A. Ahmadi Faghih, "Bioaccumulation and biosorption of stable strontium and 90Sr by *Oscillatoria homogenea* cyanobacterium", Journal of Radioanalytical and Nuclear Chemistry, vol. 272, no. 1, pp. 53-59, 2007.

[39]T. Nakiboğlu, "Deri endüstrisi atık sularından kromun çeşitli alglerle biyosorpsiyonu",

Süleyman Demirel Üniversitesi, Fen Bilimleri Enstitüsü, Çevre Mühendisliği Anabilim Dalı, Yüksek Lisans Tezi, Isparta, 2005.

JOURNAL OF SCIENCE
SAKARYA UNIVERSITY

Sakarya University Journal of Science

ISSN 1301-4048 | e-ISSN 2147-835X | Period Bimonthly | Founded: 1997 | Publisher Sakarya University
http://www.saujs.sakarya.edu.tr/en/

Title: The Protective Effect of Grape Seed and Skin Extract and Ulva rigida Against Oxidative Stress Induced by Cisplatin on The Testis of Rats

Authors: Rihab Ksouri, Souha Rabah, Sana Mezghani, Sonia Hamlaoui
Recieved: 2019-10-27 12:08:25

Accepted: 2020-01-07 15:04:25

Article Type: Research Article
Volume: 24
Issue: 2
Month: April
Year: 2020
Pages: 312-323

How to cite
Rihab Ksouri, Souha Rabah, Sana Mezghani, Sonia Hamlaoui; (2020), The Protective Effect of Grape Seed and Skin Extract and Ulva rigida Against Oxidative Stress Induced by Cisplatin on The Testis of Rats. Sakarya University Journal of Science, 24(2), 312-323, DOI: https://doi.org/10.16984/saufenbilder.638725
Access link
http://www.saujs.sakarya.edu.tr/tr/issue/52471/638725

Sakarya University Journal of Science 24(2), 312-323, 2020

The Protective Effect of Grape Seed and Skin Extract and *Ulva rigida* Against Oxidative Stress Induced by Cisplatin on The Testis of Rats

Rihab KSOURI[*1], Souha RABAH[2], Sana MEZGHANI[3], Sonia HAMLAOUI[4]

Abstract

Cisplatin, an anticancer drug used in chemotherapy, has made considerable progress recently; particularly in the treatment of testicular cancer. However, the side effects of this treatment, limit its use. Grape Seed and Skin Extract (GSSE) and *Ulva rigida* (*U. rigida*) marine seaweeds are giving compounds with high antioxidant capacity. This work aims to develop a model in vivo to evaluate the protective effect of extracts of GSSE or *U. rigida* against the oxidative stress induced by cisplatin. This stress occurring in healthy cells is one of the major causes of the adverse effects of chemotherapy. Healthy male rats received an intraperitoneal injection of cisplatin only or cisplatin and GSSE or *U. rigida* extract. At the end of the treatment, the rats were sacrificed and from the crushed testicles; the supernatant was recovered for biochemical assays. The data showed that the dose of cisplatin induces testicular toxicity, and a pro-oxidant state characterized by increased levels of malondialdehyde, carbonyl proteins, superoxide anion, calcium and iron. Besides, treatment with cisplatin increases the activity of superoxide dismutase and inhibits the activity of catalase. GSSE or *U. rigida* extract exerts a protective effect on the testes of cisplatin-treated rats, or they protect against the adverse effects of oxidative stress induced by cisplatin to restore levels near control. This study demonstrated that GSSE and *U. rigida* can protect against cisplatin-induced cytotoxicity.

Keywords: Cisplatin, GSSE, *U. rigida*, Oxidative Stress, Pro-Oxidant, Antioxidant.

[*] Corresponding Author: Ksrhb96@gmail.com
[1]University Tunis El Manar, Laboratory of Functional Neurophysiology and Pathologies, Tunis, Tunisia. ORCID: 0000-0002-6241-2989
[2]University Tunis El Manar, Laboratory of Functional Neurophysiology and Pathologies, Tunis, Tunisia.
[3]University Tunis El Manar, Biological Sciences Department, Tunis, Tunisia.
[4]ISEP BG La Soukra, Physiology – Biology Department, Tunis, Tunisia.

1. Introduction

Cancer presents a global public health challenge that affects countries around the world becoming one of the leading causes of death. According to the World Health Organization (WHO), the number of cancers could reach 15 million by new cases per year from the beginning of 2020. Nowadays, medicine has several weapons against this scourge thanks to hormone therapy, radiotherapy and chemotherapy. Chemotherapy has significantly evolved in the last few decades thanks to the discovery of new chemotherapeutic molecules. However, this progress remains as every evolution a double-edged sword, because most anti-cancer treatments are often with side effects such as hair loss, nausea, vomiting and fatigue, caused mainly by inequality of the balance between pro and antioxidants generating oxidative stress in healthy cells. Some side effects may be limited or even avoided by appropriate care and medication. In chemotherapy, in particular, a lot of progress has been made in recent years to improve the quality of life of patients treated with chemotherapy. Synthesis chemical's molecules are used as pretreatment or post-treatment to reduce damage from chemotherapy. Nevertheless, most of these molecules did not give a satisfactory result because of the toxicity associated with certain chemical molecules or because of their intolerance. It is thus important to continue to develop new molecules with greater tolerance and less toxicity. Currently, searches are increasingly moving towards the medicinal plants and herbal medicine known by their beneficial effects on health. In this context, our work aims to search in extracts of *Ulva rigida* (*U. rigida*) and seeds and grape skin (GSSE: Grape Seed and Skin Extract) an antioxidant effect. This effect will be evaluated against the oxidative stress induced by cisplatin, a molecule used in chemotherapy on the testes of healthy rats, to minimize the side effects related to this molecule during chemotherapeutic treatment.

2. Materials and Methods

2.1 Animals

Thirty male Wistar rats weighed between 110 and 290 g (8 to 10 weeks old) from the Pasteur Institute of Tunis were used for these experiments in accordance with the local ethics committee of Tunis University, and care of animals was in conformity with NIH recommendations (National Research Council 1985). They are raised and grown in the laboratory in a pet shop at a constant temperature (21 + 1°C) and submitted to a photoperiodic regime (12h dark/12h artificial light). Food and drink are provided an ad libitum.

2.2 Treatments

Rats were divided according to their weights and the type of injection into six lots into 6 groups of 5 animals each. Group 1 received ethanol 10% (control), group 2 ethanolic extract of garlic (2.5 g/kg bw), group 3 ethanolic extract of *U.rigida* (2.5 g/kg bw), group 4 cisplatin (5mg/kg/bw) as a dose that may induce a toxicity according to literature [1, 2], group 5 cisplatin plus GSSE and group 6 cisplatin plus *U.rigida*. Animals were daily administered IP with one of these treatments. The treatment was performed at fixed times for 7 days according to the following protocol:

Table 1 : Protocol of follow-up of the different injections during 7 days

Group 1	D1		Ethanol 10%		D7
Group 2	D1		GSSE (2.5g/kg/bw)		D7
Group 3	D1		*U.rigida* (2.5g/kg/bw)		D7
Group 4	D1		Cisplatin (5mg/kg/bw)		D7
Group 5	D1	GSSE	Cisplatin (day 4)	GSSE	D7
Group 6	D1	*U.rigida*	Cisplatin (day 4)	*U.rigida*	D7

2.3 Preparation of the extract of *U. rigida*

The green seaweed *U. rigida* was harvested in spring in a rocky habitat on the sea coasts of the Ras Djebel region (Bizerte, Tunis) and transported in the ice to the laboratory. The samples were cleaned of the epiphytes, washed successively with distilled water, dried overnight at 30°C and then grounded with an electronic mortar to obtain a powder. The mixture is dissolved at the rate of 5g of powder in 30 ml of 10% ethanol and centrifuged at 5000 rpm for 30 minutes [3]. The supernatant is recovered and then injected to the animals intraperitoneally with a dose of 2.5mg/kg/bw after calculation and

2.4 Preparation of the extract of GSSE

We used the vinification waste of the *Carignan Vitis Vinifera* variety which is available in the north of Tunisia. GSSE extract is produced from residues of winemaking that were obtained from the wine cooperative Ain Ghelal, Tunis. It's an extract consisting of 50% seeds and 50% pulp. The mixture is dissolved at the rate of 5 g of powder in 10 ml of 10% ethanol, centrifuged at 3000 rpm for 10 min and thus the supernatant is recovered then injected to the animals intraperitoneally with a dose of 2.5g/kg/bw knowing that GSSE was used at a dosage 500 mg/kg/bw and it was safe and near the optimal concentration recognized. Also, GSSE was tested at wide-ranging doses, reaching 4 g/kg/bw with no sign of toxicity [4].

2.5 Sacrifice of animals

The rats were sacrificed and the testes taken were weighed, crushed and then homogenized using an ULTRA-TURRAX in a Tris Base buffer solution (TBS, 50mM, pH=7.4) at a rate of 1g $2ml^{-1}$. The homogenates were centrifuged (10 000 rpm, 10 min, 4°C) and the supernatant is gently removed and placed in eppendorfs and stored at -20°C for subsequent biochemical assays.

2.6 Biochemical assays

2.6.1 Determination of superoxide anion $O_2^{\circ -}$:

DHE is a non-fluorescent compound that is rapidly oxidized to fluorescent ethidium (λ excitation=488 nm and λ emission=575 nm) under the action of $O_2^{\circ -}$. The samples are incubated with the dihydroethidine probe (DHE, 2µM) for 15 min in the dark. The stock solution of DHE was prepared in dimethyl sulfoxide (DMSO, 1.6mM). This solution is later used at the final

concentration of 2µM. After incubation for 15min at 37°C, the analysis is performed by a fluorescence microplate reader (Bio-Tek FL800TBI).

2.6.2 Determination of malondialdehyde (MDA):

This colorimetric assay consists of reacting the thiobarbituric acid (TBA) reactive substance on one of the end products of lipid peroxidation (MDA) [5]. The reaction is carried out in acid and hot medium to form a pink coloring pigment whose intensity is proportional to the concentration of MDA in the sample. A 25µl of each sample is mixed with 125 µl TCA-BHT (trichloroacetic acid, Butylhydroxytoluene) and centrifuged at 1000 rpm for 5 minutes at 4°C. The supernatant was mixed with 0.5N HCl, 50 µl Tris-TBA (thiobarbituric acid) and then heated at 80°C for 10 minutes. After incubation at 80°C for 10 minutes, the absorbance measured at 530 nm is directly proportional to the amount of MDA present in the reaction medium.

2.6.3 Determination of carbonylated proteins:

The oxidation of the proteins by the ROS (reactive species of oxygen) leads to the formation of a carbonyl group (C=O) in the protein. The determination of the carbonylated proteins was carried out according to Levine et al., (1990) [6]. After precipitation of the proteins with 20% TCA and centrifugation at 11 000 rpm for 3 minutes at 4°C, the pellet then was on the edge in buffer with 10mM DNPH. Stirring was performed every 10min during the time of incubation. After 3 washes with ethanol-ethyl acetate, the pellet was dissolved in 20mM potassium phosphate containing 6M guanidine chloride. The density was then read at 366nm.

2.6.4 Determination of intracellular mediators

Calcium: By the use of a commercial kit (Biomaghreb, Tunis), we measured the intracellular calcium following Stern and Lewis, (1957)[7]. A purple colorful complex is formed after the interaction of calcium with cresolphtalein at basic pH, measurable at 570nm. Briefly, 50µL of testicular extract was added to 650µL of the mixture containing 2-amino-2-methyl-1-propanol (500 mmol L^{-1}), Cresolphthalein (0.62 mmol L^{-1}) and 8-hydroxyquinoline buffer (69 mmol L^{-1}). Assuming that the complex was stable for one hour, incubations were realized at room temperature for 5 min.

Iron: The level of free iron in the testes was determined by Leardi et al., (1998) [8] using a commercial kit (Biomaghreb, Tunis). At acidic pH 4.8, ferric iron Fe^{3+} is released from transferrin. Ascorbic acid reduces it to ferrous iron Fe^{2+}, which gives ferrozine a colored complex in violet measurable at 562 nm. A 50 µL of our samples was added to 250µL of reaction mixture containing ascorbic acid (5g L^{-1}) and ferrozine (40 mM) with incubation at 37°C for 10 min. The density is measured at a wavelength λ=562 nm.

2.6.5 Assaying the activity of antioxidant enzymes

The superoxide dismutase (SOD): The assay of SOD activity is based on the method described by Misra and Fridovich, 1972 [9] which relies on the use of epinephrine and bovine catalase to generate superoxide radicals. It relies on the ability of SOD to inhibit the oxidation of epinephrine to a pink-coloured compound, adenochrome, by trapping the superoxide anion flux. A 10µl of the sample is mixed in a solution of $Na_2CO_3/NaHCO_3$ buffer (62.5mM, pH 10.2) with 10µl of bovine catalase (0.4U μl^{-1}), 20

µl of epinephrine (5mg ml^{-1}). The density is measured per minute for 1 to 4 minutes at λ=480 nm.

Catalase (CAT): The principle of the assay is based on the decomposition of H_2O_2 into H_2O and O_2 in the presence of catalase activity in the solution. The decomposition of H_2O_2 is determined by the fall in absorbance at λ = 480 nm. A 20 µl of the tissue extract is mixed in a solution of phosphate buffer (50 mM, pH 7) containing 33 mM H_2O_2. The catalase activity, in the samples, is evaluated using a spectrophotometer (Bio-Rad) followed by the kinetics of the disappearance of H_2O_2 at the wavelength of 240 nm [10].

2.6.6 Determination of total protein

It is a colorimetric assay using the Biuret method [11], which consists in quantifying the number of proteins contained in the sample. In fact, the proteins form blue-violet complexes in the presence of Cu^{2+} in an alkaline medium, so the quantity of the proteins is proportional to the intensity of the coloration. The density is determined at λ=546nm. The amount of protein contained in each sample was directly determined from a calibration curve. The proteins were measured using a commercial kit (Bio-Maghreb). A 20µl of the sample was mixed with 1ml of the working reagent. The reading of the density is carried out after mixing and incubation of the solution for 5min at room temperature.

2.7 Statistical test

Statistical analyses were performed using the GraphPadPrism software (GraphPad Software). The data are expressed on average (± SEM) of at least 4 independent animals. A two-way ANOVA test followed by a Bonferroni post-test is used for the intergroup comparison. The value found by the calculation can affirm that the groups are different with a risk of error p. The GSSE, *U.rigida* and Cisplatin groups are compared with the control group. The group treated with Cis and GSSE, Cis and *U.rigida* are compared with the Cisplatin group.

3. Results and Discussion

As a whole, our study consists at looking in the natural extracts of GSSE and *U.rigida*, a beneficial effect against the cytotoxicity induced by cisplatin, chemotherapeutical agent, in the cells of the testes of rats.

3.1 Effect of treatments on body weight

This study conducted to determine the variation of rats the weight in each batch. The rats are weighed each day at the same time; the variation is represented below at Figure 1.

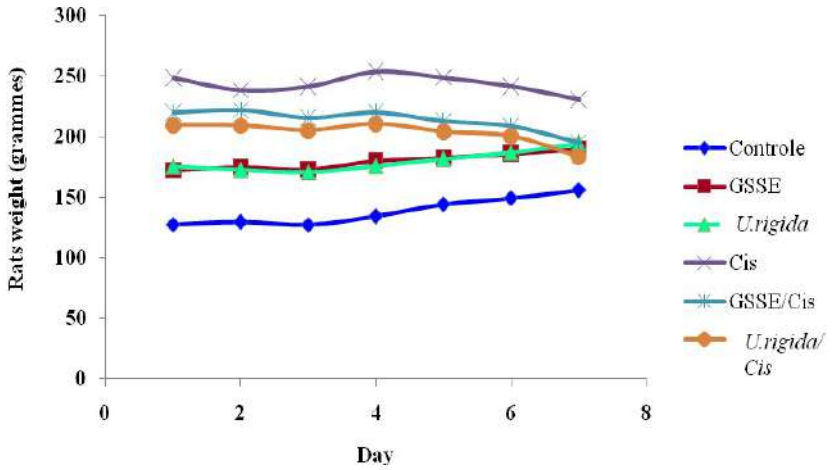

Figure1: Variation of the body weight of rats during 7 days of treatment. The results are expressed by the mean ± SEM (n = 5).

The variation in the body mass of the rats, during our study (Figure1), shows that the weight of the animals increases throughout the treatment period (7 days), except animals treated with cisplatin (cisplatin alone or in co-treatment with GSSE or *U. rigida*) where a non-significant reduction in the weight of the animals is observed.

In the present work, we observed an increase in the weight of the rats following treatment with an extract of GSSE or *U. rigida*. This corroborates the data showing that these extracts are used as nutritional supplements thanks to the plethora of minerals, proteins and vitamins [12, 13]. Treated rats by cisplatin only do not show a decrease in their weight which is not in correlation with other work which has shown that treatment with cisplatin induces a decreased body weight [14].

This could be explained by a difference between the duration of treatment used in both studies. In addition, the rats treated with extracts from GSSE or *U. rigida* with cisplatin revealed a decrease in their weight which could be explained by the toxicity of cisplatin.

3.2 Effects of the treatments on oxidation and the production of $O_2^{\circ-}$, MDA and carbonylated protein

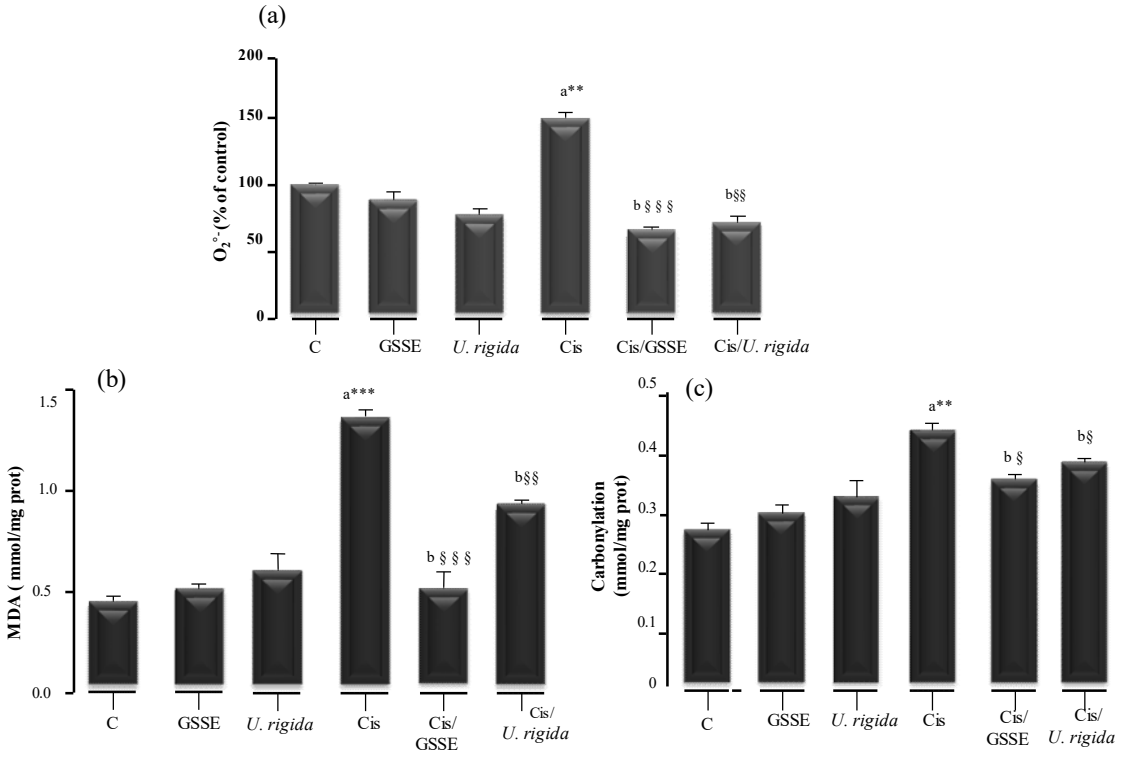

Figure 2. Effect of GSSE and *U.rigida* on cisplatin-induced changes in testicles lipoperoxidation, carbonylation and $O_2^{\circ-}$

Rats were on a daily basis administered with 10% ethanol (C), GSSE , *U.rigida* , cisplatin (Cis), *U.rigida* plus Cisplatin (Cis/*U.rigida*), or GSSE plus Cisplatin (Cis/GSSE) were administered to rats for 1 week (Fig. 2), $O_2^{\circ-}$ content (Fig. 2A), lipoperoxidation (Fig. 2B) and carbonylation (Fig. 2C) were determined. Results are expressed by means ±S.E.M. (n=5); **$p < 0.01$ where samples were compared with control (C). §§ $p < 0.01$where samples were compared with cisplatin (Cis).

We determined $O_2^{\circ-}$, MDA and carbonylated proteins as indexes of oxidative stress. Cisplatin significantly increased testis $O_2^{\circ-}$ (Fig 2A), MDA (Fig 2B) and carbonylated proteins (Fig 2C). Cisplatin has been described to induce testicular toxicity with stimulation of the production of free radical [15]. This has been confirmed in our study where we have detected in cisplatin-treated rats increased production of anion superoxide in the testicles. It is admitted that the superoxide radical crosses the biological membrane and its accumulation in cells causes damage irreversible oxidative effects on biomolecules including membrane lipids, proteins and nucleic acids [16]. This damage results in damaged cells that can lead to cell death. In agreement with these data, we have observed an increase in the level of MDA, a product of lipid peroxidation of acids polyunsaturated fat, an increase in the level

of carbonylated proteins which is the consequence of the oxidation of proteins. Membrane lipid peroxidation at the level of testicular has also been demonstrated in other studies [16, 17].

3.3 Effect of treatments on intracellular mediators of oxidative stress

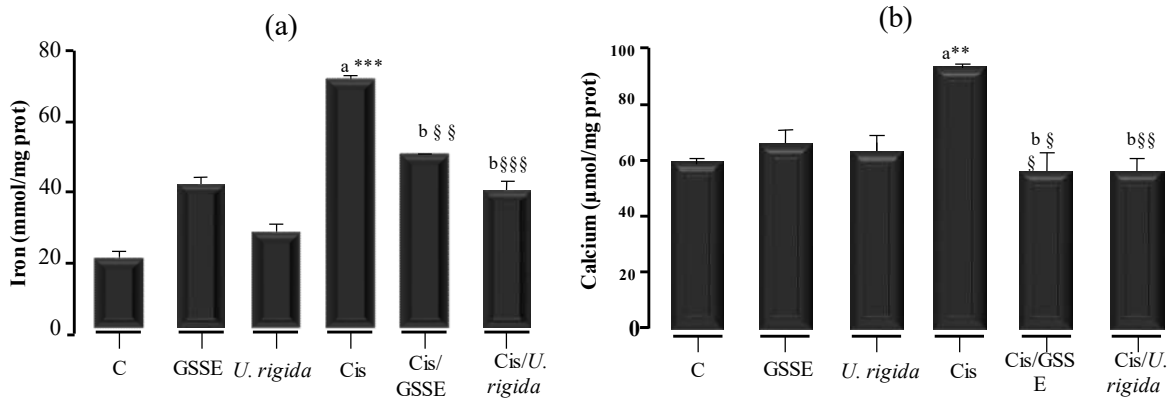

Figure.3: Effect of GSSE, *U.rigida* on cisplatin-induced intracellular mediators.

Rats were on a daily basis administered with 10% ethanol (C), GSSE, *U.rigida*, Cisplatin (Cis), *U.rigida* plus Cisplatin (Cis/*U.rigida*), or Cisplatin plus GSSE (Cis/GSSE) for 7 days and we determined levels of testis free iron (Fig. 3a) and calcium (Fig. 3b).

We expressed Results as means ±S.E.M. (n=5); **$p < 0.01$ where lots were compared with control (C). §§ $p < 0.01$ where lots were compared with cisplatin (Cis).

We next required determining the putative involvement of intracellular mediators in cisplatin, GSSE and *U.rigida* mode of action (Fig.3). We have seen an increase in calcium levels on treated rats by cisplatin (Fig 3.B). This increase could be the cause of cell death caused by the oxidative stress generated by the treatment. Indeed, the Ca^{2+} is the primordial trigger of apoptosis, it accumulates in the mitochondria increasing its permeability leading to the release of apoptogenic factors such as cytochrome C which will activate caspases leading to irreversible death of cells by apoptosis [18, 19]. Moreover, the massive entry of Ca^{2+} into the Mitochondria blocks the electron transport chain which results in excessive production of ROS.

It is well established that oxidative stress leads to increased concentration of iron following hemolysis and attack of transport proteins by ROS [20]. This increase in iron concentration (Fig 3.A) allows the mobilization of intracellular Ca^{2+} [21].

In fact, iron stimulates the production of the hydroxyl radical, following the Fenton reaction, resulting to activation of xanthine oxidase which causes elevation Ca^{2+} levels [22]. This is consistent with our results showing an increased cellular concentration of iron and Ca^{2+} in the testes of rats subjected to oxidative stress caused by cisplatin.

However, pretreatment of animals with GSSE or *U. rigida* followed by an injection of cisplatin and then a post-treatment with these extracts shows a very significant decrease in the Ca^{2+} and iron levels in the two groups compared to the rats treated with cisplatin alone.

3.4 Effect of treatments on the activity of antioxidant enzymes

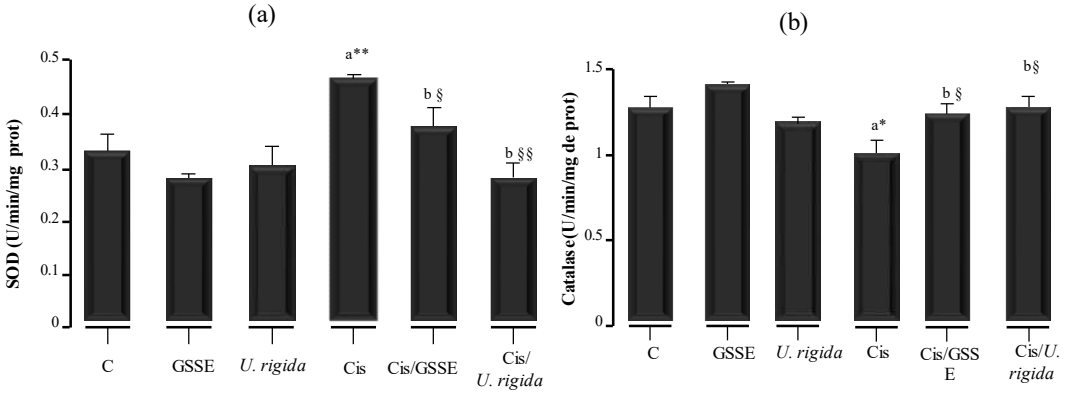

Figure.4: Effect of GSSE, *U.rigida* and cisplatin on testis antioxidant enzyme activities.

Rats were regulary administered with 10% ethanol (C), GSSE, *U.rigida*, Cisplatin (Cis), *U.rigida* plus Cisplatin (Cis/*U.rigida*) or Cisplatin plus GSSE (Cis/GSSE) for 7 days and testis free iron (Fig. 3a) and calcium (Fig. 3b) levels were outlined.

Results are described as means ±S.E.M. (n=5). ** $p < 0.01$ where lot where compared with control (C). §§ $p < 0.01$ where lots where compared with cisplatin (Cis).

In another part of our work, we followed the behaviour of the defensive enzymatic antioxidant in the presence of cisplatin and extracts of GSSE and *U. rigida*. The SOD and CAT are the first lines of defence against the toxic effects of ROS. Our results show that the activity of the SOD is largely stimulated at the level of testes of rats treated with cisplatin. It could be postulated that apart oxidative stress, the cells sought enzymatic defence. This issue does not agree with other results which showed a low activity of antioxidant enzymes including SOD [23]. Cisplatin upregulated SOD activity (Fig4.A) compared to control but decreased CAT (Fig4.B). Concerning CAT activities, cisplatin treatment appears to disrupt its operation. This disturbance can be explained by the alteration of the structure of this enzyme. We noticed that the use of extracts from GSSE or *U. rigida* in pre-treatment by cisplatin and then post-treatment is not followed by the stimulation of the activity of the SOD. This suggests that these extracts can protect cells against stress oxidative so that the cells did not find the need to strongly stimulate the enzymatic defense to protect against oxidative stress-induced by cisplatin. In view of the activity of catalase, the treatment with the extracts makes it possible to recover an activity comparable to that measured in control rats. This proves the protective effect of the extracts against the alteration of catalase

structure by the oxidative stress generated by cisplatin.

3.5 Overview of the effect of the extract of GSSE and *U.rigida* against oxidative stress product's

Treatment with the extract of GSSE or *U. rigida* protects against damage oxidative stress induced by cisplatin. It has been shown that the treatment of rats by these extracts decreases the production of the superoxide anion, one of the radicals responsible for the damage caused by oxidative stress. In addition, it has been shown that extracts of *U. rigida* or GSSE are able to protect lipids and cellular proteins from damage oxidative effects induced by oxidative stress. These results highlight the antioxidant potential of these extracts. In this context, work has revealed that the GSSE can protect against oxidative stress thanks to its power to trap ROS [4]. Even; Tian et al., (2018) [24] have shown that grape extracts have the ability to mitigate oxidative stress and to protect against inhibition of testosterone synthetase caused by cisplatin in the testes. Regarding *U. rigida*, previous work is done in our laboratory clearly demonstrate that this seaweeds possess a strong antioxidant power linked to the richness of its extracts in proteins, in compounds, phenolic and polysaccharides known for their remarkable antioxidant capacities [3, 12]. In addition, studies carried out in the laboratory showed that extracts of the seaweeds protect the cells against apoptosis induced by oxidative stress [25]. Moreover, our study reveals that extracts from the GSSE and *U. rigida* are devoid of any toxicity and has a high content of proteins, lipids, minerals and vitamins that have encouraged its extensive use as a dietary supplement for humans and animals [12, 26].

4. Conclusion and Perspectives

Ultimately, all of this work contributes to the understanding of the molecular and cellular mechanisms involved in the toxicity of cisplatin on healthy cells during chemotherapy, and the beneficial antioxidant role of GSSE and *U.rigida's* extracts against this toxicity. These results strongly encourage the use of GSSE and *U.rigida* as an alternative to the use of molecules derived from chemical synthesis whose side effects are undesirable and often complicate.

In the perspective of this work, we will highlight the sterility and / or the decrease of fertility observed in rats treated with cisplatin. We will propose by biochemical and histological approaches to follow the effect of cisplatin on spermatogenesis and sperm mortality and to look for a protective effect in the extracts of GSSE and / or *U. rigida*.

5. References

[1] M.-T. Lin, J.-L. Ko, T.-C. Liu, P.-T. Chao, and C.-C. Ou, "Protective Effect

of D-Methionine on Body Weight Loss, Anorexia, and Nephrotoxicity in Cisplatin-Induced Chronic Toxicity in Rats," (in eng), *Integrative cancer therapies,* vol. 17, no. 3, pp. 813-824, 2018.

[2] Y. V. Natochin, L. V. Reznik, V. T. Bakchteeva, and E. A. Lavrova, "Renal function and renal platinum content in uninephrectomized rats following cisplatin administration," (in eng), *Ren Fail,* vol. 15, no. 2, pp. 157-62, 1993.

[3] S. Mezghani, D. Csupor, I. Bourguiba, J. Hohmann, M. Amri, and M. Bouaziz, "Characterization of Phenolic Compounds of Ulva rigida (Chlorophycae) and Its Antioxidant Activity," *European*

Journal of Medicinal Plants, vol. 12, no. 1, pp. 1-9, 2016.

[4] S. Hamlaoui-Gasmi *et al.*, "Grape seed and skin extract mitigates garlic-induced oxidative stress in rat liver," (in eng), *Can J Physiol Pharmacol,* vol. 90, no. 5, pp. 547-56, May 2012.

[5] J. A. Buege and S. D. Aust, "Microsomal lipid peroxidation," (in eng), *Methods Enzymol,* vol. 52, pp. 302-10, 1978.

[6] R. L. Levine *et al.*, "Determination of carbonyl content in oxidatively modified proteins," (in eng), *Methods Enzymol,* vol. 186, pp. 464-78, 1990.

[7] J. Stern and W. H. Lewis, "The colorimetric estimation of calcium in serum with ocresolphthalein complexone," (in eng), *Clin Chim Acta,* vol. 2, no. 6, pp. 576-80, Dec 1957.

[8] A. Leardi *et al.*, "Desferioxamine increases iron depletion and apoptosis induced by ara-C of human myeloid leukaemic cells," vol. 102, no. 3, pp. 746-752, 1998.

[9] H. P. Misra and I. Fridovich, "The role of superoxide anion in the autoxidation of epinephrine and a simple assay for superoxide dismutase," (in eng), *J Biol Chem,* vol. 247, no. 10, pp. 3170-5, May 25 1972.

[10] H. Aebi, "Catalase in vitro," (in eng), *Methods Enzymol,* vol. 105, pp. 121-6, 1984.

[11] S. T. Ohnishi and J. K. Barr, "A simplified method of quantitating protein using the biuret and phenol reagents," (in eng), *Analytical biochemistry,* vol. 86, no. 1, pp. 193-200, 1978/05// 1978.

[12] S. Mezghani, I. Bourguiba, I. Hfaiedh, and M. Amri, "Antioxidant potential of Ulva rigida extracts: protection of HeLa cells against H(2)O(2) cytotoxicity," (in eng), *Biol Bull,* vol. 225, no. 1, pp. 1-7, Sep 2013.

[13] M. Mokni *et al.*, "Grape seed and skin extract protects kidney from doxorubicin-induced oxidative injury," (in eng), *Pak J Pharm Sci,* vol. 29, no. 3, pp. 961-8, May 2016.

[14] Y. O. Ilbey, E. Ozbek, A. Simsek, A. Otunctemur, M. Cekmen, and A. Somay, "Potential chemoprotective effect of melatonin in cyclophosphamide- and cisplatin-induced testicular damage in rats," (in eng), *Fertil Steril,* vol. 92, no. 3, pp. 1124-32, Sep 2009.

[15] A. R. Fallahzadeh *et al.*, "Evaluation of the Effect of Pentoxifylline on Cisplatin-Induced Testicular Toxicity in Rats," (in eng), *Toxicol Res,* vol. 33, no. 3, pp. 255-263, Jul 2017.

[16] E. A. Ahmed, H. M. Omar, S. elghaffar, S. M. Ragb, and A. Y. Nasser, "The antioxidant activity of vitamin C, DPPD and L-cysteine against Cisplatin-induced testicular oxidative damage in rats," (in eng), *Food Chem Toxicol,* vol. 49, no. 5, pp. 1115-21, May 2011.

[17] I. Singh, Y. Goyal, and P. Ranawat, "Potential chemoprotective role of resveratrol against cisplatin induced testicular damage in mice," (in eng), *Chem Biol Interact,* vol. 273, pp. 200-211, Aug 1 2017.

[18] S. W. Tait and D. R. Green, "Mitochondria and cell death: outer membrane permeabilization and beyond," (in eng), *Nat Rev Mol Cell Biol,* vol. 11, no. 9, pp. 621-32, Sep 2010.

[19] N. Zamzami and G. Kroemer, "Apoptosis: mitochondrial membrane

permeabilization--the (w)hole story?," (in eng), *Curr Biol,* vol. 13, no. 2, pp. R71-3, Jan 21 2003.

[20] L. M. Bystrom, M. L. Guzman, and S. Rivella, "Iron and reactive oxygen species: friends or foes of cancer cells?," (in eng), *Antioxid Redox Signal,* vol. 20, no. 12, pp. 1917-24, Apr 20 2014.

[21] P. M. Pahl and L. D. Horwitz, "Cell permeable iron chelators as potential cancer chemotherapeutic agents," (in eng), *Cancer Invest,* vol. 23, no. 8, pp. 683-91, 2005.

[22] T. Az-ma, N. Saeki, and O. Yuge, "Cytosolic Ca2+ movements of endothelial cells exposed to reactive oxygen intermediates: role of hydroxyl radical-mediated redox alteration of cell-membrane Ca2+ channels," (in eng), *Br J Pharmacol,* vol. 126, no. 6, pp. 1462-70, Mar 1999.

[23] S. A. Adejuwon, O. M. Femi-Akinlosotu, and J. O. Omirinde, "Cisplatin-induced testicular dysfunction and its amelioration by Launaea taraxacifolia leaf extract," (in eng), *Andrologia,* vol. 47, no. 5, pp. 553-9, Jun 2015.

[24] M. Tian *et al.*, "Grape seed procyanidins extract attenuates Cisplatin-induced oxidative stress and testosterone synthase inhibition in rat testes," (in eng), *Syst Biol Reprod Med,* vol. 64, no. 4, pp. 246-259, Aug 2018.

[25] S. Mezghani, P. N'Guessan, A. Carrier, and M. Amri, "The Ethanol Precipitate of Ulva rigida Protects HeLa Cells from Hydrogen Peroxide-Induced Apoptosis," vol. 39, no. 1, pp. 48-54, 2015.

[26] G. G. Satpati and R. Pal, "Biochemical composition and lipid characterization of marine green alga Ulva rigida- a nutritional approach," *Journal of Algal Biomass Utilization,* vol. 2, no. 4, pp. 10-13, 2011.

JOURNAL OF SCIENCE
SAKARYA UNIVERSITY

Sakarya University Journal of Science

ISSN 1301-4048 | e-ISSN 2147-835X | Period Bimonthly | Founded: 1997 | Publisher Sakarya University
http://www.saujs.sakarya.edu.tr/en/

Title: Using PSO and Genetic Algorithms to Optimize ANFIS Model for Forecasting Uganda's Net Electricity Consumption

Authors: Abdal Kasule, Kürşat Ayan
Recieved: 2019-10-04 18:15:09

Accepted: 2020-01-08 15:27:19

Article Type: Research Article
Volume: 24
Issue: 2
Month: April
Year: 2020
Pages: 324-337

How to cite
Abdal Kasule, Kürşat Ayan ; (2020), Using PSO and Genetic Algorithms to Optimize ANFIS Model for Forecasting Uganda's Net Electricity Consumption. Sakarya University Journal of Science, 24(2), 324-337, DOI: https://doi.org/10.16984/saufenbilder.629553
Access link
http://www.saujs.sakarya.edu.tr/tr/issue/52471/629553

Sakarya University Journal of Science 24(2), 324-337, 2020

Using PSO and Genetic Algorithms to Optimize ANFIS Model for Forecasting Uganda's Net Electricity Consumption

Abdal KASULE*[1], Kürşat AYAN[2]

ABSTRACT

Uganda seeks to transform its society from a peasant to a modern and largely urban society by the year 2040. To achieve this, electricity as a form of modern and clean energy has been identified as a driving force for all the sectors of the economy. For this reason, electricity consumption forecasts that are realistic and accurate are key inputs to policy making and investment decisions for developing Uganda's electricity sector. In this study, we present an ANFIS long-term electricity forecasting model that is easy to interpret. We use the model to forecast Uganda's electricity consumption. The ANFIS model takes population, gross domestic product, number of subscribers and average electricity price as input variables and electricity consumption as the output. We use particle swarm optimization (PSO) algorithm and genetic algorithm (GA) to optimize the parameters of the model. A forecast accuracy of 94.34% is achieved for GA-ANFIS, while 90.88% accuracy is achieved for PSO-ANFIS as compared to 87.79% for multivariate linear regression (MLR) model. Comparison with official forecasts made by Ministry of Energy and Mineral Development (MEMD) revealed low forecast errors.

Keywords: Electricity consumption forecasting, Adaptive Neuro-Fuzzy Inference System, Genetic algorithm, Particle swarm optimization algorithm, Uganda.

1. INTRODUCTION

The national vision statement, "A Transformed Ugandan Society from a Peasant to a Modern and Prosperous Country within 30 years" was approved by the cabinet of Uganda in the year 2007. Through consultations with stakeholders, the National Planning Authority (NPA) developed the Uganda Vision2040 [3] to operationalize this Vision statement and it was launched on 18th April 2013. To achieve the required transformation, electricity as a form of modern energy is identified as a driving

* Corresponding Author.

[1] Sakarya University, abdal.kasule1@ogr.sakarya.edu.tr, ORCID ID: 0000-0002-4619-4256

[2] İstanbul Medeniyet University, kursat.ayan@medeniyet.edu.tr, ORCID ID: 0000-0002-4619-4256

[3] http://npa.ug/wp-content/themes/npatheme/documents/vision2040.pdf accessed on 3rd-Sept-2016

force, not only for industrial and commercial sectors but also for domestic and transport sectors among others. Presently the mostly used source of energy in Uganda is traditional biomass (wood and charcoal) and this comprises 88.8% of the total energy use. It is used in both rural and urban areas for heating and cooking. Electricity is mainly hydro and contributes only 1.7% of the total energy use. Only 20% of Uganda's population have access to electricity (MEMD[4], annual report 2015). Despite the low energy access rates, electricity supply is still of poor quality. It is characterized by blackouts, deficiencies in supply leading to load shedding. It is estimated that a total of 41,738 MW of electricity will be required by the year 2040 for 80% of the total population to have access to electricity at 3,668kWh electricity per capita consumption. In light of the above, the Power Sector Investment Plan (2009-2030) was reviewed and the results of the review were presented in the Demand Forecast Report 2015. The Demand forecast report forecasted electricity consumption from 2015 up to 2040. The objective of both studies was to "provide adequate and reliable power based on the demand to spur Uganda's economic development". The findings of the two studies are now used as basis for decision making regarding planning and investment in Uganda's electricity sector. The situation has not changed much though and the forecasted consumption in the Demand Forecast Report has not been realized. We note that there is a very big difference between the forecasted values for all forecast scenarios in the Demand forecast report and the observed consumption for the years 2015-2017 as shown in Table 1 below.

Table 1.
Percentage relative errors between actual consumption and MEMD forecasts for the different forecast scenarios.

Year	Actual Consumption	Forecasts (GWh)				% Relative errors			
	(GWh)	Low case	Base case	High case	Vision 2040	Low case	Base case	High case	Vision 2040
2015	3,219	4,407	4,645	5,082	25,506	36.9	44.3	57.9	692.4
2016	3,489	5,451	6,665	8,193	31,090	56.2	91.0	134.8	791.1
2017	3,715	5,853	7,114	8,815	37,035	57.6	91.5	137.3	898.9

Source: Uganda Bureau of Statistics, Demand Forecast Report 2015.

In Table 1, "Actual Consumption" is the recorded electricity consumption for the corresponding year in GWh, "Low case", "Base case", "High case" and "Vision 2040" are MEMD electricity forecast scenarios developed for different annual growth rates of Uganda's economy. Since the forecasts were intended for planning purposes in the power sector, the big difference between the forecasted and observed consumption are misleading. These big differences can lead to inadequate planning and place more burden on the electricity generation and production costs. The result is inappropriate investment decisions for the country's energy systems and electricity sector in particular. For this reason, there is need for alternative forecasts with much lower deviations from the actual consumption in order to make appropriate investment decisions. Various techniques and methods have been used to forecast electricity consumption. Among the most popular techniques is regression analysis which is based on formulation of mathematical relationships between independent and dependent variables. However, in cases where the mathematical relationships are not known or hard to formulate it becomes a challenge and in such cases appropriate and effective models are hard to build. To avoid the above limitations of regression analysis, we propose an Adaptive Neuro-Fuzzy Inference System (ANFIS) model to forecast electricity consumption as an alternative

[4] Ministry of Energy and Mineral Development

solution. ANFIS can be used to build models whose mathematical relationships are hard to formulate or not known. For such cases, ANFIS modelling's only requirement is to provide independent variables (inputs) and dependent variables (targets) data, specify ANFIS parameters such as membership functions, a learning algorithm and through a training process ANFIS learns the relationships between the suggested inputs and targets. In this study we present an easy to interpret as well as accurate ANFIS model to forecast Uganda's electricity consumption with low forecast errors between the actual and forecasted consumption. We use population, gross domestic product, number of subscribers and average electricity price as inputs (independent variables) and electricity consumption as the target (dependent variable). Traditionally ANFIS parameters have been optimized using back propagation and a hybrid algorithm of least squares and back propagation algorithms. These algorithms are gradient based and are often trapped in local minima. Genetic algorithm (GA) and particle swarm optimization (PSO) algorithm are population based algorithms and have been widely used when it is difficult to obtain derivatives [1]. Thus in a bid to avoid the scenario of being trapped in local minimum we use GA and PSO to tune the parameters of ANFIS forecasting model. We compare results with official MEMD forecasts and a multivariate linear regression (MLR) model that uses the same variables as independent and dependent variables. The novelty of the study is to provide forecasts that are realistic with less forecast errors between the actual and forecasted consumption. These forecasts will help in formulation of appropriate investment decisions and policies in regard to electricity generation, transmission and distribution planning and expansion. These decisions and policies will help Ugandan society transform from a peasant to a largely urban and industrialized society as outlined in the Uganda Vision 2040.

The rest of the paper is organized as follows; in section 2 we present related and methods and materials in section 3. In section 4 we discuss the results and we give a conclusion in section 5.

2. RELATED WORK

ANFIS has been used in many fields such as control systems, image processing, time series forecasting, and load forecasting. For example [2] developed ANFIS by hybridizing subtractive clustering technique with GA and applied it to forecast electricity consumption for the Iranian industrial sector. The GA was used to find the optimum value of cluster radius which guaranteed the minimum number of rules and error. For both accuracy and the number of rules, the hybrid approach performed better than the conventional ANFIS based on gird partitioning, fuzzy c-means, and subtractive clustering. A hybrid PSO-ANFIS approach for short term wind power prediction in Portugal is used in [3]. The parameters of membership functions were tuned using PSO algorithm to lower the error between the observed and predicted wind power. A hybridized ANFIS, computer simulation and time series algorithm was used with monthly electricity consumption in Iran from 1995 to 2005 to predict electricity consumption [4]. A novel genetic-based adaptive neuro-fuzzy inference system (GBANFIS) for short-term load forecasting expert systems and controllers is presented in [5]. GA is first used to find the most suitable feature of inputs to construct the model and at a later stage GA is used optimize weights among rules. GBANFIS is used to forecast Iranian monthly energy demand and shows better results when compared to regression, GA, simulated-based GA, Artificial Neural Network (ANN), simulated-based ANN, fuzzy decision tree, and simulated-based ANFIS approaches. In [6] fuzzy sets were used to investigate the effect of weather, time, historical data, and random disturbances on load forecasting during the generation process. After the

investigation, they predicted Jordanian short term loads for generation scheduling and unit commitment decisions. A scaled conjugate gradient algorithm (CGA) and back propagation (BP) algorithm was used to train ANN and evolving fuzzy neural network (EFuNN) to predict electricity demand in the State of Victoria, Australia [7]. They conclude that the performance of neuro-fuzzy system was better than that of neural networks and Autoregressive Integrated Moving Average (ARIMA) models. The number of customers connected to the electricity distribution network, the temperature and the precipitation of rain are used in [8] as exogenous variables for Seasonal autoregressive integrated moving average with exogenous variables (SARIMAX) and ANFIS models to forecast electric load time series. The ANFIS model gave lower forecast error values than the SARIMAX model. Hence concluded that ANFIS model performed better than SARIMAX model for electric load time series forecast. [9] combined Back Propagation (BP) neural network, Adaptive Network-based Fuzzy Inference System (ANFIS) and Difference Seasonal Autoregressive Integrated Moving Average (diff-SARIMA) to forecast short-term electricity consumption. BP and ANFIS were able to deal with the nonlinearity of the data, and diff-SARIMA dealt with linearity and seasonality in the data. Though the forecasting results of the combined method had reduced errors and better accuracy than the individual methods, ANFIS model showed better forecast results among the individual methods. An ANFIS based model for solving the medium term electric load-forecasting using time series monthly data is presented by [10]. Comparison with Autoregressive (AR) and an Autoregressive Moving Average (ARMA) models showed that the ANFIS model's results were better than those of AR and ARMA models. Using weather data, [11] developed and compared linear regression, artificial neural networks and ANFIS models for load prediction and found that ANFIS model gave more accurate results. For Canada's Ontario province, [12] used ANFIS to model electricity demand using data from the year 1976-2005. The inputs to the model were population, gross domestic product, number of employment, dwelling count, hottest and coldest temperatures of the day. Their results showed that employment affected electricity demand most. ANFIS was used for next week electric load forecasting [13]. The input variables consisted of half hour weekly load time series data. Similarly [14] used ANFIS to model and predict electricity demand using population, Gross Domestic Product (GDP), Gross National Income (GNI), imports and exports data for India. short-term load forecasting models using fuzzy logic and ANFIS were developed in [15]. They used historical load, temperature and season as input variables. Forecasting ability of ANFIS model is demonstrated in [16] and is applied to regional electricity loads in Taiwan. A neurofuzzy methodology using historical energy data for load prediction to estimate the energy consumption for several future years is presented in [17]. Jordanian industrial sector electricity consumption was modeled and predicted using MLR and neuro-fuzzy models [18]. The variables used in these models were electricity tariffs, fuel prices, production outputs, capacity utilizations, number of establishments, number of employees, and structural effects. A comparison of the models using the root mean squared error showed that the neuro-fuzzy model performed better than the MLR model. [19] presented a deep neural network algorithm for short-term load forecasting. The algorithm describes two main processes i.e. feature extraction and load forecasting. Feature extraction is performed by convolution layers and pooling layers. The forecasting process is performed when Pooling3 layer is flattened into one dimension to construct a fully connected structure to the output

layer. The experiment results show that the proposed algorithm displays very high forecasting accuracy in comparison with Support Vector Machines, Random Forests, Decision Trees, Multi-Layer Perceptron and Long Short Term Memory that are commonly used in load forecasting. Youshan and Qi [20] proposed and utilized a Regressive Convolution Neural Network (RCNN) model to extract features from data. The extracted features are used to train a Regressive Support Vector Machine (SVR) to predict the electricity consumption. Results show that the forecasting accuracy of the proposed approach is high compared to BP neural network and SVM. Youshan et al [21] using historical data proposed a modified particle swarm optimization-back propagation neural network model to forecast electricity consumption for a mineral company of Anshan in China. Comparison of the proposed algorithm's convergence and forecast accuracy with Back Propagation, PSO and fuzzy neural network showed better results.

3. METHODS AND MATERIALS

Our goal is to model Uganda's net electricity consumption using ANFIS. The model structure should be easy to interpret at the same time exhibit a significant level of forecasting accuracy. We train the model (optimize the parameters of input and output membership functions) and use the optimized/trained ANFIS model to forecast Uganda's long-term net electricity consumption. We take socio-economic variables as inputs to the model and electricity consumption as the output. In general, forecasting approaches and methodologies aim to minimize the error term between the observed/actual and the forecasted values. Therefore all forecasting methods use some form of error function (loss function) as the objective function. Commonly used error functions include sum of squared errors (SSE), mean square error (MSE), root mean square error (RMSE) and mean absolute percentage error (MAPE). In this study we use MSE, Eq. (1) as the objective function for the training algorithm.

$$\min f = \frac{1}{n}\sum(Y_i^{actual} - Y_i^{predicted})^2 \qquad (1)$$

where Y_i^{actual} is the observed consumption (target) and $Y_i^{predicted}$ is the computed consumption using ANFIS model (output) for the observed period.

3.1. Dataset

Electricity consumption is affected by many factors such as weather, socio-economic and demographic factors. Weather factors normally affect short term electricity consumption while socio-economic and demographic factors affect long term electricity consumption. In this study the dataset comprised of historical data for electricity consumption as the dependent variable, and socio-economic factors i.e. population, gross domestic product (GDP), total exports, total imports, total number of electricity subscribers/customers (residential, commercial and industrial consumers), and average electricity price as independent variables from 1990 to 2016. Population and GDP data was obtained from the world bank population [5] and GDP [6] data APIs, electricity consumption, number of subscribers and electricity prices data was obtained from the 1997 statistical abstract of the Ministry of planning and economic development, Uganda Bureau of Statistics statistical abstracts[7] from 2002 to 2016 and Electricity Regulatory Authority[8] of Uganda.

[5] api.worldbank.org/v2/en/indicator/SP.POP.TOTL?downloadformat=excel retrieved on 12-Sept-2017

[6] api.worldbank.org/v2/en/indicator/NY.GDP.MKTP.CD?downloadformat=excel retrieved on 12-Sept-2017

[7] www.ubos.org/publications/statistical-abstract last accessed 10th-Sept-2017

[8] www.era.or.ug/index.php/statistics-tariffs/tariffs, last accessed 10th-Sept-2017

3.2. Overview of Adaptive Neuro-Fuzzy Inference System (ANFIS)

ANFIS is a combination of neural networks and fuzzy systems. The fuzzy system component defines the membership functions while the neural network component is used to automatically extract fuzzy rules from numerical data and adaptively tunes the parameters of the membership function through a learning process. ANFIS was introduced in 1993 as a basis for constructing "IF-THEN" rules to map the input to output space through appropriate membership functions [22]. Jang's work is an extension Takagi and Sugeno's 1985 work on fuzzy identification and modelling of systems [23]. Fuzzy "IF–THEN" rules also define the relationship between ANFIS's premise and consequent parameters [1]. Each rule describes a local behavior of the mapping. In the Sugeno fuzzy model, a basic fuzzy rule is represented as;

$IF\ X_1\ is\ a_1\ and\ X_2\ is\ a_2\ and\ X_3\ is\ a_3\ and\ X_4\ is\ a_4\ THEN\ Y = f(X_1, X_2, X_3, X_4)$,

where X_1, X_2, X_3 and X_4 are fuzzy sets in the antecedent inputs (influential variables) and Y is a crisp function representing the output (electricity consumption). Inputs and outputs in ANFIS are represented by membership functions. The type and number of membership functions, number of inputs and outputs and the number of rules determines the number of parameters to be tuned/optimized through a learning process. Fuzzy rules are generated from the input space through a partitioning process. Commonly used partitioning processes are grid partition, subtractive clustering and fuzzy c-means clustering. Each of these partitioning processes have advantages and disadvantages; such as complexity of the rules and computation time among others. In this study we use fuzzy c-means clustering as a partitioning process to reduce the complexity and number of rules and parameters to be optimized. The fuzzy c-means clustering allows data points to belong to multiple clusters and it is identified by a membership value in each cluster. The membership value of each data point in cluster is specified by a membership function on the basis of its distance between the cluster's center and the data point. ANFIS structure with four inputs and one output used in this study is shown in Figure 1 below.

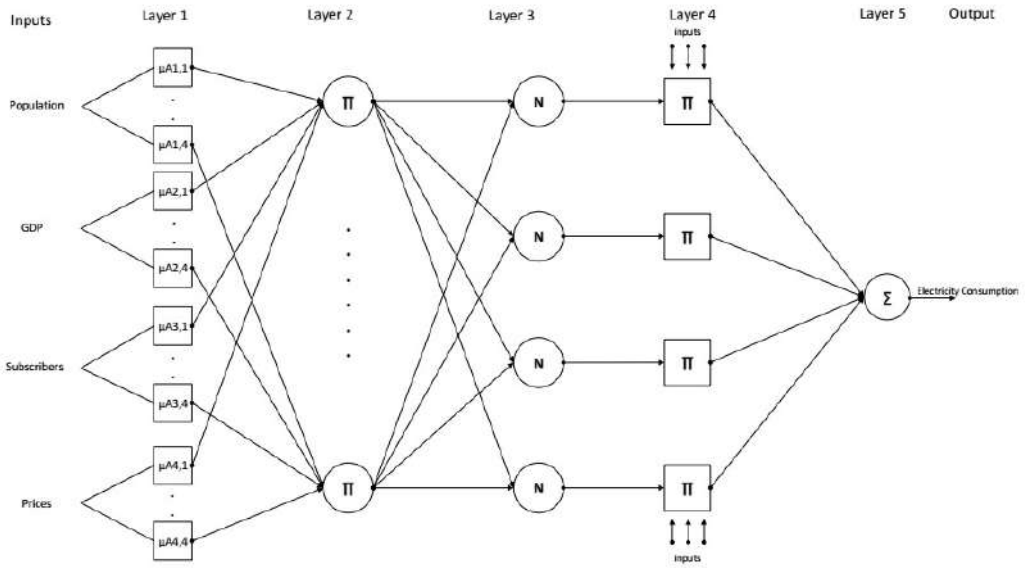

Figure 1 ANFIS structure with four inputs and one output

In layer 1, we have inputs and their membership functions $\mu A(x)$. Nodes in this layer are adaptive, i.e. the parameters are changed during the training process. The outputs of each node is of the form

$O_{1,i} = \mu A_i(x)$, a result of computing membership functions.

Commonly used membership functions include generalized bell, Gaussian, triangular, and trapezoidal functions. We use the Gaussian function for the input membership functions as shown in Eq. (2) below.

$$\mu A(x_i) = \exp\{\frac{-(x_i - c_i)^2}{2\sigma_i{}^2}\} \quad (2)$$

where c_i and σ_i are called premise parameters. These parameters are adjusted through a learning process to get an optimal state of ANFIS. In layer 2 the rules are formed. The output of layer 2 is the firing strength w_i of each rule. The firing strength is a product of membership functions in layer one, mathematically the output of each node in layer 2 can be expressed as Eq. (3) below.

$$O_{2,i} = w_i = \mu A_i(X_1)\mu B_i(X_2)\mu C_i(X_3)\mu D_i(X_4), i = 1,2,3,4. \quad (3)$$

where $X_1, X_2, X_3 \; and \; X_4$ are the inputs.
In layer 3, the firing strength of each rule is normalized using Eq. (4) below.

$$O_{3,i} = \overline{w_i} = \frac{w_i}{\sum_{i=1}^{4} w_i} \quad (4)$$

The next layer defines the output membership functions, for this study we Sugeno fuzzy model that uses linear functions shown in Eq. (5) as membership functions.

$$f_i = p_i x_1 + q_i x_2 + r_i x_3 + s_i x_4 + t_i, i = 1,2,3,4. \quad (5)$$

where p_i, q_i, r_i, s_i, t_i are called consequent parameters and x_i are the inputs. Like the premise parameters in layer 1, consequent parameters are also adjusted through a learning process to get an optimal ANFIS model. The normalized firing strength of each rule is applied on the corresponding output membership function to get the output of each rule as shown in Eq. (6)

$$O_{4,i} = \overline{w_i} f_i = \overline{w_i}(p_i x_1 + q_i x_2 + r_i x_3 + s_i x_4 + t_i), i = 1,2,3,4. \quad (6)$$

The final output of layer 5 is a summation of all incoming signals of the firing strengths and output membership functions as shown in Eq. (7).

$$O_{5,i} = \sum \overline{w_i} f_i = \sum_{i=1}^{4} \overline{w_i}(p_i x_1 + q_i x_2 + r_i x_3 + s_i x_4 + t_i) \quad (7)$$

3.3. Overview of Particle Swarm Optimization (PSO) algorithm

Developed in 1995 by Eberhart and Kennedy, PSO algorithm is a computational intelligence technique that gets inspiration from the social behavior of a flock of birds or a school of fish. PSO algorithm originates from artificial life, social psychology, computer and engineering science. The swarm intelligence concept as used in PSO algorithm applies the collective behavior of agents that locally interact with their environment to create global functional patterns that are coherent [24]. A population of random solutions is used to initialize PSO algorithm and search for optimal solution is done by updating the positions of the particles at each successive iteration using Eq. (8).

$$x_i^{k+1} = x_i^k + v_i^{k+1} \quad (8)$$

In Eq. (7) x_i^{k+1} is the new position, x_i^k is the previous position and v_i^{k+1} is the updated velocity. Velocity is updated using Eq. (9).

$$v_i^{k+1} = v_i^k + c_1 rand_1\left(pbest_i^k - x_i^k\right) + c_2 rand_2(gbest^k - x_i^k) \quad (9)$$

In Eq. (8), c_1 and c_2 are social and cognitive coeeficients, $rand_1$ and $rand_2$ are random numbers uniformly distributed in the [0, 1] interval. A user defined fitness function is used to derive particle and global best positions. Every particle's

movement at each iteration evolves to an optimal or near-optimal solution. The process is repeated until improved positions that satisfy a set criteria are discovered.

3.4. Overview of Genetic Algorithm (GA)

GA is a stochastic optimization technique based on evolution of biological processes. GA starts with a random initialization of solutions in the search space, this initial set of solutions is called a population. Using genetic operators, the population is improved over multiple iterations until a specified stopping criteria is reached. The basic operators of GA are selection, crossover and mutation. Selection is used to choose individuals for reproduction. The selection procedure is based on the probability of fitness of individuals with in the population. The higher the fitness of an individual, the higher the probability of being selected. Selection probability is calculated based on the Eq. (10) below.

$$P_i = \frac{F_i}{\sum_{k=1}^{n} F_k} \qquad (10)$$

F_i in Eq. (9) is the fitness value of solution i, and n is the population size. Common selection procedures are roulette wheel selection, fitness ranking and tournament selection. After the selection procedure, crossover operator is applied to the selected individuals. Using a crossover rate genetic material of two or more solutions is combined to form a better solution. The mutation operator is used to create diversity in the new population to enable a wider search space.

3.5. ANFIS model for long term electricity consumption forecasting

ANFIS model for long term electricity forecasting is modeled based on the Sugeno fuzzy inference system. It takes four inputs i.e. population, gross domestic product, number of subscribers and electricity price and the output is electricity consumption. The model was implemented using MATLAB 2017 on a dual core processor with 4GB of RAM. The structure of ANFIS model is shown in Figure 2.

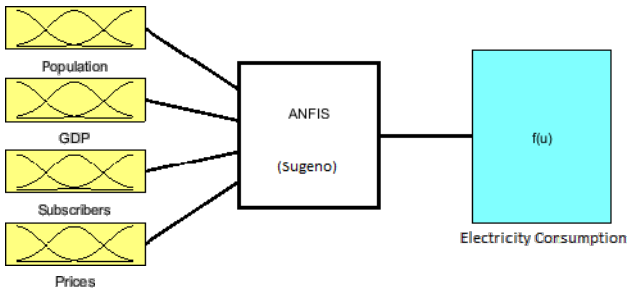

Figure 2 ANFIS model for electricity consumption forecasting

The Gaussian function has only two parameters to tune as opposed to three for the triangular, and four for the trapezoidal function. Because of the limited data available, we choose the Gaussian function for the membership functions of inputs in order not to have many premise parameters to optimize. Because the more the parameters to optimize become the more data is needed. More so [25] examined the four mostly used membership functions on the performance of ANFIS while solving various classification problems and concluded that the Gaussian membership function demonstrated higher degree of accuracy with lesser computational complexity as compared to its counterparts. The linear function is used for output membership function. Interpretability of ANFIS relates to its structure. Thus to easily interpret an ANFIS model we look at the number and structure of "IF-THEN" rules, and the number of input variables i.e. the smaller the number of rules and the less number of input variables, the easier it is to interpret the ANFIS model. Accuracy on the other hand relates to how precisely an ANFIS model can correctly estimate the modeled system. Accuracy is usually measured as a percentage [26]. The higher the percentage the more accurate an ANFIS model is. In order to achieve interpretability, we used

fuzzy c-means clustering to divide our dataset into four clusters, each cluster containing inputs and their corresponding outputs. One rule is generated for each cluster, giving a total of four rules as shown Figure 3 below.

```
'1. If (in1 is in1cluster1) and (in2 is in2cluster1) and (in3 is in3cluster1) and (in4 is in4cluster1) then (out1 is out1cluster1) (1)'
'2. If (in1 is in1cluster2) and (in2 is in2cluster2) and (in3 is in3cluster2) and (in4 is in4cluster2) then (out1 is out1cluster2) (1)'
'3. If (in1 is in1cluster3) and (in2 is in2cluster3) and (in3 is in3cluster3) and (in4 is in4cluster3) then (out1 is out1cluster3) (1)'
'4. If (in1 is in1cluster4) and (in2 is in2cluster4) and (in3 is in3cluster4) and (in4 is in4cluster4) then (out1 is out1cluster4) (1)'
```

Figure 3 ANFIS rules

In the rules above *in1*=population, *in2*=gross domestic product, *in3*=number of subscribers, *in4*=average electricity price and *out1*=electricity consumption. Similarly "*inX is inXclusterY*" means input X in cluster Y, and "*out1 is out1clusterY*" means output 1 in cluster Y. Each input is defined by four membership functions and each output is defined by one membership function. The number of tunable parameters for each input is eight (2x4=8) and each output has five (5) parameters, giving a total of thirteen (13) tunable parameters for each cluster. For all the four clusters the total number of parameters is fifty two (52). A learning algorithm is used to tune the parameters of ANFIS through a learning process. In this study we use PSO algorithm and GA as learning algorithms to tune the parameters of ANFIS.

3.5.1. Training ANFIS with PSO algorithm and GA

The training process by a learning algorithm tunes the parameters of the membership functions to construct a mapping and learn relationships between inputs and outputs.

```
1.  Load dataset
2.  Create ANFIS forecasting model
        Set the parameters of ANFIS
3.  Train ANFIS using training dataset
        Choose algorithm (PSO or GA)
4.  Output trained ANFIS
5.  Test trained ANFIS using test dataset
        Calculate RMSE and MAPE
6.  Make forecasts using forecast dataset
```

Figure 4 Pseudo code for the main procedure for training ANFIS

In this study we use PSO algorithm and GA to tune membership functions' parameters of inputs and polynomial coefficients of output of the ANFIS model shown in Figure 2. The pseudo code for the main procedure for training the model is shown in the Figure 4 above. In PSO-ANFIS and GA-ANFIS models, ANFIS is considered as particle or individual representing a potential solution to the optimization problem. The premise and consequent parameters of ANFIS are the dimensions of the problem. The data set was divided randomly into a training and a testing data set in the ratio 0.7:0.3. The parameters of PSO algorithm and GA were set as follows, population size=100, maximum number of iterations=1000, lower and upper bound interval [-10, 10], $c_1 = c_2 = 2.1$, crossover rate=0.7 and mutation rate=0.15. The algorithm evaluates the objective function defined in Eq. (1) until a stopping criteria or maximum number of iterations is reached. The Y_i^{actual} is regarded as the target and the $Y_i^{predicted}$ is the ANFIS output at each every iteration.

3.6. Model performance assessment

To assess the forecasting ability and accuracy of PSO-ANFIS and GA-ANFIS we use the root mean square error (RMSE) and mean absolute percentage error (MAPE). The lower the values the better the forecasting ability. RMSE and MAPE are calculated using the formulas below.

Table 2
RMSE and MAPE values to assess the performance of models

PSO-ANFIS forecast		GA-ANFIS forecast		MLR	
RMSE	MAPE (%)	RMSE	MAPE (%)	RMSE	MAPE (%)
1.4707	9.1164	0.8977	5.6543	1.6490	12.2135

$$RMSE = \sqrt{\frac{1}{N}\sum(Y_i^{actual} - Y_i^{predicted})^2} \quad (11)$$

$$MAPE = \frac{1}{N}\sum \left| \frac{Y_i^{actual} - Y_i^{predicted})}{Y_i^{observed}} \right| * 100 \quad (12)$$

In Eqs. (11) and (12), N is the number of observations, Y_i^{actual} is the observed electricity consumption and $Y_i^{predicted}$ is the forecasted electricity. To use the trained ANFIS model to forecast electricity consumption, forecasted input variables obtained using multilayer perceptron network for time series forecasting were used [27].

4. RESULTS AND DISCUSSION

The objective of this study was to propose ANFIS forecast model as an alternative approach to Uganda's electricity consumption forecasting. By taking social economic factors that influence electricity consumption as inputs to ANFIS model, we were able to train the model using PSO and GA. The proposed model is not only easy to interpret, it also gives low forecast errors. ANFIS models are generally complex black box models and not always easy to interpret because of the so many inputs and many number of rules. We managed to reduce this complexity to make our model easy to interpret by taking only four inputs. Using FCM, our inputs were divided into four clusters and four rules. Each rule takes number of customers, electricity prices, GDP and population as inputs in each cluster, passes the input to either PSO or GA training algorithm and gives electricity consumption as the output. The training process was done a number of times and each time the values of RMSE and MAPE were recorded. The target was to get the best (lowest) values of RMSE and MAPE. The best RMSE and MAPE values for both algorithms are shown in the Table 2. From Table 2, GA-ANFIS gives lower values for both RMSE and MAPE than both PSO-ANFIS and MLR models. The forecasting accuracy of a model is a common parameter that is used to determine how good or bad a forecast model is. This parameter is usually measured as a percentage. A high forecasting accuracy indicates a good model. On the other hand a low forecast accuracy means a bad model. In this study, we use MAPE to measure the percentage error in the forecast, hence subtracting this error from one hundred gives the forecast accuracy of the model. As shown in Table 2, GA-ANFIS model gives a forecast accuracy of 94.3457% compared to that of 90.8836% for PSO-ANFIS and 87.7865% for MRL model. We can say that GA-ANFIS is a better forecasting model than PSO-ANFIS forecasting model and MRL model. The optimized ANFIS models after training are shown in Figures 5 and 6 below.

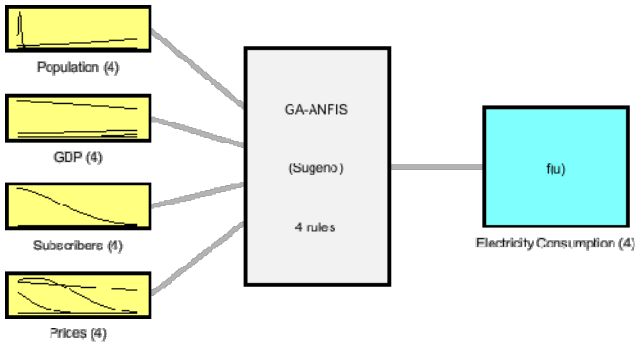

Figure 5 ANFIS model optimized using GA

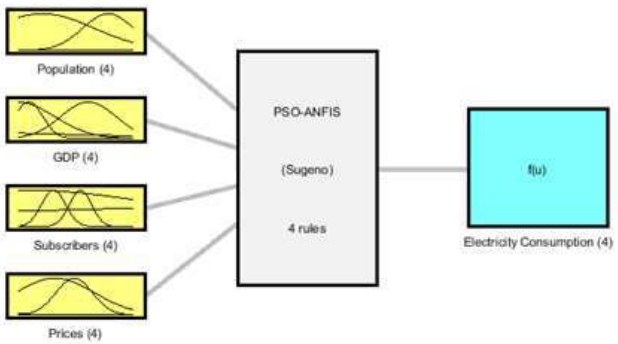

Figure 6 ANFIS model optimized using PSO algorithm

Using these optimized GA-ANFIS and PSO-ANFIS we forecast Uganda's electricity consumption from year 2015 up to year 2040. The forecasted consumption along with the actual consumption, MEMD base case and Vision 2040 scenario forecasts and regression model forecasts are shown in Table 3. As expected each model shows a general increase in electricity consumption from 2015 up to 2040. As the consumption increases, the error between the actual and forecasted consumption also increases though not to a bigger magnitude as that of the MEMD forecasts. For planning purposes this error is manageable. The graph in Figure 7 show the forecasts. The percentage relative errors of our forecasts in comparison to the MEMD forecast for the years 2015, 2016 and 2017, are very low while those MEMD and regression model are very high, especially those for Vision 2040 forecast as Table 4.

5. CONCLUSIONS

Uganda's development goals as stated in Uganda vision 2040, identify electricity as a key variable in the development process. Therefore, planning in the electricity sector should be emphasized more than ever before. One of the critical inputs to the planning process is realistic and achievable forecast targets. In this study we have modelled Uganda's electricity consumption forecasting using ANFIS and tuned the parameters of the model using PSO algorithm and GA. The ANFIS model takes four socio-economic variables as inputs and electricity consumption as output. From the results of the study we can make the following conclusions;

i. Based on the RMSE and MAPE values as shown in Table 2, the results indicate that the GA-ANFIS model a better model as compared to the PSO-ANFIS and MRL models.

Table 3
Comparison of forecast results and MEMD forecast report

Year	Actual Consumption	MEMD Forecast (GWh)		MLR Model	PSO-ANFIS	GA-ANFIS
	(GWh)	Base case	Vision 2040	(GWh)	(GWh)	(GWh)
2015	3,219	4,645	25,506	3,854	3,219	3,269
2016	3,489	6,665	31,090	4,416	3,780	3,637
2017	3,715	7,114	37,035	5,246	4,444	4,284
2018		7,591	43,358	6,325	5,347	5,099
2019		8,099	50,077	7,861	6,614	6,264
2020		8,638	57,214	9,318	7,825	7,358
2021		9,211	64,790	10,990	9,182	8,629
2022		9,819	72,825	12,784	10,638	9,997
2023		10,370	81,344	14,502	12,049	11,298
2024		10,992	90,370	16,227	13,465	12,602
2025		11,648	99,927	17,969	14,914	13,906
2026		12,338	110,033	19,714	16,343	15,228
2027		13,064	120,723	21,535	17,866	16,579
2028		13,828	132,026	23,395	19,404	17,966

2029	14,632	143,973	25,285	20,947	19,400
2030	15,453	156,320	27,346	22,728	20,901
2031	16,289	169,042	29,411	24,395	22,479
2032	17,138	182,087	31,470	26,102	24,016
2033	17,994	195,410	33,538	27,797	25,578
2034	18,857	208,961	35,608	29,458	27,160
2035	19,721	222,688	37,686	31,201	28,698
2036	20,584	236,534	39,755	32,880	30,273
2037	21,441	250,440	41,829	34,623	31,816
2038	22,289	264,345	43,901	36,310	33,390
2039	23,124	278,183	45,981	38,056	34,926
2040	23,941	291,889	48,055	39,751	36,494

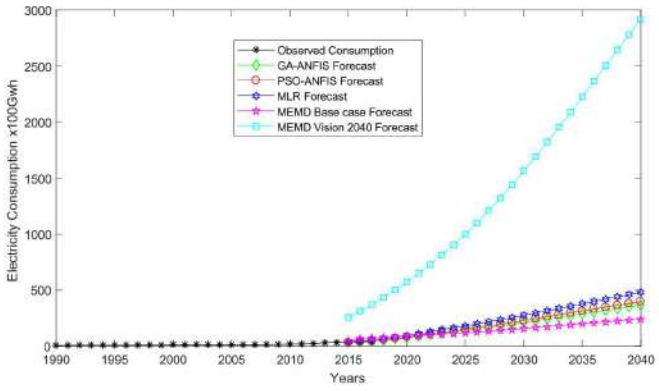

Figure 7 Comparison of forecasts

ii. In regard to easy interpretability we managed to model ANFIS with only four rules using with four inputs and one output. We were able to achieve forecast accuracy of 94.3457%, for GA-ANFIS, 90.8836% for PSO-ANFIS. Both ANFIS models exhibited better accuracy than the MLR model whose accuracy was 87.7865%.

iii. ANFIS model for long term electricity forecasting has given more realistic and achievable targets as seen in the relative errors between the observed consumption and ANFIS forecasts in comparison to the official forecasts of the Ministry of Energy and Mineral Development.

Results arising from this study provide important reference materials for policy makers and utility companies to access Uganda's electricity consumption needs and targets in order to align them with the national development goals outlined in Uganda Vision 2040.

Forecasting literature suggests that various forecasting approaches and methods when combined together give better forecast results with minimal forecast errors. There are various methods to combine forecast methods. As further research, we propose that the PSO-ANFIS and GA-ANFIS forecast models can combined into one model. Results of the combined model can be compared with results of the individual models.

Table 4
Percentage relative errors

Year	MEMD		MLR	ANFIS	
	Base case	Vision 2040		PSO-ANFIS	GA-ANFIS
2015	44.30	692.36	19.73	0.00	1.55
2016	90.48	788.54	26.57	8.03	3.94
2017	91.49	896.90	41.21	19.62	18.06

REFERENCES

[1] K. V. Shihabudheen and G. N. Pillai, "Recent advances in neuro-fuzzy system: A survey," *Knowledge-Based Syst.*, vol. 152, pp. 136–162, 2018.

[2] S. Mollaiy-Berneti, "Optimal design of adaptive neuro-fuzzy inference system using genetic algorithm for electricity demand forecasting in Iranian industry," *Soft Comput.*, vol. 20, no. 12, pp. 4897–4906, 2016.

[3] H. M. I. Pousinho, V. M. F. Mendes, and J. P. S. Catalão, "A hybrid PSO – ANFIS approach for short-term wind power prediction in Portugal," *Energy Convers. Manag.*, vol. 52, no. 1, pp. 397–402, 2011.

[4] A. Azadeh, M. Saberi, A. Gitiforouz, and Z. Saberi, "A hybrid simulation-adaptive network based fuzzy inference system for improvement of electricity consumption estimation," *Expert Syst. Appl.*, vol. 36, no. 8, pp. 11108–11117, 2009.

[5] S. M. R. Kazemi, M. M. Seied Hoseini, S. Abbasian-Naghneh, and S. H. A. Rahmati, "An evolutionary-based adaptive neuro-fuzzy inference system for intelligent short-term load forecasting," *Int. Trans. Oper. Res.*, vol. 21, no. 2, pp. 311–326, 2014.

[6] R. Mamlook, O. Badran, and E. Abdulhadi, "A fuzzy inference model for short-term load forecasting," *Energy Policy*, vol. 37, pp. 1239–1248, 2009.

[7] A. Abraham and B. Nath, "A neuro-fuzzy approach for modelling electricity demand in Victoria," *Appl. Soft Comput.*, vol. 1, pp. 127–138, 2001.

[8] C. M. Pereira, N. N. De Almeida, and M. L. F. Velloso, "Fuzzy modeling to forecast an electric load time series," *Procedia Comput. Sci.*, vol. 55, no. Itqm, pp. 395–404, 2015.

[9] Y. Yang, Y. Chen, Y. Wang, C. Li, and L. Li, "Modelling a combined method based on ANFIS and neural network improved by DE algorithm: A case study for short-term electricity demand forecasting," *Appl. Soft Comput. J.*, vol. 49, pp. 663–675, 2016.

[10] C. Ucenic and A. George, "A Neuro-fuzzy Approach to Forecast the Electricity Demand," in *Proceedings of the 2006 IASME/WSEAS International Conference on Energy & Environmental Systems*, 2006, vol. 2006, pp. 299–304.

[11] J. R. G. Sarduy, K. G. Di Santo, and M. A. Saidel, "Linear and non-linear methods for prediction of peak load at University of São Paulo," *Meas. J. Int. Meas. Confed.*, vol. 78, pp. 187–201, 2016.

[12] G. Zahedi, S. Azizi, A. Bahadori, A. Elkamel, and S. R. Wan, "Electricity demand estimation using an adaptive neuro-fuzzy network : A case study from the Ontario province-Canada," *Energy*, vol. 49, pp. 323–328, 2013.

[13] B. Mordjaoui, M.; Boudjema, "Forecasting and Modelling Electricity Demand Using Anfis Predictor," *J. Math. Stat.*, vol. 7, no. 4, pp. 275–281, 2011.

[14] S. Saravanan, S. Kannan, and C. Thangaraj, "Prediction of India's Electricity Consumption using ANFIS," *ICTACT J. Soft Comput.*, vol. 5, no. 3, pp. 985–990, 2015.

[15] H. Çevik, H.; Çunkaş, "Short-term load forecasting using fuzzy logic and ANFIS," *Neural Comput Appl.*, vol. 26, pp. 1355–1367, 2015.

[16] M. Ying, L.; Pan, "Using adaptive network based fuzzy inference system to forecast regional electricity loads," *Energy Convers. Manag.*, vol. 49, pp. 205–211, 2008.

[17] M. Haydari, Z.; Kavehnia, F.; Askari, M.; Ganbariyan, "Time-Series Load Modelling and Load Forecasting Using Neuro-Fuzzy Techniques," in *2007 9th International Conference on Electrical Power Quality and Utilization*, 2007.

[18] M. Al-Ghandoor, A.; Samhouri, "Electricity Consumption in the Industrial Sector of

Jordan : Application of Multivariate Linear Regression and Adaptive Neuro-Fuzzy Techniques," *Jordan J. Mech. Ind. Eng.*, vol. 3, no. 1, pp. 69–76, 2009.

[19] P. Kuo and C. Huang, "A High Precision Artificial Neural Networks Model for Short-Term Energy Load Forecasting," Energies, vol. 11, no. 1, pp. 1–13, 2018.

[20] Y. Zhang and Q. Li, "Network and Support Vector Regression Model for Electricity Consumption," In Future of Information and Communication Conference, Springer, vol. 1, pp. 33-45, 2019.

[21] Y. Zhang, L. Guo, Q. Li, and J. Li, "Electricity consumption forecasting method based on MPSO-BP neural network model," Proceedings of the 2016 4th International Conference On Electrical Electronics Engineering and Computer Science (ICEEECS), vol. 50, pp. 674–678, 2016.

[22] J. R. Jang, "ANFIS : Adap tive-Ne twork-Based Fuzzy Inference System," *IEEE Trans. Syst. Man. Cybern.*, vol. 23, no. 3, pp. 665–685, 1993.

[23] T. Takagi and M. Sugeno, "Fuzzy Identification of Systems and Its Applications to Modeling and Control," *IEEE Trans. Syst. Man. Cybern.*, vol. 15, no. 1, pp. 116–132, 1985.

[24] R. G. Del Valle, Y.; Venayagamoorthy, G. K.; Mohagheghi, S.; Hernandez, J. C.; Harley, "Particle swarm optimization: basic concepts, variants and applications in power systems," *IEEE Trans. Evol. Comput.*, vol. 12, no. 2, pp. 171–195, 2008.

[25] N. Talpur, M. N. M. Salleh, and K. Hussain, "An investigation of membership functions on performance of ANFIS for solving classification problems," *IOP Conf. Ser. Mater. Sci. Eng.*, vol. 226, no. 1, 2017.

[26] D. P. Rini, S. M. Shamsuddin, and S. S. Yuhaniz, "Particle swarm optimization for ANFIS interpretability and accuracy," *Soft Comput.*, vol. 20, no. 1, pp. 251–262, 2016.

[27] A. Kasule and K. Ayan, "Forecasting Uganda's Net Electricity Consumption Using a Hybrid PSO-ABC Algorithm," *Arab. J. Sci. Eng.*, 2018.

JOURNAL OF SCIENCE
SAKARYA UNIVERSITY

Sakarya University Journal of Science

ISSN 1301-4048 | e-ISSN 2147-835X | Period Bimonthly | Founded: 1997 | Publisher Sakarya University
http://www.saujs.sakarya.edu.tr/en/

Title: The Effects of Green Tea Leaf Extract on Cytogenetical and Physiological Parameters of Allium cepa L. exposed to Salinity

Authors: Dilek Çavuşoğlu
Recieved: 2019-03-19 14:13:44

Accepted: 2020-01-09 14:02:34

Article Type: Research Article
Volume: 24
Issue: 2
Month: April
Year: 2020
Pages: 338-346

How to cite
Dilek Çavuşoğlu; (2020), The Effects of Green Tea Leaf Extract on Cytogenetical and Physiological Parameters of Allium cepa L. exposed to Salinity. Sakarya University Journal of Science, 24(2), 338-346, DOI: https://doi.org/10.16984/saufenbilder.541835
Access link
http://www.saujs.sakarya.edu.tr/tr/issue/52471/541835

Sakarya University Journal of Science 24(2), 338-346, 2020

The Effects of Green Tea Leaf Extract on Cytogenetical and Physiological Parameters of *Allium cepa* L. exposed to Salinity

Dilek ÇAVUŞOĞLU[1]

Abstract

The aim of this study investigated the effects of 50 mg L^{-1} green tea leaf extract in decreasing harmful effects of 0.175 M salinity stress on the mitotic activity, chromosomal aberrations, seedling growth (fresh weight, radicle length and radicle number), micronucleus frequency which is the simplest indicator, the most effective of cytological damage and bulb germination of *A. cepa* L. In only green tea leaf extract medium, the radicle length and radicle number of bulbs were partially reduced compared to the control bulbs germinated in the distilled water medium. While their germination percentage and fresh weight statistically indicated the same values. Besides, the mitotic index and chromosomal abnormalities in the root tip meristematic cells of *Allium cepa* bulbs germinated in alone green tea leaf extract medium increased compared to germinated control bulbs in the distilled water medium, whereas the micronucleus frequency showed statistically the same value compared to the control. In other words, it can be said that salt stress significantly inhibited the seedling growth and bulb germination of *Allium cepa*. What's more, it significantly reduced the mitotic index in the root tip meristems of the bulbs and increased the number of chromosomal abnormalities and micronuclues frequency. On the other hand, inhibitory effects of salt on the mitotic activity, seedling growth, bulb germination, chromosomal abnormalities and micronuclues frequency significantly decreased with the application of green tea leaf extract. The germination percentage, radicle lenght, radicle number, fresh weight, mitotic index, micronuclues frequency and chromosomal aberrations of the seedlings grown in 0.175 M salinity were 23 %, 10.3 mm, 12.7, 7 g, 1.2 %, 13 % and 17 % respectively, while these values became 75 %, 13.4 mm, 17.2, 13.8 g, 6.3 %, 9 % and 9.3 % in the seedlings treated with 50 mg L^{-1} green tea leaf extract.

Keywords: green tea leaf extract, chromosomal aberrations, mitotic index, salt stress, bulb germination

[1] Corresponding Author. dilekcavusoglu@isparta.edu.tr
Department of Plant and Animal Production, Isparta University of Applied Sciences, Turkey ORCID ID: 0000-0002-7963-8204

1. INTRODUCTION

Saltness is an expanding problem. The soil affected by salt is increasing worldwide through irrigation vegetation and clearance, both of which raise the water table bringing dissolved salts to the surface. One of the most serious peripheral factors that limit the efficiency of crop plants that have a major impact on agricultural productivity is defined as salt stress. Saltness on plants has three potential leffects: ı) conflict with the intake of essential nutrients ıı) reduction of water potential, ııı) direct toxicity absorbed by any Cl and Na [1, 2]. Salinity stress caused is one of the most serious environmental factors, which inhibits plant development and growth. Also it decreases crop productivity worldwide. Salt has the most harmful effect in germination cycle. In many cases, salt tolerance increases as long as plant development progresses. Plant's reactions to salt; it can vary according to the development period in which the plant is located, the concentration of salt that the stress factor, on the time it affects on the plant of salt; it may also vary depending on climate and soil properties. Primary cytogenetically effects occurring at the beginning of salt stress include retarded expansion and cell division [3]. It was found that salt had negative effects on plant growth and development by preventing the seed germination, seedling growth, enzyme activation, nucleic acid and protein synthesis and mitosis. On the other hand, salt may interfere with growth and development by disrupting endogenous hormone balance in favor of absicic acid, increasing free radical production, and causing changes in the morphological and anatomical structures of plants. During long-term exposure to salt stress, accumulation of salt ions in plant aerial parts via the transpiration stream leads to ionic stress [3, 4]. To adaptively respond and survive under salinity, plants require changes of various cellular, physiological and metabolic mechanisms, which are controlled by the regulated expression of specific stress-related genes through cascades of complex regulatory networks [5].

Green tea is one of the most ancient consumed beverages by over 2/3 of the world population. The principal constituents of green tea leaf extract (GTLE) are tannins, essential oil and caffeine. Green tea leaf extract contains catechin, gallaocatechin, epicatechin gallate, epicatechin, epigallocatechin, epigallocatechin gallate which the most active polyphenol. GTLE has anti-imflammatory, anti-bacterial, anti-allergenic, anti-viral, anti-arthritic, anti-angiogenic, anti-mutagenic, anti-diabetic, anti-cancer properties, neuroprotective, anti-aging (defensive the skin from damage arised from ionizing radiation and others, increasing collagen volume and assisting wound healing/ insect stings), protective effect against oxidative damage-dependent diseases (i.e. Parkinson, Alzheimer, heart disease, atherosclerosis), benefical effect in alcohol intoxication, effect of reducing the oxidation of food products and extend their shelf life, thermogenesis (enhancing weight loss), cholesterol-lowering effects, preventive effect of tooth decay [6, 7].

The *Allium cepa* bioassay, which was applied in this study, has excellent correlation with mammalian systems. These bioassay is a fast, inexpensive, sensitive method and easily handled toxicity test, which has advantages over other short-term tests that require previous preparations of tested samples. The *Allium cepa* test facilitates testing different toxicity endpoints *viz.* mitotic index, root growth inhibition [8], the chromosomal aberrations, nuclear abnormalities and occurrence of micronuclei [9]. For this reason, *Allium cepa* was used as a test material in this study. There is no study on the influences of green tea leaf extract on the seedlings growth, bulb germination, chromosomal aberrations, mitotic activity and micronucleus frequency under saline and normal conditions. Therefore, this work was designed to investigate the efficiency of green tea leaf extract on the chromosomal aberrations, seedling growth, micronuclues frequency, bulb germination and mitotic activity in *Allium cepa* L. subject to salt stress.

2. MATERIALS and METHODS

2.1. Green Tea Leaf Extract, The Bulb and Salt Concentrations

Uniform and healty small bulb (*Allium cepa* L., 2n=16) that used for the assay were obtained from Erdoğan Ekinci Ltd. Şti., Antalya, Turkey. Green tea leaf extract (60 capsules of 380 mg) was purchased from Sepe Natural. By a preliminary investigation carried out, firstly it was determined as 0.175 M salt concentration (tried out concentrations of 0.10, 0.125, 0.15, 0.175, 0.20, 0.225, 0.25, 0.275, 0.30 M) which largely preventing the germination of *Allium cepa* L. Then it was designated as 50 mg L^{-1} green tea leaf extract concentration (tried out concentrations of 1, 5, 10, 20, 30, 40, 50, 100, 200, 300, 400, 500, 600, 700, 800, 900 and 1000 mg L^{-1} dose of green tea leaf extract) alleviating the adverse effects of this salt concentration (0.175 M) on the bulb germination and seedling growth. Thus, 50 mg/L green tea leaf extract and 0.175 M NaCl (salt) concentration used for this study.

2.2. Germination of the Bulbs

The germination assay of the bulbs was carried out with *Allium cepa* bulbs, that are physiologically homogeneous. Bulbs were germinated at incubated at 20˚C in the darkness and they were surface-disinfected in 2.5% sodium hypochloride solution for ten minutes. Then, they washed in ultra-distilled water for 24 hours. For germination, 20 bulbs from each treatment group were placed in 1700-mL plastic boxes. For 7 consecutive days, the study included four groups of boxes with bulbs:

- Control (group I), to which bulbs were treated with distilled water
- Group II, to which bulbs were treated with alone 0.175 M NaCl
- Group III, to which bulbs were treated with a 50 mg L^{-1} dose of GTLE
- Group IV, to which bulbs were treated with both GTLE (50 mg L^{-1}) and NaCl (0.175 M)

These bulbs into plastic boxes were germinated at incubated. When the roots reached about a length of ten cm (approximately 7 days after the beginning of the assay), their radicle numbers and germination percentages were recorded. The radicle lengths were measured in mm, additionally the fresh weights in g/seedling were determined.

2.3. Cytological Analysis

For cytological and physiological studies, root tips were excised after a few days. Cytological preparations pretreated with saturated para-dichlorobenzene for 4 hrs, carried out by fixation of roots in a mixture of 3: ethanol / 1: glacial acetic acid at room temperature for 24 hrs. Then stored at 70 % ethanol in 4ºC until used for analyses. Hydrolysis were done by 5 N HCl for 45 min, root tips were stained using the Feulgen, squashed and then smashed in a drop acetic acid of 45% [10]. Microscopic slides made permanent by mounting in balsame. Mitotic index was expressed in percentage by counting cells of different mitotic phases in total number of cells. Mitotic phases were also expressed as percentage of total number of cells. Chromosomal aberrations were recorded. The mitotic index was calculated by means of this formula, 2,000 cells (three slides = 6,000 total cells).

Mitotic index (%) = Number of cells in mitosis × 100 / total number of cells

Observations of counted cells in each application groups were performed using an Olympus CX41 microscope and photographed at X500 magnification.

2.4. Statistical Analysis

Data collected from physiological and cytogenetical parameters using the SPSS program according to Duncan's multiple range test in triplicate, all statistical analyses were performed [11].

3. RESULTS

3.1. Effects of Green Tea Leaf Extract on the Seedling Growth and Bulb Germination

Table 1 results clearly demonstrate that while germination percentage and fresh weight of group III showed statistically the same values as control (group I), their radicle number and radicle length partly decreased according to control bulbs germinated in distilled water.

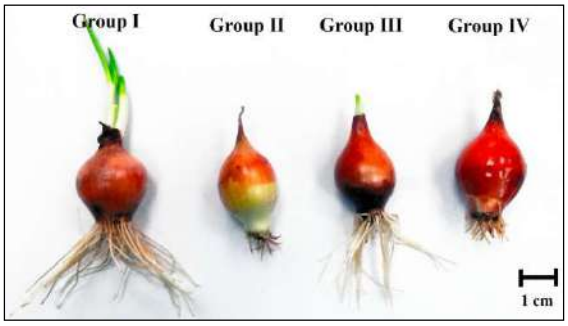

Figure 1. Root tip cells of *Allium cepa* showing germination situations at the end of 7 day. Group I (control): distilled water, Group II: 0.175 M NaCl alone, Group III: 50 mg L^{-1} GTLE and Group IV: 50 mg L^{-1} GTLE+0.175 M NaCl, Scale bar = 1 cm

NaCl showed an inhibitory activity on all growth parameters examined. For instance, control bulbs germinated in distilled water after 7 days showed 100% germination, whereas this value was 23 % in group II bulbs germinated at 0.175 M salinity. That is to say, NaCl prevented 77 % *Allium cepa* bulb germination. The restricting effect of NaCl stress on the bulb germination markedly mitigated by green tea leaf extract (GTLE) application. Group IV bulbs treated with GTLE at said salt level showed 75 % germination (Fig. 1). In addition, GTLE continued its success on the seedling growth parameters like fresh weight, radicle number and radicle length. Radicle length, radicle number and fresh weight of group II bulbs grown in 0.175 M salted were 10.3 mm, 12.7 and 7.0 g, respectively while these values became 13.4 mm, 17.2 and 13.8 g in group IV (Tab. 1).

Table 1. Effect of green tea leaf extract on some growth parameters of *Allium cepa*

Groups	Growth parameters			
	Germination percentage (%)	Radicle length (mm)	Radicle number	Fresh weight (g/seedling)
Group I	*100 ±0.0^{c}	63.5 ± 0.5^{d}	63.2 ± 0.6^{d}	14.2 ± 0.8^{b}
Group II	23 ± 2.8^{a}	10.3 ± 0.3^{a}	12.7 ± 0.5^{a}	7.0 ± 0.5^{a}
Group III	100 ± 0.0^{c}	53.9 ± 0.2^{c}	39.4 ± 0.6^{c}	15.4 ± 1.2^{b}
Group IV	75 ± 5.0^{b}	13.4 ± 0.6^{b}	17.2 ± 0.5^{b}	13.8 ± 0.6^{b}

* The difference between the values in each column and the same letters isn't significant at the 0.05 level (±SD). Group I (control): distilled water, Group II: 0.175 M NaCl alone, Group III: 50 mg L^{-1} GTLE and Group IV: 50 mg L^{-1} GTLE + 0.175 M NaCl

3.2. Effects of Green Tea Leaf Extract on The Mitotic Activity, Chromosomal Aberrations and Micronucleus Frequency

Exposure to 0.175 M salt revealed significant inhibition of the mitotic index and induction of the chromosomal aberrations and micronucleus frequency. That is to say, the mitotic index in root-tip meristematic cells of *Allium cepa* germinated in containing 0.175 M salt media showed a 89% reduction compared to group I bulbs and the mitotic aberrations and micronucleus frequency flashily increased. Micronucleus frequency of group III bulbs germinated in only GTLE medium was remained the same compared to group I (control) samples. This application increased the mitotic index and chromosomal aberrations (Tab. 2). Simultaneous GTLE+NaCl treatment (group IV) may be successful in improving reverse effects of salt on all cytogenetical parameters. Statistically, all values mentioned here are highly significant at level of significance $P \leq 0.05$. Table 2 summarizes all cytogenetic parameters obtained from the control and other treated bulbs.

Table 2. Effect of green tea leaf extract on some cytogenetic parameters of *Allium cepa*

Groups	Mitotic index (%)	Micronucleus frequency (%)	Chromosome aberrations (%)
Group I	*11.6 ± 1.0^{c}	0.0 ± 0.0^{a}	0.0 ± 0.0^{a}
Group II	1.2 ± 0.2^{a}	13.0 ± 1.0^{c}	17.0 ± 0.4^{d}
Group III	16.2 ± 0.6^{d}	0.0 ± 0.0^{a}	4.6 ± 1.0^{b}
Group IV	6.3 ± 0.1^{b}	9.0 ± 1.0^{b}	9.3 ± 0.3^{c}

* The difference between the values in each column and the same letters isn't significant at the 0.05 level (±SD). Group I (control): distilled water, Group II: 0.175 M NaCl alone, Group III: 50 mg L^{-1} GTLE and Group IV: 50 mg L^{-1} GTLE+0.175 M NaCl

The micronucleus formations observed during the microscopic examination of root tip meristematic cells of *Allium cepa* are shown in Figure 2 and abnormal mitosis phases are shown in Figure 3. The chromosomal abnormalities were observed nuclear disintegration, accumulation of micronuclei in cell, chromosomal rings, ball metaphase/telophase, stickiness in metaphase, metaphase/anaphase with chromosome losses, telophase/anaphase with chromosome bridges, vagrant chromosome in anaphase/telophase with broken chromosome bridges, disorientation at anaphase, diagonal at telophase. The greatest abnormalities percentage in root-tip cells treated with salt or GTLE were nuclear peak and micronucleus in this study.

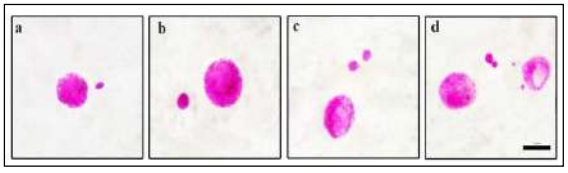

Figure 2. The micronucleus formations observed in *Allium cepa* L. meristematic cells exposed to Group II and Group IV; a, b: micronucleus c, d: accumulation of micronuclei in cell, Scale bar=10 µm

4. DISCUSSION

4.1. Physiological and Cytogenetical Effects of Green Tea Leaf Extract under Non-Stress Conditions

Unless there are generally stress conditions, there is no need for exogenously add any plant growth regulator during germination. Exogenously addition of a plant growth regulator in non-stress conditions can cause negative or positive effect on the seedling growth and bulb germination [12]. But, there is no study about the influences of green tea leaf extract on the seedling growth and bulb germination under non-stress conditions. Therefore, for the first time, the effects of GTLE application on the seedling growth, bulb germination, chromosomal aberrations, mitotic activity and micronucleus frequency under stress-free conditions requested to be tested in the laboratory study. Results of this study showed that the radicle number and radicle length of the bulbs germinated in only GTLE treatment were partially reduced but their fresh weight and germination percentages of the mentioned bulbs statistically showed the same values compared to those of the control bulbs germinated in distilled water (Table 1).

Moreover, some growth regulators may cause particularly cell disortions, chromosomal aberrations and mitotic irregularities especially if stress conditions aren't present [13, 14]. Although a number of researchers state that some plant extracts that have been widely used in recent years have significant mutagenic effects [15], there is no extent study relating to the impacts of GTLE on the chromosomal abnormalities, micronucleus frequency and mitotic activity subject to non-stress conditions. For this reason, this study was examined the first time whether GTLE affected these parameters at normal conditions. This data obtained in the present study indicated that the mitotic index in root tip meristem cells of *Allium cepa* (Group III) bulbs exposed to GTLE application in non-stress conditions increased 39% according to ones of the group I bulbs germinated in distilled water medium. That is, 50 mg L^{-1} GTLE treatment showed a triggering

influence on the mitotic activity by accelerating cell division.

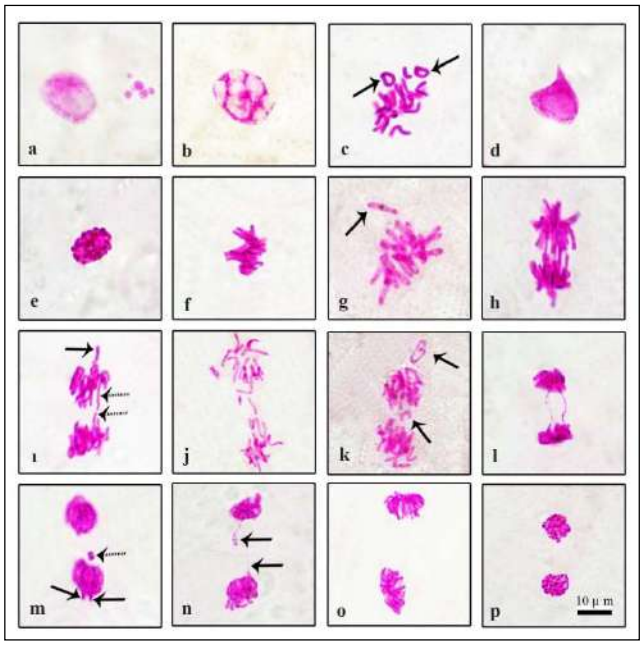

Figure 3. Different types of chromosomal aberrations observed in *Allium cepa* L. meristematic cells exposed to Group II, Group III and Group IV; a: accumulation of micronuclei in cell b: nuclear disintegration c: chromosomal rings= arrows d: nuclear peak e: ball metaphase f: stickiness in metaphase g: metaphase with loss chromosome= arrow h: anaphase with chromosome bridges ı: vagrant chromosome (arrow) in anaphase with broken chromosome bridges=patterned j: disorientation at anaphase k: anaphase with chromosome losses= arrows l: telophase with chromosome bridges m: vagrant chromosomes (arrows) in telophase with micronucleus= patterned n: telophase with broken chromosome bridges= arrows o: diagonal at telophase p: ball telophase (Scale bar = 10 µm)

4.2. Physiological and Cytogenetical Effects of Green Tea Leaf Extract under Saline Conditions

It is well-known that saltinity stress has diverse influences on plant physiological processes such as increased ion toxicity and respiration rate, mineral distribution, change in plant growth, membrane permeability [16] and decreased of photosynthesis efficiency [17].

The results from table 1 clearly demonstrated that as expected, the seedling growth and bulb germination of *Allium cepa* inhibited under salinity medium. Salinity stress can be preventive in many ways. Seed germination can be prevented by causing to change in water situation of the seed, thus prevent water intake [18]. Results of the present study displaying the diminish in water content and the fresh weight of the seedlings in salted conditions can be explained by the inability of roots to receive enough water due to high osmotic pressure in medium. Restrictive treatment of salt on the fresh weight, radicle number and radicle length might result from reducing cell division, protein synthesis and nucleic acid [19].

On the contrary, by GTLE application, inhibitory effect of salt stress on parameters such as the bulb germination, seedling growth (fresh weight, radicle number and radicle length) was significantly eliminated (Tab. 1). Unfortunately, to date, there isn't extant literatüre data relating to effects of GTLE on the seedling growth and bulb germination exposed to saline conditions. This GTLE alleviates salt stress on the bulb germination and seedling growth could be noticed by decreasing the osmotic influence of salt. For example, at 0.175 M NaCl treatment, GTLE application raised markedly growth parameters of seedlings compared to the control indicates this probability (Tab. 1).

Effects of the determined concentrations of a test chemical on the chromosome aberration and mitotic index are used respectively as parameters of cytotoxicity and genotoxicity [20]. The inhibitory and cytotoxic effects of salt stress on the mitotic activity have long been known. A high concentration of salt causes total inhibition of the chromosomal abnormalities and mitotic activity in root-tip cells according to some researchers [21]. With this study, it should be noted that salinity negatively affects the mitotic activity, chromosome behaviors and micronucleus frequency in *Allium cepa* root meristem cells. Data of this study showed that salt showed a greater number of the chromosomal abnormalities and micronucleus frequency compared to controls and reduced the mitotic index by 89 % and this reduced was achieved by reducing the number of cells entering mitotic division. For example, the micronucleus frequency and chromosomal aberration in the root tip meristematic cells of the

bulbs germinated exposed to distilled water were 0.0 %, 0.0 % while it were 13.0 %, 17.0 % at 0.175 M saltness (Tab. 2). Besides, simultaneous GTLE+NaCl application could be succeeded in alleviating of the detrimental influence of salinity on the chromosome aberration, micronucleus frequency and mitotic activity. Limit of mitotic inhibition by this treatment reached to 6.3 %. So, the chromosomal aberration decreased by 45%, the frequency of micronucleus decreased by 30% with the application of simultaneous GTLE+NaCl. This result shows GTLE repair role against salt injuries during *Allium cepa*'s mitosis.

Chromosome aberrations (CAs) are change in chromosomal material or exchange in the structure of the chromosome resulting from breakage. CAs induction could affect the fertility, vigour, competitive or yield ability of the exposed plants [22]. The presence of nuclear disintegration (Fig. 3b) offer cytological evidences for the inhibitory action on DNA biosynthesis [23]. Diagonal orientation (Fig. 3o) is caused by a slight tilt in the spindle apparatus [24]. Vagrant chromosomes (Fig. 3ı, m) which might arise as a consequence of disturbances in the mitotic spindle were categorized as indicatives of aneugenic action. The micronucleus (Fig. 3a, m) is composed either of all of the chromosomes that do not migrate during anaphase as a result of spindle dysfunction or of small chromatin fragments which arise as a consequence of chromosomal break. The loss chromosomes (Fig. 3g, k) are typically associated with mitotic spindle malfunction [25]. Chromosomal ring (Fig. 3c) is the result of chromosome losses in the telomere domain [26]. The ball metaphase (Fig. 3e) may be due to the localized activity of spindle apparatus in the centre, so that the centromeres remain in the equator and arms spread in different directions in the form of a ball. The bridges (Fig. 3h, l) are probably caused by joining and interruption to chromatids or chromosomes. Stickiness in metaphase (Fig. 3f) is an indicates that chemical substance has a high toxicity and might cause the cell deaths by inducing unrecoverable damages [27]. Disorientation at anaphase (Fig. 3j) may be due to spindle apparatus disturbance which allows that the chromosomes to spread irregularly over the cell [28]. Shortly, green tea leaf extract may be function as a stimulator triggering the protein synthesis required for the normal cell division and accelerate the mitotic cycle.

There is no literatures data on the influences of GTLE application under salted conditions on cytogenetical and physiological parameters examined in the study. Therefore, for the first time, this study results have been reported particularly in saline conditions. As a result, this study shows that GTLE can significantly increase the activations such as the seedling growth and bulb germination in either alone or saline conditions. But the mechanisms by which salt inhibits growth are controversial and complex, also they might vary according to cultivar and species. An universal mechanism hasn't been established yet. While the causes of salty have been determined, it is still very poor to understand the mechanisms by which salty prevents plant growth. Therefore further work should be done to learn more about the effect of GTLE on cell division, cell cycle and germination molecular metabolism. This literature study can serve to present new conceptual tools for designing salt tolerance hypotheses in plants.

5. REFERENCES

[1] T.J. Flowers and A.R. Yeo, "Ion relations of plant under drought and salinity", Australian Journal of Plant Physiology, vol. 13, pp. 75–91, 1986.

[2] T.J. Flowers and A.R. Yeo, "Breeding for salinity resistance in crop plants: where next?", Australian Journal of Plant Physiology, vol. 22, pp. 875–884, 1995.

[3] P. Carillo, M.G. Annunziata, G. Pontecorvo, A. Fuggi, and P. Woodrow, "Salinity stress and salt tolerance", in: Abiotic stress in plants - mechanisms and adaptations, pp. 21–38, 2011.

[4] A.K. Parida and A.B. Das, "Salt tolerance and salinity effects on plants: a

review", Ecotoxicology and Environmental Safety, vol. 60, pp. 324–349, 2005.

[5] U. Deinlein, A.B. Stephan, T. Horie, W. Luo, G. Xu, and J.I. Schroeder, "Plant salt-tolerance mechanisms", Trends Plant Science, vol. 19, pp. 371–379, 2014.

[6] D.G. Nagle, D. Ferreira, and Y.D. Zhou, "Molecules of interest epigallocatechin-3-gallate (EGCG): chemical and biomedical perspectives", Phytochemistry, vol. 67, pp. 1849–1855, 2006.

[7] S.Y. Asadi, P. Parsaei, M. Karimi, S. Ezzati, A. Zamiri, F. Mohammadizadeh, and M. Rafieian-Kopaei, "Effect of green tea (*Camellia sinensis*) extract on healing process of surgical wounds in rat", International Journal of Surgery, vol. 11, no. 4, pp. 332-7, 2013.

[8] G. Fiskesjo, "The *Allium* test as a standard in environmental monitoring", Hereditas, vol. 102, no. 1, pp. 99–112, 1985.

[9] W.F. Grant, "Chromosome aberration assays in *Allium*: a report of the united states environmental protection agency's gene-tox program", Mutation Research/Reviews in Genetic Toxicology, vol. 99, pp. 273–291, 1982.

[10] P.C. Sharma and P.K. Gupta, "Karyotypes in some pulse crops", Nucleus, vol. 25, pp. 181–185. 1982.

[11] D.B. Duncan, "Multiple range and multiple F tests", Biometrics, vol. 11, pp. 1-42, 1955.

[12] D. Çavuşoğlu, "Effects of L-lysine on cytogenetical and physiological parameters in *Allium cepa* L. under salt stress", Bangladesh Journal of Botany, vol. 48, no. 3, pp. 625-632, 2019.

[13] D. Çavuşoğlu, "Physiological and cytogenetical effects of L-tyrosine in *Allium cepa* L. exposed to NaCl stress", Fresenius Environmental Bulletin, vol. 28, no. 12A, pp. 9753-9759, 2019.

[14] K. Çavuşoğlu, S. Cadıl, and D. Çavuşoğlu, "Role of potassium nitrate (KNO_3) in alleviation of detrimental effects of salt stress on some physiological and cytogenetical parameters in *Allium cepa* L.", Cytologia, vol. 82, no. 3, pp. 279-286, 2017.

[15] MC. Karaismailoğlu, "Investigation of the cytotoxic and genotoxic effects of *Artemisia annua* methanol extract with the *Allium* test", Ekoloji, vol. 23, pp. 64-74, 2014.

[16] N.K. Gupta, S.K. Meena, S. Gupta, and S.K. Khandelwal, "Gas exchange, membrane permeability, and ion uptake in two species of Indian jujube differing in salt tolerance", Photosynthetica, vol. 40, pp. 535-539, 2002.

[17] O.H. Sayed, "Chlorophyll fluorescence as a tool in cereal crop research", Photosynthetica, vol. 41, pp. 321-330, 2003.

[18] T.J. Flowers, and T.D. Colmer, "Plant salt tolerance: adaptations in halophytes," Annals of Botany, vol. 115, no. 3, pp. 327-331, 2015.

[19] K.F. Mccue and A.D. Hanson, "Drought and salt tolerance: towards understanding and application", Trends Biotechnology, vol. 8, pp. 358-362, 1990.

[20] H. Nefic, J. Musanovic, A. Metovic, and K. Kurteshi, "Chromosomal and nuclear alterations in root tip cells of *Allium cepa* L. induced by *alprazolam*", Medical Archives, vol. 67, pp. 388–392, 2013.

[21] S. Radic, M. Prolic, M. Pavlica, and B. Pevalek-Kozlina, "Cytogenetic effects of osmotic stress on the root meristem cells of *Centaurea ragusina* L.", Environmental and Experimental Botany, vol. 54, pp. 213-218, 2005.

[22] M. Kara, M.A. Tanda, and A. Ateş, "Cytogenetic effects of the insecticide cypermethin on the root meristems of *Allium*

cepa L." Turkish Journal of Biology, vol. 18, pp. 323–331, 1994.

[23] F.I. Akaneme and I.V. Iyioke, "Mutagenic potentials of the sterilizing fluid-purital on root tip mitosis of *Allium cepa*", Bio-Research, vol. 6, pp. 293–297, 2008.

[24] P.K. Renjana, S. Anjana, and J.E. Thoppil, "Evaluation of genotoxic effects of baking powder and monosodium glutamate (MSG) using *Allium cepa* assay", International Journal of Pharmacy and Pharmaceutical Sciences, vol. 5, 132-139, 2013.

[25] D.M. Leme and M.A. Marin-Morales, "*Allium cepa* test in environmental monitoring: a review on its application", Mutation Research, vol. 682, pp. 71–81, 2009.

[26] N. Khanna and S. Sharma, "*Allium cepa* root chromosomal aberration assay", Indian Journal of Pharmaceutical and Biological Research, vol. 1, pp. 105-119, 2013.

[27] S. Türkoğlu, "Genotoxicity of five food preservatives tested on root tips of *Allium cepa* L." Mutation Research, vol. 626, no. 1-2, pp. 4-14, 2007.

[28] S.M. Amer and E.M. Alı, "Cytological effects of pesticides. V. effects of some herbicides on *Vicia faba*", Cytologia, vol. 39, pp. 633-643, 1974.

JOURNAL OF SCIENCE
SAKARYA UNIVERSITY

Sakarya University Journal of Science

ISSN 1301-4048 | e-ISSN 2147-835X | Period Bimonthly | Founded: 1997 | Publisher Sakarya University
http://www.saujs.sakarya.edu.tr/en/

Title: Synthesis and Characterisation of Polyaromatic Chalcones with Electron Donation

Authors: Alparslan Atahan
Recieved: 2019-07-20 16:43:02

Accepted: 2020-01-09 14:09:40

Article Type: Research Article
Volume: 24
Issue: 2
Month: April
Year: 2020
Pages: 347-356

How to cite
Alparslan Atahan; (2020), Synthesis and Characterisation of Polyaromatic Chalcones with Electron Donation. Sakarya University Journal of Science, 24(2), 347-356, DOI: https://doi.org/10.16984/saufenbilder.594611
Access link
http://www.saujs.sakarya.edu.tr/tr/issue/52471/594611

Sakarya University Journal of Science 24(2), 347-356, 2020

Synthesis and Characterisation of Polyaromatic Chalcones with Electron Donation

Alparslan ATAHAN*[1]

ABSTRACT

In this study, a series of chalcone derivatives was successfully synthesized via condensation of 1-acetylpyrene with dimethylamine, diphenylamine or carbazole containing benzaldehyde derivatives at basic conditions. Spectral characterisations were acquired by 1 and 2 dimensional NMR techniques and FTIR. In addition, UV-vis and thermal analysis studies were performed to determine their absorption properties and thermal behaviours, respectively. Lastly, surface and film generation properties were investigated by the means of SEM images on ITO glass to determine usability potential in organic electronics.

Keywords: Chalcone, Pyrene, Triphenylamine, Carbazole, Characterisation.

1. INTRODUCTION

Chalcones which have 1,3-diaryl-2-propen-1-one skeleton are a family of aromatic ketones and have huge fascination due to their simple chemistry and pervasive applications in medicinal [1,2], and material chemistries [3,4]. In addition, they are quite functional as chemical intermediates in the synthesis of many significant compounds such as quinolines [5], pyrimidines [6], aza-BODIPY's [7], chromones [8], and oxazoles [9] etc.

As a bioactive molecule, it is well known that natural and synthetic chalcone derivatives exhibit wide spectrum of chemotherapeutic properties such as antimicrobial [10], antioxidant [11], anticancer [12], enzyme inhibitor [13], anti-inflammatory [14], antimalarial [15] and more. These mentioned properties can be attributed to their linear and nearly planar structure and extended conjugation.

Alongside of their broad-spectrum bioactivity and importance in synthetic chemistry, they have characteristic electronic structure due to conjugation and donor-acceptor structure and this property makes them functional compounds in photophysics [16] as well. In this context, they have a wide range of applications as promising materials for non-linear optics [17], also in electro-active fluorescence [18]. In addition, chalcones are useful compounds as fluorescent sensors for the recognition of some cations [19].

*Corresponding Author: alparslanatahan@duzce.edu.tr
[1]Düzce University, Faculty of Technology, Department of Polymer Engineering, 81620, Düzce, TURKEY.
ORCID: 0000-0001-8904-9377

Chalcone structures are easily prepared via Claisen-Schmidt condensation between acetophenone and benzaldehyde or their substituted derivatives [20]. In the same way, their polyaromatic (i.e., anthracene, phenathrene, pyrene) counterparts can be obtained via replacing one (or two) ring(s) by a polyaromatic group, generating the so-called polyaromatic chalcones. These structures are commonly prepared by systematic chemical modifications via condensation using polyaromatic aldehyde and required substituted acetophenone or vice versa [21, 22]. The addition of a polyaromatic scaffold into chalcone compounds can bring about significant improvement in their physical properties such as absorption, fluorescence, and beneficial sensing capacity against cations, anions, or some molecules [23-25]. It is believed that these improved performances depend on the chemical unification of these electronically specific groups in the chalcone structure.

In this context, pyrene is a well-known polyaromatic hydrocarbon and has also quite interesting properties including high fluorescence [26], high optical contrast [27], and white-light emission [28]. Moreover, various pyrene derivatives exhibit surprising exciplex emission at higher concentrations or solid state [29,30]. In other words, π-stacking or intermolecular interaction of among pyrene rings can change whole photophysical characteristics and this phenomenon promotes an increase or quench at emission.

Since the promising potential of mentioned structures in significant areas, it is important to report novel compounds and their critical properties. Taking into account this fact and our previous studies [31,32], herein, the objective has been to generate polyaromatic chalcones which are containing various electron donating groups. In order to accomplish this objective, mentioned polyaromatic chalcones have been successfully prepared and characterised by ^{1}H NMR, ^{13}C NMR, COSY, and FTIR. UV-vis studies and thermal gravimetric analyses have been performed to determine their absorption properties and thermal behaviours, respectively. Lastly, SEM images on ITO glass have been taken to determine surface and film generation properties which are important for usability in organic electronics.

In structural characterisation, proposed structures have been confirmed and *trans* conformations have been observed for all the target compounds. From UV-vis studies, it has been shown that the target compounds have a main absorption band between ~380-430 nm. In thermal characterisation, the target compounds were quite stable and masses were preserved up to about 350 ºC. Finally, SEM images showed that the compounds have good film generation properties on ITO glass.

2. MATERIALS AND METHODS

2.1 *General*

Chalcone compounds (**3a-c**) were synthesized via Claisen-Schmidt condensation at basic conditions. All the reagents and chemicals were purchased from Sigma-Aldrich**,** Merck or Fluka and they were AR grade with high purity. Used solvents were dried, distilled and purified according to the standard methods. Silica Gel TLC plates were used to monitor the reactions and crude products were purified by crystallization or silica gel column chromatography. NMR spectra were carried out by 400 MHz Bruker NMR Spectrometer in DMSO-d6. Chemical shifts were reported in ppm from tetramethylsilane ($(CH_3)_4Si$) for ^{1}H and ^{13}C. FTIR spectra were recorded by Shimadzu Prestige-21 spectrometer combined with an ATR system. Melting points were determined by Electrothermal IA-9200 apparatus. TGA analyses were performed Shimadzu DTG 60H - DSC 60 Thermal Analysis System. Absorption studies were realized by a PG Instruments T80 double beam spectrophotometer by using a quartz cells. FEI Quanta FEG 250 Scanning Electron microscope was used to get SEM images on ITO glass.

2.2 *Chemistry*

The target compounds were obtained as shown in Figure 1 followed by preparing starting compounds (1-acetylpyrene, 4-diphenylamino benzaldehyde, 4-(carbazol-9-yl)benzaldehyde) according to literature procedures [33-35].

Chemical structures were illuminated by ^{1}H-NMR, ^{13}C-NMR, COSY and FT-IR.

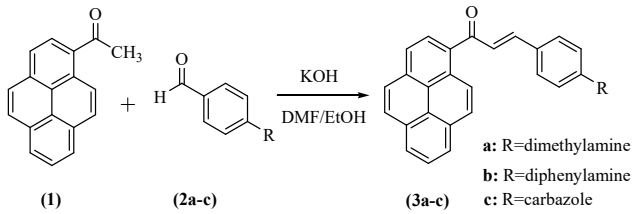

Figure 1. Synthesis of target compounds (3a-c)

2.2.1 *Synthesis of 1-acetyl pyrene*

Synthesis of 1-acetyl pyrene was accomplished according to the literature procedure [33]. Structure verification and purity control were realized by hydrogen NMR spectroscopy. M.p.: 172-173 ºC, yield: 65 %.

2.2.2 *Synthesis of 4-diphenylaminobenzaldehyde*

4-Diphenylaminobenzaldehyde was synthesized as reported in the literature procedure [34]. Structure verification and purity control were realized by hydrogen NMR spectroscopy. M.p.: 132-135 ºC, yield: 92 %.

2.2.3 *Synthesis of 4-(carbazol-9-yl)benzaldehyde*

4-(carbazol-9-yl)benzaldehyde was prepared as reported elsewhere [35]. Structure verification and purity control were realized by hydrogen NMR spectroscopy. M.p.: 154-157 ºC, yield: 87 %.

2.2.4 *Synthesis of chalcones (3a-c)*

The target chalcone compounds were successfully synthesized by Claisen-Schmidt condensation reaction as explained below. 0.122 g (0.5 mmol) of 1-acetylpyrene and 1.0 equi-molar amount of corresponding aldehyde were mixed in 20 mL of ethanol/DMF mixture (50/50 %, v/v) in the presence of 1.0 equivalent (0.028 g) KOH as catalyst and magnetically stirred at ambient temperature. After understanding the completion of the reactions by thin layer chromatography in three to five days, volatiles evaporated and resulting mixtures quenched with cold water. The precipitates were air-dried and re-crystallized in DCM/hexane or EtOAc/hexane to get pure chalcone products.

*(E)-3-(4-(dimethylamino)phenyl)-1-(pyren-1-yl)prop-2-en-1-one (**3a**)*

This target compound was reported previously [33]. ^{1}H NMR (400 MHz, DMSO-d_6) δ: 8.51 (d, *J*: 9,2 Hz, 1H), 8.41-8.26 (m, 7H), 8.14 (t, *J*: 7.6 Hz, 1H), 7.61 (d, *J*: 8,8 Hz, 2H), 7.51 (d, *J*: 15,6 Hz, 1H), 7.37 (d, *J*: 15,6 Hz, 1H), 6.71 (d, *J*: 8,8 Hz, 2H), 2.99 (s, 6H); ^{13}C NMR (100 MHz, DMSO-d_6) δ: 195.1, 152.6, 147.3, 135.2, 132.7, 131.3 (2C), 131.2, 130.6, 129.2, 129.1, 128.7, 127.8, 127.2, 126.6, 126.5, 126.2, 125.0, 124.9, 124.5, 124.2, 122.1, 122.0, 112.2(2C), 40.1(2C); FTIR: 3039, 2970, 1639, 1560, 1514, 1166, 840, 698 cm^{-1}; M.p.: 166-168 ºC; yield: 87 %.

*(E)-3-(4-(diphenylamino)phenyl)-1-(pyren-1-yl)prop-2-en-1-one (**3b**)*

^{1}H NMR (400 MHz, DMSO-d_6) δ: 8.54 (d, *J*: 9,2 Hz, 1H), 8.39-8.35 (m, 4H), 8.31-8.24 (m, 3H), 8.12 (t, *J*: 7.6 Hz, 1H), 7.64 (d, *J*: 8.4 Hz, 2H), 7.54 (d, *J*: 16.0 Hz, 1H), 7.49 (d, *J*: 16.0 Hz, 1H), 7.35 (t, *J*: 7.6 Hz, 4H), 7.14 (t, *J*: 7.6 Hz, 2H), 7.10 (d, *J*: 8.0 Hz, 4H), 6.86 (t, *J*: 8.4 Hz, 2H); ^{13}C NMR (100 MHz, DMSO-d_6) δ: 195.2, 150.3, 146.6 (2C), 145.8, 134.5, 133.0, 131.2, 130.9 (2C), 130.6, 130.3 (4C), 129.5, 129.3, 128.9, 127.7, 127.6, 127.2, 126.9, 126.7, 126.4, 125.9 (4C), 125.1, 125.0 (2C), 124.9, 124.8, 124.5, 124.1, 120.9 (2C); FTIR: 3040, 2980, 1656, 1575, 1504, 1282, 842, 700 cm^{-1}; M.p.: 153-155 ºC; yield: 90 %.

(E)-3-(4-(9H-carbazol-9-yl)phenyl)-1-(pyren-1-yl)prop-2-en-1-one (3c)

^{1}H NMR (400 MHz, DMSO-d_6) δ: 8.69 (d, *J*: 9,2 Hz, 1H), 8.54 (d, *J*: 8.0 Hz, 1H), 8.47-8.30 (m, 6H), 8.26 (d, *J*: 8.0 Hz, 2H), 8.19-8.14 (m, 3H), 7.88 (d, *J*: 16.0 Hz, 1H), 7.81 (d, *J*: 16.0 Hz, 1H), 7.73 (d, *J*: 8.0 Hz, 2H), 7.49-7.44 (m, 4H), 7.32 (t, *J*: 6,4 Hz, 2H); ^{13}C NMR (100 MHz, DMSO-d_6) δ: 195.0, 144.6, 140.2 (2C), 139.3, 134.0, 133.7, 133.4, 131.2, 131.1 (2C), 130.6, 129.8, 129.6, 129.2, 128.1, 127.8, 127.4, 127.3 (3C), 126.9, 126.8 (2C), 126.6, 125.0, 124.9, 124.5, 124.1, 123.5 (2C), 121.1 (2C), 120.9 (2C), 110.3 (2C);

FTIR: 3039, 2980, 1653, 1583, 1514, 1450, 1222, 831, 740 cm^{-1}; M.p.: 184-186 ºC; yield: 92 %.

2.3 *Absorption Studies*

All the absorption measurements were performed at 10^{-5} M concentration. For this, firstly, a certain amounts of **3a-c** were dissolved in 10 mL of each solvent to get 10^{-3} M solutions. 1:100 dilution of this stock solution gave 10^{-5} M solutions to be used for absorption spectra.

2.4 *Thermal Analysis*

Thermal properties were studied using 5-10 mgs of target compounds (3a-c). Thermograms were obtained in a platinum pan between room temperature and 850 °C. The curves were obtained under nitrogen atmosphere with a flow rate of 100 mL/min. The heating rate was 10 °C/min.

2.5 *Surface Analysis Studies*

Target compounds were dissolved in dichlorobenzene at 1.0 M concentration and spin coated on appropriately cleaned ITO glass. After annealing on 150 °C plate for 60 seconds, SEM images were recorded to describe surface properties.

3. RESULTS AND DISCUSSION

3.1 *General*

The target compounds were successfully synthesized by using 1-acetyl pyrene and electron donation functionalized benzaldehyde derivatives. ^{1}H-NMR, ^{13}C-NMR, COSY, and FTIR analyses completely verified the proposed structures. All the target compounds were isolated with good yields (~90% levels).

3.2 *Structural Characterisation*

In ^{1}H NMR analysis, firstly, expected specific peaks of olefinic bond and electron donation group bonded phenyl ring on chalcone structures can be clearly seen. These signal systems can be easily selected by the means of signal shape, chemical shifts and coupling constants. For example, the AA' signal systems of olefinic bond of **3a** can be seen as two doublets at δ = 7.35 and 7.55 with J = 15.6 Hz coupling constant. Like this, these signals for **3b** and **3c** can be seen at similar shape and chemical shifts (7.54, 7.49; J=16 Hz and 7.88, 7.81; J=16 Hz, respectively). In addition, phenyl ring signals associated with benzaldehyde can be seen as AA'BB' system as written above.

On the other hand, pyrene related protons have been resonated usually as multiplets at lower magnetic fields due to lower electron densities. In ^{13}C NMR spectra, carbonyl carbon signals of all chalcones can be clearly seen at around δ = 190 ppm and other carbon signals are completely in accordance with proposed structures.

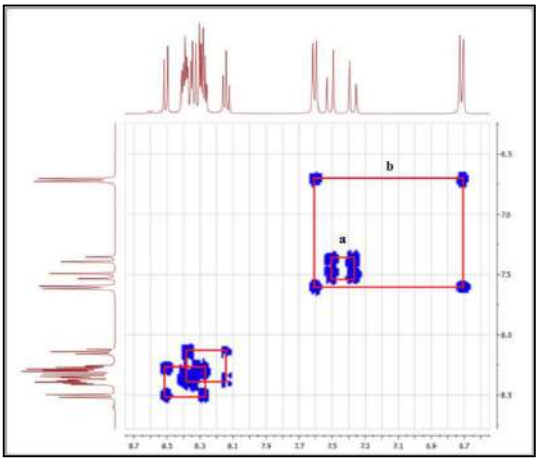

Figure 2. COSY spectrum of **3a**

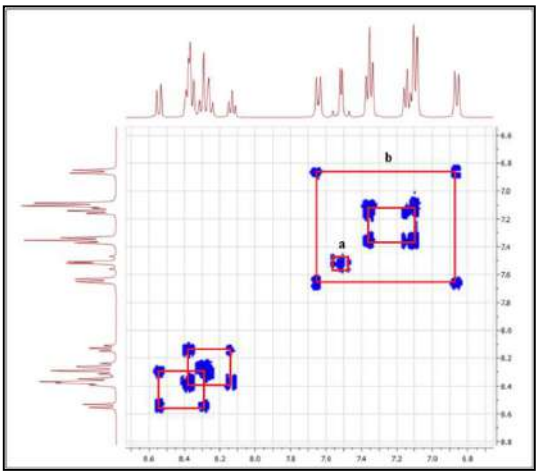

Figure 3. COSY spectrum of **3b**

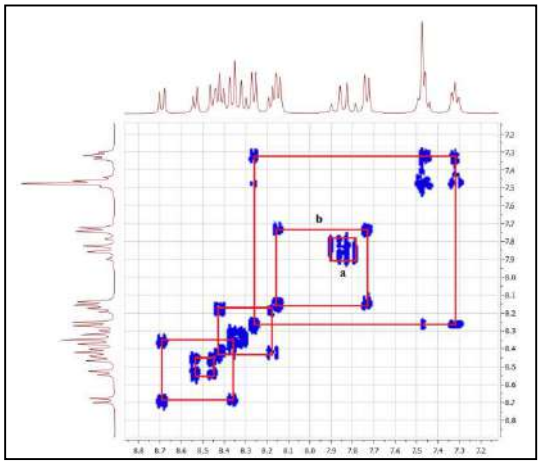

Figure 4. COSY spectrum of **3c**

At the same time, to show correlation between specific protons and associated chemical shifts, 2D-NMR technique (COSY) was applied to target compounds. In the first spectrum (Figure 2), rectangle a shows the couplings of α,β-unsaturated double bond protons of **3a** (doublets at δ = 7.35 and 7.55). In addition, the coupling of dimethylamine attached phenyl group's hydrogens can be clearly seen in rectangle b (doublets at δ = 7.61 and 6.71). Lastly, the correlations between pyrene protons can be roughly seen at lower fields in the spectrum.

Figure 3 shows the correlation spectrum of **3b** target compound and rectangle a visualizes the coupling of α,β-unsaturated double bond protons (doublets at δ = 7.54 and 7.49). In addition, rectangle b also shows the diphenylamino group bonded phenyl ring on the proposed structure (doublets at δ = 7.64 and 6.86). This spectrum also shows the pyrene related protons at lower fields as in Figure 2.

The last spectrum in Fig 4 is of the carbazole containing structure (**3c**). In the spectrum, olefinic bond and benzaldehyde related phenyl ring's protons are shown in rectangle a (doublets at δ = 7.88 and 7.81) and b (doublets at δ = 8.15 and 7.73), respectively. Moreover, the couplings of pyrene and carbazole protons can be separately seen at different chemical shifts.

3.3 *Absorption Studies*

Absorption spectra of **3a-c** were recorded in six common organic solvents at 10^{-5} M concentrations to understand the photophysical manners. All the absorption results for target compounds were summarized in Table 1 and the absorption spectra can be seen in Figure 5, Figure 6, and Figure 7, as well.

Table 1. Absorption maxima values of **3a-c** (nm)

	3a	**3b**	**3c**
Cyclohexane	402	412	394
Acetonitrile	418	418	384
Tetrahydrofuran	410	422	394
Dimethylformamide	420	424	392
Dichloromethane	414	426	392
Ethanol	428	428	396

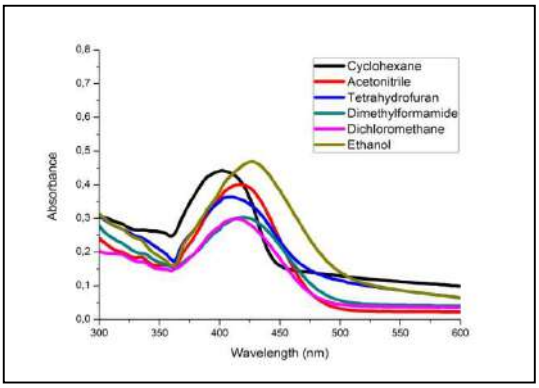

Figure 5. Absorption spectrum of **3a**

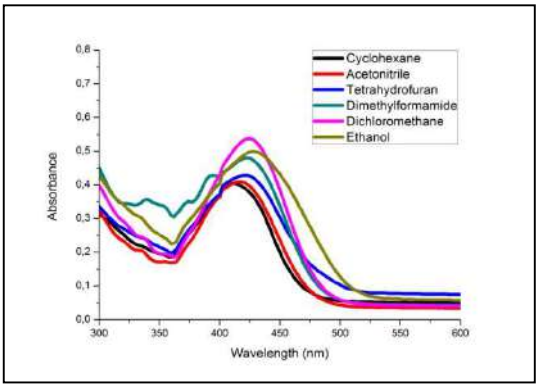

Figure 6. Absorption spectrum of **3b**

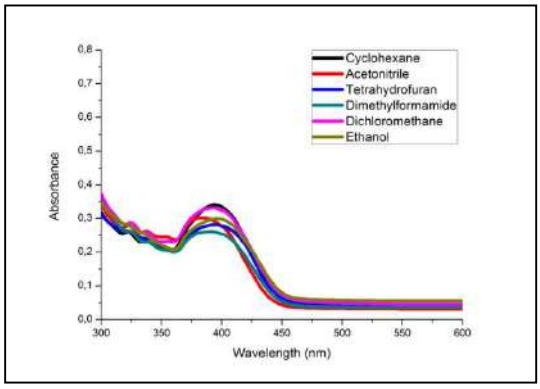

Figure 7. Absorption spectrum of **3c**

As shown in absorption spectra (Figure 5, Figure 6, Figure 7) and Table 1, target chalcone compounds exhibited one main absorption peak between ~380-430 nm for each studied solvents and these signals are assigned to the n-π* and π-π* transitions. These shapes are unstructured, and this may come from intramolecular charge transfers from electron donating groups to α,β-unsaturated carbonyl groups. By analyzing the results, a correlation was shown between λ_{abs} values and polarity of used solvents. In other words, these changings are affected from polarity and increasing polarity causes bathochromic shifts as expected. In addition, compound **3c** exhibited lower wavelength absorption when compared to others (**3a** and **3b**). This situation may come from higher electron donation ability of dimethylamino and diphenylamino groups.

3.4 *Thermal Analysis*

Thermal gravimetric analysis studies were carried out to understand the thermal perspective and obtained thermograms gave many important data about synthesized chalcone compounds (**3a-c**). As a main result, all three compounds showed good thermal stability (with max. 10 % weight loss) up to ~350 °C (Figure 6, Figure 7, and Figure 8). In a small range on this temperature, each compound exhibited different thermal behaviours with main weight losses in the range of 325-600, 350-450, and 350-450 for **3a**, **3b**, and **3c**, respectively. In Figure 8 and Figure 9, it can be seen slow degradations and weight losses while the weight loss is sharp in the thermogram of **3c** (Figure 10).

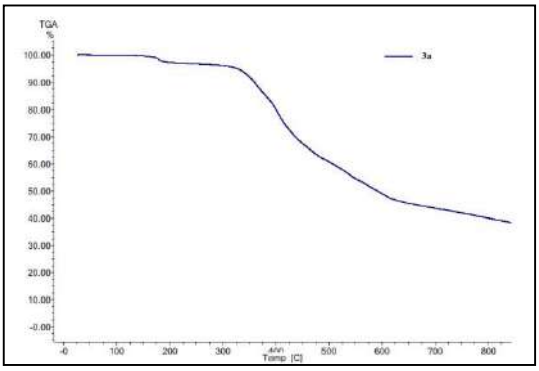

Figure 8. Thermogram of **3a**

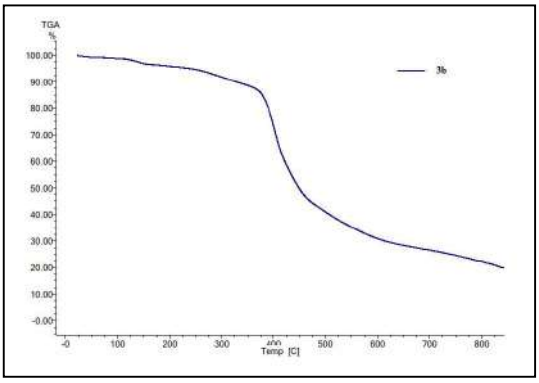

Figure 9. Thermogram of **3b**

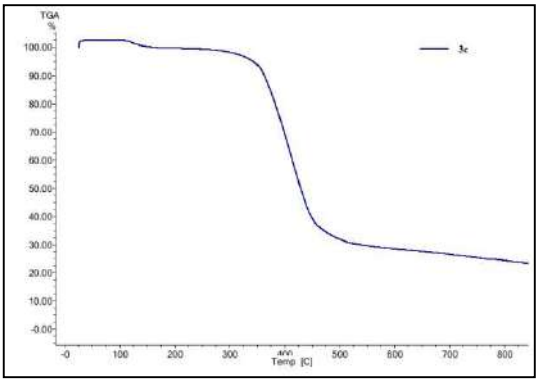

Figure 10. Thermogram of **3c**

3.5 *Surface Analysis*

To determine the possibility of using in organic electronics, the SEM images of all compounds (**3a-c**) were obtained by coating on ITO glass. A several solvent was used to generate thin film and dichlorobenzene was the most appropriate for the coating processes of these compounds. From all the images (Figure 11, Figure 12 and Figure 13), it can be understood that all the compounds have good ability to generate thin film (dark coloured

area) and have potential to be used in organic electronics.

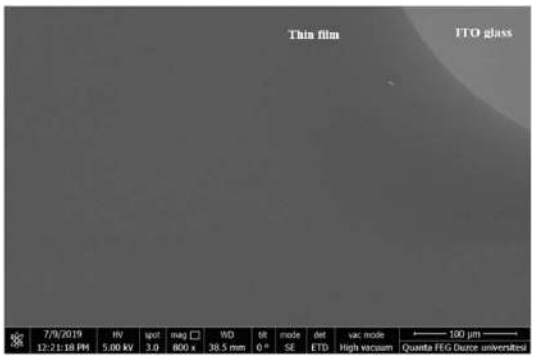

Figure 11. SEM image of **3a** thin film

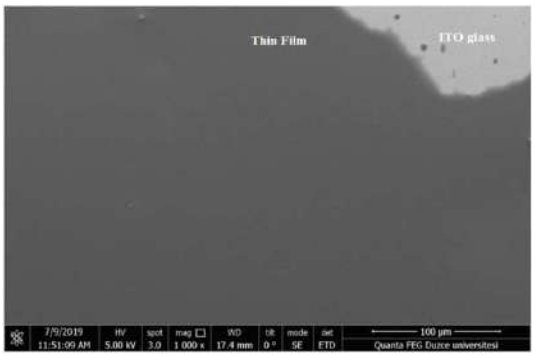

Figure 12. SEM image of **3b** thin film

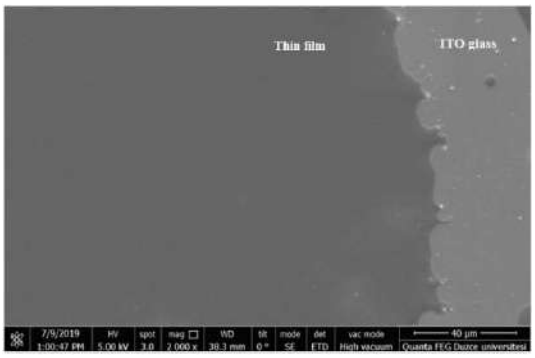

Figure 13. SEM image of **3c** thin film

4. CONCLUSIONS

Three chalcone compounds were successfully synthesized via condensation of 1-acetylpyrene with dimethylamine, diphenylamine or carbazole containing benzaldehyde derivatives at basic conditions. The yields were excellent in the range of 87-92%. In structural characterisation, it was shown trans configuration by consulting the coupling constants in ^{1}H NMR. UV-vis studies showed visible region absorption between ~380-430 nm. For each compound, λ_{max} values were quite different at different solvents and this was evidence of solvent type dependent absorption. The thermal studies showed that the target compounds were quite stable up to 350 °C. This thermal stability of the compounds can prevent from degradation and it ensures ultimately advantageous results at the end of application. Lastly, SEM images were taken to determine surface and film generation properties which are important for usability in organic electronics. The results were quite promising due to good film generation ability of each compound and these compounds might be used in organic electronics. By taking into account of electron donating and highly conjugated structures, absorption properties, high thermal stabilities, and good film generation properties, synthesized compounds can be promising candidates for organic electronics and dependent area.

ACKNOWLEDGMENTS

The author is thankful to Department of Chemistry in Faculty of Arts and Sciences of Düzce University and Prof. Dr. Sefa DURMUŞ for all kind support.

5. REFERENCES

[1] D. K. Mahapatra, S. K. Bharti, V. Asati, S. K. Singh, “Perspectives of medicinally privileged chalcone based metal coordination compounds for biomedical applications”, European Journal of Medicinal Chemistry, vol. 174, pp. 142-158, 2019.

[2] I. Karaman, H. Gezegen, M. B. Gürdere, A. Dingil, and M. Ceylan, “Screening of biological activities of a series of chalcone derivatives against human pathogenic microorganisms”, Chemistry & Biodiversity, vol. 7, pp. 400-408, 2010.

[3] S. R. Maidur, P. S. Patil, “Z-scan studies of third-order nonlinear optical and optical limiting properties of chalcones doped Poly(methyl methacrylate) thin films for visible laser protection”, Optical Materials, vol. 84, pp. 28-37, 2018.

[4] R. Agilandeshwari, V. Meenatchi, S. P. Meenakshisundaram, "Synthesis, growth, structure and characterisation of chalcone crystal: A novel organic NLO material", Journal of Molecular Structure, vol. 1118, pp. 356-366, 2016.

[5] H. Gezegen, A. Dingil, and M. Ceylan, "Three-Step Synthesis of 2,4-Diaryl-5,6,7,8-tetrahydroquinoline Derivatives", Journal of Heterocyclic Chemistry, vol. 47, pp. 1017-1024, 2010.

[6] S. A. Khan, A. M. Asiri, N. S. M. Al-Ghamdi, M. Asad, M. E. M. Zayed, S. A. K. Elroby, F. M. Aqlan, M. Y. Wani, K. Sharma, "Microwave assisted synthesis of chalcone and its polycyclic heterocyclic analogues as promising antibacterial agents: In vitro, in silico and DFT studies", Journal of Molecular Structure, vol. 1190, pp. 77-85, 2019.

[7] H. Yamane, K. Tanaka, Y. Chujo, "Synthesis of a near-infrared light-absorbing polymer based on thiophene-substituted Aza-BODIPY", Polymer Journal, vol. 50, pp. 271-275, 2018.

[8] M. Bansal and R. Kaur, "Electromeric effect of substitution at 6th position in 2-(Furan-2-yl)-3-hydroxy-4 *H*-chromen-4-one (FHC) on the absorption and emission spectra", Journal of Chemical Sciences vol. 127, no. 3, pp. 405-412, 2015.

[9] X. Yang, X. Guo, M. Qin, X. Yuan, H. Jing and B. Chen, "Metal-free iodine(III)-promoted synthesis of 2,5-diaryloxazoles", Organic & Biomolecular Chemistry, vol. 16, pp. 3104-3108, 2018.

[10] D. Usjak, B. Ivkovic, D. D. Bozic, L. Boskovic, M. Milenkovic, "Antimicrobial activity of novel chalcones and modulation of virulence factors in hospital strains of Acinetobacter baumannii and Pseudomonas aeruginosa", Microbial Pathogenesis, vol. 131, pp. 186-196, 2019.

[11] G. Singh, A. Arora, P. Kalra, I. K. Maurya, C. E. Ruizc, M. A. Estebanc, S. Sinha, K. Goyal, R. Sehgal, "A strategic approach to the synthesis of ferrocene appended chalcone linked triazole allied organosilatranes: Antibacterial, antifungal, antiparasitic and antioxidant studies", Bioorganic & Medicinal Chemistry, vol. 27, pp. 188-195, 2019.

[12] L. F. Castano, V. Cuartas, A. Bernal, A. Insuasty, J.Guzman, O. Vidal, V. Rubio, G. Puerto, P. Lukac, V. Vimberg, G. Balikova-Novtona, L. Vannucci, J. Janata, J. Quiroga, R. Abonia, M.Nogueras, J. Cobo, B. Insuasty, "New chalcone-sulfonamide hybrids exhibiting anticancer and antituberculosis activity" European Journal of Medicinal Chemistry, vol. 176, pp. 50-60, 2019.

[13] N. Gencer, Ç. Bilen, D. Demir, A. Atahan, M. Ceylan and M. Küçükislamoğlu, "In vitro inhibition effect of some chalcones on erythrocyte carbonic anhydrase I and II", Artificial Cells, Nanomedicine, and Biotechnology, vol. 41, pp. 384-388, 2013.

[14] A. Özdemir, M. D. Altıntop, G. Turan-Zitouni, G. Akalın Çiftçi, İ. Ertorun, Ö. Alataş, Z. A. Kaplancıklı, "Synthesis and evaluation of new indole-based chalcones as potential antiinflammatory agents", European Journal of Medicinal Chemistry, vol. 89, pp. 304-309, 2015.

[15] R. H. Hans, E. M. Guantai, C. Lategan, P. J. Smith, B. Wan, S. G. Franzblau, J. Gut, P. J. Rosenthal, K. Chibale, "Synthesis, antimalarial and antitubercular activity of acetylenic chalcones", Bioorganic & Medicinal Chemistry Letters, vol. 20, pp. 942-944, 2010.

[16] M. Gaber, S.A. El-Daly, T.A. Fayed, Y.S. El-Sayed, "Photophysical properties, laser activity and photoreactivity of a heteroaryl chalcone A model of solvatochromic fluorophore", Optics & Laser Technology, vol. 40, pp. 528-537, 2008

[17] S. Satheeshchandra, D. Haleshappa, S. Rohith, A. Jayarama, N. Shetty, "Novel benzofuran based chalcone material for potential nonlinear optical application", Physica B: Condensed Matter vol. 560, pp. 191-196, 2019.

[18] A. Kamal, K. Kumar, V. Kumar, R. Kumar Mahajan, "Electrochemical and Chromogenic Sensors Based on Ferrocene Appended Chalcone for Selective Quantification of Copper (II)",

Electrochimica Acta, vol. 145, pp. 307-313, 2014.

[19] J. Prabhu, K. Velmurugan, R. Nandhakumar, "Development of fluorescent lead II sensor based on an anthracene derived chalcone", Spectrochimica Acta Part A: Molecular and Biomolecular Spectroscopy, vol. 144, pp. 23-28, 2015.

[20] H. Karaca, Catalytic Oxidation of 2-Mercaptoethanol by Cobalt(II) phthalocyanines Bearing Chalcone with Furan and Thiophene Sakarya University Journal of Science, vol. 22, no. 6, pp. 1699-1703, 2018.

[21] A. Karuppusamy, T. Vandana, P. Kannan, "Pyrene based chalcone materials as solid state luminogens with aggregation-induced enhanced emission properties" Journal of Photochemistry and Photobiology A: Chemistry, vol. 345, pp. 11-20, 2017.

[22] S. R. Maidur, P. S. Patil, "Linear optical and third-order nonlinear optical properties of anthracene chalcone derivatives doped PMMA thin films". Optik - International Journal for Light and Electron Optics, vol. 190 pp. 54-67 2019.

[23] B. Delavaux-Nicot, J. Maynadie, D. Lavabre, S. Fery-Forgues, "Two electroactive ferrocenyl chalcones as original optical chemosensors for Ca^{2+} and Ba^{2+} cations in CH_3CN", Journal of Organometallic Chemistry, vol. 692, pp. 3351-3362, 2007.

[24] Y. Sun, H. Chen, D. Cao, Z. Liu, H. Chen, Y. Deng, Q. Fang, "Chalcone derivatives as fluorescence turn-on chemosensors for cyanide anions" Journal of Photochemistry and Photobiology A: Chemistry, vol. 244, pp. 65-70, 2012.

[25] Z. Luo, B. Liu, T. Qin, K. Zhu, C. Zhao, C. Pan, L. Wang, "Cyclization of chalcone enables ratiometric fluorescence determination of hydrazine with a high selectivity", Sensors and Actuators B, vol. 263, pp. 229-236, 2018.

[26] L. Pineiro, M. Novo, W. Al-Soufi, "Fluorescence emission of pyrene in surfactant solutions", Advances in Colloid and Interface Science, vol. 215, pp. 1-12, 2015.

[27] B. Wang, J. Zhao, C. Cui, M. Wang, Z. Wang, Q. He, "Electrochemical synthesis, characterization and electrochromic properties of a copolymer based on 1,4-bis(2-thienyl)naphthalene and pyrene", Optical Materials, vol. 34, pp. 1095-1101. 2012.

[28] X. Feng, C. Qi, H. T. Feng, Z. Zhao, H. H. Y. Sung, I. D. Williams, R. T. K. Kwok, J. W. Y. Lam, A. Qin and B. Z. Tang, "Dual fluorescence of tetraphenylethylene substituted pyrenes with aggregation-induced emission characteristics for white-light emission", Chemical Sciences, vol., 9, pp. 5679-5687, 2018.

[29] Y. Zhang, B. He, J. Liu, S. Hu, L. Pan, Z. Zhao, and B. Z. Tang, "Aggregation-induced emission and working mechanism of 1-benzoyl and 1-benzyl pyrene derivatives, Physical Chemistry Chemical physics, vol. 20, pp. 9922-9929, 2018.

[30] F. Lu, T. Takaya, K. Iwata, I. Kawamura, A. Saeki, M. Ishii, K. Nagura, T. Nakanishi, "A Guide to Design Functional Molecular Liquids with Tailorable Properties using Pyrene-Fluorescence as a Probe", Scientific Reports, Vol. 7, no. 3416, pp.1-12, 2017.

[31] E. Fındık, A. Dingil, I. Karaman, M. Ceylan, "Synthesis of Terpenoid-Like Bischalcones from α- and β-Ionones and Their Biological Activities", Synthetic Communications vol. 1, no 39, pp. 4362-4374, 2009.

[32] F. Sönmez, S. Sevmezler, A. Atahan, M. Ceylan, D. Demir, N. Gencer, O. Arslan, M. Küçükislamoğlu, "Evaluation of new chalcone derivatives as polyphenol oxidase inhibitors", Bioorganic & Medicinal Chemistry Letters, vol. 21, pp. 7479-7482, 2011.

[33] E. M. Hussein, S. A. Ahmed and I. I. Althagafi, "A convenient regioselective synthesis of spirooxindolinopyrrolizidines incorporating the pyrene moiety through a [3+2]cycloaddition reaction", Heterocyclic Communications, vol. 23, no. 5, pp. 379-384, 2017.

[34] H. J. Lee, J. Sohn, J. Hwang, and S. Y. Park, "Triphenylamine-Cored Bifunctional Organic Molecules for Two-Photon Absorption and Photorefraction" Chemical Materials, vol. 16, pp. 456-465, 2004.

[35] O. Bagheri, H. Dehghani, "Effect of Isonicotinate derivatives as additive on the photovoltaic performance of Carbazole-dye sensitized nanostructured TiO_2 solar cells", Electrochimica Acta, vol. 186, pp. 43-49 2015.

JOURNAL OF SCIENCE
SAKARYA UNIVERSITY

Sakarya University Journal of Science

ISSN 1301-4048 | e-ISSN 2147-835X | Period Bimonthly | Founded: 1997 | Publisher Sakarya University
http://www.saujs.sakarya.edu.tr/en/

Title: Hurwitz Stability of Matrix Segment and The Common Solution Set of 2 and 3-Dimensional Lyapunov Equations

Authors: Şerife Yılmaz
Recieved: 2019-06-03 10:47:26

Accepted: 2020-01-16 15:43:22

Article Type: Research Article
Volume: 24
Issue: 2
Month: April
Year: 2020
Pages: 357-364

How to cite
Şerife Yılmaz; (2020), Hurwitz Stability of Matrix Segment and The Common Solution Set of 2 and 3-Dimensional Lyapunov Equations. Sakarya University Journal of Science, 24(2), 357-364, DOI:
https://doi.org/10.16984/saufenbilder.573551
Access link
http://www.saujs.sakarya.edu.tr/tr/issue/52471/573551

Sakarya University Journal of Science 24(2), 357-364, 2020

Hurwitz Stability of Matrix Segment and The Common Solution Set of 2 and 3-Dimensional Lyapunov Equations

Şerife YILMAZ[1]

Abstract

In this study, a necessary and sufficient condition is given for the stability of the convex combinations of n-dimensional two Hurwitz stable matrices. There is a close relationship between Hurwitz stability of the matrix segment and common solution to the Lyapunov equations corresponding to those matrices. Therefore, the results obtained in this area are important. In the case of existence, an algorithm that determines common solutions set is also given. A number of illustrative examples using this algorithm are given.

Keywords: Hurwitz stability, matrix segment, common quadratic Lyapunov function

1. INTRODUCTION

Let A_1 and A_2 be n-dimensional square real matrices, that is $A_1, A_2 \in \mathbb{R}^{n\times n}$. If all eigenvalues of a square matrix lie in the open left half plane, it is called Hurwitz stable matrix. A stable matrix can also be characterized by Lyapunov inequality: if A_1 is a Hurwitz stable matrices, there exists a positive definite P such that

$$A_1^T P + P A_1 < 0 \tag{1}$$

is hold (see [1,2]). When considering stable matrices A_1 and A_2 if the following inequalities

$$\begin{aligned} A_1^T P + P A_1 < 0, \\ A_2^T P + P A_2 < 0 \end{aligned} \tag{2}$$

are simultaneously satisfied for a $P > 0$, the matrix P is called common solution to the matrices A_1 and A_2.

The problem of the existence of a common $P > 0$ has been extensively investigated for the last two decades (see [3-8], and references therein). A

[1]Department of Mathematics and Sciences Education, Faculty of Education, Burdur Mehmet Akif Ersoy University, Istiklal Campus 15030 Burdur, Turkey. E-mail: serifeyilmaz@mehmetakif.edu.tr, Orcid Id: 0000-0002-7561-3288

sufficient condition for the asympotitical stability of the linear system given by the finite number of matrices, which are called switched system, is the existence of their common solution. With the exception of some special cases (for instance, second order matrices), the theoretical solution to the general n-dimensional problem has not been found yet [4-8].

Define the matrix segment

$$[A_1, A_2] = \{C(\alpha): C(\alpha) = \alpha A_1 + (1-\alpha)A_2, \quad \alpha \in [0,1]\}. \tag{3}$$

With the stability of the segment $[A_1, A_2]$, we mean that all matrix $A \in [A_1, A_2]$ is stable.

In [5], a necessary and sufficient condition for the existence of a common solution to second order matrices is given. According to this result, the stability of the matrix segments $[A_1, A_2]$ and $[A_1, A_2^{-1}]$ are equivalent to the existence of a common solution $P > 0$.

Notice that the existence of the solution of the problem is related to the stability of the convex combinations of the matrices.

The paper is organized as follows: Section 2 introduces the relation between bialternate product and stability of matrices. A necessary and sufficient condition for the segment stability will be derived via this product. Section 3 considers the common solution to the Lyapunov equation for two and three-dimensional matrices. Section 4 considers finding common solutions. By using the minimization of the functions defined on a box, an algorithm will be constructed. In the case of existence, the bisection method determinates common solutions. A number of illustrative examples are provided.

2. THE STABILITY CRITERIA FOR CONVEX COMBINATIONS OF TWO MATRICES

For 2×2 real matrices, a necessary and sufficient condition for the matrix segment in (3) to be stable is that both A_1 and A_2 are stable, and that the matrix $A_1 A_2^{-1}$ has no negative eigenvalues (see [5,9,10]).

Let A be an $n \times n$ matrix. We denote the bialternate product of $2A$ and the identity matrix I_n by $L(A)$:

$$L(A) = (2A) \cdot I_n.$$

As usual the bialternate product is denoted by "$\cdot$". The dimension of $L(A)$ is $\frac{n(n-1)}{2} \times \frac{n(n-1)}{2}$ and if the eigenvalues of A are $\lambda_1, \lambda_2, \dots, \lambda_n$ then the eigenvalues of $L(A)$ are written $\lambda_i + \lambda_j$ where $i = 1,2,\dots,n-1$ and $j = i+1, i+2, \dots, i+n$ (see [11-13]).

Now we give the following stability theorem for a matrix A, in terms of the above mentioned bialternate product.

Theorem 1 [14, p. 37]: The matrix A is stable if and only if the coefficients of the characteristic polynomials of the matrices A and $L(A)$

$$\begin{aligned} p_A(s) &= \det(sI_n - A) \\ &= s^n + a_{n-1}s^{n-1} + \cdots + a_1 s + a_0, \\ P_{L(A)}(s) &= \det\big(sI_m - L(A)\big) \\ &= s^m + b_{m-1}s^{m-1} + \cdots + b_1 s + b_0. \end{aligned}$$

are positive. That is, $a_i > 0$ and $b_j > 0$ for $i = 1,2,\dots,n-1$, $j = 1,2,\dots m-1$, where $m = n(n-1)/2$.

Note that in the case of A is stable, the following inequalities hold

$$\begin{aligned} p_A(0) &= \det(0 \cdot I_n - A) \\ &= (-1)^n \det(A) > 0, \\ P_{L(A)}(0) &= \det\big(0 \cdot I_m - L(A)\big) \\ &= (-1)^m \det\big(L(A)\big) > 0. \end{aligned}$$

Lemma 1: Let $A_1, A_2 \in \mathbb{R}^{n\times n}$ be stable matrices. For all $\alpha \in [0,1]$, $(-1)^n \det C(\alpha) > 0$ if and only if the matrix $A_1 A_2^{-1}$ has no negative real eigenvalues.

Proof: Since A_1 and A_2 are stable, $(-1)^n \det(A_1) > 0$ and $(-1)^n \det(A_2) > 0$.

Sufficiency: For $\alpha \in (0,1)$,

$$\begin{aligned}\det C(\alpha) &= \det[\alpha A_1 + (1-\alpha)A_2] \\ &= \det([\alpha A_1 A_2^{-1} + (1-\alpha)I_n]A_2) \\ &= \det[\alpha A_1 A_2^{-1} + (1-\alpha)I_n]\det(A_2) \\ &= \alpha^n \det\left[A_1 A_2^{-1} + \frac{1-\alpha}{\alpha} I_n\right]\det(A_2).\end{aligned}$$

Since $\frac{1-\alpha}{\alpha} \in (0,\infty)$ and $A_1 A_2^{-1}$ has no negative real eigenvalues,

$$\det\left[A_1 A_2^{-1} + \frac{1-\alpha}{\alpha} I_n\right] \neq 0.$$

Hence, $\det C(\alpha) > 0$ for $\alpha \in (0,1)$.

Necessity: If $(-1)^n \det C(\alpha) > 0$ for all $\alpha \in (0,1)$ then $\det\left[A_1 A_2^{-1} + \frac{1-\alpha}{\alpha} I_n\right] \neq 0$ and so the matrix $A_1 A_2^{-1}$ has no negative eigenvalues.

Lemma 2: Let $A_1, A_2 \in \mathbb{R}^{n\times n}$ be stable matrices and $C(\alpha)$ be as in (3). For all $\alpha \in [0,1]$,

$$(-1)^m \det L(C(\alpha)) > 0$$

if and only if the matrix $L(A_1)L^{-1}(A_2)$ has no negative real eigenvalues.

Proof is analogously to Lemma 1.

Theorem 2: Let $A_1, A_2 \in \mathbb{R}^{n\times n}$ be stable matrices and $C(\alpha)$ be as in (3). For all $\alpha \in [0,1]$, $C(\alpha)$ is stable if and only if the matrices $A_1 A_2^{-1}$ and $L(A_1)L^{-1}(A_2)$ have no negative real eigenvalues.

Proof: From Theorem 1, $(-1)^n \det C(\alpha) > 0$ and $(-1)^m \det L(C(\alpha)) > 0$ for all $\alpha \in [0,1]$ since $C(\alpha)$ is stable. Therefore, the matrices $A_1 A_2^{-1}$ and $L(A_1)L^{-1}(A_2)$ have no negative eigenvalues from Lemma 1 and 2.

Sufficiency: Assume that $A_1 A_2^{-1}$ and $L(A_1)L^{-1}(A_2)$ have no negative eigenvalues. Consider the eigenvalues of the matrix $C(\alpha)$. By the continuity theorem of eigenvalues [16, p. 52], there exists continuous functions $\lambda_i: [0,1] \to C$ $(i = 1,2,\dots,n)$ such that $\lambda_1(\alpha), \lambda_2(\alpha), \dots, \lambda_n(\alpha)$ are the eigenvalues of $C(\alpha)$. Here $Re\ \lambda_i(0) < 0$ $(i = 1,2,\dots,n)$, since the matrix $C(0)$ is stable. Proceeding by contraposition, suppose that $C(\alpha_*)$ is not Hurwitz stable for an $\alpha_* \in (0,1)$. Therefore, there exists an index $i_0 \in \{1,2,\dots,n\}$ such that $Re\ \lambda_{i_0}(\alpha_*) \geq 0$. In view of the continuity of $\lambda_{i_0}(\alpha)$ with respect to α, there must exists an $\tilde{\alpha} \in (0,1)$ such that $Re\ \lambda_{i_0}(\tilde{\alpha}) = 0$. The matrix $C(\tilde{\alpha})$ has an eigenvalue which lies on the imaginary axes. If the eigenvalue is real then

$$\det C(\tilde{\alpha}) = \lambda_1(\tilde{\alpha}).\cdots.\lambda_{i_0}(\tilde{\alpha}).\cdots.\lambda_n(\tilde{\alpha}) = 0$$

which contradicts the result of Lemma 1. If the eigenvalue is not real, $\lambda_{i_0}(\tilde{\alpha}) = j\tilde{\omega}$ where $\tilde{\omega} > 0$. The complex conjugate of $j\tilde{\omega}$ is also an eigenvalue of $C(\tilde{\alpha})$. The matrix $L(C(\tilde{\alpha}))$ has the eigenvalue $j\tilde{\omega} + (-j\tilde{\omega}) = 0$ and this imply $\det L(C(\tilde{\alpha})) = 0$ which contradicts Lemma 2. This contradictions show that $C(\alpha)$ is stable for all $\alpha \in [0,1]$.

3. THE COMMON SOLUTION TO THE LYAPUNOV EQUATION FOR TWO AND THREE-DIMENSIONAL MATRICES

In this section, we can give the important theorem on common quadratic solution two−dimensional Lyapunov equations for two stable matrices.

Theorem 3 [5]: Let $A_1, A_2 \in \mathbb{R}^{2\times 2}$ be stable matrices. A necessary and sufficient condition for the matrices A_1 and A_2 have common solution to its Lyapunov equation (2) is that the matrices $A_1 A_2$ and $A_1 A_2^{-1}$ have no negative real eigenvalue. An equivalent condition is that the segments $[A_1, A_2]$ and $[A_1, A_2^{-1}]$ are stable.

Note that, if A is a 2×2 dimensional matrix then the matrix $L(A)$ is a number and is equal to trace(A).

For the common solution set of two-dimensional Lyapunov equation of the matrices A_1 and A_2, define the symmetric matrices

$$P(x) = \begin{bmatrix} x_1 & x_2 \\ x_2 & x_3 \end{bmatrix},\ Q_2(y) = \begin{bmatrix} y_1 & y_2 \\ y_2 & y_3 \end{bmatrix},$$

$$R_2(z) = \begin{bmatrix} z_1 & z_2 \\ z_2 & z_3 \end{bmatrix}.$$

Let A_1 and A_2 be stable matrices. Assume that A_1A_2 and $A_1A_2^{-1}$ have no negative real eigenvalue. Consider the following Lyapunov equations:

$$A_1^TP(x)+P(x)A_1=-Q_2(y),$$
$$A_2^TP(x)+P(x)A_2=-R_2(z)$$

where $x,y,z\in\mathbb{R}^3$. For given $Q_2(y)>0$, there exists an $x\in\mathbb{R}^3$ such that the matrix $P(x)>0$ is a unique solution to the first equation. That is, from the solution of the first equation

$$x=\big(\phi_1(y),\phi_2(y),\phi_3(y)\big)$$

is obtained. Analogously, for $R_2(z)>0$ there exists an $x\in\mathbb{R}^3$ such that the matrix $P(x)>0$ is a unique solution to the second equation. As a result,

$$x=\big(\eta_1(z),\eta_2(z),\eta_3(z)\big)$$

is obtained. Finally, if these two results are combined, the equation for the common solution is

$$\big(\phi_1(y),\phi_2(y),\phi_3(y)\big)=\big(\eta_1(z),\eta_2(z),\eta_3(z)\big).$$

From this linear equations system,

$$y=\big(\gamma_1(z),\gamma_2(z),\gamma_3(z)\big).$$

We investigate three-dimensional box where the symmetric matrix $R_2(z)$ is positive definite on it.

The matrix

$$Q_2(z)=\begin{bmatrix}\gamma_1(z) & \gamma_2(z)\\ \gamma_2(z) & \gamma_3(z)\end{bmatrix}$$

must be positive definite for z such that $R_2(z)>0$. If $Q_2(z)>0$ and $R_2(z)>0$ then

$$P(z)=\begin{bmatrix}\eta_1(z) & \eta_2(z)\\ \eta_2(z) & \eta_3(z)\end{bmatrix}$$

is a common solution to A_1 and A_2.

The matrices $Q_2(z)$ and $R_2(z)$ are positive definite if its leading principle minors are positive. Define the functions

$$\begin{aligned}&f_1(z)=\gamma_1(z),\\ &f_2(z)=\gamma_1(z)\gamma_3(z)-\gamma_2^2(z),\\ &f_3(z)=z_1z_3-z_2^2,\\ &f_4(z)=z_1.\end{aligned}\qquad(4)$$

These functions are multivariate polynomials.

Let's give some basic properties of positive definite matrices. From $P=[p_{ij}]>0$ it follows that $u^TPu>0$ for all $0\neq u\in\mathbb{R}^n$. Taking $u=(0,\dots,0,1,0,\dots,0)^T$ we acquire

$$p_{ii}>0\quad(i=1,2,\dots,n).\qquad(5)$$

The positive definite matrices comprise the cone interior. Therefore, the entry z_3 of $R_2(z)$ can be taken $z_3=1$.

Define the box $B=[0,1]\times[-1,1]$. If the matrices A_1 and A_2 have a common positive definite solution, there exists an $x\in B$ such that $P(x)$ is a common solution also.

In the case of three and higher dimensional matrices, there is no theoretical solution. To solve the problem, there are gradient based numerical algorithms (see [6,7]). In this work, we propose an algorithm which is based on sign-definite decomposition.

This paper differs from the mentioned works since it is determined a subbox which contains common solutions.

Let A_1 and A_2 be three-dimensional matrices. Assume that A_1 and A_2 have a common positive definite solution.

As in the two-dimensional case, common solution can be acquire.

For the matrices,

$$P(x)=\begin{bmatrix}x_1 & x_2 & x_3\\ x_2 & x_4 & x_5\\ x_3 & x_5 & x_6\end{bmatrix},\ Q_3(y)=\begin{bmatrix}y_1 & y_2 & y_3\\ y_2 & y_4 & y_5\\ y_3 & y_5 & y_6\end{bmatrix},$$

$$R_3(z) = \begin{bmatrix} z_1 & z_2 & z_3 \\ z_2 & z_4 & z_5 \\ z_3 & z_5 & z_6 \end{bmatrix},$$

where $x, y, z \in \mathbb{R}^6$, the solution of the Lyapunov equations

$$\begin{aligned} A_1^T P(x) + P(x) A_1 &= -Q_3(y), \\ A_2^T P(x) + P(x) A_2 &= -R_3(z) \end{aligned} \tag{6}$$

is

$$x = (\phi_1(y), \phi_2(y), \dots, \phi_6(y))$$

and

$$x = \left(\eta_1(z), \eta_2(z), \dots, \eta_6(z)\right) \tag{7}$$

respectively.

As in the two-dimensional case, the matrix $Q_3(z)$ can be constructed

$$Q_3(z) = \begin{bmatrix} \gamma_1(z) & \gamma_2(z) & \gamma_3(z) \\ \gamma_2(z) & \gamma_4(z) & \gamma_5(z) \\ \gamma_3(z) & \gamma_5(z) & \gamma_6(z) \end{bmatrix}.$$

The functions that will be used to provide positive definiteness of $Q_3(z)$ and $R_3(z)$ are

$$\begin{aligned} g_1(z) &= \gamma_1(z), \\ g_2(z) &= \gamma_1(z)\gamma_4(z) - \gamma_2^2(z), \\ g_3(z) &= \det Q_3(z), \\ g_4(z) &= z_1 z_4 - z_2^2 \\ g_5(z) &= \det R_3(z) \\ g_6(z) &= z_1 \end{aligned} \tag{8}$$

So, these functions are multivariate polynomials.

4. AN APPLICATION OF SIGN-DEFINITE DECOMPOSITION

The sign of a multivariate polynomial function $h(a)$ over a box can be given by decomposition (see [17]).

Define the box

$$D = \{a \in \mathbb{R}^k : \ a_i^- \le a_i \le a_i^+, \quad i = 1,2, \dots, k\}.$$

Given any box can be transported to the first orthant in the parameter space. Therefore, one can assume that $a_i^- \ge 0$ without loss of generality. Then $h(a)$ can be written as

$$h(a) = h^+(a) - h^-(a)$$

where $h^+(a) \ge 0$ and $h^-(a) \ge 0$ for all $a \in D$. The functions $h^+(a)$ and $h^-(a)$ correspond to the positive and negative coefficients of $h(a)$.

Define the two extreme vertices of the box D

$$\begin{aligned} a^- &= (a_1^-, a_2^-, \dots, a_k^-), \\ a^+ &= (a_1^+, a_2^+, \dots, a_k^+). \end{aligned}$$

Lemma 3 ([17]): If $h^+(a^-) - h^-(a^+) > 0$ then $h(a) > 0$, If $h^+(a^+) - h^-(a^-) < 0$ then $h(a) < 0$ for all $a \in D$.

Using the sufficient conditions from Lemma 1, one can test positivity of f_i on the box B.

In order to apply this conditions, the B box (and accordingly the function f_i) must be transformed into the first orthant.

Here, we provide an algorithm for the common solution to 2-dimensional two matrices. We investigate the points $(z_1, z_2) \in B$ where the functions in (4) f_i $(i = 1,2,3,4)$ are positive. Here, we omitted the function $f_4(z)$.

This algorithm can also be adapted to 3-dimensional matrices. Notice that, among the functions g_i $(i = 1,2, \dots,6)$ given in (8), $g_6(z)$ can be omitted. In the case of existence, the following algorithm gives affirmative answer.

Algorithm 1:

Let B be initial box.

1. Calculate
   $m_i = f_i^+(b^-) - f_i^-(b^+)$,
   $M_i = f_i^+(b^+) - f_i^-(b^-) \quad (i = 1,2,3)$.
   where b^- and b^+ are extreme vertices of the box investigated.
2. If $\min\{m_1, m_2, m_3\} > 0$ then $f_1(z) > 0$, $f_2(z) > 0$ and $f_3(z) > 0$ for all z in the

box. Therefore, $Q_2(z) > 0$ and $R_2(z) > 0$. Otherwise, go to step 3.

3. If one of the M_i's is nonpositive, there is no z in the box so that $Q_2(z) > 0$ or $R_2(z) > 0$. This box should be eliminated. Otherwise, go to step 4.
4. The investigating box is divided into two subboxes along an axis. Return to step 1.

This processes are repeated until finding a subbox containing common solutions is provided or there is no subbox to be examined.

5. EXAMPLES

We will give the applications of the Algorithm 1.

Example 1. Consider the following Hurwiz stable matrices

$$A_1 = \begin{bmatrix} -2 & 4 \\ 1 & -7 \end{bmatrix}, \quad A_2 = \begin{bmatrix} -2 & 1 \\ -1 & -1 \end{bmatrix}.$$

The matrices A_1A_2 and $A_1A_2^{-1}$ have no negative real eigenvalues. From Theorem 3, they have common solution. The matrix $Q_2(z)$ is obtained with regard to z as

$$Q_2(z) = \begin{bmatrix} \frac{7}{9}z_1 - \frac{8}{9}z_2 + \frac{4}{9} & \frac{20}{9}z_2 - \frac{4}{9}z_1 - \frac{29}{18} \\ \frac{20}{9}z_2 - \frac{4}{9}z_1 - \frac{29}{18} & \frac{1}{3}z_1 + \frac{4}{3}z_2 + \frac{19}{3} \end{bmatrix}$$

and the common solution P can be written as

$$P(z) = \begin{bmatrix} \frac{2}{9}z_1 - \frac{1}{9}z_2 + \frac{1}{18} & \frac{1}{18}z_1 + \frac{2}{9}z_2 - \frac{1}{9} \\ \frac{1}{18}z_1 + \frac{2}{9}z_2 - \frac{1}{9} & \frac{1}{18}z_1 + \frac{2}{9}z_2 + \frac{7}{18} \end{bmatrix}$$

From the equation (4), we have the following functions

$$f_1(z_1, z_2) = \frac{7}{9}z_1 - \frac{8}{9}z_2 + \frac{4}{9},$$

$$f_2(z_1, z_2) = \frac{5}{81}z_1^2 + \frac{295}{81}z_1 - \frac{496}{81}z_2^2 + \frac{220}{81}z_1z_2 + \frac{172}{81}z_2 + \frac{71}{324},$$

$$f_3(z_1, z_2) = z_1 - z_2^2.$$

The sign of the functions f_1, f_2, f_3 on the box $B = [0,1] \times [-1,1]$ is determined by Algorithm 1. After 116 steps in 0.022s, calculations give the following table. The calculations have been made by using the mathematical software Maple on a computer with an i5 1.4 GHz processor.

Table 1. Results of the elimination process

step	Subboxes	m	M_1, M_2, M_3	Operations
1	$[0,1] \times [-1,1]$	$-$	$+,+,+$	divide
2	$\left[0,\frac{1}{2}\right] \times [-1,1]$	$-$	$+,+,+$	divide
3	$\left[\frac{1}{2},1\right] \times [-1,1]$	$-$	$+,+,+$	divide
⋮	⋮	⋮	⋮	⋮
16	$\left[0,\frac{1}{4}\right] \times \left[-1,-\frac{1}{2}\right]$	$-$	$+,-,+$	eliminate
⋮	⋮	⋮	⋮	⋮
66	$\left[\frac{1}{4},\frac{7}{8}\right] \times \left[-1,-\frac{1}{2}\right]$	$-$	$+,-,+$	eliminate
⋮	⋮	⋮	⋮	⋮
116	$\left[\frac{7}{8},1\right] \times \left[0,\frac{1}{4}\right]$	$+$	$+,+,+$	stop

For all $z \in \left[\frac{7}{8},1\right] \times \left[0,\frac{1}{4}\right]$, $P(z) > 0$ is common solution to A_1 and A_2. For instance, take $z = \left(\frac{15}{16},\frac{1}{8}\right)$ the matrix

$$P = \begin{bmatrix} \frac{1}{4} & -\frac{1}{32} \\ -\frac{1}{32} & \frac{15}{32} \end{bmatrix}$$

is common solution to A_1 and A_2. When the Algorithm 1 continues for 2000 steps, the common solution set (subboxes) is obtained as in Figure 1.

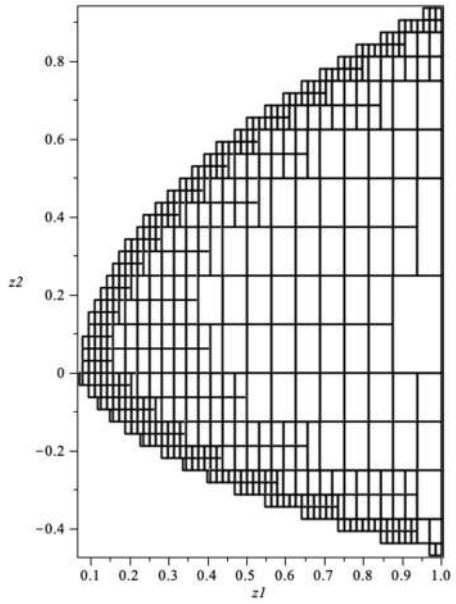

Figure 1. The subboxes are contained common solutions.

Example 2. Consider the following Hurwitz stable matrices

$$A_1 = \begin{bmatrix} -1 & -3 & -4 \\ 2 & -3 & -2 \\ 1 & 1 & -2 \end{bmatrix}, \quad A_2 = \begin{bmatrix} -4 & -3 & 1 \\ 5 & 1 & -1 \\ -2 & 0 & -3 \end{bmatrix}.$$

Eigenvalues of $A_1 A_2^{-1}$ and $L(A_1)L^{-1}(A_2)$, are

$$3.3244, \quad 0.3242 \pm 0.4138i,$$
$$0.5103, \quad 0.9922 \pm 1.0773i$$

respectively. We conclude that the segments $[A_1, A_2^{-1}]$ is stable by Theorem 2 since they have no negative real eigenvalues.

For initial box

$$B = [0,1] \times [-1,1] \times [-1,1] \times [0,1] \times [-1,1],$$

Algorithm 1 has given an affirmative result:

$$S = \left[\frac{17}{64}, \frac{35}{128}\right] \times \left[\frac{-1}{64}, \frac{-1}{128}\right] \times \left[\frac{-25}{64}, \frac{-3}{8}\right] \times \left[\frac{3}{128}, \frac{1}{32}\right] \times \left[\frac{1}{64}, \frac{1}{32}\right].$$

The matrix

$$P(z) = \begin{bmatrix} \eta_1(z) & \eta_2(z) & \eta_3(z) \\ \eta_2(z) & \eta_4(z) & \eta_5(z) \\ \eta_3(z) & \eta_5(z) & \eta_6(z) \end{bmatrix}$$

is the common solution of the Lyapunov equations (6) for all $z \in S$, where

$$\eta_1(z) = \frac{619}{3515}z_1 - \frac{113}{703}z_2 - \frac{258}{3515}z_3 + \frac{2659}{7030}z_4 - \frac{166}{3515}z_5 + \frac{86}{3515},$$

$$\eta_2(z) = \frac{273}{7030}z_1 - \frac{80}{703}z_2 - \frac{108}{3515}z_3 + \frac{1047}{3515}z_4 + \frac{94}{3515}z_5 + \frac{36}{3515},$$

$$\eta_3(z) = -\frac{18}{3515}z_1 + \frac{26}{703}z_2 + \frac{246}{3515}z_3 - \frac{83}{7030}z_4 + \frac{567}{3515}z_5 - \frac{82}{3515},$$

$$\eta_4(z) = \frac{819}{7030}z_1 - \frac{240}{703}z_2 - \frac{324}{3515}z_3 + \frac{2767}{7030}z_4 + \frac{282}{3515}z_5 + \frac{108}{3515},$$

$$\eta_5(z) = -\frac{219}{7030}z_1 + \frac{41}{703}z_2 - \frac{261}{3515}z_3 - \frac{106}{3515}z_4 + \frac{813}{3515}z_5 + \frac{87}{3515},$$

$$\eta_6(z) = \frac{61}{7030}z_1 - \frac{5}{703}z_2 + \frac{169}{3515}z_3 + \frac{43}{7030}z_4 - \frac{82}{3515}z_5 + \frac{1059}{7030}.$$

Here, $z_6 = 1$ can be taken (see equation (5)).

6. REFERENCES

[1] R. Bellman, Introduction to Matrix Analysis, SIAM, Philadelphia, 1997.

[2] H.K. Khalil, Nonlinear Systems, Prentice Hall, New Jersey, (2002).

[3] D. Liberzon, Switching in System and Control, Birkhauser, Boston, (2003).

[4] H. Lin, P.J. Antsaklis, Stability and stabilizability of switched linear systems: A survey of recent results, IEEE Transactions on Automatic Control, Vol.54, N.2, pp. 308-322, 2009.

[5] R.N. Shorten, K.S. Narendra, Necessary and sufficient conditions for the existence of a common quadratic Lyapunov function for a finite number of stable second order linear time-invariant systems, International Journal of Adaptive Control and Signal Processing, Vol.16, pp. 709-728, 2002.

[6] V. Dzhafarov, T. Büyükköroğlu, Ş. Yılmaz, On one application of convex optimization to stability of linear systems, Trudy Inst. Mat. i Mekh. UrO RAN, Vol.21, N.2, pp. 320-328, 2015.

[7] D. Liberzon, R. Tempo, Common Lyapunov functions and gradient algorithms, IEEE Transactions on Automatic Control, Vol.49, N.6, pp. 990-994, 2004.

[8] M. Góra, Some methods of construction of a common Lyapunov solution to a finite set of complex systems, Linear Algebra and its Applications, Vol.530, pp. 77-93, 2017.

[9] C. King, M. Nathanson, On the existence of a common quadratic Lyapunov function for a rank one difference, Linear Algebra and its Applications, Vol.419, pp. 400-416, 2006.

[10] T.J. Laffey, H. Šmigoc, Common solution to the Lyapunov equation for 2×2 complex matrices, Linear Algebra and its Applications, Vol.420, pp. 609-624, 2007.

[11] A.T. Fuller, Conditions for a matrix to have only characteristics roots with negative real parts, Journal of Mathematical Analysis and Applications, Vol.23, pp. 71-98, 1968.

[12] W. Govarets, B. Sijnave, Matrix manifolds and Jordan Structure of the bialternate matrix product, Linear Algebra and its Applications, Vol.292, pp. 245-266, 1999.

[13] L. Elsner, V. Monov, The bialternate matrix product revisited, Linear Algebra and its Applications, Vol.434, pp. 1058-1066, 2011.

[14] R.K. Yedevalli, Robust Control of Uncertain Dynamic Systems: A linear state space approach, Springer, New York, 2014.

[15] R.K. Yedevalli, Robust Control of Uncertain Dynamic Systems: A linear state space approach, Springer, New York, 2014.

[16] B.R. Barmish, New Tools for Robustness of Linear Systems, Macmillan, New York, 1994.

[17] L.H. Keel and S.P. Bhattacharyya, Robust stability via sign-definite decomposition, IEEE Transactions on Automatic Control, Vol.56, N.1, pp. 140-145, 2011.

JOURNAL OF SCIENCE
SAKARYA UNIVERSITY

Sakarya University Journal of Science

ISSN 1301-4048 | e-ISSN 2147-835X | Period Bimonthly | Founded: 1997 | Publisher Sakarya University
http://www.saujs.sakarya.edu.tr/en/

Title: The Classification of OECD Countries in Terms of Life Satisfaction Using Partial Least Squares Discriminant Analysis

Authors: Esra Polat
Recieved: 2019-10-14 14:36:39

Accepted: 2020-01-28 13:47:04

Article Type: Research Article
Volume: 24
Issue: 2
Month: April
Year: 2020
Pages: 365-376

How to cite
Esra Polat; (2020), The Classification of OECD Countries in Terms of Life Satisfaction Using Partial Least Squares Discriminant Analysis. Sakarya University Journal of Science, 24(2), 365-376, DOI: https://doi.org/10.16984/saufenbilder.632820
Access link
http://www.saujs.sakarya.edu.tr/tr/issue/52471/632820

Sakarya University Journal of Science 24(2), 365-376, 2020

The Classification of OECD Countries in Terms of Life Satisfaction Using Partial Least Squares Discriminant Analysis

Esra POLAT[1]

Abstract

Life satisfaction (LS) measures how people assess their lives as a whole, not their present emotions. Measuring emotions can be very subjective, but it is still a useful completion to more objective data when comparing quality of life across countries. Many questionnaires are used to measure especially LS and happiness. The Partial Least Squares Discriminant Analysis (PLSDA) is a statistical method for classification and includes an ordinary Partial Least Squares Regression, where the dependent variable is categorical that represents each observation's class membership. In this study, the purpose is to classify 35 OECD countries correctly to their predefined classes (above or below the average LS level of OECD) by using year 2017 Better Life Index data. In the analyses PLSDA, a flexible supervised classification method, is used. PLSDA is a preferable alternative method in case of some assumptions not satisfied for classical discriminant analysis. The results showed that PLSDA has a satisfying classification performance and self-reported health (SH) is only effective variable in determining the LS levels of countries.

Keywords: Better Life Index, classification, life satisfaction, OECD countries, Partial Least Squares Discriminant Analysis

1. INTRODUCTION

There is much more than Gross Domestic Product (GDP) numbers and economic statistics. Therefore, the current economic and financial crisis has refocused interest in other factors. The trick is to decide what works for a better life and the way of measuring progress. In most OECD countries, inequality is broadening and more money does not make people feeling better. So that what else should be measured that thought to affect the life happiness? The OECD interested on this question over ten years ago; and work such as the Stiglitz-Sen-Fitoussi Commission in France, and in recent times national attempts such as the UK's programme Measuring National Well-Being [1].

[1] Corresponding Author: espolat@hacettepe.edu.tr
Hacettepe University, Faculty of Science, Department of Statistics, ORCID ID: 0000-0001-9271-485X

In 2011, the OECD Better Life Initiative took an interactive step with the Better Life Index, an international comparable well-being indicator (How's Life? Report) and its interactive tool, the Better Life Index (BLI) inviting users to look at how their country measures up on the subjects that significant for them, a wide range of topics from education to air pollution, from health to income etc. [1].

A key reason for measuring well-being is to understand whether, where and how life is getting better for people. In "How's Life? 2017: Measuring Well-being" report provides an overview of OECD countries' achievements across 11 dimensions of current well-being and four different "capital stocks" that help to sustain well-being overtime. It features a various set of statistics, ranging from household wealth to times spent on leisure, and from air pollution to how safe people feel walking alone at night. Since the last 10 years have been a turbulent time in most OECD economies, the particular focus on changes in people's well-being. It seeks to address the simple question: Is life today better or worse than it was in 2005, before the financial crisis took hold? [2].

Life satisfaction (LS) is highest in Denmark, Norway and other Scandinavian countries, also in Switzerland, New Zealand, Canada and Australia - countries with high levels of employment, quality of jobs and population health [3]. In countries with the lowest LS, employment levels and, usually, life expectancy are below the OECD average. The BLI indicates that having strong relationships with friends and deriving pleasure from a good work-life balance and personal safety is associated with high LS. Scandinavian countries score high in these areas, also in Spain where data that underpin BLI indicate that 96% of people know someone they can trust in the moment of need, one of the OECD's highest rates [3].

The BLI shows that there is little difference in LS between men and women in 35 countries. Nevertheless, in OECD countries individuals with bachelor's degree have tendency to have higher LS than those who are merely primary school graduated. BLI includes 35 countries and measures well-being over 11 dimensions (civic engagement, community, education, environment, health, housing, income, jobs, life satisfaction, safety, work-life balance). This index clears that if a country has a good performance in economic, this means not directly it will indicate same good performance in terms of well-being. For example, Mexico and Turkey indicate a good performance in some form of civic engagement. South Africa scores inadequately compared to rich countries in terms of many indicators, however, it has a relatively strong public conscience and work-life balance [3].

Personal security is also a problem in some rich countries. BLI shows that in Australia, New Zealand and US people feel unsafety in high level. The countries who perform well above the average in work-life balance have various economic levels such as Hungary, Ireland, Italy and Russia. Estonia, Germany, Japan, Korea and Poland are among the countries with the best general education and skill levels. Decent housing is a significant component of well-being. BLI reveals that good housing conditions are often connected with good economic outcomes. Canadians and Americans demonstrate a tendency to benefit from best housing circumstances [3].

BLI's online interactive tool also permits users to directly tell what is substantial to their own well-being. Up to now, in 180 countries this tool has been used by more than 110000 people. In general, online users rank education, health and LS as the most essential elements for their well-being. The education is commonly considered to be the most important of the 11 well-being dimensions in Latin America. However, regional differences appear. LS and work-life balance are among the top precedencies in North America even though community environment and health are the base interests in Europe [3].

LS measures how people evaluate their lives as a whole, not their present emotions. Considering the all OECD countries using a scale between 0 and 10, people gave an average score of 6.5 for scoring their overall LS. However, LS is not

shared equally in the OECD. In some countries such as Portugal, Greece, Turkey - with an average of 5.5 scores or less, seen relatively low level of overall LS. At the other end of the scale, scores reach 7.5 in Denmark, Iceland, Finland, Switzerland and Norway [4].

The term of a better life first appeared in the 2000s. In 2001, the OECD published a report on the better lives of countries [5]. Osberg and Sharpe [6] developed an economic well–being index by merely in view of economic variables for chosen OECD countries: Australia, Canada Sweden, Norway, U.K, U.S. Kerenyi [7] also studied on and introduced a BLI for countries. Kasparian and Rolland [8] developed a better quality of life index based on diverse data from OECD countries. Stevenson and Wolfers [9] interested on the relationship between income and well-being so that evaluations made on LS. Mizobuchi [10] suggested a combined indicator of overall well-being, to measure the performance of each country in supplying well-being to its citizens. He applied Data Envelopment Analysis to form a group of 11 separate well-being indicators into a combined indicator, using the World Bank's production base estimates for each country. Akar [11] assessed BLI as an alternative tool for measuring well-being for Turkey. As a result of this it is found that the lowest BLI value belongs to Turkey among OECD countries. Durand [12] discussed the advantages and disadvantages of several approaches for introducing and spreading information on multidimensional well-being to different people, containing the OECD BLI. The progress made in developing measures of well-being is exemplified and the statistical agenda for improving present indicators and building-up new ones is outlined [5]. Gundogan Aşık and Altın Yavuz [5] compared six different methods for modeling the LS using the OECD BLI Data. They have found that if solely classification is interested, the robust discriminant analysis can be used for modeling of LS. But robust logistic ridge regression could be used in case of determining the effective levels for LS. Başol [13] aimed to discover the dynamics affecting the LS in OECD countries by using the year 2016 BLI data. The results of this research using structural equation modeling technique and model development strategy showed; health and positive work quality positively affect LS; income and negative job quality negatively affect LS.

PLSDA is a good alternative to classical discriminant analysis, since in some circumstances classical one could not be used while PLSDA could be performed; for instance, the situations such as the number of explanatory variables exceeding the number of observations ($p>>n$). Moreover, it can be performed on data even if in case of missing values and multicollinearity problem and non-normality [14]. The purpose of this study is classify 35 OECD countries by using PLSDA according to their LS level (above or below the average score of 6.5 across the OECD) by using the potential effective 23 variables on LS that constituting quality of life.

2. PARTIAL LEAST SQUARE DISCRIMINANT ANALYSIS

PLSDA is a supervised classification method, since it must have primary information about the class memberships of the samples. Barker and Rayens [15] compared PLSDA with Linear Discriminant Analysis (LDA) and mentioned that PLSDA has advantages over classical Discriminant Analysis (DA) such as choosing of variables and reduction of noise [16].

The PLSDA method use the same algorithm for Partial Least Squares Regression (PLSR), the only difference is Y has discrete values used for showing class memberships of each observation. PLSR searches for a direct relationship between dependent variable and the explanatory variables. X matrix with nxp dimension shows the independent variables; n is the number of observations and p is the number of explanatory variables. Y matrix with nxq dimension corresponding to the dependent variable. Here, q represents the number of dependent variables. X and Y are decomposed by scores (or components, or latent variables) and the size of the data is reduced as shown in Eq. (1) and Eq. (2) [16].

$$X = TP' + E \tag{1}$$

$$Y = UQ' + F \quad (2)$$

T and U are the score matrices for X and Y, respectively; P shows the loading matrix of X; E is the error term for X; Q is the loading matrix for Y and F is the residual matrix for Y. In PLSR while choosing components, their relationship with Y is also considered different from Principal Component Regression (PCR). The optimal number of components are generally lower than PCR. T components are orthogonal and they are estimated as in Eq. (3) by using W^*, the weight matrix [16].

$$T = XW^* \quad (3)$$

The T components are good predictors of Y and the PLSDA model is written as in Eq. (4). F shows the deviations between the real and predicted response.

$$Y = TQ' + F \quad (4)$$

Inserting Eq. (3) in Eq. (4) the model can be updated lastly as in Eq. (5) and turns to a regression model as in Eq. (6).

$$Y = XW^*Q' + F \quad (5)$$

$$Y = X\beta + F \quad (6)$$

The regression coefficients are obtained as $\beta = W^*Q'$, where W^* can be obtained as in Eq. (7). W is defined using a set of weighting loadings, which maximizes the covariance between X and Y [17]. The detailed information about PLSR model and its classical algorithm's steps could be found in Wold et al. [18].

$$W^* = W\left(PW\right)^{-1} \quad (7)$$

In case of two classes in the data set, in PLSDA the matrix Y is coded to 0 or 1 (G=2). In case of multiple classes (G>2), several models could be constructed with 0 and 1 encoding, or the PLS2 algorithm is used by constructing a matrix (nxG), in which each column shows a class [16, 19]. An important stage of constructing a PLSDA model is the determination of the ideal number of LVs. For this purpose, usually cross-validation (CV) is used. In this method the data set is divided by training samples and validation samples and the models are built with the separated observations for validation sample. The prediction errors are computed for separated samples using various numbers of LVs. The process is repeated until all samples are predicted. The PLSDA model gives a number by using Eq. (5), not reading completely 0 or 1. Hence, constructing threshold values is necessary for defining the class limits. The threshold is estimated by using Bayesian theorem in many approaches [19] or by constructing confidence limits for each classified object. Usually resampling techniques such as bootstrap could be used for the calculation of these confidence intervals [16].

3. CLASSIFICATION PERFORMANCE MEASURES

The calculated classification measures are described in Ballabio et al. [20]. These measures are used to assess the performance of classification methods such as classical DA or PLSDA. The classification results can be showed in confusion matrix (or contingency table). Since G represents the number of classes, the ***confusion matrix*** dimension is G x G. It could be showed as in Table 1. Each element c_{gk} shows the number of samples belonging to class g and assigned to class k. Hence, the diagonal elements c_{gg} show the number of correctly assigned observations, while off-diagonal elements show the numbers of unclassified observations [20, 21].

Table 1. Representation of confusion matrix (in case of G classes)

		Assigned Class				
		1	2		G	
True Class	1	c_{11}	c_{12}	⋯	c_{1G}	n_1
	2	c_{21}	c_{22}	⋯	c_{2G}	n_2
	⋯	⋯	⋯	⋯	⋯	⋯
	G	c_{G1}	c_{G2}	⋯	c_{GG}	n_G
		n'_1	n'_2		n'_G	n

Three popular class-based measures (sensitivity, precision and specificity) are used for estimating the classification performance obtained on each class. They are computed on each class individually and show different sides of the classification [20].

Sensitivity defining the model ability of correctly recognizing samples of the g-th class and is given as in Eq. (8) [20, 21]:

$$Sn_g = \frac{c_{gg}}{n_g} \tag{8}$$

Here, c_{gg} (the diagonal elements of confusion matrix) showing the correctly classified samples, n_g is the total number of objects that member of the g-th class. In case of all the samples that member of the g-th class are correctly assigned $\left(c_{gg} = n_g\right)$, Sn_g equals to 1. The unassigned objects of the g-th class are not taken under consideration for the sensitivity computation.

Precision represents the capability of a classification model not containing objects of other classes in the examined class. It shows the ability of a classifier avoiding wrong predictions in that class and given by Eq. (9) [20, 21]:

$$P_{rg} = \frac{c_{gg}}{n'_g} \tag{9}$$

Here, the total number of objects assigned to the g-th class showed by n'_g. If all the objects assigned to class g correspond to the samples member of class g, P_{rg} equals to 1.

Specificity characterizes the capability of a classifier to reject the samples of all the other classes and is given as in Eq. (10) [20, 21]:

$$Sp_g = \frac{\sum_{k=1}^{G}\left(n'_k - c_{gk}\right)}{n - n_g} \quad \text{for} \quad k \neq g \tag{10}$$

Each element of confusion matrix c_{gk} represents the number of objects belonging to class g and assigned to class k. Hence, n'_k shows the total number of objects classified to the k-th class: $n'_k = \sum_{g=1}^{G} c_{gk}$. This measure computed as the ratio of "samples not member of the g-th class also not assigned to the g-th class" over "the total number of samples not member of the g-th class ($n-n_g$)". Sp_g equals to 1, in case of the objects not member of class g are never classified to g. Not classified objects are not taken under consideration for the specificity computation.

Until now the three measures that we examined give the classifier performances on each specific class, however, they do not yield total assessment of the classification quality. Hence, by clustering class measures in different ways, global measures of classification performances are computed.

Accuracy (AC) is another index helps for evaluating the classification quality. It is also named as overall agreement/predictive ability/classification rate/success rate, total accuracy. It is given as in Eq. (11) and shows the ratio of correctly classified objects. It takes the values between 0 (no correctly classified objects) to 1 (perfect classification) [20, 21]:

$$AC = \frac{\sum_{g=1}^{G} c_{gg}}{n} \tag{11}$$

n is the total number of samples and not classified objects are not used for the accuracy computation. "Misclassification error" is the complementary of it and defined as the ratio of objects classified to a wrong class.

Non error rate (NER) is the mean of the class sensitivities [20]:

$$NER = \frac{\sum_{g=1}^{G} Sn_g}{G} \tag{12}$$

Error Rate (ER) is given as: $ER = 1 - NER$, using the non-error rate.

Ratio of not assigned samples is the fraction of the objects that could not have assigned in the modelled classes. Not assigned samples are not used in the specificity, sensitivity, non error rate and error rate computations [20].

Classification results could be presented by using graphs such as ***ROC (Receiver Operating Characteristics) curves***. In Classification toolbox for MATLAB [22], as a result of PLSDA these curves are also given.

A ROC curve is a plot of sensitivity and specificity, used for classification studies of two class date sets. Its discrimination threshold is not fixed. By using contingency table, a single value of sensitivity and specificity can be computed. So that each contingency table shows one point in the ROC space. For each threshold value, a classification rule is computed and the related contingency table is obtained. The best possible classification method would produce a point in the upper left corner of the ROC space, standing for maximum sensitivity and specificity, however, a random classification yields points along the diagonal line from the left bottom to the top right corners. ROC curves are computed for each class, separately, by changing the threshold of assignations. The area under the ROC curve (AUC) can be used as estimator of the class discrimination; it is shown in the plot title for each class [20]. ROC is a probability curve and AUC shows degree or measure of separability. It shows model ability of distinguishing between classes.

Formula and extra details on these classification measures are given in html help files created for the Classification Toolbox for MATLAB [22, 23].

4. APPLICATION AND RESULTS

The Better Life Index is applied to 35 OECD members. These OECD countries are; Australia, Austria, Belgium, Canada, Chile, Czech Republic, Denmark, Estonia, Finland, France, Germany, Greece, Hungary, Iceland, Ireland, Israel, Italy, Japan, Korea, Latvia, Luxembourg, Mexico, Netherlands, New Zealand, Norway, Poland, Portugal, Slovak Rebuplic, Slovenia, Spain, Sweden, Switzerland, Turkey, United Kingdom, United States [2, 5].

The data set is obtained from OECD 2017 BLI data. LS used as the dependent variable and coded as two classes for each of 35 OECD countries. 6.5 is the average LS score across the OECD.

$$y_i = \begin{cases} 0, & \text{Countries with a LS score less than 6.5 / low LS level} \\ 1, & \text{Countries with a LS score greater than 6.5 / high LS level} \end{cases}$$

The independent variables are 23 sub-dimensions given in OECD BLI data set. 10 dimensions and their sub-dimensions can be examined in Table 2. The analysis made by using Classification Toolbox (MATLAB) and XLSTAT (Excel) programs. XLSTAT running on Excel and lets users for analyzing, customizing and sharing their results within Microsoft Excel [22, 23, 24].

Table 2. OECD Better Life Index 2017 dimensions and sub-dimensions

Dimensions	**Sub-Dimensions**
Housing	• Dwellings without basic facilities **(DW)** • Housing expenditure **(HE)** • Rooms per person **(RP)**
Income	• Household net adjusted disposable income **(HI)** • Household net financial wealth **(HFW)**
Jobs	• Labour market insecurity **(LM)** • Employment rate **(ER)** • Long-term unemployment rate **(LUR)** • Personal earnings **(PE)**
Community	• Quality of support network **(QN)**
Education	• Educational attainment **(EA)** • Student skills **(SS)** • Years in education **(YE)**
Environment	• Air pollution **(AP)** • Water quality **(WQ)**
Civic engagement	• Stakeholder engagement for developing regulations **(SE)** • Voter turnout **(VT)**
Health	• Life expectancy **(LE)** • Self-reported health **(SH)**
Safety	• Feeling safe walking alone at night **(SWA)** • Homicide rate **(HR)**
Work-Life Balance	• Employees working very long hours **(EH)** • Time devoted to leisure and personal care **(TLP)**

Resource:https://stats.oecd.org/Index.aspx?DataSetCode=BLI

The data set could be analyzed by using classical DA. However, there are several assumptions for DA that must be checked. Firstly, an assumption that the discriminating variables follow the multivariate normality must be checked.

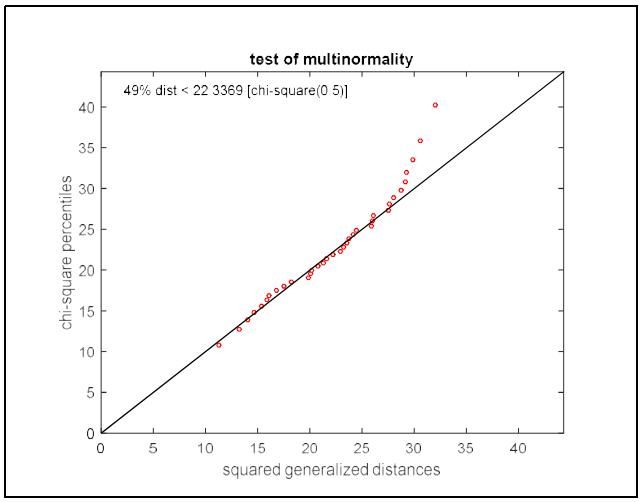

Figure 1. The chi-square Q-Q plot

Multivariate normality test has been implemented by using Mahalanobis Distances. Figure 1 shows that there are some deviations from the straight line, therefore, possible deviations from a multivariate normal distribution. It can be concluded that, this data set not meets multivariate normality assumption since the plot indicates departures from multivariate normal distribution explicitly.

Multicollinearity exists in any model when two or more independent variables in the model are related to each other. There are several different numerical methods for exploring multicollinearity connections. VIF and Tolerance values are statistics which the researches usually prefer. The multicollinearity detection is done by using Microsoft Excel XLSTAT program. In practice, if any of the VIF values is equal or larger than 10, there is a near collinearity. From Table 3 it is clear that the VIF values for RP, HI, LM, ER, LUR, PE, SS, WQ are 13.398, 17.475, 11.142, 13.995, 13.552, 22.475, 11.112, 18.865, respectively. Hence, there is a multicollinearity problem for this dataset.

Table 3. Multicollinearity statistics result

Statistic	**DW**	**HE**	**RP**	**HI**
Tolerance	0.136	0.340	0.075	0.057
VIF	7.379	2.937	13.398	17.475
Statistic	**HFW**	**LM**	**ER**	**LUR**
Tolerance	0.189	0.090	0.071	0.074
VIF	5.295	11.142	13.995	13.552
Statistic	**PE**	**QN**	**EA**	**SS**
Tolerance	0.044	0.105	0.142	0.090
VIF	22.475	9.556	7.054	11.112
Statistic	**YE**	**AP**	**WQ**	**SE**
Tolerance	0.350	0.102	0.053	0.294
VIF	2.856	9.769	18.865	3.400
Statistic	**VT**	**LE**	**SH**	**SWA**
Tolerance	0.295	0.163	0.116	0.175
VIF	3.385	6.123	8.600	5.711
Statistic	**HR**	**EH**	**TLP**	
Tolerance	0.166	0.173	0.180	
VIF	6.015	5.774	5.549	

Since multivariate normality assumption and independence among predictors are not satisfied, instead of classical DA, PLSDA could be implemented on the data set. Before it is mentioned that PLSDA is not affected by these assumptions. Firstly, for PLSDA the ideal number of LVs must be determined. For this purpose, error rate CV against number of LVs graph could be used [23].

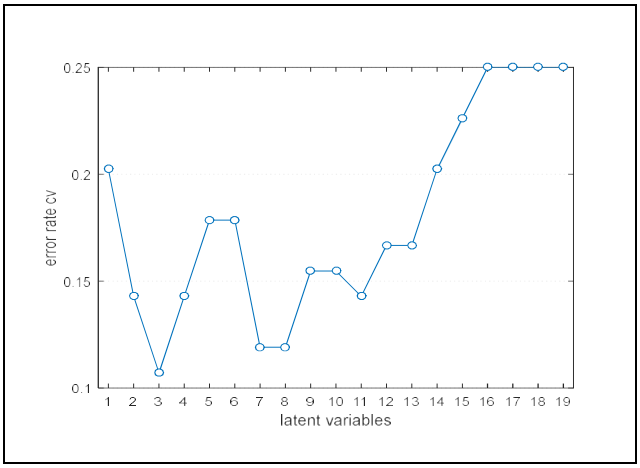

Figure 2. Error rate in CV versus number of components in PLSDA. CV was implemented 5 groups, obtained by venetian blinds method

From Figure 2, it is clear that by choosing 3 LVs much simple classification model is computed and CV error is very low for 3 LVs. After the ideal number of LVs is determined, PLSDA model can be obtained on the training samples. The final PLSDA model is obtained by choosing 3 LVs and 5 CV groups for validation. The confusion matrices constructed for fitting and CV as given in Table 4. The outputs of the classification model are collected in confusion matrix and it is the preliminary stage of evaluating the classification performance. The last column of the Table shows the number of unclassified objects for each class. From Table 4, it can be observed that, in fitting, 1 out of 21 high samples are classified into low class (3 in CV), 1 out of 14 low samples are classified into high class (1 in CV), and finally there is not any samples that are not assigned. It is clear from Table 4 that %94.29 of the countries are correctly classified for the training sample. For prediction sample it is seen from Table 4 that %88.57 of the countries are correctly classified.

Table 4. Confusion matrices for fitting and CV with 5 venetian blinds groups

	Predicted Class		
Real Class	**High**	**Low**	**Not assigned**
Fitting			
High	20	1	0
Low	1	13	0
Cross validation			
High	18	3	0
Low	1	13	0

Table 4 reveals that in case of two classes the confusion matrix could be shown as in below (in which the high class is defined as positive, P and low class as negative, N):

		Predicted Class	
		High (P)	Low (N)
Real Class	High (P)	TP	FN
	Low (N)	FP	TN

Here, TP (True Positive) represents the number of high objects correctly classified as high, TN (True Negative) shows the number of low objects correctly classified as low, FN (False Negative) represents the number of high objects wrongly classified as low and FP (False Positive) shows the number of low objects wrongly classified as high.

TP/(TP+FN) is used for computing the high class sensitivity. Class sensitivity values range between 0 and 1 and defining the model capability to correctly distinguish objects that are member of that class. For instance, if not any of the high samples are assigned to low class (FN equals to 0), the sensitivity for high class can be equal to 1.

On the contrary, TN/(FP+TN) is used for high class specificity. The class specificity values range between 0 and 1 and defining the model capability of rejecting objects of all other classes. For instance, if not any of the low samples are assigned to high class (FP equals to 0), the specificity for high class can be equal to 1 [23].

In Table 5, the classification performance measures of PLSDA model are presented. It is known that when there are only two classes, sensitivity and specificity of two classes are symmetrical, as a result, all the time sensitivity of the high class equals to specificity of the low class and vice versa. The results of fitting (in case of all training samples used for modelling) shows that the low class's specificity and sensitivity values are 0.95 and 0.93, respectively. Taking under consideration only the classified samples, this means that 93 % of the low training samples (13 out of 14) are correctly classified as low and 95 % of the high training samples (20 out of 21) are correctly classified as high. Because of sensitivity and specificity values show similarity, it can be concluded that the type of error is balanced, hence, there is not special trend in the model for recognizing high samples as low, or vice versa. The model NER and ER in fitting are equal to 0.94 and 0.06, respectively. Finally, the classification performance of CV can be compared with model fitting. Cross-validated and fitting results are more similar for high class and less similar for low class. Although small difference can be seen, still it could be concluded that the PLSDA classification model can be supposed to be reliable and stable, since the classification performance is not badly affected by samples taken out from the training set during the CV procedure.

Table 5. Classification performance measures for both fitting and CV (for 5 venetian blinds groups)

	High		
	sensitivity	**specificity**	**precision**
Fitting	0.95	0.93	0.95
Cross validation	0.86	0.93	0.95
	Low		
	sensitivity	**specificity**	**precision**
Fitting	0.93	0.95	0.93
Cross validation	0.93	0.86	0.81
	NER	**ER**	**AC**
Fitting	0.94	0.06	0.94
Cross validation	0.89	0.11	0.89

The evaluation of the classification performance of a model could also be made by using ROC curves. A perfect model's AUC will be close to 1 means that having a good measure of separability. A poor model's AUC will be close to 0 meaning that having the worst measure of separability. This kind of poor model predicts 0s as 1s and 1s as 0s (means lows as highs, highs as low). Moreover, in case of AUC is 0.5, it refers to model's incapability of separation. In Figure 3, ROC curves for high (upper) and low (lower) classes are shown. Table 5 also reveals that the ROC curves of both classes are nearly perfect. The plots on the right of Figure 3 are ROC curves, as showing the sensitivity and specificity values as the class threshold for assigning samples to the class is changed. The class threshold is chosen at the point where the number of FPs and number of FNs is minimized and hence, its value corresponds to the point where the specificity line crosses the sensitivity line.

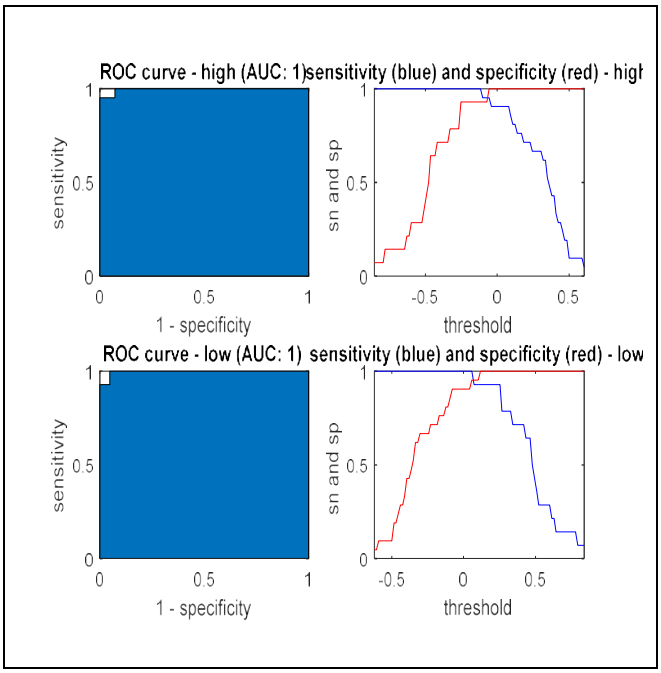

Figure 3. ROC curves (LEFT SIDE) and plots of specificity (red) sensitivity (blue) values (RIGHT SIDE)

Since PLSDA's origin comes from PLSR algorithm, the regression coefficients of the variables are obtained using this algorithm. The significant variables, for classifying objects to their correct classes, will have positive coefficients that contributing in increment of the class calculated response. Until now all results are obtained in Classification Toolbox, but in order to see which variable/variables are important in discriminating the classes, the results are obtained in XLSTAT.

The standardized coefficients are given in Table 6. It can be used to compare the relative weight of the variables in the model. For the computation of confidence intervals of coefficients, PLSR do not use the classical formulae based on the normality hypotheses used in Ordinary Least Squares regression. A bootstrap method gives confidence intervals estimations. If the absolute value of a coefficient is higher, weight of the variable in the model is also higher. In case of interval estimation of standardized coefficients contains 0, the weight of the variable in the model is unimportant [14].

Table 6. Standardized coefficients of the model

Variable	Coeff.	Std. Dev.	LB (95%)	UB(95%)
DW	-0.078	0.202	-0.489	0.332
HE	0.092	0.184	-0.281	0.465
RP	0.173	0.157	-0.147	0.492
HI	0.036	0.105	-0.178	0.250
HFW	0.003	0.143	-0.289	0.294
LM	-0.239	0.208	-0.661	0.184
ER	0.119	0.141	-0.168	0.406
LUR	-0.184	0.156	-0.502	0.133
PE	0.131	0.079	-0.029	0.292
QN	-0.007	0.121	-0.253	0.239
EA	-0.025	0.188	-0.406	0.356
SS	-0.290	0.162	-0.619	0.039
YE	0.084	0.159	-0.240	0.408
AP	0.008	0.172	-0.340	0.357
WQ	0.021	0.114	-0.211	0.253
SE	-0.158	0.251	-0.668	0.352
VT	0.051	0.202	-0.358	0.461
LE	-0.011	0.157	-0.329	0.308
SH	**0.394**	**0.168**	**0.052**	**0.736**
SWA	-0.030	0.125	-0.283	0.224
HR	0.236	0.173	-0.116	0.589
EH	-0.104	0.206	-0.523	0.316
TLP	0.020	0.178	-0.342	0.382

The results in Table 6 indicates that the only important variable that determine the statuses of high and low LS levels of OECD countries is “self-reported health (SH)” that means percentage of people whose feeling healthy is the most important determinant of LS.

5. CONCLUSION

Quality of life of countries mainly can be understood from LS variable. The countries policies for making progress about their economic prosperity will be inevitably affected by researches on influences of other variables of quality of life on LS. Here, a significant variable LS that effects the quality of life is taken under consideration. A comparison between the welfare levels of countries in terms of many different areas can be derived by LS. Particularly in these days, the welfare of the countries identified merely by the income does not show that the welfare of the country is well. There are many different determinants of LS, that OECD surveys sum up them under titles like income, housing, jobs, education, community, environment, health, civic engagement, work-life balance and safety. Different from previous studies on this field, in this study, the sub-dimensions under these variables are used to find the most effective variable in determining the countries’ LS levels. The analyzes showed that data set is non-normal and also there is a multicollinearity problem. Therefore, classical DA couldn’t be used and PLSDA is preferred. As a result of PLSDA %94.29 of the countries are correctly classified for the training sample and %88.57 of the countries are correctly classified for validation sample. PLSDA has a good classification performance. Moreover, it is found that self-reported health (SH) is the only important variable in determining life satisfaction levels of 35 OECD countries.

Systematic health surveys are done by most of OECD countries for enabling participants to report on various statuses of their health. "How is your health?" is a frequently asked question for collecting data about self-perception health status. In spite of this question is non-objective, the responses are used to be a well estimator of people's future healthcare. In the OECD, around 69% of the adult population tell their health is "good" or "very good". Although 88% of adults say their health is "good" in New Zealand and Canada, less than 40% of people express their health as "good" or "very good" in Korea and Japan. Cultural, regional or other elements could affect the answers of this popular health question.

Men most likely to report better health compared to women, as the OECD average says 71% of men define their health status as "good" or "very good", however, this is only 67% for women. The differences between men and women are highest in countries such as Portugal, Turkey, France, United Kingdom. The answers are also changing according to age and social status. As it is expected older adults, also unemployed, having less education or income people state bad health status. In OECD countries, nearly 78% of adults,

with an available income in the top 20%, report their health as "good" or "very good". However, 61% of those, with an available income in the bottom 20%, give same answers.

As a result, it could be mentioned that self-reported health percentages obtained in each country could be explained by different factors. Each country must investigate the factors under people feelings about their health statuses. These feelings could be shaped on economical, sociological, physiological, even if climatic etc. factors. Each country must determine own policies for enhancing LS level in their home.

6. REFERENCES

[1] https://www.oecd.org/forum/issues/forum-issue-better-life-index.htm.

[2] OECD (2017), How's Life? 2017: Measuring Well-being, OECD Publishing, Paris. http://dx.doi.org/10.1787/how_life-2017-en

[3] https://www.oecd.org/social/the-path-to-happiness-lies-in-good-health-and-a-good-job-the-better-life-index-shows.htm

[4] http://www.oecdbetterlifeindex.org/topics/life-satisfaction/

[5] E. Gundogan Aşık, A. Altın Yavuz, "Investigatıon of life satisfactıon in OECD countries with multivariate analysis method", Journal of Social and Humanities Sciences Research (JSHSR), Vol. 5, no. 26, pp. 2547-2561, 2018.

[6] L. Osberg and A. Sharpe, "An index of economic well-being for selected OECD countries", Review of Income and Wealth, vol. 48, pp. 291-316, 2012.

[7] A. Kerenyi, "The better life index of the organisation for economic co-operation and development", Public Finance Quarterly, vol. 56, pp. 518–538, 2011.

[8] J. Kasparian and A. Rolland, "OECD's better life index: Can any country be well ranked?", Journal of Applied Statistics, vol. 39, pp. 2223– 2230, 2012.

[9] B. Stevenson and J. Wolfers, "Subjective Well-Being and Income: Is There Any Evidence of Satiation", American Economic Association, vol. 103, pp. 598-604, 2013.

[10] H. Mizobuchi, "Measuring world better life frontier: a composite indicator for OECD better life index", Soc Indic Res, vol. 118, pp. 987–1007, 2014.

[11] S. Akar, "Türkiye'de daha iyi yaşam endeksi: OECD ülkeleri ile karşılaştırma". Journal of Life Economics, vol. 1, no. 1, pp. 1-12, 2014.

[12] M. Durand, "The OECD better life initiative: how's life and the measurement of well-being", Review of Income and Wealth, vol. 61, no. 1, pp.4-17, 2015.

[13] O. Başol, "An evaluation on life satisfaction in OECD countries ", "IS, GUC" Industrial Relations and Human Resources Journal, vol. 20, no. 3, pp. 71-86, 2018.

[14] E. Polat, "Determination of the effective economic and/or demographic indicators in classification of European Union member and candidate countries using Partial Least Squares Discriminant Analysis", Journal of Data Science, vol. 16, no. 1, pp. 79-92, 2018.

[15] M. Barker, W.S. Rayens, "Partial least squares for discrimination", Journal of Chemometrics, vol. 17, pp. 166 – 173, 2003.

[16] M.R. Almeida, D.N. Correa, W.F.C. Rocha, and F.J.O. Scafi, "Discrimination between authentic and counterfeit banknotes using Ramanspectroscopy and PLS-DA with uncertainty estimation", Microchemical Journal vol. 109, pp. 170-177, 2013.

[17] H. Martens and M. Martens, "Modified Jack-knife estimation of parameter uncertainty in bilinear modelling by partial least squares regression (PLSR)". Food Quality and Preference, vol. 11, no. 1-2, pp. 5-16, 2000.

[18] S. Wold, M. Sjöström, and L. Eriksson, "PLS-regression: a basic tool of chemometrics", Chemometrics and Intelligent Laboratory Systems, vol. 58, pp. 109-130, 2001.

[19] B.M. Wise, N.B. Gallagher, R. Bro, J.M. Shaver, W. Windig, and R.S. Koch, R.S. "PLS Toolbox 4.0 for use with Matlab", 3905 West Eaglerock Drive, Wenatchee, WA, Eigenvector Research Inc. http://www.eigenvector.com, 2006.

[20] D. Ballabio, F. Grisoni, and R. Todeschini, "Multivariate comparison of classification performance measures", Chemometrics and Intelligent Laboratory Systems, vol. 174, pp. 33-44, 2018.

[21] D. Ballabio, R. Todeschini, "Chapter 4-Multivariate Classification for Qualitative Analysis" in Book: "Infrared Spectroscopy for Food Quality Analysis and Control" , pp.83-104, 2009. https://doi.org/10.1016/B978-0-12-374136-3.00004-3

[22] Classification toolbox for MATLAB. file:///C:/Program%20Files/MATLAB/MATLAB%20Production%20Server/R2015a/classification_toolbox_5.2/help/index.htm

[23] D. Ballabio and V. Consonni, "Classification Tools in Chemistry. Part 1: Linear Models. PLS-DA", Analytical Methods, vol. 5, pp. 3790-3798, 2013.

[24] XLSTAT, Partial Least Squares Discriminant Analysis PLSDA Tutorial. https://help.xlstat.com/s/article/partial-least-squares-discriminant-analysis-plsda-tutorial?language=en_US

JOURNAL OF SCIENCE
SAKARYA UNIVERSITY

Sakarya University Journal of Science

ISSN 1301-4048 | e-ISSN 2147-835X | Period Bimonthly | Founded: 1997 | Publisher Sakarya University
http://www.saujs.sakarya.edu.tr/en/

Title: A Survey on Illicit Drug Use among University Students by Binary Randomized Response Technique: Crosswise Design

Authors: Nilgün Özgül
Recieved: 2019-10-02 15:56:13

Accepted: 2020-02-04 15:26:06

Article Type: Research Article
Volume: 24
Issue: 2
Month: April
Year: 2020
Pages: 377-388

How to cite
Nilgün Özgül; (2020), A Survey on Illicit Drug Use among University Students by Binary Randomized Response Technique: Crosswise Design. Sakarya University Journal of Science, 24(2), 377-388, DOI:
https://doi.org/10.16984/saufenbilder.628405
Access link
http://www.saujs.sakarya.edu.tr/tr/issue/52471/628405

Sakarya University Journal of Science 24(2), 377-388, 2020

A Survey on Illicit Drug Use among University Students by Binary Randomized Response Technique: Crosswise Design

Nilgün ÖZGÜL[1]

Abstract

This paper aims to introduce Randomized Response Techniques (RRT's) and show that how RRT's are implemented in surveys in which sensitive behaviors are investigated. For this purpose, the most popular designs of the Binary RRT are summarized and an experimental study is conducted on drug use among dormitory students at a public university in Ankara, Turkey. Despite the wide applicability of the drug use studies in Turkey, surprisingly any applications using indirect questioning techniques are not observed in the literature. In this study, for the first time, drug use behavior is investigated with Crosswise design which is the most frequently used indirect questioning technique and indirect questioning method (Crosswise design) is compared with direct questioning method to evaluate the effectiveness of the RRT. Results revealed that when Crosswise design is provided on asking sensitive questions, considerably minor response refusals are happened and significantly higher drug-use estimates are observed.

Keywords: Randomized Response Technique, Sensitive Questions, Prevalence Estimation, Crosswise design

[1] Corresponding Author: nozgul@hacettepe.edu.tr
Hacettepe University, Faculty of Science, Department of Statistics, Beytepe Campus, Ankara, Turkey. ORCID ID: http://orcid.org/0000-0003-0331-9044

1. INTRODUCTION

In natural and social sciences, some research topics are related to sensitive behaviors such as mobbing, political view, tax evasion, illegal income Semitism, gambling, alcoholism, drug addiction, doping usage, sexual and physical abuse, homosexual activities, abortion, illegal hunting and many others. In surveys that collect data with direct techniques on sensitive topics, respondents are often underreported on sensitive information, even they refuse to answer. So, nonresponse on sensitive questions is normally higher than for other questions in a survey. In such surveys, a well-known technique to obtain valid and reliable information on sensitive questions is the Randomized Response Technique (RRT), introduced by [1]. The RRT is an effective indirect questioning technique that ensures privacy and may well succeed respondents' reluctance to express sensitive or probably illicit information. Therefore, respondents are more tend to collaborate and give true answers to sensitive questions. *RRTs* use a randomization device (a die, a deck of cards or a spinner) efficiently to reduce non-respondents rates resulting from sensitive, embarrassing or even illicit questions. In RRT, with the usage of a randomization device, the respondent gives a randomized answer concerning his/her true status. Due to the interviewer is unknowing of the result of the randomization device, the use of these techniques protects the anonymity of the answers of respondents. It also appeared that the results of the RRT's become more precise when the topic under investigation is more sensitive [2].

RRTs are sub classified as binary and quantitative RRTs. Binary RRT's are used to estimate the proportion of some sensitive behavior in a population. Quantitative RRTs are used to estimate the mean value of some behavior in a population [3]. In this study, the most popular Binary RRT's will introduce and real applications in literature will be given.

The paper is organized as: In section two, the most popular designs of the Binary RRT that have been proposed in the literature are summarized and real-life examples for each design will be given. Also, in this section, the crosswise design which is one of the most popular design used in recent studies is adapted to the stratified sampling. In section three, empirical studies on drug use in university students in Turkey are summarized. In section four, the application on drug use among dormitory students in a public university is described and the results are given. Section five concludes the paper.

2. THE MOST POPULAR DESIGNS IN BINARY RRT

In this section, the most popular designs in Binary RRT are summarized and instructions used in these designs are explained. The Binary RRT's will be described together with the equations to compute the population estimates and their variances. In each design, the equations are derived based on a probability distribution. Since the probability of distribution of the randomized design is known, the prevalence of the sensitive characteristic can be estimated on the basis of probability theory. In each design, the fundamental principle to compute prevalence estimate and its variance is establishing a probabilistic relationship between reported answers and unreported true scores [4]. On the other hand, some RRT procedures may confuse respondents and cause refusing answers. Many respondents hesitate that the RRT protects their sensitive behaviors even when they completely understand the instructions [5]. Therefore, for each design, the instructions are described clearly for successful implementation.

The most popular designs in Binary RRT classified into four types:

1. Warner's Design (Mirrored Question Design)
2. Unrelated Question Design
3. Forced Response Design
4. Crosswise Design

2.1. Warner's Design

Binary RRT is pioneering work of Warner [1]. Warner [1] proposed RRT for the first time to collect true response on sensitive questions by protecting the respondents' privacy. In Warner's design, respondents are requested to use a

randomization device (dice, coin or cards), whose outcome is unobserved by the interviewer. Let exemplify Warner [1] RRT with an example. For example, to estimate the "proportion of people who tried drug", two statements are written on the cards in a deck. The respondents are asked to answer one of two statements:

1. I tried drug (p).
2. I did not try drug (1-p)

The respondent randomly picks a card, and simply responds "true" or "not true" to the statement without revealing to the interviewer which statement is selected. The respondent is simply responding to the statement shown on the randomly drawn card (see Figure 1)

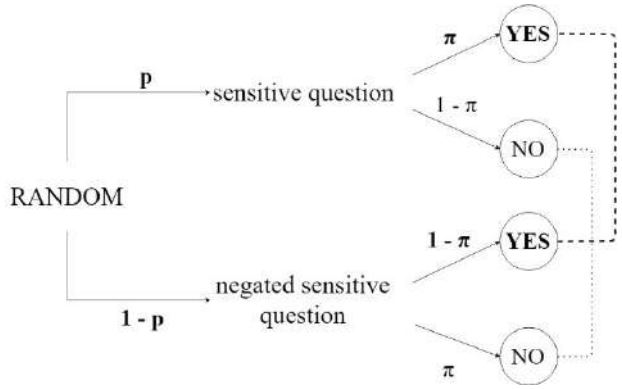

Figure 1. Warner's Design

Elementary probability theory can then be used to get an unbiased estimate $(\hat{\pi})$ of the prevalence of drug use in the population. So mathematically, π is the true proportion of the subjects with the sensitive characteristic, and p is the proportion of cards written on them with "I tried drug", (1-p) is the proportion of cards written on them with "I did not try drug". According to the Figure 1, the probability of a "yes" response, λ, is

$$\lambda = p\pi + \left(1-p\right)\left(1-\pi\right) \tag{1}$$

Solving for π, Warner [1] estimator is given as

$$\hat{\pi}_w = \frac{\hat{\lambda} - \left(1-p\right)}{2p-1}, \quad p \neq 0.5 \tag{2}$$

Here, $\hat{\lambda}$ is the observed proportion of "yes" answers in the sample:

$$\hat{\lambda} = \frac{n_1}{n} \tag{3}$$

Note that the proportions p and 1 − p are known, as are the number of "yes" responses n_1 and the sample size n. Hence, we can calculate the estimate values of π and sample variance.

The sample variance of Warner [1] estimator is

$$var\left(\hat{\pi}_w\right) = \frac{\hat{\lambda}\left(1-\hat{\lambda}\right)}{\left(n-1\right)\left(2p-1\right)^2} \tag{4}$$

As an early study of Warner design, Chaloupka [6] used this design to examine the illegal collection of shells in protected Great Barrier Reef in Australia. As a recent example, Gingerich [7] used this design to estimate the effect of a bureaucrat's partisan and electoral ambitions on participation in acts of political corruption in Bolivia, Brazil, and Chile. Other applications include capital punishment [2] and legalizing marijuana use [8].

2.2. Unrelated Question Design

Unrelated question design is developed by Greenberg et al. [9]. Unlike the Warner's design, in this design, an unrelated question is used in order to increase respondents' adaptation with survey instructions. Thus, unlike Warner's technique from the previous section, at least some of the respondents would have the reassurance that they answered a wholly unrelated question, resulting in more respondent cooperation than Warner's technique. Under this design, there are two questions which one is sensitive and other one is unrelated, non-sensitive question. The randomization device assigns whether a respondent should answer a sensitive question or an unrelated, non-sensitive question.

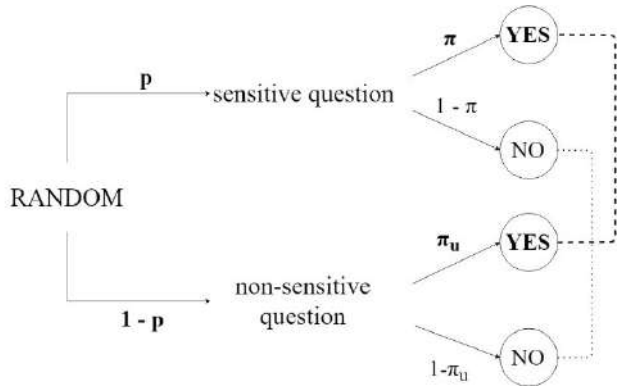

Figure 2. Unrelated Question Design

Let exemplify Greenberg et al. [9] RRT with an example. For example, to estimate the "proportion of people who tried drug". Two questions are written on the cards in a deck. The respondents are requested to answer one of two questions:

1. Have you ever tried drug in your lifetime? (Sensitive question is selected with p probability).

2. Is your mother born in January?'' (Non-sensitive question is selected with 1-p probability)

The respondent randomly picks a card, and simply responds "yes" or "no" to the question without expressing to the interviewer which question is selected. The respondent is simply responding to the question shown on the randomly drawn card (see Figure 2)

Elementary probability theory can then be used to get an unbiased estimate $(\hat{\pi})$ of the prevalence of drug use in the population. So mathematically, π is the true proportion of the subjects with the sensitive characteristic, and p is the proportion of cards written on them with sensitive question "Have you ever tried drug in your lifetime?" π_u is the known population prevalence of unrelated, non-sensitive characteristic and (1-p) is the proportion of cards written on them non-sensitive question with "Is your mother born in January?". According to the Figure 2, the probability of a "yes" response, λ, is

$$\lambda = p\pi + (1-p)(1-\pi_u) \tag{5}$$

Solving for π, Greenberg et al. [9] estimator is given as

$$\hat{\pi}_G = \frac{\hat{\lambda} - (1-p)\pi_u}{p} \tag{6}$$

Here, $\hat{\lambda}$ is the observed proportion of "yes" answers in the sample:

Note that the proportions p and 1 − p are known, as are the number of "yes" responses n_1 and the sample size n and the prevalence of population of unrelated question. Hence variance of $\hat{\pi}$ is calculated under known parameters.

The sample variance of Greenberg et al. [9] estimator is

$$var(\hat{\pi}_G) = \frac{\hat{\lambda}(1-\hat{\lambda})}{(n-1)p^2} \tag{7}$$

For example, Lara et al. [10] applied the unrelated question design to study abortion rates in Mexico.

The instructions used in this study:

> Here is a folder, one colored red and the other green. The red folder contained a sheet of paper with a red dot and the following question:
>
> ''Did you ever interrupt a pregnancy?''
>
> The words "yes" and "no" were printed below the question.
>
> The green folder contained a sheet of paper with a green dot and the following question:
>
> ''Were you born in April?''
>
> Again, the words "yes" and "no" were printed below. Then, fold the sheets of paper into the same shape, so that it is impossible to identify one from the other, and to place them in an opaque bag. Now, I shake the bag, please reach inside and select one folded sheet of paper and say your answer, either yes or no.

Here, the interviewer does not know which question the respondent had chosen and was answering. The respondent would then say her/his answer out loud, either yes or no. The interviewer then recorded the respondent's response.

As a recent example, Chen et al. [11] applied this design in the survey of issues relevant to commercial sex among men who have sex with men (MSM) in Beijing, China. Other applications of the unrelated question include abortion in Turkey [12], a criminology study of self-reported arrests in Philadelphia [13].

2.3. Forced Response Design

Forced response design is developed by Boruch [14]. Under Boruch's design, the randomization device assigns whether a respondent truthfully answers the sensitive question or simply replies with an automatic (forced) answer, `yes'or `no" response regardless of the true answer to the sensitive question. The result of the randomizing device is known only to the respondent, not to the interviewers.

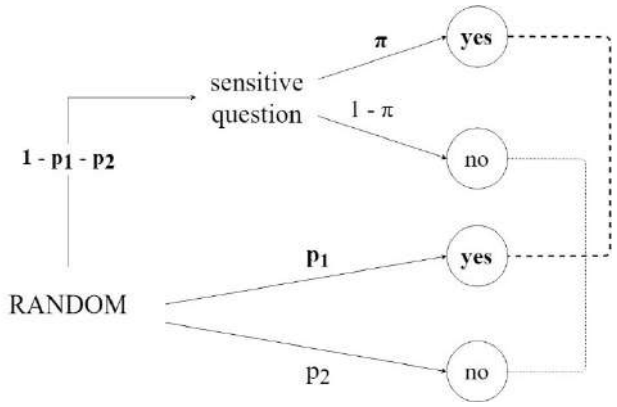

Figure 3. Forced Response Design

In Boruch [14] design, each respondent's answer provided with a randomization device, such as a die or a deck of cards. There are three statements in this design:

(i) report "yes"

(ii) report "no",

(iii) report the true answer of the sensitive variable, say "yes" or "no" with proportion p_1, p_2 and p_3 respectively.

So mathematically, π is the true proportion of the subjects with the sensitive characteristic, and p_1 is the proportion of "yes" reports, p_2 is the proportion of "no" reports and p_3 is the proportion of cards written on them with sensitive question "Have you ever tried drug in your lifetime?". According to the Figure 3, the probability of a "yes" response, λ, is

$$\lambda = p_1 + (1 - p_1 - p_2)\pi \tag{8}$$

Solving for π, Boruch [14] estimator is given as

$$\hat{\pi}_B = \frac{\hat{\lambda} - p_1}{1 - p_1 - p_2} \tag{9}$$

Here, $\hat{\lambda}$ is the observed proportion of "yes" answers in the sample:

Note that the proportions p_1 and p_2 are known, as are the number of "yes" responses n_1 and the sample size n. Hence variance of $\hat{\pi}$ is calculated under known parameters.

The sample variance of Boruch [14] estimator is

$$var(\hat{\pi}_B) = \frac{\hat{\lambda}(1 - \hat{\lambda})}{(n-1)(1 - p_1 - p_2)^2} \tag{10}$$

For example, a study of xenophobia and anti-Semitism in Germany [15]. Krumpal [15] used coin flip method for this design.

The instructions are reproduced here,

> "Now we would like to know your personal opinion on different segments of the population. One of these segments is foreigners living in Germany. We are aware of the fact that many people are very hesitant about giving their personal opinion on topics like this because they are very private. With this in mind, the University of Leipzig has developed a novel question technique that guarantees your privacy and makes the interview more comfortable.
>
> When answering the following questions, you can keep your personal opinion secret by flipping a coin. This might sound a bit unusual, however, I would like to ask you to help us and try out this

new method together with us. Could you please get three coins as well as a piece of paper and a pen? (…)

Please flip the three coins each time before I ask you a question. However, please do not tell me the results! Depending on the result of the coin flip, please answer as follows. I am happy to give you some time to write down the rules, if you would like:

- If you flip tails 3 times, please always answer "yes".

- If you flip heads 3 times, please always answer "no".

- If you flip a combination of heads and tails, for example tails 2 times and heads 1 time, please always tell your true personal opinion.

As you can see, coincidence will decide whether you answer the question truthfully or whether you give a predetermined answer. This way your privacy will always be protected. I will not know the result of your coin flip and therefore I will never know why your answer is "yes" or "no". Did you understand the coin-flip method? (…)

Sometimes you will answer "yes" or "no" due to the result of your coin flip, even though this is not your real personal opinion. Please do not worry about that. You are doing the right thing if you follow the rules of the coin-flip method and always answer according to the result of the coin-flip.

I will now read out aloud some statements to you which you might have heard at some point before. Please tell me each time, according to your coin flip, whether or not you would somewhat agree with the statement. We will now start with the first statement. (…) Please flip your three coins now without telling me the result. According to your coin flip, would you somewhat agree with the following statement?

"There are too many foreigners in Germany" (...)."

This design is popular among applied researchers and there are numerous examples. A study of fabrication in job applications [16], social security fraud in Netherland [17], use of performance enhancing drugs [18] and vote choice regarding a Mississippi abortion referendum [19].

2.4. Crosswise Design

Crosswise design (CD) is developed by Yu et al. [20]. This design is like unrelated question design. In this design, the sensitive question is asked together with a non-sensitive question that has a known population distribution (such as whether one's mother's birthday occurs in certain months). In this design, respondents are requested to give a joint answer to two questions rather than responding directly to the sensitive questions. The respondents are asked to indicate only whether their answers to two questions are the same (both "yes" and both "no") or different (one answer is "yes" and the other answer is "no"). In this design, the probability distribution of the non-sensitive question should be known and unequal to 0.5 for prevalence estimation of sensitive characteristic. In addition to this, provided that the answer to the unrelated question is unknown, the respondent's answer to the sensitive question remains confidential. The respondents could easily understand that the crosswise design protects their privacy because the interviewer is unaware of the possible answers, "the same" or "different". Furthermore no one is forced to give a "yes" or "no" answer.

So mathematically, π is the true proportion of the subjects with the sensitive characteristic, and p is the known population prevalence of non-sensitive question. According to the Figure 4, the probability of a "same" response, λ_s, is

$$\lambda_s = p\pi + \left(1-p\right)\left(1-\pi\right) \tag{11}$$

Solving for π, Yu et.al. [20] Crosswise design estimator is given as

$$\hat{\pi}_c = \frac{\hat{\lambda}_s - \left(1-p\right)}{2p-1}, \quad p \neq 0.5 \tag{12}$$

Here, $\hat{\lambda}_s$ is the observed proportion of "same" answers in the sample.

Note that the proportions p and 1 − p are known, as are the number of "same" responses. Hence, we can calculate the estimate values of π and sample variance.

The sample variance of Yu et.al. [20] Crosswise design estimator is

$$var\left(\hat{\pi}_c\right)=\frac{\hat{\lambda}_s\left(1-\hat{\lambda}_s\right)}{\left(n-1\right)\left(2p-1\right)^2} \quad (13)$$

Note that the crosswise design is formally equal to the Warner [1] original design. However, it follows a different logic than the Warner's design. In crosswise design, the respondents have to answer two questions simultaneously and they don't have to give directly "yes" or "no" answer.

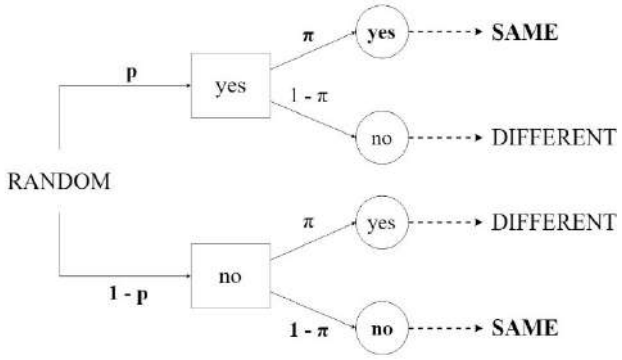

Figure 4. Crosswise Design

Recent studies have pointed out that the CD successfully reduces under-reporting of socially undesirable behavior. This design is also popular among applied researchers and there are numerous examples, recently. [21] conducted CD between Swiss and German university students to estimate plagiarism prevalence. [22] conducted a study to investigate drug use prevalence, especially anabolic steroids, among bodybuilding athletes in Iran. [23] implemented CD to estimate the prevalence of illicit drug use among the students of Tehran University of Medical Sciences. [24] used this design to investigate illicit drug use prevalence among students studying at Universities in Shahroud (Northeast of Iran). Other CD studies are summarized as, tax evasion [25], sexual behavior [26], attitudes towards Muslims [27], organ donation [28].

2.4.1. Stratified Crosswise design

In this section, crosswise design is suggested in stratified sampling. Let the population be divided into L non-overlapping homogeneous strata with N_h units in the h^{th} stratum and n_h be the number of units drawn by Simple Random Sampling without Replacement (SRSWOR) from the h^{th} stratum. $n=\sum_{h=1}^{L}n_h$ and $N=\sum_{h=1}^{L}N_h$ give the total sample size and the total population size, respectively. For the h^{th} strata, $W_h=N_h/N$ is the stratum weight. An individual respondent in the sample from h^{th} stratum is instructed to report a joint answer to two questions.

the probability of a "same" response in h. stratum λ_{sh}, is

$$\lambda_{sh}=p_h\pi_h+\left(1-p_h\right)\left(1-\pi_h\right). \quad (14)$$

Solving for π_h, crosswise design estimator in h. stratum is

$$\hat{\pi}_{ch}=\frac{\hat{\lambda}_{sh}-\left(1-p_h\right)}{2p_h-1},\quad p_h\neq 0.5 \quad (15)$$

Crosswise design estimator in stratified sampling is given as

$$\hat{\pi}_{c_{st}}=\sum_{h=1}^{l}W_h\hat{\pi}_{ch},\quad h=1,2,...,l \quad (16)$$

The sample variance of crosswise design estimator in stratified sampling is

$$var\left(\hat{\pi}_{c_{st}}\right)=\sum_{h=1}^{l}W_h^2\frac{\hat{\lambda}_{sh}\left(1-\hat{\lambda}_{sh}\right)}{\left(n_h-1\right)\left(2p_h-1\right)^2} \quad (17)$$

Here, $\hat{\lambda}_{sh}$ is the observed proportion of "same" answers in the h. stratum, p_h is the known population prevalence of non-sensitive question in h.stratum.

3. DRUG USE IN UNIVERSITY STUDENTS IN TURKEY

Empirical studies on university students in Turkey are based on direct questioning about socially undesirable behavior such as drug use. Altındağ et al. [29] investigated the prevalence of illicit drug, smoking and alcohol use in fist year students of Harran University (n=253) and lifetime illicit drug use prevalence was identified as 2.3%. Akvardar et al. [30] investigated the prevalence of illicit drug, smoking and alcohol use in medical students from three different medical schools in Turkey (n=447) and they found that 4% of the students reported using illicit drugs (cannabis, ecstasy, cocaine) at least once in their lifetime. Mayda [31] studied to determine the prevalence of substance, cigarette, alcohol use in students of Forestry Faculty of Düzce University (n=398) and he found that the substance use among students is 9.3%. Turhan et al. [32] made a cross-sectional study in students of Mustafa Kemal University (n=396) and lifetime illicit drug use were identified as 9.6%. Ulukoca et al. [33] researched the prevalence of cigarette, alcohol, and substance use among the students of Kırklareli University (n=902) and 10.4% of students had tried using substances at least once in their life, with marijuana (4.1%) and solvents (3.2%) reported as the substances most commonly tried. Yüncü and Atlam [34] evaluated the relationship between cigarette, alcohol, substance experience among gender, faculty, class, living environment, substance use of families among students of Ege University (n=1522). 13.4% of students had tried using substances at least once in their life with cannabis (12.5%), ecstasy (MDMA) (2%), cocaine (0.6%) and heroin (0.1%) were mostly used illegal drugs. They found that the illicit drug use prevalence is significantly different among men (22.2%) a women student (7.6%). Türk and Yavuz [35] investigated the meaning of penal sanctions with regard to substance use on students from different universities in Turkey (n=227). In the study, the students reported they used the below substances at least once; 17.9% marijuana, 3.4% heroin, 4.5% cocaine, 2.6% LSD, 4.5% ecstasy, 3% bonsai. The current study on drug use was carried on by Coşkun et al. [36]. They determined the change on alcohol and drug use among the first and last year university students of Gaziantep University (n=2217) and they found that 8.6% of the men and 2.1% of the women had used drug at least once. 8.3% of the last year students had used drug at least once while 4.6% of the first-year students had used drug at least once.

4. APPLICATION

This study aims to introduce binary RRTs and show the real application of RRTs in Turkey. By this aim, a RRT application is carried out in Ankara, Turkey. The survey's target population included the dormitory students at a public university in Ankara, Turkey. First of all, a pretest (n= 60) was conducted to students in order to with which binary RRT, they would feel safe and comfortable. The binary RRTs which are introduced in section 2 were presented to the students with instructions. After the presentation, the students were asked "which RRT design do you feel safe and comfortable for answering your sensitive behaviors?". Most of the students (%78) reported that they would be more confident when Crosswise design (CD) is conducted. After pretest result, crosswise design was implemented to estimate illicit drug use prevalence. To evaluate crosswise design (CD) ensures better estimates of illicit drug use than direct questioning (DQ) method, two different questionnaires: a direct-questioning version and a CD version were conducted on dormitory students. The private dormitory has 1980 students. Students were selected using stratified random sampling method. The survey is conducted with 712 students with 0.03 margin of error. The sample is consisting of %46 women and %54 men.

Students were randomly selected using a ratio of 3 for the CD (n=534) to 1 for DQ (n=178). For both techniques, the students were selected with stratified random sampling method which has two stratum and the stratum is gender.

Due to the sensitive research topic, for both conditions, the students were all informed about the aims of the study.

In the 'direct questioning' technique, a confidentiality assurance was read out loud to the respondent. "

We are aware of the fact that many people are very hesitant about revealing their sensitive behaviors because they are very private. With this in mind, we would like to assure you that all answers given will be kept confidential and will not be passed on to anyone else. I will now read aloud a question to you. Please answer the question by simply telling us 'Yes' and 'No'. Now, I read the question. "Have you ever tried illicit drug in your lifetime?"

The instructions used in the CD technique:

We are aware of the fact that many people are very hesitant about revealing their sensitive behaviors because they are very private. With this in mind to ensure the protection of your personal rights, we will use an indirect questioning technique that guarantees that your answers will be totally anonymous.

Therefore, you will not be requested to answer any question directly, but rather, you will be asked" two questions at the same time by simply telling us whether the answers to the questions are (a) the same or (b) different.

The questions:

Question 1: is your mother's birthday in January, February, or March.?

Question 2: Have you ever tried illicit drug in your lifetime?

In crosswise design application, the non-sensitive question is about respondent's mother's birthday: ''is your mother's birthday in January, February, or March?''. The known probability of answering ''yes'' to the mother's birthday question is .2471 (i.e., 90.25 days/365.25 days).

178 students were interviewed by DQ and 534 students were interviewed by the CD. For CD technique, the prevalence estimation is calculated by Eq. (16). The general result is showed in Table 1. As Table 1 illustrates, 6.1% (SE = 1.47) of the students in the DQ technique reported that they had tried illicit drug at least once in their lifetime. By CD technique, the prevalence of illicit drug use is estimated as 22.6% (SE = 4.12). As expected, one-sided z test indicates a significantly higher prevalence estimate of illicit drug use for the CD technique compared with the DQ Technique (CD = 22.6%, DQ = 6.1%, $p < .001$). The illicit drug use prevalence among students is compared according to the gender in both DQ and CD Technique. In CD technique, estimated illicit drug use prevalence is higher among male students than female students (Male: 33.19 %, Female = 10.00 %, $p < .05$). Similar result is also observed when DQ technique is conducted (Male: 9.00%, Female = 2.60%, $p < .001$). The results are showed in Table 2.

Table 1. Prevalence estimate of illicit drug use according to the questioning techniques

Variable	**Questioning Technique**	
Illicit Drug Use	**DQ**	**CD**
Prevalence Estimate (%)	6.1	22.6
Standard Error (%)	1.47	4.12
%95 Confidence Interval	3.2-9.00	14.5-30.7
n	178	534
z score (sig.)	3.78 (0.000)	

Table 2. Illicit drug use prevalence according to the Gender

Variable		**Questioning Technique**	
Illicit Drug Use	**Gender**	**DQ**	**CD**
Prevalence Estimate (%)	**Female** (%95 CI)	2.60 (0.6-4.6)	10.00 (0.0-21.49)
	Male (SE)	9.00 (5.7-12.3)	33.19 (21.93-44.45)
z score (sig.)		3.25 (0.000)	2.83 (0.002)

5. CONCLUSION

This study introduces the Binary RRTs and shows the real application of a RRT design in Turkey. The randomizing procedure is crucial for the success of the RRT, as it shows the answers of the respondents are protected by probability theory. In this study, Crosswise design is preferred in estimation of the prevalence of illicit drug use. It has seen that crosswise design provides more confidence for respondents and easier to apply to the other designs. The present study compared indirect and direct questioning techniques in estimating illicit drug use and with crosswise design, considerably minor response refusals are obtained and significantly higher drug-use estimates are observed by gaining more privacy in the data collection process. So, it can be concluded that Crosswise design gives the most efficient statistical estimation compared to alternative RRT designs. Moreover, the present research will provide to extend the recognition of the RRTs in sensitive surveys and encourage researchers to study on sensitive topics in Turkey. Future studies can be extended for analyzing all sociodemographic characteristics of the students and can be replicated for all university students in Turkey.

6. REFERENCES

[1] S.L. Warner, "Randomized response: A survey technique for eliminating evasive answer bias", Journal of the American Statistical Association, vol. 60, pp. 63-69, 1965.

[2] G.J.L.M Lensvelt-Mulders, J.J. Hox and P.G.M. Van der Heijden, "How to Improve the Efficiency of Randomised Response Designs", Quality and Quantity, vol. 39, pp. 253 – 265, 2005.

[3] N. Özgül, Proportion and Mean Estimators in Randomized Response Models, Ph.D. Thesis, Hacettepe University, Ankara, 2013.

[4] U. Engel, B. Jann, P. Lynn, A. Scherpenzeel, P. Sturgis, "Improving Survey Methods: Lessons from Recent Research", Routledge, New York, 2014.

[5] E. Coutts, and B. Jann, "Sensitive Questions in Online Surveys: Experimental Results for the Randomized Response Technique (RRT) and the Unmatched Count Technique (UCT)", Sociological Methods & Research, vol. 40, no. 1, pp. 169–193, 2011.

[6] M.Y. Chaloupka, "Application of the randomized response technique to marine park management: an assessment of permit compliance", Environmental Management, vol. 9, no. 5, pp. 393-398, 1985.

[7] D.W. Gingerich, "Understanding of the books politics: Conducting inference on the determinants of sensitive behavior with randomized response surveys", Political Analysis, vol. 18, no. 3, pp. 349-380, 2010.

[8] S. Himmelfarb, "The multi-item randomized response technique", Sociological methods & research, vol. 36, no. 4, pp. 495-514, 2008.

[9] B.V. Greenberg, A.A. Abdul-Ela, W.R. Simmons, D.G. Horvitz, "The unrelated question randomised response model: Theoretical framework", Journal of the American Statistical Association, vol. 66, pp. 243–250, 1969.

[10] D. Lara, S.G. Garcia, C. Ellertson, C. Camlin and J. Suarez, "The measure of induced abortion levels in Mexico using random response technique", Sociological Methods & Research, vol. 35, no. 2, pp. 279-301, 2006.

[11] X. Chen, Q. Du, Z. Jin, T. XU, J. Shi, G. Gao, "The Randomized Response Technique Application in the Survey of Homosexual Commercial Sex among Men in Beijing", Iranian J Publ Health, vol. 43, no. 4, pp. 416-422, 2014.

[12] S. Tezcan and A.R. Omran, "Prevalence and reporting of induced abortion in turkey: two survey techniques", Studies in family planning, vol. 12, no. 6-7, pp. 262-271, 1981.

[13] P.E. Tracy and J.A. Fox, "The validity of randomized response for sensitive measurements", American Sociological Review, pp. 187-200, 1981.

[14] R.F. Boruch, "Assuring confidentiality of responses in social research: A note on strategies", The American Sociologist, vol. 6, pp. 308–311, 1971.

[15] I. Krumpal, "Estimating the prevalence of xenophobia and anti-semitism in Germany: A comparison of randomized response and direct questioning", Social science research, vol. 41, no. 6, pp. 1387-1403, 2012.

[16] J.J Donovan, S.A. Dwight and G.M. Hurtz, "An assessment of the prevalence, severity, and verifiability of entry-level applicant faking using the randomized response technique", Human Performance, vol. 16, no. 1, pp. 81-106, 2003.

[17] P.G.M. Van der Heijden, G. Van Gils, J. Bouts, J.J Hox, "A comparison of randomized response, CASAQ, and direct questioning; eliciting sensitive information in the context of social security fraud", Kwantitatieve Methoden, vol. 59, pp. 15-34, 1998.

[18] J.H. Stubbe, A.M. Chorus, L.E. Frank, O. Hon and P.G. Heijden, "Prevalence of use of performance enhancing drugs by fitness centre members", Drug testing and analysis, vol. 6, no. 5, pp. 434-438, 2014.

[19] B. Rosenfeld, K. Imai and J. Shapiro, "An empirical validation study of popular survey methodologies for sensitive questions", American Journal of Political Science, vol. 60, no. 3, pp. 783-802, 2016.

[20] J.W. Yu, G.L. Tian, M.L. Tang, "Two new models for survey sampling with sensitive characteristic: design and analysis", Metrika, vol. 67, pp. 251-263, 2008.

[21] B. Jann, J. M. Jerke, I. Krumpal, "Asking Sensitive Questions Using the Crosswise Model: An experimental Survey Measuring plagiarism", Public Opinion Quarterly, vol. 76, no. 1, pp. 32-49, 2012.

[22] M.R. Nakhaee, F. Pakravan, N. Nakhaee, "Prevalence of Use of Anabolic Steroids by Bodybuilders Using Three Methods in a City of Iran", Addict Health, vol. 5, no. 3-4, pp. 77-82, 2013.

[23] M. Shamsipour, M. Yunesian, A. Fotouhi, B. Jann, A. Rahimi-Movaghar, F. Asghari and A.A. Akhlaghi, "Estimating the prevalence of illicit drug use among students using the crosswise model", Substance Use & Misuse, vol. 49, no. 10, pp. 1303–1310, 2014.

[24] A. Khosravi, S.A. Mousavi, R. Chaman, F. Khosravi, M. Amiri, M. Shamsipour, "Crosswise Model to Assess Sensitive Issues: A Study on Prevalence of Drug Abuse Among University Students of Iran", Int J High Risk Behav Addict, vol. 4, no. 2, e24388, 2015.

[25] M. Korndörfer, I. Krumpal and S.C. Schmukle, "Measuring and explaining tax evasion: Improving self-reports using the crosswise model", Journal of Economic Psychology, vol. 45, pp. 18-32, 2014.

[26] K. Vakilian, S. Mousavi and A. Keramat, "Estimation of Sexual Behavior in the 18-to 24-Years-old Iranian Youth based on a Crosswise Model Study", BMC Research Notes, vol. 7, no. 1, pp. 1-4, 2014.

[27] D. Johann and K. Thomas, "Testing the Validity of the Crosswise Model: A Study on Attitudes Towards Muslims Survey Methods: Insights from the Field", 2017, Retrieved from https://surveyinsights.org/?p=8887.

[28] M. Höglinger, B. Jann, A. Diekmann," Uncovering a Blind Spot in Sensitive Question Research: False Positives Undermine the Crosswise-Model RRT", Political Analysis, vol. 25, no. 1, pp. 131-137, 2017.

[29] Y. Akvardar, Y. Demiral, G. Ergör, A. Ergör, M. Bilici and Ö.A. Özer,"Substance use in a sample of Turkish medical students", Drug and alcohol dependence, vol. 72, no. 2, pp. 117-121, 2003.

[30] A. Altındağ, M. Yanık, E. Yengil and A.H. Karazeybek, "Şanlıurfa'da üniversite öğrencilerinde madde kullanımı", Bağımlılık Dergisi, vol. 6, no. 2, pp. 60-64, 2005.

[31] A.S. Mayda, "Düzce Üniversitesi Orman Fakültesi Öğrencilerinde Sigara, Alkol Ve Madde Kullanımı Sıklığı Ve Kullanmaya Başlama Nedenleri", Düzce Tıp Dergisi, vol. 12, no. 3, pp. 7-14, 2010.

[32] E. Turhan, T. İnandı, C. Özer, S. Akoğlu, "Üniversite öğrencilerinde madde kullanımı, şiddet ve bazı psikolojik özellikler", Turkish Journal of Public Health, vol. 9, no. 1, pp. 33-44, 2011.

[33] N. Ulukoca, Ş. Gökgöz and A. Karakoç, "Kırklareli Üniversitesi Öğrencileri Arasında Sigara, Alkol ve Madde Kullanım Sıklığı", Fırat Tıp Dergisi, vol. 18,no. 4, pp. 230-234, 2013.

[34] Z. Yüncü and D.H. Atlam, "Üniversitesi Öðrencilerinde Sigara, Alkol,Madde Kullaným Bozukluğu ve Ailesel Madde Kullanımı Arasındaki İlişki", Klinik Psikiyatri, vol. 20, pp. 161-170, 2017.

[35] B. Türk and M.F. Yavuz, "Caydırıcılığın Madde Kullanımı Açısından Üniversite Öğrencilerinde Değerlendirilmesi", Adli Tıp Bülteni, vol. 23, no. 3, pp. 143-150, 2018.

[36] F. Coşkun, B. Özçırpıcı and S. Özgür, "Gaziantep Üniversitesi Merkez Kampüsü'ndeki lisans öğrencilerinde alkol ve madde kullanma durumu", Ortadoğu Tıp Dergisi, vol. 11, no. 2, pp. 143-147, 2019.

JOURNAL OF SCIENCE
SAKARYA UNIVERSITY

Sakarya University Journal of Science

ISSN 1301-4048 | e-ISSN 2147-835X | Period Bimonthly | Founded: 1997 | Publisher Sakarya University
http://www.saujs.sakarya.edu.tr/en/

Title: Assessment of Major Air Pollution Sources in Efforts of Long Term Air Quality Improvement in İstanbul

Authors: Orhan Sevimoğlu
Recieved: 2019-07-04 10:01:18

Accepted: 2020-02-17 15:09:40

Article Type: Research Article
Volume: 24
Issue: 2
Month: April
Year: 2020
Pages: 389-405

How to cite
Orhan Sevimoğlu; (2020), Assessment of Major Air Pollution Sources in Efforts of Long Term Air Quality Improvement in İstanbul. Sakarya University Journal of Science, 24(2), 389-405, DOI: https://doi.org/10.16984/saufenbilder.586655
Access link
http://www.saujs.sakarya.edu.tr/tr/issue/52471/586655

Sakarya University Journal of Science 24(2), 389-405, 2020

Assessment of Major Air Pollution Sources in Efforts of Long Term Air Quality Improvement in İstanbul

Orhan SEVİMOĞLU*[1]

Abstract

Air pollution affected quality of life and public health due to high concentration levels of air pollutants in Istanbul, especially in 1990s. Major air pollution sources in Istanbul caused elevation of the air pollutants in ambient air of the megacity. To protect human health, the levels of PM_{10} and SO_2 were reduced by taking effective actions such as the reduction of utilization of coal, fuel oil, wood combustion for residential heating, expending natural gas network and improving the quality of diesel and gasoline. Intelligent Traffic Systems (ITS) were applied to reduce the air pollutant emission from transportation by reducing travelling time. Overall, this study evaluates air pollution sources in Istanbul based on previous source apportionment studies that guide the emission reduction strategies. The improvement on PM_{10} and SO_2 demonstrated as 50% and 98% reduction respectively since 1990s to 2014.

Keywords: megacity, air pollution sources, emission, air quality management

1. INTRODUCTION

Air pollution is considered as one of the environmental problems in megacities due to decrease of comfort [1] and adverse health effects [2]. Air pollution researchers focus not only on outdoor/indoor air pollution [3] but also emphasize on greenhouse gas emissions from natural and anthropogenic sources that take into account the impact on climate change [4]. The dynamics of climate interactions are not completely understood, although there is a general scientific agreement that anthropogenic activities are contributing to global climate change [5] and to ambient air pollution [6].

Istanbul is a megacity with a population that elevated from 6.6 million in 1990s to 15 million up to 2015 due to increasing business and industrial activities such as road construction, skyscrapers, housing, business centers, airports, railways and metro lines. All these developments in the city are a necessity for the public and market needs. The planning and developments of megacity requires a focus on environmental awareness, sustainability and infrastructure to protect its environment and the public health.

*Corresponding Author: sevimoglu@gtu.edu.tr
[1]Gebze Technical University, Department of Environmental Engineering, Gebze, Kocaeli, Turkey. ORCID ID: 0000-0003-4861-5154

Therefore, air quality management requires source apportionment that needs the measurement of the major air pollution parameters, trace compounds representing sources, atmospheric parameters (temperature and pressure, wind speed, and directions), and emission inventories [7]. So, a significant amount of air pollutants and Greenhouse Gases (GHG) are released to the atmosphere from natural and anthropogenic sources [8] as a result of natural decomposition, combustion, natural and industrial activities [9]. Air pollution and GHG abatement efforts should be managed together that both are from the same sources [10, 11]. For this reason, air quality management of megacities should be determined with analytical approaches by creating strategies to reduce their own air pollutants [12]. Therefore, a comprehensive control protocol focusing on multiple criteria pollutants and emission sources was proposed to mitigate air pollution in Istanbul. The variation in concentration values of the major air pollutants (PM_{10}, SO_2, NO_x, O_3, CO) in the urban air of Istanbul has been carefully monitored by the municipal experts and researchers for last 25 years.

Nonetheless, recently, the mitigation and adaptation works in air pollutant reduction have been carried out by focusing in the area of transportation, traffic, waste disposal and energy requirement for the public for the last several decades in the concept of air quality improvement. There is a significant contribution and support from the Istanbul Metropolitan Municipality (IMM) and the Ministry in reducing emissions of greenhouse gases and air pollutants.

The control efforts of air pollution emission from the sources could also reflect decreasing of the concentration of pollutants. Major reduction efforts of air pollutants have been implemented on particle sources by reducing the consumption of gasoline, natural gas, coal, fuel oil, and liquefied petroleum gas (LPG). Therefore, the mitigation works focus on improvement of transportation network such as arriving the target in a short time with public transportation and shifting coal combustion to natural gas, improvement on waste management that all these developments reflect as a decrease in the emission of major air pollutants to the atmosphere as well as GHG. This study focuses on emphasizing of assessment and identification of air pollution and GHG sources in the metropolitan city of Istanbul and explicating of the improvement works for the reduction of the concentrations of air pollutants, especially PM_{10} and SO_2, to bring the levels of vicinity of Turkish Ambient Air Quality Standards (TAAQS) in Istanbul.

2. MATERIAL AND METHOD

2.1. Air quality management in urban area of Istanbul

Air quality management consists of controlling the criteria air pollutants, GHG emissions, and monitoring of pollutants entering from external sources (Figure 1). Air pollution of Istanbul was a critical level for public health in 1990s [13]. Istanbul Metropolitan Municipality has initiated works for the reduction of the concentrations of major criteria air pollutants; particulate matter, ground-level ozone, carbon monoxide, sulfur oxides, nitrogen oxides. The major air pollution sources such as vehicle exhaust, road dust, combustion emission from residential heating and energy supply adversely affect air quality in the urban area of Istanbul. The implementation plans were prepared in order to control the emission of the pollutants from the sources to ambient air.

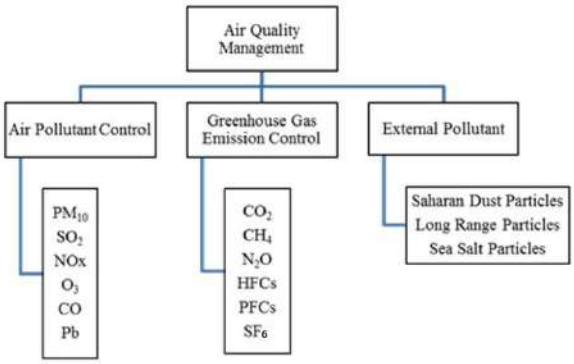

Figure 1. Control parameters in air quality management

On the other hand, the reduction of GHG emission is promoted by the reduction of the air pollutants that originate from GHG sources. The effort of

reducing GHG emissions result in reduction of the air pollutants as well. Istanbul is also exposed to the external particle transport through airflow path from time to time [14]. This constitutes stress on the urban air quality parameters. The external pollution sources cannot be managed in the concept of urban air quality. For instance, the particles from the Balkans and Saharan Dust should be noted as two important external sources for Istanbul. Sea salt particles should be also considered as a PM source for urban area since its three sides are covered by the sea [15]. All these PM emissions naturally occur and impact on the Megacity.

2.2. Istanbul ambient air quality background

The air quality of Istanbul was investigated and reported by many researchers in the past three decades. Researchs were conducted previously focusing on measuring criteria pollutants to determine the level of pollutants in the ambient air quality of Istanbul Metropolitan Area (IMA). Both PM_{10} and SO_2 parameters were focused on due to the high concentration levels 155 and 219 $\mu g/m^3$ respectively in 1990s that obviously have adverse health effects [16]. The concentrations of air pollutants were presented on variations among the sampling years in Istanbul between 1990 and 2014 (Table 1). The reported yearly average PM_{10} was mainly below TAAQS or exceeded from time to time over the years. The most significant decline was seen in SO_2 concentration in these two decades. NO_x concentrations increased over the years due to emission from sources such as vehicle exhaust, natural gas burning, and marine vessels passing through Bosphorus.

3. RESULTS

3.1. Assessment of sources of major air pollutants in Istanbul urban area

The major sources of air pollutants and greenhouse gases in Istanbul urban area are presented based on emitting by the pollutant types in Table 2. Major air pollution sources are cooking operations, domestic heating including wood, lignite (coal), natural gas, fuel oil, traffic sources including LPG, diesel and gasoline combustion in vehicles, and dust sources such as road/surface soil dust and tobacco smoking. In addition, long-range contribution from sea salt and Saharan Dust particles were reported for Istanbul ambient air [15] that could be responsible for the elevation of PM_{10} concentration [14].

Table 1. Measurements of air pollutants in previous research studies ($\mu g\ m^{-3}$) (O_3= ppb).

	PM_{10}	**PM_{10} winter**	**PM_{10} summer**	**PM_{10} Spring**	**NOx**	**SO_2**	**O_3**	**CO**	
TAAQS (in 2014)	**100**	**100**	**100**	**100**	**60**	**20**	**120**	**10000**	
01.1990		225				450			[87]
07.1990			45			75			[87]
1991	103.8	155				219			[16]
1993-1994						308			[17]
1994-1995						249.8			[17]
2000	65				50	30	25	1200	[18]
2002 European Side					138	38		1550	[19]
2002 Asian Side					98	18		1700	[19]
2002-2003		65.3	55.6			22.95			[20]
2005-2009	58								[21]
2007-2009					60		15.2		[22]
2007	69±27.9				91±65.1	12.1±10.1		686±428	[23]
2008	39.1	44.5	29.8						[15]
13.01.2008			129						[15]
12.04.2008				107					[15]
11.2007- 06.2009	39.1	48		55.2					[24]
01.01.2010-31.12.2012	50				56	10	29		[25]
2003-2013	53.60	57.45	49.75			10.43		718	[26]

Table 2. Major sources of air pollutants in Istanbul

Major Sources of Air Pollutants	Criteria Air Pollutants Emission				GHG Emission		Source Type
	PMx	SO_2	NOx	CO	CO_2	CH_4	
Meat-Cooking Operations	X						1
Paved Road Dust	X						1
Wood Burning	X			X	X		1
Coal Burning	X	X	X	X	X		1
Fuel Oil Burning	X	X	X	X	X		1
Tobacco Smoke	X			X	X		1
Diesel Vehicles	X	X	X	X	X		1
Gasoline Vehicles	X	X	X	X	X		1
Natural Gas Combustion	X		X		X		1
Vegetative Detritus	X						2
Maritime Emission	X	X	X	X	X		1
Landfill Gas					X	X	1
Sea Salt Particles	X						2
Saharan Dust	X						2
Aviation Emission	X	X	X		X		1

1: Anthropogenic, controllable, 2: Natural, uncontrollable

The landfill sites are a GHG emission source in the borderline of Istanbul Province [27]. 44% of the total area of Istanbul Province is covered by forests [82] and green lands could be considered significant PM source as vegetative detritus [28]. Vegetative detritus, sea salt particles, Saharan dust particles are naturally occurring uncontrollable PM sources. Istanbul as a coastal city is under the influence at maritime emissions as well [29]. In the following sections, the assessment of the major air pollution sources and implemented emission reduction works will be discussed.

3.1.1. Cooking influence on air quality

Different types of meat cooking emit varied emission factors with chemical compositions [30]. Meat cooking is significant part of food consumption in public that is a considerable source of organic aerosol emissions to the urban air [83]. Charbroiling extra lean meat produce fine aerosol emissions of 7 g/kg of meat cooked. In contrast, frying meat generate fine aerosol emissions recorded at 1 g/kg of meat [31]. The meat consumption per person was about 13.07 kg per year and chicken meat consumption was about 19.43 kg per year in 2013 in Istanbul [32]. Fine aerosol emission was about 2148 kg per day (assumed for the meat consumption of half charbroiling and other half frying) for the population of Istanbul. The fine organic carbon particle emissions from meat cooking to ambient air were found about 1400-4900 kg per day for Los Angeles in 1982 [30]. Schauer [7] reported organic aerosol ratios for cooking as 20.78%, 13.99%, 20.29% and 21.63% in Pasadena, Downtown Los Angles, West Los Angeles and Rubidoux in 1989, respectively. Another study was conducted in Pittsburgh with average yearly OC concentration originating from meat cooking determined as 0.45 mg-C m^{-3} as 16% in total OC concentration [33]. It was reported that the cooking was also a significant OC contributor, accounting for 0.6–3.1 μg C m^{-3} in the range of 6–24% of fine OC in Hong Kong [34]. These research studies suggest meat cooking as a considerable PM source in megacities. The cooking emission was unexpressed by the researchers of the previous studies related to ambient air quality in Istanbul. However, the Particulate Organic Matter (POM) were measured from November 2007 to June 2009 and average POM was reported as 9.8 μg m^{-3} of annual average value of PM_{10} (39.1 μg m^{-3}) in Istanbul [24]. Depending on previous research, the contribution of organic matter originating from

the meat cooking or cooking operations can be evaluated as at least 3% in contribution to the POM of PM_{10}. Further research is necessary for true estimation of fine aerosols from meat cooking. The odor emission from facilities such as restaurants and cooking centers is controlled by applying "Causing Odor Control of Emission Regulations" [35] in the concept of air quality management.

3.1.2. Paved road dust particles

The research PM apportionment indicated that the road dust is a considerable source of atmospheric aerosol in ambient air [36]. There is a significant contribution to ambient air for the inhalable particle mass of road dust that contains hazardous trace elements and compounds that has adverse health effects [37, 38]. The road dust contribution to ambient air in PM_{10} was reported 13% in Paris [39]. The road dust concentration out of six major sources (secondary sulfate, secondary nitrate, motor vehicle, road dust, sea salt, and oil combustion) was about 4.13 out of 16.37 $\mu g\ m^{-3}$, corresponding to 25.22% of $PM_{2.5}$ in New York City during July 2001 [40]. In another research study between October 2009 and October 2010 in Rochester, New York, the airborne soil was of 12.8% of the total $PM_{2.5}$ concentrations that was determined by Positive Matrix Factorization (EPA PMF, version 4.1) [41]. The road dust proportion was 25–27% in PM_{10} aerosols that were collected during 1989 every sixth day at six sites in Santa Barbara County, CA [42]. The road dust contribution was reported of 22% to PM_{10} in Istanbul [24]. Considering previous research studies, it can be stated that the road dust contributes at least 10% to atmospheric PM_{10} formation. The movement of 3.5 million registered on the street and transit vehicles cause re-suspension of road dust particles that has a noteworthy proportion in PM_{10} of Istanbul ambient air [84]. In order to decrease the contribution of road dust particles to the ambient PM, the mechanical street sweeping was implemented to the main streets by the IMM and the local municipalities since 2002 [43].

3.1.3. Wood burning

Wood is used for residential heating and industrial use [44] that is a source of particles in the residential areas [45]. The wood consumption in Istanbul was reported 350.000 ton/year in 1990 [46] and 890.857 ton/year in 2007 [47]. Although 95% of the natural gas distribution network is available for the household in Istanbul as of 2014, the use of wood for heating spaces in the residential buildings is still in use during in Fall and Winter seasons, especially in suburban areas by the low-income families. On the other side, the bakery stores use different types of wood in Istanbul [48]. There is no information about wood emission in the apportionment study of Istanbul. However, particle emission from wood burning to the ambient particles at different locations in previous studies may shed a light. For example, Pittsburgh Supersite work in 2001 [49] suggested that PM contribution from the wood burning was about % 4-5 based on PMF model. The other research study reported that the wood burning contribution was 1.4-10.4% in $PM_{2.5}$ [7]. The wood burning in residential heating and industrial use should be considered as a PM contributor even in a small fraction such as 1-2% of PM_{10} for the air quality management of Istanbul. There is no ban in use of wood for the residential heating and industry, although the natural gas use is available for 95% of the metropolitan area.

3.1.4. Lignite coal and natural gas combustion

Lignite coal was affordable and easy to supply for the public as a major fuel of residential heating in Istanbul in 1990s. At the time consumption of lignite coal was about 5.8 Million tons per year [46]. Therefore, a large amount of PM and SO_2 pollutants from coal burning in the residential area caused a decrease in air quality of city by especially elevation of SO_2 concentration in ambient air [13]. The concentrations of SO_2 were high above the TAAQS in 1990s (Figure 2).

In order to reduce SO_2 concentrations, the natural gas network was widespread in the city of Istanbul to make available the clean energy source for residential and industrial use. Consumption of natural gas increased ten times from 1994 to 2004

(Table 3) [79]. "Regulation on Control of Air Pollution Caused by Heating" published in 2005 determines the quality of the coal in use for heating purposes in residential area was implemented. Based on this regulation, the total sulfur content is allowed at most 2% in dry weight in at least 4800 Kcal/kg (±200 tolerance). So, SO_2 concentration decreased from 145 to 22 μg m^{-3} about six times less from 1994 to 2004.

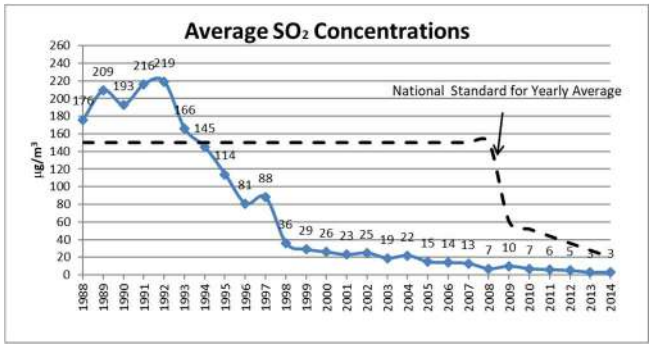

Figure 2. Yearly average of 24-h SO_2 concentrations [50].

The lignite usage degreased 18 fold and natural gas usage increased 10 fold. As a result, SO_2 concentrations drop 29 fold as of 2014. Consequently, the decrease of the SO_2 concentration result in reducing the amount of lignite usage less than 1-million-ton coal is still in use by the public for residential heating [47]. Although natural gas network is available for the public, there is no regulation to prevent the usage of coal.

3.1.5. Fuel oil burning

Fuel oil (No. 6) is sometimes referred to as furnace or heavy fuel oil (HFO) or residual oil that is commonly used for residential and commercial heating purposes in steam and power generation using industrial boilers in Istanbul. During 1990s, the amount of fuel oil use was 250,000 tons per year [46]. This volume has dropped to about 30,000 tons per year in 2014 [51], which should be taken into account in terms of the amount of lower emission due to the less consumption. The combustion of HFO contributes SO_4^{-2} significantly to the total PM mass [52]. The fuel oil combustion contributes accounting for 18% of the PM_{10} mass in the city of Colima, Western Central Mexico [53]. Cheng [54] reported that $PM_{2.5}$ contains (~10%) fine particles from residual oil combustion in Hong Kong from 2004 to 2005. The source apportionment in five cities of Netherland revealed the residual oil combustion in $PM_{2.5}$ is about 1-3% from 2007 to 2008 [55]. All these previous research indicate a contribution of fine particles from HFO combustion in the formation of PM_{10} in Istanbul.

3.1.6. Tobacco smoke

The trace compounds of tobacco smoke were detected in ambient aerosol as a source of biomass burning [56, 83] with less than 1% in $PM_{2.5}$ [7]. Smokers in the population of Turkey were about 14.8 million (27.1%) of 75.6 million in 2012 [57]. Though, there is no exact number of smokers in Istanbul. However, there might be about 2.66 million smokers in Istanbul in 2012 based on Istanbul population (13.6 Million). Smoking was banned in closed areas of public since 2008 in Turkey. A mean $PM_{2.5}$ emission rate of 12.7 mg/cigarette was reported [58]. If it is assumed that one person smokes per day one cigarette in open area, 11.5 kg $PM_{2.5}$ emits to the ambient in Istanbul. Beyond the contribution of cigarette smoke to atmospheric pollution, it is important that 27% of the smokers of the urban population were exposed by ambient air pollution in addition to direct inhalation of cigarette smoke. Therefore, the adverse effect of tobacco use on public health should be taken into account due to additional pollution exposure [59].

Table 3. Natural gas consumption in last two decades.

Years	**1994**	**2004**	**2014**
Number of Subscribers	300,000	2,606,300	5,660,095
Number of subscribers using gas (Unit)	215,000	2,280,704	5,357,080
Amount of Consumed Gas (Year/m^3)	353,111,160	3,025,985,565	4,943,890,773
Amount of Consumed Gas per subscriber using gas (m^3/subscriber)	1642	1326	922

Hence, the necessary measures for the reduction of tobacco use should be taken even though PM proportion of tobacco smoke is very low in ambient air due to adverse health effect.

3.1.7. Diesel and gasoline vehicle emissions

One of the major sources of air pollution in the IMA is vehicle exhaust from gasoline and diesel vehicles [24]. Their exhaust emits fine particles including organic carbon (OC), elemental carbon (EC), trace metals, cations (Na^+, K^+, NH_4^+), and anions (Cl^-, NO^{3-}, SO_4^{2-}) [60] as well as gaseous pollutants including NOx, VOCs, and CO. Traffic emission has a considerable proportion in the total of GHG emissions in megacities [61]. The reduction of traffic jam and transportation time will lead to the reduction of emissions of both GHG and air pollutants from vehicle exhaust. Istanbul is an important junction point connecting two continents that is an indispensable route for transit transport. The vehicle emissions are from local use and transit vehicles. The determination of their proportion is not simple. There were 3,383,812 vehicles registered in Istanbul Province in 2014. 67% of these vehicles were cars, the others include minibus, bus, truck, motorcycle, tractor, and special vehicles. In 2014, 495,714 tons of gasoline and 2,760,567 tons of diesel fuel were sold. The sold gasoline/diesel fuel ratio is 0.18. As a result, gasoline consumption is lower than diesel. It is known that significant quantities of gasoline vehicles were converted into CNG-powered vehicles to lower the fuel cost. That also reflects to lower pollution emissions originating from gasoline equipped vehicle exhaust. On the other hand, the diesel equipped vehicle exhaust is effective in decreasing air quality [85]. In order to reduce the emissions from vehicle exhaust, lowering all types fuel consumption such as follows: acceleration of the traffic flow in peak hours, increasing the use of public transport, implementation of the prohibited zone to enter in the city center, use of intelligent traffic control systems, given traffic density information for the drivers that contributes in reducing the fuel consumption by changing optimum route.

3.1.8. Vegetative detritus emission

Plants emit GHG and fine particles to ambient air. Anthropogenic and natural particles (e.g., soil and exhaust particles) sink on the leaves under suitable conditions [62]. Due to wind-induced mechanical shear and rubbing of leaves against each other, foliage and leaf deposits become airborne particles that are resuspended into the atmosphere [63]. The leaf surface abrasion particles are identified in ambient PM by measuring the trace organic markers and trace elements [64]. There is a large forest area of 2424 km^2 in the northern part of Istanbul Province and 80.7 km^2 green areas in the IMA. Both green areas should be considered as vegetative detritus source that emit formed particles to ambient air. Rogge [63] reported that vegetative detritus particle proportion was 1.25-2.5% in total OC of $PM_{2.5}$ for four cities of Los Angeles. Shrivastava [33] reported biomass burning and vegetative detritus together contributing to OC of $PM_{2.5}$ as about 8.3% in Pittsburgh Area. Due to no data reported about vegetative detritus particle contribution to ambient air for Istanbul, which is likely a minor proportion in PM_{10} needs to be determined. Vegetative detritus particles naturally occur, so there is no model to reduce emission from plants.

3.1.9. Maritime emission

Ship emissions are significantly increasing globally and have remarkable impact on air quality of seaside and inland [65]. Istanbul strait connect to the Black Sea and Marmara Sea that has an intensive maritime traffic with about 50,000 ship passing through per year. In addition to the maritime traffic on Istanbul Strait, the ships that are in use in domestic transport, fishing, sport or strolling ships should be also considered [66]. The exhaust gas emissions from ships in the Sea of Marmara and the Istanbul Strait are calculated by utilizing the data acquired in 2003. Total emissions from ships in the study area were estimated as 5,451,224 t y^{-1} for CO_2, 111,039 t y^{-1} for NO_x, 87,168 t y^{-1} for SO_2, 20,281 t y^{-1} for CO, 5,801 t y^{-1} for VOC, 4,762 t y^{-1} for PM [65]. Bove [67] reported that the source apportionment study presented the contribution of maritime particles as 15% in the urban area of Genoa (Italy). The

contributions from shipping emissions to PM and gaseous pollutant concentrations show a large spatial variability with 1-7% to annual mean PM_{10} levels with maximal contributions in the Mediterranean basin and the North Sea [29]. The PM and NO_x contribution from the ship emission to Istanbul ambient air should be considered as a negative impact on air quality. However, there is no legislation to control or limit the emissions of ships passing through the Istanbul Strait due to international agreements.

3.1.10. Sea salt particles

Sea-salt particles associated with ions (Na^+, Cl^- and Mg^{2+}) contribute to the ambient air particles in the coastal area [68]. Sea salt aerosols, as represented by Na^+, were consistently confined to the coarse mode, peaking between 1–18 μm depending on location and time [69]. So, Istanbul Province has two parts and each part of its three sides is surrounded by the Marmara Sea, the Black Sea and the Istanbul Strait. The land is under the influence of winds from the north-western and the south-western/eastern sides. Sea salt particles are transported to the European and Asian parts by the wind that sweeps the sea surface and carries the sea salt particles to the inner regions. The aerosol sampling study represented ionic mass contributions up to 42% of the PM_{10} mass that has 8% sodium in Istanbul [24]. So, Na ion was 3.36% in PM_{10} that indicated the sea salt particles contributed to ambient particles in the coastline ambient air.

3.1.11. Long range particle transport

African dust travels over the Mediterranean Sea to impact the urban areas in cities of Europe such as Madrid (Spain) [70], Athens (Greece) [71], Istanbul (Turkey) [72, 73]. The Saharan dust episode cause the elevation of ambient PM concentration due to external PM entrance [74, 75] that effects public health [76, 80, 81]. Chemical composition of PM revealed the concentration of PM_{10} reached 87 μg m^{-3} in 13th of April 2008 that composed of 57% crustal material [15]. Perez [77] reported the PM elevation seen in PM_{10-1} during the Saharan dust event. The Saharan particles were deposited as dry and wet deposition [78]. Therefore, Saharan Dust episode can be considered as long range particles that contribute in elevation of PM_{10} in Istanbul.

3.1.12. GHG emission from landfill

About 15,000 tons/daily municipal solid waste (MSW) was disposed to landfills in the city of Istanbul in 2009 [27]. About 50 million tons and 25 Million tons of MSW were disposed to both Odayeri and Kömürcüda landfills where located in rural site of the megacity from 1995 to 2014, respectively. LFG from both landfill sites has been emitted theoretically to the atmosphere since 1995 until 2009 about 850 Million m^3 (Odayeri) and 400 Million m^3 (Kömürcüda) [27]. Due to the reduction in GHG emissions in the concept of the environmental awareness by IMM, Waste-to-Energy Projects were applied to both landfills to produce electricity by utilizing LFG. After installation of power plants, the total produced electricity is about 1,112,756 MWh from 2009 to 2014 [79]. These projects aimed to reduce GHG from the landfills in the concept of adaptation work. Hence, a minimum of about 110 thousand houses are provided with the electricity from both waste to energy production plants considered as renewable energy source.

3.1.13. Aviation emission

Aviation emits gases (Nitrogen Oxides), volatile organic compounds (VOCs), sulfur oxides (SOx), soot, and other particles [88]. Emissions close to the surface have impact on the concentrations of ozone, and fine particles at the urban area [89]. Air craft emissions impact on local air quality while landing, take-off, and non-LTO (non-Landing-Take-Off) period above 1 km above from the surface [90]. In terms of city air quality, the travels of the aircraft within the city limits should be taken into consideration due to the emission of pollutants. There were two active airports in Istanbul during this study period, namely Atatürk Airport and Sabiha Gökçen Airport. These two airports emit significant greenhouse gas emissions. The calculated greenhouse gas emission values are; 904,465.32 tons CO_2-eq which has been verified as the

equivalent greenhouse gas emission of 2014 at Atatürk Airport [91]. The greenhouse gas emissions from Sabiha Gökçen Airport was reported as 682,916 tons of CO_2-eq from the transportation-related fuel consumption in 2014 [92]. The emission reduction studies of aviation-induced greenhouse gases and air pollutants should be considered carefully.

3.2. Assessment of PM_{10} and SO_2 concentrations between 2010 - 2014

There is no significant variation in PM_{10} and SO_2 values between 2010-2014 (Figure 3). Yearly average SO_2 concentrations were in the range of 3-7 μg/m^3 last five years which are lower than TAAQS. It is obvious that the reduction of consumption of lignite coal cause the decrease of the SO_2 concentration in the long term.

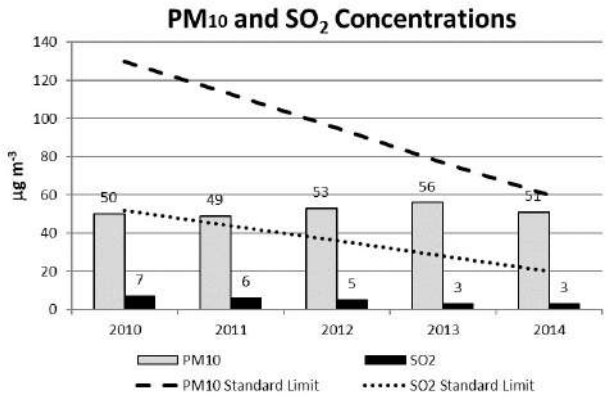

Figure 3. PM_{10} and SO_2 concentrations from 2010 to 2014 in Istanbul [79].

On the other hand, PM_{10} values are in the range of 49-56 μg/m^3 which are slightly lower than TAAQS. It can be interpreted that the implementation works have reduced emissions of PM_{10} which lead to a constant value. Table 4 shows the major reduction works focusing on vehicle exhaust, dust particles and residential combustion sources (natural gas, lignite, fuel oil, wood) which has the most significant sources of PM_{10}.

4. RESULTS

This study determined the sources of air pollutants in order to ensure an effective air quality management in the megacity of boundary. The concentration values of the pollutant parameters were examined retrospectively, and their changes were examined. Accordingly, the actions to be taken in the metropolitan area have been determined to reduce the emission values of pollutant sources.

Major air pollution sources were evaluated at the metropolitan area of Istanbul based on a long-term air quality improvement plan. Air quality management consist of controlling the emission of major sources that are cooking, road dust, wood burning, coal, natural gas, fuel oil, cigarette smoke, diesel and gasoline exhaust, and GHG emission from the landfills. These sources emit air pollutants and GHG that contribute to PM formation and other major pollutants in the urban ambient air. Vegetative detritus and sea salt particles are natural sources and long rang transport particles (Saharan dust) that contribute to elevation of the concentration of PM as well.

It was a priority for air quality management to reduce the concentration of PM_{10} and SO_2 for public health since 1990 to 2014 for the Istanbul case. PM_{10} has been reduced to about 50% since 1990s. Despite all reduction efforts of PM emissions, the PM_{10} has remained in the range of 49-56 μg/m^3 from 2010 to 2014, although there is an intensive urban growth. The stability of PM_{10} is an indication that the works of the measures for air quality control management mentioned above.

The emission reduction efforts were mainly applied on reduction of fossil fuel consumption in the metropolitan area. According to the previous source apportionment studies in road dust and vehicle exhaust gases constitutes higher rate of involvement in PM_{10}. Contributions from these two sources should be tracked carefully by air quality researchers. Without examining major sources of air pollution, only greenhouse gas reduction efforts will not be effective in improving air quality studies. SO_2 was reduced

98% since 1990 to 2014 due to reduction of lignite coal consumption with high sulfur content.

Table 4. Major implementations of emission reductions.

Major Sources of Air Pollutants	Implementations of Emission Reduction
Meat-Cooking Operations	Filter application on exhaust hood of cooking facilities, Chimney Cooker Hood in residential kitchens.
Paved Road Dust	Main artery roads cleaning to collect road dust by sufficient number of street sweepers, using multipurpose street, barriers, and tunnels washing vehicles. Germination to roadside area.
Wood Burning	New retrofitted stove design to improve combustion efficiency.
Coal Burning	New retrofitted stove design to improve combustion efficiency, regulated lignite sale with less than 2% sulfur content. Selling coal-sacks with sealed and marked.
Fuel oil Burning	Improved the performance of oil-fired furnaces and boilers in fuel consumption and burning, improved the quality of fuel-oil.
Cigarette Smoke	Rehabilitation initiative worked for addicts to reduce tobacco use, informed community about the health hazard of smoking, regulated all tobacco products, established Smoke-Free Public Places Act
Diesel and Gasoline Equipped Vehicles	Acceleration of traffic flow in peak hours, encourage to use public transport, implementation of the prohibited zone to enter in the city center, use of intelligent traffic systems, to provide drivers with the necessary information about road conditions in order to use less fuel, established new roads and tunnels to reduce travel distance, promote public to use cars with less consume fuel, promote public to use advanced EURO model diesel vehicles.
Natural Gas	Development of intelligence heating system in residence, advanced technology in natural gas boiler, isolation of building, informed tips for public to use less natural gas and fuels. Encourage the use of natural gas, if available to access
Vegetative Detritus	Naturally occurred.
Maritime Emission	Promoting the use of MARPOL Annex VI compliant ships, no forced application.
Landfill	Implemented waste to energy projects to reduce GHG emission at three landfills (Hasdal, Odayeri, Kömürcüoda) in Istanbul.
Sea Salt Particles	Naturally occurred
Saharan dust particles	Naturally occurred
Aviation Emission	Reduced the waiting time for landing and take-off of aircraft, managed the fuel consumption, improvement of aircraft models, use high quality aircraft fuel.

This study helps assess sources for the abatement of air quality problems for the development of megacities. It requires a serious effort to reduce existing emissions, primarily, the reduction of road dust emission, vehicle exhaust emission, and residential heating emission will contribute to the reduction of both air pollutants.

Major emission reduction work was applied on both PM_{10} and SO_2 parameters to bring them to the level of TAAQS in Istanbul area. The coal

(local Turkish lignite) containing high sulfur content was used a vast amount for the domestic heating until the beginning of 1995 that promoted high SO_2 and PM emissions to the ambient air. On the other hand, all major sources emit particles in all ranges to ambient air that contribute to the formation of PM_{10}. All mentioned control parameters were applied to pollution sources to reduce these concentrations.

5. REFERENCES

[1] M. Derbez, B. Berthineau, V. Crochet, C. Pignon, J. Ribéron, G. Wyatt, C. Mandin, S. Kirchner, "A 3-year follow-up of indoor air quality and comfort in two energy-efficient houses". Building and Environment, vol. 82, pp. 288-299, 2014.

[2] H. Altuğ, E.O. Gaga, T. Döğeroğlu, B. Brunekreef, G. Hoek, W.V. Doorn, "Effects of ambient air pollution on respiratory tract complaints and airway inflammation in primary school children". Science of the Total Environment, vol. 479–480, pp. 201-209, 2014.

[3] S. Hasheminassab, N. Daher, M.M. Shafer, J.J. Schauer, R.J. Delfino, C. Sioutas, "Chemical characterization and source apportionment of indoor and outdoor fine particulate matter (PM2.5) in retirement communities of the Los Angeles Basin". Science of the Total Environment, vol. 490, pp. 528–537, 2014.

[4] G. El Dib, "Impacts of atmospheric pollution on climate change – laboratory studies". Energy Procedia, vol. 6, pp. 600-609, 2011.

[5] N. Oreskes, "The Scientific Consensus on Climate Change", Science, vol. 306(5702), pp. 1686, 2004.

[6] M. Karaca, M. Tayanç, H. Toros, "Effects of urbanization on climate of İstanbul and Ankara", Atmospheric Environment, vol. 29(23), pp. 3411-3421, 1995.

[7] J.J. Schauer, W.F. Rogge, L.M. Hildemann, M.A. Mazurek, G.R. Cass, B.R.T. Simoneit, "Source apportionment of airborne particulate matter using organic compounds as tracers", Atmospheric Environment, vol. 30(22), pp. 3837-3855, 1996.

[8] A. Saral, S. Demir, Ş. Yıldız, "Assessment of odorous VOCs released from a main MSW landfill site in Istanbul-Turkey via a modelling approach", Journal of Hazardous Materials, vol. 168(1), pp. 338-345, 2009.

[9] U. Im, N. Daskalakis, K. Markakis, M. Vrekoussis, J. Hjorth, S. Myriokefalitakis, E. Gerasopoulos, G. Kouvarakis, A. Richter, J. Burrows, L. Pozzoli, A. Unal, T. Kindap, M. Kanakidou, "Simulated air quality and pollutant budgets over Europe in 2008", Science of the Total Environment, vol. 470–471, pp. 270-281, 2014.

[10] L. Bhagavatula, C. Garzillo, R. Simpson, "Bridging the gap between science and practice: An ICLEI perspective", Journal of Cleaner Production, vol. 50, pp. 205-211, 2013.

[11] Z. Şen, "An application of a regional air pollution estimation model over Istanbul urban area", Atmospheric Environment, vol. 32(20), pp. 3425-3433, 1998.

[12] S. Kumar, S.A. Gaikwad, A.V. Shekdar, P.S. Kshirsagar, R.N. Singh, "Estimation method for national methane emission from solid waste landfills", Atmospheric Environment, vol. 38(21), pp. 3481–3487, 2004.

[13] M. Tayanç, "An assessment of spatial and temporal variation of sulfur dioxide levels over Istanbul, Turkey", Environmental Pollution, vol. 107(1), pp. 61-69, 2000.

[14] T. Kindap, A. Ünal, S.-H. Chen, Y. Hu, M.T. Odman, , M. Karaca, "Long-range aerosol transport from Europe to Istanbul, Turkey",

Atmospheric Environment, vol. 40(19), pp. 3536–3547, 2006.

[15] M. Koçak, C. Theodosi, P. Zarmpas, U. Im, A. Bougiatioti, O. Yenigun, Mihalopoulos, N. "Particulate matter (PM10) in Istanbul: Origin, source areas and potential impact on surrounding regions", Atmospheric Environment, vol. 45(38), pp. 6891-6900, 2011.

[16] S. İncecik, "Investigation of Atmospheric Conditions in Istanbul Leading to Air Pollution Episodes", Atmospheric Environment, vol. 30(15), pp. 2739-2749, 1996.

[17] Y.S. Ünal, S. İncecik, Y.Borhan, S. Mentes, "Factors Influencing the Variability of SO2 Concentrations in Istanbul", Journal of Air Waste Management Association, vol. 50(1), pp. 75-84, 2000.

[18] G. Onkal-Engin, İ. Demir, H. Hiz, "Assessment of urban air quality in Istanbul using fuzzy synthetic evaluation", Atmospheric Environment, vol. 38(23), pp. 3809–3815, 2004.

[19] H. K. Özcan, "Long Term Variations of the Atmospheric Air Pollutants in Istanbul City", International Journal of Environmental Research and Public Health, vol. 9(3), pp. 781-790, 2012.

[20] Ü.A. Şahin, O.N. Ucan, C. Bayat, O. Tolluoğlu, "A New Approach to Prediction of SO2 and PM10 Concentrations in Istanbul, Turkey: Cellular Neural Network (CNN)", Environmental Forensics, vol. 12(3), pp. 253-269, 2011.

[21] Y.S. Ünal, H. Toros, A. Deniz, S. İncecik, "Influence of meteorological factors and emission sources on spatial and temporal variations of PM10 concentrations in Istanbul metropolitan area", Atmospheric Environment, vol. 45(31), pp. 5504-5513, 2011.

[22] U. İm, S. İncecik, M. Güler, A. Tek, S. Topcu, Y.S. Unal, O. Yenigün, T. Kindap, M.T. Odman, M. Tayanç, "Analysis of surface ozone and nitrogen oxides at urban, semi-rural and rural sites in Istanbul, Turkey", Science of the Total Environment, vol. 443, pp. 920–931, 2013.

[23] T. Elbir, N. Mangir, M. Kara, S. Simsir, T. Eren, S. Ozdemir, "Development of a GIS-based decision support system for urban air quality management in the city of Istanbul", Atmospheric Environment, vol. 44(4), pp. 441-454, 2010.

[24] C. Theodosi, U. Im, A. Bougiatioti, P. Zarmpas, O. Yenigun, N. Mihalopoulos, Aerosol chemical composition over Istanbul. Science of the Total Environment, vol. 408, pp. 2482–2491, 2010.

[25] H. Toros, H. Erdun, Ö. Çapraz, B. Özer, E.B. Daylan, A.İ. Öztürk, "Air Pollution and Quality Level in Metropolitan Turkey for Sustainable Life". European Journal of Science and Technology, vol. 1(2), pp. 12-18, 2013.

[26] E. Yurtseven, S. Vehid, M. Bosat, S. Köksal, C.N. Yurtseven, "Assessment of Ambient Air Pollution in Istanbul during 2003-2013", Iranian Journal of Public Health, vol. 47(8), pp. 1137-1144, 2018.

[27] O. Sevimoğlu, "Assessment of Limiting Factors for Potential Energy Production in Waste to Energy Projects", Fresenius Environmental Bulletin, vol. 24(7), pp. 2362 – 2373, 2015.

[28] P. Fu, K. Kawamura, M. Kobayashi, B.R.T. Simoneit, "Seasonal variations of sugars in atmospheric particulate matter from Gosan, Jeju Island: Significant contributions of airborne pollen and Asian dust in spring", Atmospheric Environment, vol. 55, pp. 234-239, 2012.

[29] M. Viana, P. Hammingh, A. Colette, X. Querol, B. Degraeuwe, I. Vlieger, J.

Aardenne, "Impact of maritime transport emissions on coastal air quality in Europe". Atmospheric Environment, vol. 90, pp. 96-105, 2014.

[30] W.F. Rogge, L.M. Hildemann, M.A. Mazurek, G.R. Cass, B.R.T. Simoneit, "Sources of fine organic aerosol. 1. Charbroilers and meat cooking operations", Environmental Science Technology, vol. 25(6), pp. 1112–1125, 1991.

[31] L.M. Hildemann, G.R. Markowski, G.R. Cass, "Chemical composition of emissions from urban sources of fine organic aerosol". Environmental Science Technology, vol. 25(4), pp. 744-759, 1991.

[32] Turkey Statistical Institute (TSI), "Turkey's Statistical Yearbook", 2013, http://www.turkstat.gov.tr/Kitap.do?metod=KitapDetay&KT_ID=0&KITAP_ID=1, [Accessed: Feb. 12, 2020].

[33] M.K. Shrivastava, R. Subramanian, W.F. Rogge, A.L. Robinsona, "Sources of organic aerosol: Positive matrix factorization of molecular marker data and comparison of results from different source apportionment models", Atmospheric Environment, vol. 41(40), pp. 9353–9369, 2007.

[34] Y.-C. Li, J.Z. Yu, S. Sai, H. Ho, J.J. Schauer, Z. Yuan, A.K.H. Lau, P.K.K. Louie, "Chemical characteristics and source apportionment of fine particulate organic carbon in Hong Kong during high particulate matter episodes in winter 2003", Atmospheric Research, vol. 120–121, pp. 88–98, 2013.

[35] Gazette, "Causing Odor Control of Emission Regulations", No: 27692, 4 September 2010.

[36] W.F. Rogge, P.M. Medeiros, B.R.T. Simoneit, "Organic Compounds in Dust from Rural and Urban Paved and Unpaved Roads Taken During the San Joaquin Valley Fugitive Dust Characterization Study", Environmental Engineering Science, vol. 29(1), pp. 1-13, 2012.

[37] S. Han, J.-S. Youn, Y.-W. Jung, "Characterization of PM10 and PM2.5 source profiles for resuspended road dust collected using mobile sampling methodology", Atmospheric Environment, vol. 45(20), pp. 3343-3351, 2011.

[38] K. Hussain, M. Rahman, A. Prakash, R.R. Hoque, "Street dust bound PAHs, carbon and heavy metals in Guwahati city – Seasonality, toxicity and sources", Sustainable Cities and Society, vol. 19, pp. 17-25, 2015.

[39] F. Amato, O. Favez, M. Pandolfi, A. Alastuey, X. Querol, S. Moukhtar, B. Bruge, S. Verlhac, J.A.G. Orza, N. Bonnaire, T. Le Priol, J.-F. Petit, J. Sciare, "Traffic induced particle resuspension in Paris: Emission factors and source contributions", Atmospheric Environment, vol. 129, pp. 114-124, 2016.

[40] Z. Li, P.K. Hopke, L. Husain, S. Qureshi, V.A. Dutkiewicz, J.J. Schwab, F. Drewnick, K.L. Demerjian, "Sources of fine particle composition in New York City", Atmospheric Environment, vol, 38(38), pp. 6521–6529, 2004.

[41] Y. Wang, P.K. Hopke, X. Xia, O.V. Rattigan, D.C. Chalupa, M.J. Utell, "Source apportionment of airborne particulate matter using inorganic and organic species as tracers", Atmospheric Environment, vol. 55, pp. 525-532, 2012.

[42] J.C. Chow, J.G. Watson, D.H. Lowenthal, R.J. Countess, "Sources and chemistry of PM10 aerosol in Santa Barbara County, CA", Atmospheric Environment, vol. 30(9), pp. 1489-1499, 1996.

[43] E. Avşar, A.·Hanedar, I.·Toroz, K. Alp, B. Kaynak, "Investigation of P10 Concentrations And Noise Levels of The Road Sweepers Operating In Istanbul-Turkey: A Case Study", Fresenius

Environmental Bulletin, vol. 19(9), pp. 2033-2039, 2010.

[44] J. Zhou, T. Wang, Y. Zhang, N. Zhong, P.M. Medeiros, B.R.T. Simoneit, "Composition and sources of organic matter in atmospheric PM10 over a two year period in Beijing", Atmospheric Research, vol. 93(4), pp. 849-861, 2009.

[45] M.A. Bari, G. Baumbach, J. Brodbeck, M. Struschka, B. Kuch, W. Dreher, G. Scheffknecht, "Characterisation of particulates and carcinogenic polycyclic aromatic hydrocarbons in wintertime wood-fired heating in residential areas", Atmospheric Environment, vol. 45(40), pp. 7627-7634, 2011.

[46] K. Alp, V. Eroğlu, O. Borat, "Istanbul da hava Kirlenmesi ve önleme tedbirlerinin değerlendirilmesi (in Turkish)", In Proceedings Air Pollution Control Symposium, Istanbul Technical University, 8-18 March, 1993

[47] M. Kara, N. Mangır, A. Bayram, T. Elbir, A Spatially High Resolution and Activity Based Emissions Inventory for the Metropolitan Area of Istanbul, Turkey", Aerosol Air Quality Research, 14, 10–20, 2014.

[48] B.M. Didyk, B.R.T. Simoneit, L.A. Pezoa, M.L. Riveros, A.A. "Flores, Urban aerosol particles of Santiago, Chile: organic content and molecular characterization", Atmospheric Environment, vol. 34(8), pp. 1167-1179, 2000.

[49] N.J. Pekney, C.I. Davidson, A. Robinson, L. Zhou, P. Hopke, D. Eatoug, W.F. Rogge, "Major Source Categories for PM2.5 in Pittsburgh using PMF and UNMIX", Aerosol Science and Technology, vol. 40(10), pp. 910-924, 2006.

[50] O. Sevimoglu, "Greenhouse Gas Mitigation Works and Measures Taken Against Climate Change: Case of Istanbul", VII. Atmospheric Science Symposium, Istanbul, pp. 686-697, 28-30 April 2015.

[51] Enerji Piyasaları Denetleme Kurulu (EPDK), Petrol Piyasası Sektör Raporu, 2014.https://www.epdk.org.tr/Detay/Icerik/3-0-107/yillik-sektor-raporu, [Accessed Feb. 14, 2020].

[52] S. Becagli, D.M. Sferlazzo, G. Pace, A. Di Sarra, C. Bommarito, G. Calzolai, C. Ghedini, F. Lucarelli, D. Meloni, F. Monteleone, M. Severi, R. Traversi, R. Udisti, "Evidence for heavy fuel oil combustion aerosols from chemical analyses at the island of Lampedusa: a possible large role of ships emissions in the Mediterranean", Atmospheric Chemistry and Physics, vol. 12, pp. 3479–3492, 2012.

[53] A.A. Campos–Ramos, A. Aragon–Pina, A. Alastuey, I. Galindo–Estrada, X. Querol, "Levels, composition and source apportionment of rural background PM10 in western Mexico (State of Colima)", Atmospheric Pollution Research, vol. 2(4), pp. 409-417, 2011.

[54] Y. Cheng, S., Lee, Z. Gu, K. Ho, Y. Zhang, Y. Huang, J.C. Chow, J.G. Watson, J. Cao, R. Zhang, "$PM_{2.5}$ and $PM_{10-2.5}$ chemical composition and source apportionment near a Hong Kong roadway", Particuology, vol. 18, pp. 96-104, 2015.

[55] D. Mooibroek, M. Schaap, E.P. Weijers, R. Hoogerbrugge, "Source apportionment and spatial variability of PM2.5 using measurements at five sites in the Netherlands", Atmospheric Environment, vol. 45(25), pp. 4180-4191, 2011.

[56] W.F. Rogge, L.M. Hildemann, M.A. Mazurek, G.R. Cass, B.R.T. Simoneit, "Sources of fine organic aerosol. 6. Cigarette smoke in the urban atmosphere", Environmental Science Technology, vol. 28(7), pp. 1375–1388, 1994.

[57] Worlds Health Organization (WHO), "Report on the Global Tobacco Epidemic, 2013: Enforcing bans on tobacco advertising, promotion and sponsorship", 2013. https://apps.who.int/iris/bitstream/handle/10665/85380/9789241505871_eng.pdf;jsessionid=50136D6997B82D936E43969DD43B897D?sequence=1. [Accessed Feb. 14, 2020].

[58] W.W. Nazaroff, N.E. Klepeis, "Environmental tobacco smoke particles. In: Lidia Morawska and Tunga Salthammer (eds), Indoor Environment: Airborne Particles and Settled Dust", Wiley-VCH, Weinheim, pp. 467, 2003.

[59] S. Mentese, N.A. Mirici, M.T. Otkun, C. Bakar, E. Palaz, D. Tasdibi, S. Cevizci, O. Cotuker, "Association between respiratory health and indoor air pollution exposure in Canakkale, Turkey", Building and Environment, vol. 93(1), pp. 72-83, 2015.

[60] J.G. Watson, J.C. Chow, L.W.A. Chen, D.H. Lowenthal, E.M. Fujita, H.D. Kuhns, D.A. Sodeman, D.E. Campbell, H. Moosmueller, D. Zhu, N. Motallebi, "Particulate emission factors for mobile fossil fuel and biomass combustion sources". Science of the Total Environment, vol. 409(12), pp. 2384-2396, 2011.

[61] J.H., Lee, S. Lim, "The selection of compact city policy instruments and their effects on energy consumption and greenhouse gas emissions in the transportation sector: The case of South Korea", Sustainable Cities and Society, vol. 37, pp. 116-124, 2018.

[62] S. Önder, S. Dursun, "Air borne heavy metal pollution of Cedrus libani (A. Rich.) in city center of Konya (Turkey)", Atmospheric Environment, vol. 40(6), pp. 1122-1133, 2006.

[63] W.F. Rogge, L.M. Hildemann, M.A. Mazurek, G.R. Cass, B.R.T. Simoneit, "Sources of fine organic aerosol. 4. Particulate abrasion products from leaf surfaces of urban plants", Environmental Science and Technology, vol. 27(13), pp. 2700–2711, 1993.

[64] J.C. Chow, J.G. Watson, D.H. Lowenthal, P.A. Solomon, K.L. Magliano, S.D. Ziman, L.W. Richards, "PM10 source apportionment in California's San Joaquin valley" Atmospheric Environment, vol. 26(18), pp. 3335-3354, 1992.

[65] C. Deniz, Y. Durmuşoğlu, "Estimating shipping emissions in the region of the Sea of Marmara, Turkey", Science of the Total Environment, vol. 390(1), pp.255-261, 2008.

[66] U. Kesgin, N. Vardar, "A study on exhaust gas emissions from ships in Turkish Straits". Atmospheric Environment, vol. 35(10), pp. 1863-1870, 2001.

[67] M.C. Bove, P. Brotto, F. Cassola, E. Cuccia, D. Massabò, A. Mazzino, A. Piazzalunga, P. Prati, "An integrated PM2.5 source apportionment study: Positive Matrix Factorisation vs. the chemical transport model CAMx", Atmospheric Environment, vol. 94, pp. 274-286, 2014.

[68] S. Tsunogai, "Sea salt particles transported to the land", Tellus, vol. 27(1), pp. 51–58, 1975.

[69] K. Anlauf, S.-M. Li, R. Leaitch, J. Brook, K. Hayden, D. Toom-Sauntry, A. Wiebe, "Ionic composition and size characteristics of particles in the Lower Fraser Valley: Pacific 2001 field study", Atmospheric Environment, vol. 40(15), pp. 2662–2675, 2006.

[70] A. Tobías, L. Pérez, J. Díaz, C. Linares, J. Pey, A. Alastruey, X. Querol, "Short-term effects of particulate matter on total mortality during Saharan dust outbreaks: A case-crossover analysis in Madrid (Spain)". Science of the Total Environment, vol. 412–413, pp. 386-389, 2011.

[71] E. Remoundaki, A. Bourliva, P. Kokkalis, R.E. Mamouri, A. Papayannis, T. Grigoratos,

C. Samara, M. Tsezos, "PM10 composition during an intense Saharan dust transport event over Athens (Greece)", Science of the Total Environment, vol. 409, pp. 4361-4372, 2011.

[72] D.W. Griffin, N. Kubilay, M. Koçak, M.A. Gray, T.C. Borden, E.A. Shinn, "Airborne desert dust and aeromicrobiology over the Turkish Mediterranean coastline", Atmospheric Environment, vol. 41(19), pp. 4050-4062, 2007.

[73] S.-H. Chen, J. Dudhia, J. S. Kain, T. Kindap, E. Tan, "Development of the online MM5 tracer model and its applications to air pollution episodes in Istanbul- Turkey and Sahara dust transport", Journal of Geophysics and Research, vol. 113, pp. D11203, 1-24, 2008.

[74] B. Kabataş, A. Ünal, R.B. Pierce, T. Kindap, L. Pozzoli, "The contribution of Saharan dust in PM10 concentration levels in Anatolian Peninsula of Turkey", Science of the Total Environment, vol. 488–489, pp. 413-421, 2014.

[75] T. Agacayak, T. Kindap, A. Unal, L. Pozzoli, M. Mallet, F. Solmon, "A case study for Saharan dust transport over Turkey via RegCM4.1 model", Atmospheric Research, vol. 153, pp. 392-403, 2015.

[76] G. Cadelis, R. Tourres, J. Molinie, Short- "Term Effects of the Particulate Pollutants Contained in Saharan Dust on the Visits of Children to the Emergency Department due to Asthmatic Conditions in Guadeloupe (French Archipelago of the Caribbean)", Plosone, vol. 9(3): pp. e91136, 2014.

[77] N. Pérez, J. Pey, X. Querol, A. Alastuey, J.M. López, M. Viana, "Partitioning of major and trace components in PM10–PM2.5–PM1 at an urban site in Southern Europe", Atmospheric Environment, vol. 42(8), pp. 1677-1691, 2008.

[78] S. Tilev-Tanriover, A. Kahraman, "Saharan dust transport by Mediterranean cyclones causing mud rain in Istanbul", Weather, vol. 70, pp. 145-150, 2015.

[79] Istanbul Metropolitan Municipality (IMM), Progress Report, pp. 159, 2014 https://www.ibb.istanbul/Uploads/2016/12/ibb_faaliyetraporu2014.pdf, [Accessed Feb. 14, 2020]

[80] S. Mallone, M. Stafoggia, A. Faustini, G.P. Gobbi, A. Marconi, F. Forastiere, "Saharan Dust and Associations between Particulate Matter and Daily Mortality in Rome, Italy", Environmental Health Perspective, vol. 119(10), pp.1409–1414, 2011.

[81] A. Karanasiou, N. Moreno, T. Moreno, M. Viana, F. De Leeuw, X. Querol, "Health effects from Sahara dust episodes in Europe: Literature review and research gaps", Environment International, vol. 47, pp. 107-114, 2012.

[82] Orman Atlası, Orman ve Su İşleri Bakanlığı, Orman Genel Müdürlüğü, 2013, https://www.ogm.gov.tr/ekutuphane/Yayinlar/Orman%20Atlasi.pdf, [Accessed Feb 12, 2020]

[83] X. Wu, T.V. Vu, Z. Shi, R.M. Harrison, D. Liu, K. Cen, "Characterization and source apportionment of carbonaceous PM2.5 particles in China - A review", Atmospheric Environment, vol. 189, pp. 187-212, 2018.

[84] Türkiye İstatistik Kurumu (TÜİK), Seçilmiş Göstergelerle İstanbul 2013, Yayın No: 4182, ISSN: 1307-0894, 2013.

[85] C. Louis, Y. Yao Liu, P. Tassel, P. Perret, A. Chaumond, M. André, "PAH, BTEX, carbonyl compound, black-carbon, NO2 and ultrafine particle dynamometer bench emissions for Euro 4 and Euro 5 diesel and gasoline passenger cars", Atmospheric Environment, vol. 141, pp. 80-95, 2016.

[86] D. Rutherford, L. Ortolano, "Air quality impacts of Tokyo's on-road diesel emission regulations", Transportation Research Part D: Transport and Environment, vol. 13(4), pp. 239-254, 2008.

[87] A. Akkoyunlu, F. Ertürk, "Evaluation of air pollution trends in Istanbul", International Journal of Environment and Pollution, vol. 18(4), pp. 388-397, 2002.

[88] M. Mazaheri, G.R. Johnson, L. Morawska, "An inventory of particle and gaseous emissions from large aircraft thrust engine operations at an airport", Atmospheric Environment, vol. 45(20), pp. 3500-3507, 2011.

[89] M.A. Cameron, M.Z. Jacobson, S.R.H. Barrett, H. Bian, C.C. Chen, S.D. Eastham, "An intercomparative study of the effects of aircraft emissions on surface air quality", Journal of Geophysical Research: Atmospheres, vol. 122, pp. 8325-8344, 2017.

[90] D. Phoenix, A. Khodayari, D. Wuebbles, K. Stewart, "Aviation impact on air quality present day and mid-century simulated in the Community Atmosphere Model (CAM)", Atmospheric Environment, vol. 196, pp. 125-132, 2019.

[91] Devlet Hava Meydanları İşletmesi (DHMİ), İSTANBUL ATATÜRK HAVALİMANI, Sera Gazı Beyanı Doğrulama Açıklaması (2014 Yılı Dönemi). Web:https://ataturk.dhmi.gov.tr/Sayfalar/icerik-detay.aspx?oid=1231, [Accessed Feb 12, 2020]

[92] Pendik Belediyesi Strateji Geliştirme Müdürlüğü, "Pendik İlçesi Karbon Ayak İzi Çalışması", İstanbul, 2014, http://www.skb.gov.tr/wp-content/uploads/2017/01/Pendik-Ilcesi-Karbon-Ayak-Izi.pdf, [Accessed Feb 12, 2020].

Sakarya University Journal of Science

ISSN 1301-4048 | e-ISSN 2147-835X | Period Bimonthly | Founded: 1997 | Publisher Sakarya University
http://www.saujs.sakarya.edu.tr/en/

Title: The Effect of Spin-Orbit Interaction On Structural and Electronic Properties of ScIr2

Authors: Hüseyin Yasin Uzunok
Recieved: 2020-01-26 17:51:56

Accepted: 2020-02-18 16:21:06

Article Type: Research Article
Volume: 24
Issue: 2
Month: April
Year: 2020
Pages: 406-411

How to cite
Hüseyin Yasin Uzunok; (2020), The Effect of Spin-Orbit Interaction On Structural and Electronic Properties of ScIr2. Sakarya University Journal of Science, 24(2), 406-411, DOI: https://doi.org/10.16984/saufenbilder.680230
Access link
http://www.saujs.sakarya.edu.tr/tr/issue/52471/680230

Sakarya University Journal of Science 24(2), 406-411, 2020

The Effect of Spin-Orbit Interaction On Structural and Electronic Properties of $ScIr_2$

Hüseyin Yasin UZUNOK[1]

Abstract

The structural and electronic properties of face-centred cubic ScIr2 compound is investigated by using a generalised gradient approximation scheme of density functional theory with and without spin-orbit interaction. The structural results show that the spin-orbit interaction has a negligible effect for the crystallizing of $ScIr_2$ compound. The Fermi surface calculations suggest considerable nesting along $\Gamma - X$ direction that could affect the vibrational properties.

Keywords: intermetallics, density functional theory, electronic structure, spin-orbit interaction

1. INTRODUCTION

Laves phase cubic $MgCu_2$-type (C15) intermetallic compounds are taken interest from a long time due to their interesting features such as heavy fermion behaviour, Kondo effect, interesting thermodynamic properties and especially favouring superconductivity [1-8]. The superconducting properties are studied by our group for these kind of compounds such as $CaIr_2$ and $CaRh_2$ [9]. In this study, it is observed that the spin-orbit interaction has to be taken account when the transition-metal d states dominate Fermi level region. First Compton and co-workers [10], then Geballe and co-workers [11] are successfully synthesized and studied cubic Laves $ScIr_2$ compound. They found that this compound is a superconductor with a 2.07 K superconducting transition temperature. In 2000, Goncharuk and colleagues [12] are investigated $ScIr_2$ compound for its thermodynamic features by using electromotive force measurements. They have obtained Gibb energies, enthalpies, and entropies for this compound. Shrivastava and Sanyal [13] are studied structural, electronic and elastic properties of $ScIr_2$ YIr_2, and $LaIr_2$ compounds by using full-potential linearized augmented plane wave (FP-LAPW) method. The results show that all studied compounds are showing ductile properties due to the elastic analysis. In 2019, also Chowdhury and Saha [14] have investigated the physical properties of $ScIr_2$ superconductor using *ab initio* technique. They have found that the

[1] Sakarya Univesrsity, Department of Physics, 54187 Sakarya,Turkey, ORCID ID: 0000-0002-2130-1748, hyuzunok@sakarya.edu.tr.

electronic band structure reveals metallic conductivity and the major contribution comes from Ir-5d states. Even though there are several theoretical studies on structural and electronic properties of $ScIr_2$, there is no study included the spin-orbit interaction (SOI) for this properties.

Due to its interesting features, in this study, the structural and electronic properties of $ScIr_2$ is studied by using generalised gradient approximation (GGA) scheme implemented in Density Functional Theory with and without SOI. Since the compound has transition metal in its structure, the SOI effect on its electronic structure has to be researched. The structural lattice constants, bulk modulus and its pressure derivative B' are obtained by fitting the total energy as a function of the lattice parameter to the Murnaghan equation of states [15]. The electronic properties are calculated by using full-relativistic norm-conserving pseudopotentials for including SOI and compared by the results obtained via scalar-relativistic norm-conserving pseudopotentials without SOI.

2. METHOD

The first principles calculations are performed by using the Quantum Espresso package [16, 17]. The exchange-correlation calculations are determined by using the norm-conserving GGA scheme [18, 19]. While the full-relativistic norm-conserving pseudopotentials are employed for a description of interaction between the ionic cores and valence electrons with SOI, scalar relativistic norm-conserving pseudopotentials are used for the same calculations without SOI [18]. The wave function was expanded in plane waves with the energy cut-off of 60 Ry and the default charge-density value of 240 Ry is used for the norm-conserving pseudootentials. For the sampling of the Brillouin zone to obtain structural optimization, we have used a $(8 \times 8 \times 8)$ Monkhorst-Pack [20] $\vec{k}$-point mesh. For the electronic structure and the electronic density of states calculations $(24 \times 24 \times 24)$ Monkhorst-Pack [20] $\vec{k}$-point mesh is used.

3. RESULTS

3.1. Structural Properties

The $ScIr_2$ compound crystallizes in $MgCu_2$-type face-centred cubic (fcc) structure with the space group $Fd\bar{3}m$ (Wyckoff no:227). The structure is presented in Fig. 1. In this crystal structure, atomic positions are taken as Sc at 8b (0.375, 0.375, 0.375) and Ir at 16c (0.00, 0.00, 0.00). The ground state properties have been determined by calculating the total energy as a function of lattice constant (a (Å)) and fitted to the Murnaghan equation of state [15] for defining the equilibrium lattice, the bulk modulus (B), and the pressure coefficient (B') [15]. Table 1 presents the calculated values of a, B, B' and the distance between atoms along with available previous experimental and theoretical studies.

Table 1.The calculated structural properties for fcc $ScIr_2$ with available previous studies.

	a(Å)	d_{Sc-Ir} (Å)	d_{Ir-Ir} (Å)	B (GPa)	B'
This Work (With SOI)	7.450	3.1176	2.6587	209.3	4.39
This Work (Without SOI)	7.520	3.1201	2.6654	208.5	4.52
Experimental	7.348				
FP-LAPW[13]	7.399			224.2	5.02
GGA[14]	7.449			225.8	

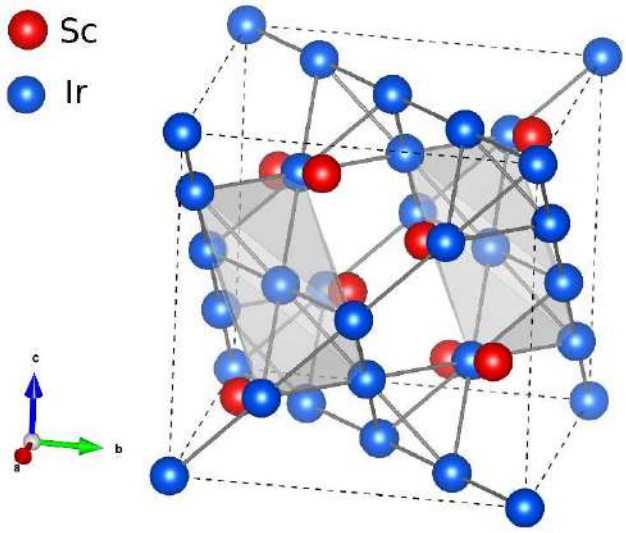

Figure 1. The fcc $MgCu_2$-type crystal structure of $ScIr_2$

The calculated results in this study are in accordance with previous experimental and theoretical results. More importantly, the results with and without SOI are very close to each other. This result is a sign for the spin-orbit interaction does not effect on the structural properties of studied $ScIr_2$ compound. The distance between Ir atoms is shorter than the sum of their covalent radii which suggest a covalent bonding between Ir atoms while the electronegativity difference between Sc and Ir atoms suggest an ionic bonding. It could be said that the $ScIr_2$ compound contains an interplay between covalent, ionic and metallic bonds.

3.2. Electronic Properties

The electronic structure of $ScIr_2$ compound without SOI is presented in Figure 2 (a). The electronic structure in this figure clearly shows the metallic nature of the studied compound because of the electronic bands that are crossing the Fermi energy level (E_F). Dispersive bands are crossing the E_F along all the symmetry directions that shows there is no insulated direction along the studied high symmetry points. The bands show nondispersive character along the $\Gamma - X$ direction which suggest the density of states at the Fermi level ($N(E_F)$) have a higher value because of this behaviour.

Figure 2 (b) is presented the electronic band calculations with (solid red lines) and without (dashed black lines) SOI for comparison. Even though there is some splitting effect occurred for six-fold and four-fold degenerated bands, since the compound is centrosymmetric, there is no splitting seen for the two-fold degenerated bands. The six-fold degeneration around -0.26 eV at the Γ high-symmetry point is split into two- and four-fold degenerated electronic band with a 0.1 eV energy difference. The split two-fold degenerated band stays under the E_F along $\Gamma - X$ direction and does not contribute the $N(E_F)$ value. Along the $\Gamma - L$ direction the SOI splitting make the split band get closer to E_F that makes more contribution to the $N(E_F)$. The SOI split four-fold degeneration into two-fold degenerated bands with a 0.04 eV difference at the W high symmetry point. Even though this splitting is quite small, the split bands get close to E_F. Overall, the SOI effect on the electronic band structure is negligible.

In order to investigate the nature of electronic bands, the total and partial density of states (DOS) with and without SOI of $ScIr_2$ are presented in Figure 2 (c), and a comparison between total DOS values with and without SOI is presented with an inset figure. From this inset figure, it is found that the effect of SOI on the total DOS of $ScIr_2$ is very small and negligible even though the $N(E_F)$ value with SOI seems higher than without SOI one. This feature could be related with the splitting effect that cause the electronic bands get near the E_F. The value of $N(E_F)$ with SOI is calculated to be 4.78 states/eV that decreases to 4.61 states/eV by turning off the SOC. These results are in accordance with previous FL-LAPW result of 4.64 states/eV [13]. The value of $N(E_F)$ consists of roughly 82 % of Ir electronic states and 18% Sc electronic states. In particular, Ir 5d state alone contribution to the $N(E_F)$ is up to 74%. This result signs that Ir 5d electrons are most influential in consisting the free electrons around the developing the E_F.

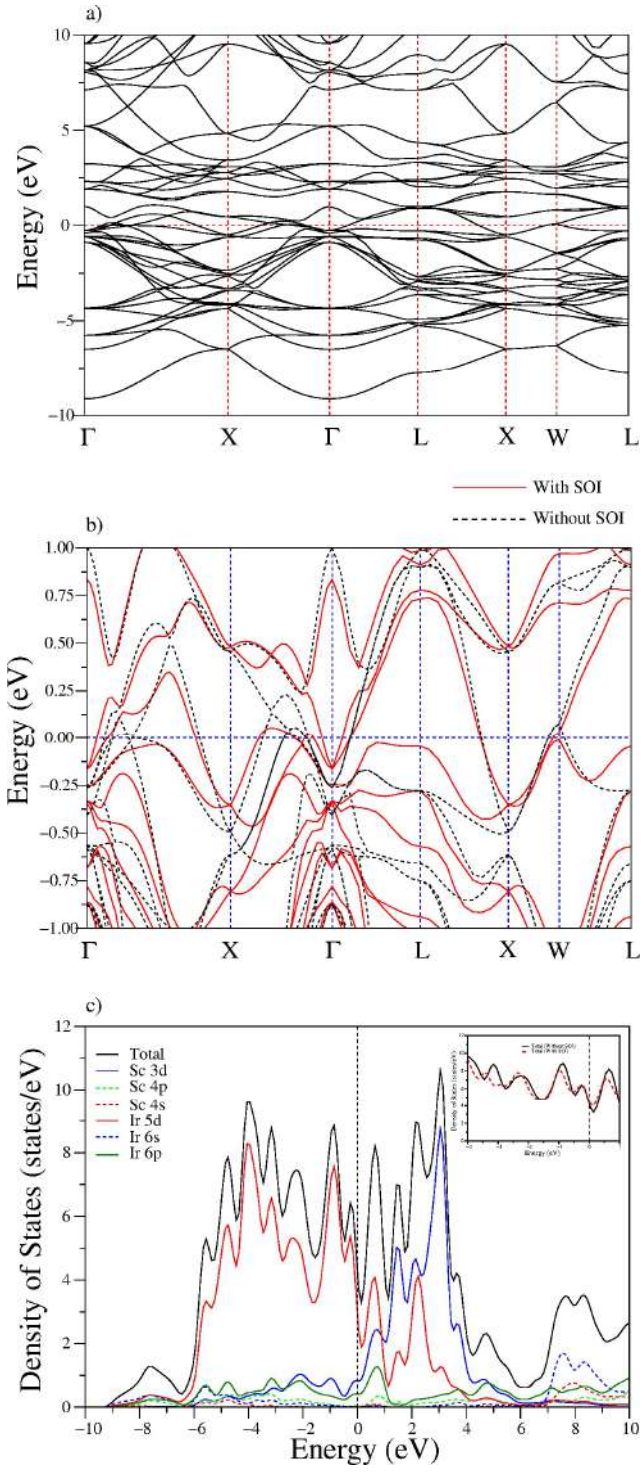

Figure 2. (a) The electronic structure of $ScIr_2$ compound without SOI, (b) The comparison between the electronic structure with (solid red lines) and without (dashed black lines) SOI, and (c) electronic DOS. The inset figure in (c) is presenting a comparison between total DOS values with and without SOI

For a better understanding the electronic properties with SOI, the Fermi surfaces of $ScIr_2$ is illustrated with and without SOI in Figure 3. The Fermi surfaces without SOI are illustrated in Figure 3 (b)-(c)-(d) and the Fermi surfaces with SOI are illustrated in Figure 3 (e)-(f)-(g)-(h). It is clear that the Fermi surfaces are divided into split sheets because of SOI. The Fermi surface in Figure 3 (b) has a hole characteristic and barely consists because the electronic band that constitute this surface is barely touched the E_F along $\Gamma - X$ direction. This Fermi surface does not consist when the SOI considered because SOI move this band away from the E_F. The Fermi surface presented in Figure 3 (c) without SOI is split into two Fermi surfaces that are given in Figure 3 (e) and Figure 3 (f). This Fermi sheets make a closed curves around the Γ and X high symmetry points which show a high nesting features [21-23] along $\Gamma - X$ direction. Similar to this feature, the Fermi surface calculated without SOI that presented in Figure 3 (d) is split into two different Fermi surfaces when the SOI taken into account. These surfaces are given in given in Figure 3 (g) and Figure 3 (h). The Fermi sheets without SOI show complex features when the SOI simplified them.

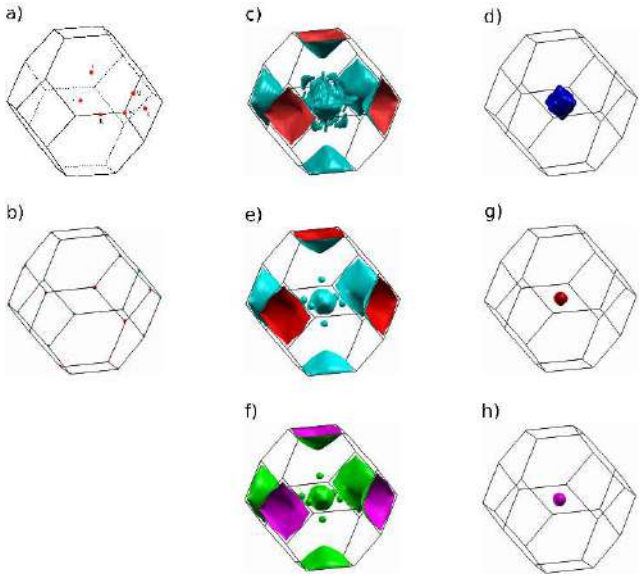

Figure 3. (a) High symmetry points of Brillouin zone of fcc structure, the Fermi surface sheets (b)-(c)-(d) without SOI, and (e)-(f)-(g)-(h) with SOI for $ScIr_2$ compound.

4. SUMMARY

The structural and electronic properties of face-centred cubic $ScIr_2$ compound is investigated by using a generalised gradient approximation scheme of density functional theory with and without spin-orbit interaction. The structural results show that the spin-orbit interaction has a negligible effect for the crystallizing of $ScIr_2$ compound. The distances between the atoms are also suggest an interplay between different kind of bonding features exist.

The electronic structure calculations are in good accordance with previous calculations[13, 14]. The SOI has a negligible effect on the electronic features of this compound even though the Fermi level is occupied by transition metal's d orbital electrons. The Fermi surfaces are shown a considerable nesting and could affect the vibrational properties of studied $ScIr_2$ compound. Hence the lattice dynamical properties have to be examined with detail.

ACKNOWLEDGMENTS

I want to thank Prof. Dr. Hüseyin Murat Tütüncü and Dr. Ertuğrul Karaca for their invaluable support.

5. REFERENCES

[1] E. Deligoz, K. Colakoglu, H. Ozisik, and Y. Cifti, "The first principles investigation of lattice dynamical and thermodynamical properties of Al2Ca and Al2Mg compounds in the cubic Laves structure," Computational materials science, vol. 68, pp. 27-31, 2013.

[2] S. Chen, Y. Sun, Y.-H. Duan, B. Huang, and M.-J. Peng, "Phase stability, structural and elastic properties of C15-type Laves transition-metal compounds MCo2 from first-principles calculations," Journal of Alloys and Compounds, vol. 630, pp. 202-208, 2015.

[3] E. Deligoz, H. Ozisik, and K. Colakoglu, "Theoretical predictions of the structural, mechanical and lattice dynamical properties of XW2 (X= Zr, Hf) Laves phases," Philosophical Magazine, vol. 94, pp. 1379-1392, 2014.

[4] M. I. Kholil, M. Z. Rahaman, and M. A. Rahman, "First principles study of the structural, elastic, electronic, optical and thermodynamic properties of SrRh2 laves phase intermetallic compound," Computational Condensed Matter, vol. 13, pp. 65-71, 2017.

[5] U. Atzmony, M. Dariel, E. Bauminger, D. Lebenbaum, I. Nowik, and S. Ofer, "Spin-orientation diagrams and magnetic anisotropy of rare-earth-iron ternary cubic laves compounds," Physical Review B, vol. 7, p. 4220, 1973.

[6] U. Atzmony and M. Dariel, "Nonmajor cubic symmetry axes of easy magnetization in rare-earth-iron Laves compounds," Physical Review B, vol. 13, p. 4006, 1976.

[7] U. Atzmony, M. Dariel, E. Bauminger, D. Lebenbaum, I. Nowik, and S. Ofer, "Magnetic Anisotropy and Spin Rotations in Ho x Tb 1− x Fe 2 Cubic Laves Compounds," Physical Review Letters, vol. 28, p. 244, 1972.

[8] Ö. Rapp, J. Invarsson, and T. Claeson, "Search for superconductivity in Laves phase compounds," Physics Letters A, vol. 50, pp. 159-160, 1974.

[9] H. Tütüncü, H. Uzunok, E. Karaca, E. Arslan, and G. Srivastava, "Effects of spin-orbit coupling on the electron-phonon superconductivity in the cubic Laves-phase compounds CaIr 2 and CaRh 2," Physical Review B, vol. 96, p. 134514, 2017.

[10] V. B. Compton and B. T. Matthias, "Laves phase compounds of rare earths and hafnium with noble metals," Acta Crystallographica, vol. 12, pp. 651-654, 1959.

[11] T. Geballe, B. Matthias, V. Compton, E. Corenzwit, G. Hull Jr, and L. D. Longinotti, "Superconductivity in binary alloy systems of the rare earths and of thorium with Pt-group metals," Physical Review, vol. 137, p. A119, 1965.

[12] L. Goncharuk, V. Sidorko, V. Khoruzhaya, and T. Y. Velikanova, "Thermodynamic parameters of scandium-iridium compounds< ScIr 3> and ScIr 2," Powder Metallurgy and Metal Ceramics, vol. 39, pp. 55-58, 2000.

[13] D. Shrivastava and S. Sanyal, "Structural, electronic and elastic properties of REIr 2 (RE= Sc, Y and La) Laves phase compounds under pressure," Indian Journal of Physics, vol. 91, pp. 183-190, 2017.

[14] U. K. Chowdhury and T. C. Saha, "An ab-initio Investigation: The Physical Properties of ScIr 2 Superconductor," Physics of the Solid State, vol. 61, pp. 530-536, 2019.

[15] F. Murnaghan, "The compressibility of media under extreme pressures," Proceedings of the National Academy of Sciences, vol. 30, pp. 244-247, 1944.

[16] P. Giannozzi, S. Baroni, N. Bonini, M. Calandra, R. Car, C. Cavazzoni*, et al.*, "QUANTUM ESPRESSO: a modular and open-source software project for quantum simulations of materials," Journal of physics: Condensed matter, vol. 21, p. 395502, 2009.

[17] P. Giannozzi, O. Andreussi, T. Brumme, O. Bunau, M. B. Nardelli, M. Calandra*, et al.*, "Advanced capabilities for materials modelling with Quantum ESPRESSO," Journal of Physics: Condensed Matter, vol. 29, p. 465901, 2017.

[18] R. Stumpf, X. Gonze, and M. Scheffler, A list of separable, norm-conserving, ab-initio pseudopotentials: Fotocopia: Fritz-Haber-Institute, 1990.

[19] J. P. Perdew, K. Burke, and M. Ernzerhof, "Generalized gradient approximation made simple," Physical review letters, vol. 77, p. 3865, 1996.

[20] H. J. Monkhorst and J. D. Pack, "Special points for Brillouin-zone integrations," Physical review B, vol. 13, p. 5188, 1976.

[21] M. Johannes, I. Mazin, and C. Howells, "Fermi-surface nesting and the origin of the charge-density wave in Nb Se 2," Physical Review B, vol. 73, p. 205102, 2006.

[22] D. Scalapino, E. Loh Jr, and J. Hirsch, "Fermi-surface instabilities and superconducting d-wave pairing," Physical Review B, vol. 35, p. 6694, 1987.

[23] S. Barman, S. Banik, A. Shukla, C. Kamal, and A. Chakrabarti, "Martensitic transition, ferrimagnetism and Fermi surface nesting in Mn2NiGa," EPL (Europhysics Letters), vol. 80, p. 57002, 2007.

JOURNAL OF SCIENCE
SAKARYA UNIVERSITY

Sakarya University Journal of Science

ISSN 1301-4048 | e-ISSN 2147-835X | Period Bimonthly | Founded: 1997 | Publisher Sakarya University
http://www.saujs.sakarya.edu.tr/en/

Title: A Study on the Gamma-ray Attenuation Parameters of Some Commercial Salt Samples

Authors: Canel Eke
Recieved: 2019-05-27 11:33:01

Accepted: 2020-03-10 11:20:56

Article Type: Research Article
Volume: 24
Issue: 2
Month: April
Year: 2020
Pages: 412-423

How to cite
Canel Eke; (2020), A Study on the Gamma-ray Attenuation Parameters of Some Commercial Salt Samples. Sakarya University Journal of Science, 24(2), 412-423,
DOI: https://doi.org/10.16984/saufenbilder.570480
Access link
http://www.saujs.sakarya.edu.tr/tr/issue/52471/570480

Sakarya University Journal of Science 24(2), 412-423, 2020

A Study on the Gamma-ray Attenuation Parameters of Some Commercial Salt Samples

Canel EKE*[1]

Abstract

The purpose of this study is to calculate self-attenuation correction factors, linear (LAC) /mass attenuation coefficients (MAC), half value layers (HVL) and tenth value layers (TVL) of different brands of commercial salt samples using gamma-ray spectrometry equipped with high resolution germanium (HpGe) detector. The gamma-rays emissions of ^{22}Na, ^{60}Co, ^{133}Ba and ^{137}Cs point sources were counted with/without sample. The obtained gamma-ray spectra were analyzed using computer software. Self-attenuation correction factors and gamma-ray attenuation parameters of eleven different brands of commercial salt sample were calculated. The experimental MACs of salt samples were compared with those of NaCl compound utilizing WinXCom software.

Keywords: Self-attenuation correction factor, gamma-ray attenuation parameter, gamma-ray spectrometry, salt samples

1. INTRODUCTION

Gamma-ray spectrometry is used to determine activity concentrations of natural and artificial radionuclides in environmental materials. The accurate and precise determination of radioactivity concentration in samples is important in many areas including radioactive waste management, health physics etc. [1]. Several correction factors have to be determined to obtain reliable activity concentrations. One of them is the self-attenuation correction factor which is described as the ratio a reference specimen count rate to that of the sample [2] The self-attenuation correction factor is calculated theoretically [3], experimentally [1,4] and by simulation methods [2, 5, 6, 7]. Usually, the self-attenuation correction factor is calculated using the Cutshall transmission method [4]. To obtain the most precise results the experimental approach should be used, in which point sources are placed upon the sample or reference specimen placed on the head of the detector [4, 6]. Values of self-attenuation correction factors vary depending on the density, geometry, the chemical

* Corresponding Author. ceke@akdeniz.edu.tr
[1] Akdeniz University, Department of Mathematics and Science Education, Division of Physics Education, Antalya, Turkey. ORCID: 0000-0002-6672-6467

composition of the measured items as well as their attenuation coefficients [1, 6, 8].

The linear attenuation coefficient (LAC) is defined as the probability of interaction per distance unit [9]. Photons interact with material by three processes, namely the Photoelectric Effect, the Compton Effect and the Pair Production. The linear attenuation coefficient is the sum of the probabilities of these interactions as shown in the following equation:

$$\mu = \tau + \sigma + \kappa \quad (1)$$

where τ, σ and κ are the aforementioned interactions, respectively. The Photoelectric Effect is dominant at low gamma-ray energies, the Compton Effect is dominant at mid-gamma ray energies, and the Pair Production is dominant at $E_\gamma > 1.022$ MeV [11]. The mass attenuation coefficient (MAC) depends on the density of the sample.

There are various methods to obtain gamma-ray attenuation parameters in different areas. Gamma-ray attenuation parameters were calculated for soil [13], cane sugar of milk [14], diethylene glycol dissolved in ethyl alcohol [15], naphthalene dissolved in ethanol [16], dilute aqueous solutions of sugar ($C_6H_{12}O_6$) [17], manganese (II) chloride [18], potassium chloride [19], ammonium sulfate [20], NaCl [31], lead nitrate [22], etc. [23, 24]. Furthermore, biological compounds [25], some amino acids [26], alcohol-soluble compounds [27, 28], medical plants [29, 30], different wood materials with different densities [31], environmental bulk sample 32], biological and geological samples [33], and many more. In literature, aqueous solution of salts samples were studied using different methods to calculate gamma-ray attenuation parameters [23, 24, 37, 38].

Gamma-ray attenuation parameters are highly relevant in radiation protection [20] because investigation of gamma-ray parameters of materials is important for applicability in science, technology, human health dosimetry, radiography, radiation shielding, etc. [23, 37]. In view of the importance of the attenuation parameters, the purpose of this study is to calculate gamma-ray attenuation parameters of salt samples and to give examples of application of the Cutshall et al. [4] transmission method using gamma-ray spectrometry. Also the experimental mass attenuation coefficients will be compared with obtained mass attenuation coefficients using WinXCom software [40] to check the accuracy of the results of this study.

2. MATERIAL AND METHOD

In this study to calculate gamma-ray parameters, eleven salt samples were used. Except for S6 which is dishwasher salt, the others are different brands commercial edible salts. S1, S2, S3, S5 and S7 are not refined while S4, S8, S9, S10 and S11 are refined. Densities of the samples are shown in Table-1 and Table-2. Densities (ρ) of samples were calculated using $\rho = {}^{m}/_{V}$ equation, where m is masses of the salt samples V is the volume of the salt samples.

The γ-ray emissions of radioactive point sources ^{22}Na (1274 keV), ^{60}Co (1173 and 1332 keV), ^{133}Ba (81, 276, 302, 356 and 383 keV) and ^{137}Cs (662 keV) were counted 1000 seconds using high purity germanium (HpGe) detector to calculate self-attenuation correction factors, linear-mass attenuation coefficients, HVL and TVL of eleven different brands of salt samples. The activities of these point sources are approximately 1 μCi (37 kBq). The samples were put into 100 ml plastic container; its diameter and height are 61 mm and 53 mm, respectively. The samples were not been sieved because their crystals get same size but samples were shaked to increase density before the measurements. Gamma-ray spectra were analyzed using Maestro-32 software [34]. Wolfram Mathematica-8 [36] software was used in calculating the self-attenuation correction factors of sample versus energy referring to ultrapure water and air fitting function.

The self-attenuation correction factor C_f is calculated using the following well know equation which is called the Cutshall transmission formula [4],

$$C_f = \frac{In\left(\frac{I}{I_0}\right)}{\frac{I}{I_0} - 1} \quad (2)$$

where, I is the count number of source inside the container with the sample and I_0 is the count number of the source inside the container (without sample). Firstly, the container was counted empty then it was filled with ultrapure water when the count number without sample was counted.

The LAC is calculated using the well-known (Lambert – Beer's Law) equation [10, 11],

$$I = I_0 e^{-\mu_l x} \quad (3)$$

$$\mu_l = -\frac{\ln\left(\frac{I}{I_0}\right)}{x} \quad (4)$$

where, μ_l is the LAC of the sample, I is the number of incident photons counts passing through absorber material, I_0 is the number of incident photons counts passing through without absorber material, viz., the empty sample container, and x is the thickness of the absorber material, viz., the sample.

The mass attenuation coefficient (MAC) depends on the density of the sample and is calculated using the following equation [9]:

$$\mu_m = \frac{\mu_l}{\rho} \quad (5)$$

where, μ_m is the mass attenuation coefficient of the sample, and ρ is the density of the sample. Also MACs were calculated using WinXCom software [40]. Total cross-sections and attenuation coefficients also partial cross-sections for incoherent and coherent scattering, photoelectric absorption and pair production can be obtained using WinXCom for elements, compounds or mixtures [40].

Half value layer (HVL) and tenth value layer (TVL) are generally relevant in gamma-ray shielding enforcement considerations. The HVL is described as thickness of shielding materials which reduces the radiation intensity by a factor of two whilst TVL reduces the intensity by a factor of 10 [12]. The HVL and TVL are calculated using following equations,

$$HVL = \frac{In2}{\mu_l} \quad (6)$$

$$TVL = \frac{In10}{\mu_l} \quad (7)$$

3. RESULTS AND DISCUSSION

Self-attenuation correction factors of salt samples referring to air or ultrapure water environment, linear attenuation coefficients (LAC), mass attenuation coefficients (MAC), half value layers (HVL) and tenth value layers (TVL) of salt samples are shown in Tables 1, 2 and 3, respectively. As an example, the self-attenuation correction factor versus energy graphic referring to air sample and ultrapure water sample, variation of the LACs as a function of the γ-ray energy of sample-1 and sample-4, variation of the MACs as a function of the γ-ray energy of sample-1 and sample-4, their transmission rates of sample-1 and sample-4 at different γ-ray energies are shown in Figures 1, 2, 3, 4 and 5, respectively.

The self-attenuation correction factor of salt samples referring to air is greater than that referring to ultrapure water as shown in Figure 1. Because densities of salt samples are greater than that of air and the density of water is higher than air also the self-attenuation correction factor mainly depends on the chemical components and on the integral density of the investigated material [35]. The function of the self-attenuation correction factor versus the energy referring to the air sample and ultrapure water sample was fitted using the fitting function $C_f=aE^{-b}+c$ where E is the gamma-ray energy, and a, b and c are the fitting parameters.

The LACs and MACs were fitted by the $y=ax^{-b}$ fitting function where y is the LAC or MAC, respectively, x is the gamma-ray energy, a and b are the best fit parameters. Because MACs are influenced by the density of the sample they are lower than the LACs. As shown in Figure 4, the values of MACs of sample-1 and sample-4 are

nearly equal although the density of sample-1 is 1.286 g/cm^3 and 1.651 g/cm^3 for sample-4. Conversely, the LACs of sample-1 and sample-4 are different since the LACs depend on the thickness of the samples. Although the thicknesses of the samples are equal in this experiment, the LACs are different. The LACs not only depend on density but also nature of samples. The MACs indicate similar values at certain energy for all samples so the compositions of salt samples are also similar. MACs of NaCl compound were calculated using WinXCom software [40] because the Na and Cl are main elements while the Mg, S, K, Ca, Mn, Fe, Br and Si are trace elements in commercial edible salt samples [39]. The MACs of salt samples obtained experimentally are lower than the results of MACs of NaCl compound obtained from WinXCom software [40] as shown in Table 4. These disparities in the results of the experimentally calculated and obtained from WinXCom [40] may be due about experimental setup especially from narrow-beam geometry in the source- detector settings [41].

The HVL and TVL increase with increasing incident gamma-ray energy (see Table 3). Thus, the transmission rate changes with the gamma-ray energy as shown in Figures 4 and 5 and the transmission rates of the sample-1 and sample-4 decrease with increasing thickness of sample.

Table 1. Self attenuation correction factors of salt samples referring to air

Sample No	Density (g/cm^3)	^{133}Ba (keV)					^{137}Cs (keV)	^{60}Co (keV)	^{22}Na (keV)	^{60}Co (keV)
		81	276	302	356	383	662	1173	1274	1332
1	1.286	1.666±0.024	1.299±0.038	1.288±0.019	1.279±0.009	1.280±0.032	1.211±0.007	1.160±0.009	1.154±0.008	1.143±0.009
2	1.264	1.667±0.024	1.313±0.039	1.311±0.020	1.283±0.009	1.277±0.032	1.224±0.007	1.162±0.009	1.160±0.008	1.148±0.009
3	1.480	1.806±0.030	1.381±0.044	1.358±0.022	1.343±0.009	1.336±0.035	1.266±0.008	1.197±0.010	1.180±0.008	1.175±0.009
4	1.651	1.889±0.033	1.442±0.049	1.397±0.023	1.374±0.010	1.384±0.038	1.290±0.008	1.212±0.010	1.202±0.009	1.191±0.009
5	1.486	1.802±0.030	1.353±0.042	1.349±0.021	1.336±0.009	1.339±0.036	1.250±0.008	1.196±0.010	1.182±0.008	1.178±0.009
6	1.400	1.782±0.029	1.349±0.042	1.349±0.022	1.328±0.009	1.331±0.035	1.270±0.008	1.194±0.010	1.182±0.008	1.176±0.009
7	1.434	1.762±0.027	1.333±0.040	1.353±0.022	1.326±0.009	1.346±0.036	1.257±0.008	1.188±0.010	1.184±0.008	1.172±0.009
8	1.586	1.829±0.030	1.397±0.044	1.367±0.022	1.361±0.010	1.367±0.037	1.284±0.008	1.210±0.010	1.191±0.009	1.193±0.009
9	1.579	1.820±0.030	1.402±0.046	1.378±0/023	1.342±0.009	1.334±0.035	1.267±0.008	1.195±0.010	1.181±0.008	1.174±0.009
10	1.615	1.863±0.032	1.397±0.045	1.390±0.023	1.352±0.010	1.398±0.040	1.267±0.008	1.201±0.010	1.186±0.008	1.183±0.009
11	1.631	1.868±0.032	1.412±0.046	1.385±0.023	1.365±0.010	1.386±0.039	1.279±0.008	1.207±0.010	1.189±0.008	1.184±0.009

Table 2. Self attenuation correction factors of salt samples referring to ultrapure water

Sample No	Density (g/cm^3)	^{133}Ba (keV)					^{137}Cs (keV)	^{60}Co (keV)	^{22}Na (keV)	^{60}Co (keV)
		81	276	302	356	383	662	1173	1274	1332
1	1.286	1.174±0.019	0.989±0.034	0.990±0.017	0.991±0.008	1.002±0.029	0.986±0.007	0.993±0.008	0.998±0.008	0.993±0.008
2	1.264	1.174±0.019	1.001±0.035	1.009±0.018	0.994±0.008	0.999±0.029	0.997±0.007	0.995±0.009	1.003±0.008	0.998±0.008
3	1.480	1.289±0.024	1.059±0.039	1.049±0.019	1.045±0.008	1.050±0.032	1.033±0.007	1.027±0.009	1.021±0.008	1.023±0.009
4	1.651	1.357±0.026	1.110±0.043	1.082±0.020	1.072±0.009	1.091±0.034	1.054±0.007	1.040±0.009	1.041±0.008	1.037±0.009
5	1.486	1.285±0.024	1.034±0.037	1.041±0.019	1.039±0.008	1.052±0.032	1.020±0.007	1.026±0.009	1.023±0.008	1.025±0.009
6	1.400	1.269±0.023	1.031±0.036	1.041±0.019	1.033±0.008	1.046±0.031	1.038±0.007	1.024±0.009	1.024±0.008	1.024±0.009
7	1.434	1.252±0.022	1.018±0.035	1.045±0.019	1.031±0.008	1.059±0.032	1.026±0.007	1.018±0.009	1.026±0.008	1.020±0.009
8	1.586	1.307±0.024	1.072±0.039	1.057±0.019	1.061±0.009	1.077±0.033	1.050±0.007	1.038±0.009	1.032±0.008	1.039±0.009
9	1.579	1.300±0.024	1.076±0.040	1.066±0.020	1.045±0.008	1.048±0.031	1.035±0.007	1.025±0.009	1.022±0.008	1.022±0.009
10	1.615	1.336±0.026	1.072±0.040	1.076±0.020	1.053±0.008	1.103±0.035	1.037±0.007	1.030±0.009	1.027±0.008	1.030±0.009
11	1.631	1.341±0.026	1.084±0.040	1.072±0.020	1.064±0.009	1.093±0.034	1.045±0.007	1.036±0.009	1.030±0.008	1.032±0.009

Table 3. Linear attenuation coefficient (LAC), mass attenuation coefficient (MAC), half value layer (HVL) and tenth value layer (TVL) of salt samples

Sample No	^{133}Ba (keV)					^{137}Cs (keV)	^{60}Co (keV)	^{22}Na (keV)	^{60}Co (keV)
	81	**276**	**302**	**356**	**383**	**662**	**1173**	**1274**	**1332**
S1									
μ_l (cm^{-1})	0.212±0.005	0.103±0.006	0.100±0.003	0.097±0.002	0.097±0.005	0.075±0.002	0.058±0.002	0.055±0.002	0.051±0.002
μ_m(cm^2/g)	0.165±0.004	0.080±0.005	0.078±0.003	0.075±0.002	0.076±0.004	0.058±0.001	0.045±0.001	0.043±0.001	0.040±0.001
HVL (cm)	3.264±0.074	6.711±0.038	6.941±0.237	7.149±0.164	7.128±0.372	9.271±0.225	12.048±0.386	12.539±0.384	13.471±0.463
TVL (cm)	10.841±0.247	22.295±1.256	23.056±0.789	23.748±0.546	23.678±1.236	30.799±0.747	40.023±1.282	41.653±1.276	44.750±1.472
S2									
μ_l (cm^{-1})	0.212±0.005	0.108±0.006	0.107±0.004	0.098±0.002	0.096±0.005	0.079±0.002	0.058±0.002	0.057±0.002	0.053±0.002
μ_m(cm^2/g)	0.168±0.004	0.085±0.005	0.085±0.003	0.078±0.002	0.076±0.004	0.062±0.001	0.046±0.001	0.045±0.001	0.042±0.001
HVL (cm)	3.262±0.074	6.420±0.352	6.455±0.254	7.062±0.177	7.198±0.375	8.782±0.210	11.886±0.378	12.061±0.362	12.978±0.443
TVL (cm)	10.838±0.246	21.328±1.168	21.445±0.842	23.460±0.589	23.911±1.245	29.175±0.697	39.485±1.256	40.066±1.202	43.113±1.472
S3									
μ_l (cm^{-1})	0.250±0.006	0.129±0.006	0.122±0.004	0.117±0.003	0.115±0.005	0.093±0.002	0.070±0.002	0.064±0.002	0.063±0.002
μ_m(cm^2/g)	0.169±0.004	0.087±0.004	0.082±0.003	0.079±0.002	0.078±0.004	0.063±0.001	0.047±0.001	0.043±0.001	0.042±0.001
HVL (cm)	2.768±0.062	5.361±0.268	5.683±0.209	5.910±0.140	6.020±0.284	7.479±0.170	9.885±0.284	10.800±0.306	11.088±0.363
TVL (cm)	9.194±0.207	17.809±0.891	18.879±0.696	19.634±0.465	19.998±0.943	24.844±0.566	32.838±0.942	35.877±1.015	36.835±1.206
S4									
μ_l (cm^{-1})	0.272±0.006	0.148±0.007	0.134±0.005	0.127±0.003	0.130±0.006	0.100±0.002	0.075±0.002	0.072±0.002	0.068±0.002
μ_m(cm^2/g)	0.165±0.004	0.090±0.004	0.081±0.002	0.077±0.002	0.079±0.004	0.061±0.001	0.045±0.001	0.043±0.001	0.041±0.001
HVL (cm)	2.547±0.057	4.688±0.220	5.175±0.187	5.463±0.129	5.333±0.237	6.904±0.154	9.244±0.258	9.686±0.261	10.204±0.334
TVL (cm)	8.461±0.191	15.574±0.731	17.190±0.621	18.148±0.429	17.717±0.788	22.936±0.512	30.709±0.856	32.177±0.868	33.898±1.111
S5									
μ_l (cm^{-1})	0.249±0.006	0.120±0.006	0.119±0.005	0.115±0.003	0.116±0.005	0.088±0.002	0.070±0.002	0.065±0.002	0.064±0.002
μ_m(cm^2/g)	0.168±0.004	0.081±0.004	0.080±0.003	0.077±0.002	0.078±0.004	0.059±0.001	0.047±0.001	0.044±0.001	0.043±0.001
HVL (cm)	2.781±0.063	5.758±0.297	5.821±0.232	6.026±0.149	5.977±0.283	7.911±0.183	9.949±0.288	10.681±0.301	10.909±0.359
TVL (cm)	9.237±0.209	19.128±0.988	19.337±0.772	20.017±0.495	19.855±0.941	26.280±0.606	33.051±0.957	35.482±0.999	36.239±1.194
S6									
μ_l (cm^{-1})	0.244±0.006	0.119±0.006	0.119±0.005	0.113±0.003	0.114±0.005	0.094±0.002	0.069±0.002	0.065±0.002	0.063±0.002
μ_m(cm^2/g)	0.174±0.004	0.085±0.004	0.085±0.003	0.080±0.002	0.081±0.004	0.067±0.002	0.049±0.001	0.046±0.001	0.045±0.001
HVL (cm)	2.840±0.064	5.820±0.300	5.812±0.224	6.159±0.151	6.095±0.289	7.358±0.167	10.059±0.293	10.646±0.299	11.007±0.361
TVL (cm)	9.434±0.213	19.335±0.996	19.308±0.743	20.460±0.501	20.245±0.961	24.443±0.555	33.415±0.972	35.364±0.993	36.563±1.200

Table 3. continue

Sample No	^{133}Ba (keV)					^{137}Cs (keV)	^{60}Co (keV)	^{22}Na (keV)	^{60}Co (keV)
	81	**276**	**302**	**356**	**383**	**662**	**1173**	**1274**	**1332**
S7									
μ_l (cm^{-1})	0.239±0.005	0.114±0.006	0.121±0.005	0.112±0.003	0.118±0.006	0.090±0.002	0.067±0.002	0.066±0.002	0.062±0.002
μ_m(cm^2/g)	0.166±0.004	0.080±0.004	0.084±0.003	0.078±0.002	0.083±0.004	0.063±0.001	0.047±0.001	0.046±0.001	0.043±0.001
HVL (cm)	2.906±0.065	6.067±0.319	5.749±0.220	6.195±0.152	5.853±0.272	7.706±0.177	10.356±0.305	10.538±0.294	11.252±0.374
TVL (cm)	9.653±0.217	20.154±1.059	19.099±0.730	20.579±0.503	19.445±0.905	25.600±0.588	34.402±1.013	35.008±0.977	37.377±1.243
S8									
μ_l (cm^{-1})	0.256±0.006	0.134±0.007	0.125±0.005	0.123±0.003	0.125±0.006	0.099±0.002	0.074±0.002	0.068±0.002	0.069±0.002
μ_m(cm^2/g)	0.162±0.004	0.085±0.004	0.079±0.002	0.078±0.002	0.079±0.004	0.062±0.001	0.047±0.001	0.043±0.001	0.043±0.001
HVL (cm)	2.704±0.061	5.168±0.251	5.550±0.207	5.639±0.134	5.551±0.250	7.020±0.157	9.338±0.261	10.177±0.278	10.101±0.331
TVL (cm)	8.981±0.201	17.166±0.832	18.435±0.687	18.734±0.444	18.441±0.831	23.319±0.522	31.022±0.867	33.807±0.925	33.555±1.100
S9									
μ_l (cm^{-1})	0.254±0.006	0.135±0.007	0.128±0.005	0.117±0.003	0.115±0.005	0.093±0.002	0.069±0.002	0.065±0.002	0.062±0.002
μ_m(cm^2/g)	0.161±0.004	0.086±0.004	0.081±0.002	0.074±0.002	0.073±0.003	0.059±0.001	0.044±0.001	0.041±0.001	0.039±0.001
HVL (cm)	2.728±0.061	5.116±0.251	5.411±0.202	5.926±0.145	6.052±0.286	7.446±0.169	10.004±0.289	10.732±0.302	11.143±0.369
TVL (cm)	9.061±0.204	16.994±0.834	17.976±0.672	19.685±0.481	20.105±0.951	24.736±0.563	33.231±0.960	35.650±1.003	37.017±1.224
S10									
μ_l (cm^{-1})	0.265±0.006	0.134±0.007	0.132±0.005	0.120±0.003	0.134±0.006	0.093±0.002	0.071±0.002	0.066±0.002	0.065±0.002
μ_m(cm^2/g)	0.164±0.004	0.083±0.004	0.082±0.002	0.074±0.002	0.083±0.004	0.058±0.001	0.044±0.001	0.041±0.001	0.040±0.001
HVL (cm)	2.611±0.059	5.168±0.254	5.257±0.195	5.774±0.139	5.161±0.229	7.449±0.169	9.705±0.277	10.461±0.289	10.620±0.349
TVL (cm)	8.673±0.195	17.166±0.843	17.462±0.646	19.181±0.461	17.145±0.760	24.745±0.563	32.241±0.920	34.752±0.962	35.280±1.158
S11									
μ_l (cm^{-1})	0.267±0.006	0.139±0.007	0.130±0.005	0.124±0.003	0.131±0.006	0.097±0.002	0.073±0.002	0.067±0.002	0.066±0.002
μ_m(cm^2/g)	0.164±0.004	0.085±0.004	0.080±0.002	0.076±0.002	0.080±0.004	0.059±0.001	0.045±0.001	0.041±0.001	0.040±0.001
HVL (cm)	2.598±0.058	5.000±0.241	5.317±0.200	5.582±0.133	5.309±0.236	7.149±0.161	9.449±0.266	10.285±0.283	10.533±0.346
TVL (cm)	8.629±0.194	16.611±0.802	17.664±0.665	18.542±0.443	17.635±0.783	23.750±0.535	31.387±0.883	34.167±0.939	34.991±1.151

Table 4. Mass attenuation coefficients (MACs) of NaCl compound

Energy	^{133}Ba (keV)					^{137}Cs (keV)	^{60}Co (keV)	^{22}Na (keV)	^{60}Co (keV)
	81	**276**	**302**	**356**	**383**	**662**	**1173**	**1274**	**1332**
μ_m(cm^2/g)	0.234	0.108	0.104	0.097	0.094	0.074	0.056	0.054	0.053

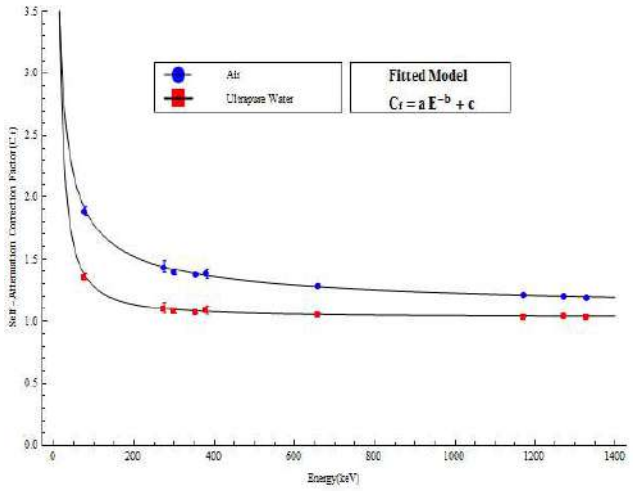

Figure 1. Self-attenuation correction factors of sample 4 versus energy referring to ultrapure water and air

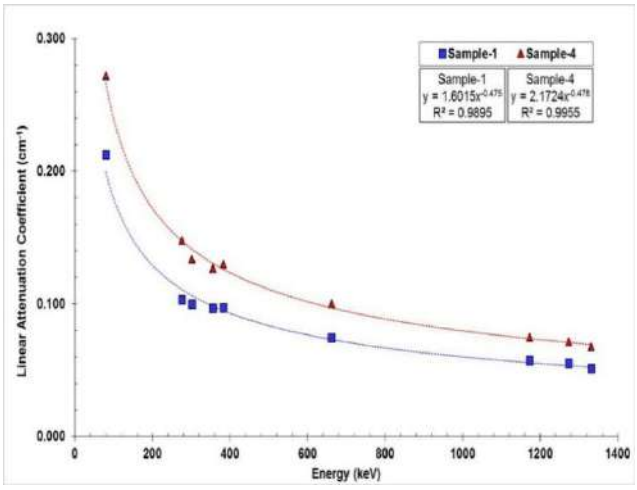

Figure 2. Variation of the LACs of sample-1 and sample-4 as functions of the γ-ray energy

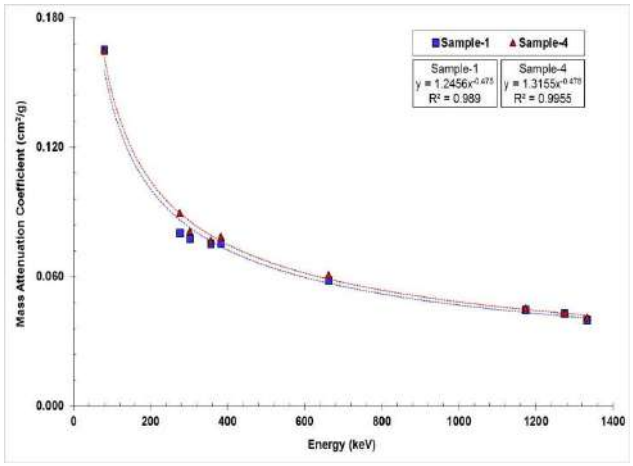

Figure 3. Variation of the MACs of sample-1 and sample-4 as functions of the γ-ray energy

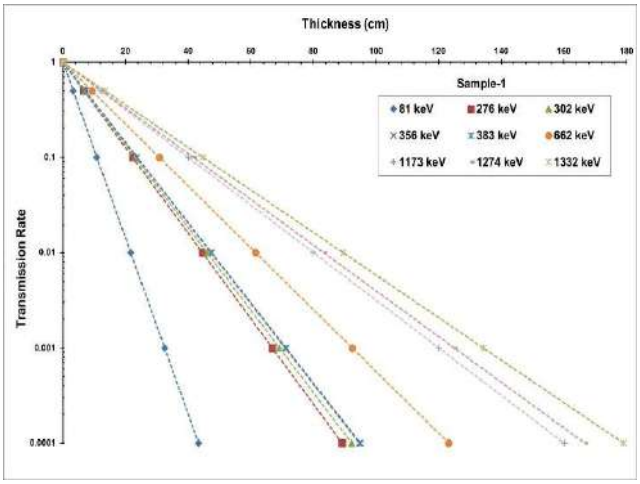

Figure 4. Transmission rate of the sample-1 at different γ-ray energies

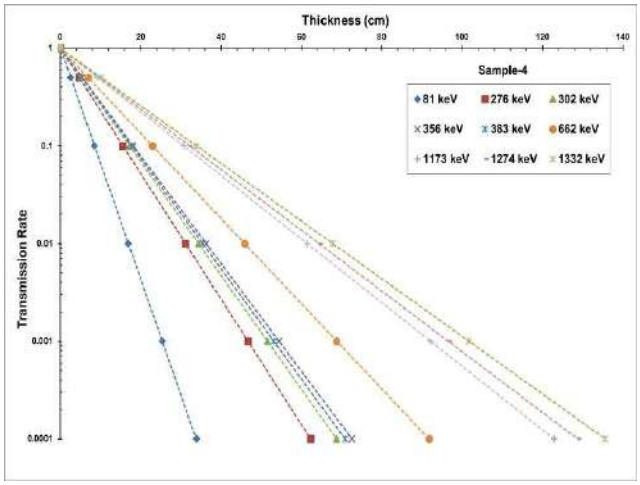

Figure 5. Transmission rate of the sample-4 at different γ-ray energies

4. CONCLUSIONS

The self-attenuation correction factors, LACs, MACs, HVLs and TVLs were calculated experimentally by gamma ray spectrometry between 81 and 1332 keV. The self-attenuation correction factor of salt samples referring to air is higher than that referring to ultrapure water. There are differences between obtained experimental MACs of salts and the results of MACs of NaCl compound obtained from WinXCom software [40]. The LACs are different values for each salt samples whereas the MACs are same values at certain energy for all samples. The HVL and TVL increase with increasing incident gamma-ray energy. The transmission

rate decrease with increasing thickness of sample at certain gamma-ray energy.

The self -attenuation coefficient is significant to accurate and reliable activity concentration of the samples. The attenuation coefficients are needed for different applications of radiation, e.g. dosimetry, radiography, tomography in industrial, agricultural and medical areas in science, technology, human health etc. [18, 20, 33]. The results of this study give information about self-attenuation correction factors, LACs, MACs, HVLs and TVLs of salt samples. Chemical components and physical properties of salt samples can be investigated using atomic and nuclear techniques the effect on attenuation coefficients in the future.

ACKNOWLEDGEMENTS

The author would like to thank Dr. Christian Segebade for useful suggestions and comments.

5. REFERENCES

[1] D. Millsap and S. Landsberger, "Self-attenuation as a function of gamma ray energy in naturally occurring radioactive material in the oil and gas industry," Applied Radiation and Isotopes, vol. 97, pp. 21-23, 2015.

[2] P. Jodłowski, P. Wachniew and C. Dinh, "Monte Carlo validation of the self-attenuation correction determination with the Cutshall transmission method in 210Pb measurements by gamma-spectrometry," Applied Radiation and Isotopes, vol. 87, pp. 387-389, 2014.

[3] M. Barrera, A. Suarez-Llorens, M. Casas-Ruiz, J. Alonso and J. Vidal, "Theoretical determination of gamma spectrometry systems efficiency based on probability functions. Application to self-attenuation correction factors," Nuclear Instruments and Methods in Physics Research Section A: Accelerators, Spectrometers, Detectors and Associated Equipment, vol. 854, pp. 31-39, 2017.

[4] N. Cutshall, I. Larsen and C. Olsen, "Direct analysis of Pb-210 in sediment samples: a self-absorption corrections," Nuclear Instruments and Methods in Physics Research, vol. 206, no. 309-312, 1983.

[5] P. Sabyasachi, C. Agarwal, A. Goswami and M. Gathibandhe, "Attenuation correction for the collimated gamma ray assay of cylindrical samples," Applied Radiation and Isotopes, vol. 98, pp. 23-28, 2015.

[6] P. Jodłowski, "A revision factor to the Cutshall self-attenuation correction in ^{210}Pb gamma spectrometry measurements," Applied Radiation and Isotopes, vol. 109, pp. 566-569, 2016.

[7] S. Landsberger, C. Brabec, B. Canion, J. Hashem, C. Lu, D. Millsap and G. George, "Determination of ^{226}Ra, ^{228}Ra and ^{210}Pb in NORM products from oil and gas exploration: Problems in activity underestimation due to the presence of metals and self-absorption of photons," Journal of Environmental Radioactivity, vol. 125, pp. 23-26, 2013.

[8] M. Bonczyk, B. Michalik and I. Chmielewska, "The self-absorption correction factors for ^{210}Pb concentration in mining waste and influence on environmental radiation risk assessment," Isotopes in Environmental and Health Studies, vol. 53, pp. 104-110, 2017.

[9] N. Tsoulfanidis, Measurement and Detection of Radiation (Second Edition), United States of America: Taylor&Francis, 1995.

[10] G. Knoll, Radiation Detection and Measurement (Third Edition), United States of America: John Wiley&Sons, Inc., 2000.

[11] G. Gilmore, Practical Gamma-ray Spectrometry (Second Edition), England: John Wiley&Sons, Ltd, 2008.

[12] S. Ahmed, Physics and engineering of radiation detection, UK: Academic Press Inc. Published by Elsevier, 2007.

[13] C. Laxman and R. Dayanand, "Attenuation Coefficient of Soil Samples by Gamma ray Energy," Research Journal of Recent Sciences, vol. 1, no. 9, pp. 41-48, 2012.

[14] L. Chaudhari, "Attenuation coefficient of cane sugar of milk samples using gamma source," Scholarly Research Journal for Interdisciplinary Studies, vol. 3, no. 20, pp. 1088-1092, 2015.

[15] C. Udagani and T. Ramesh, "Detection and quantitative determination of diethylene glycol in ethyl alcohol using gamma- ray spectroscopy," Journal of Food Science and Technology, vol. 52, no. 8, pp. 5311-5316, 2015.

[16] U. Dindore, S. Rajmane, S. Dongarge and U. Biradar, "Measurement technique of linear and mass attenuation coefficient of naphthalene soluble in ethanol by gamma ray energy at 1.33 M eV," International Journal of Engineering Technology, Management and Applied Sciences, vol. 4, no. 3, pp. 88-93, 2016.

[17] P. Malwadkar and S. Dongarge, "Linear attenuation coefficient of water soluble suger ($C_6H_{12}O_6$) at 0.662 MeV gamma energy by varying concentration," International Journal of Engineering Technology Science and Research, vol. 3, no. 3, pp. 158-162, 2016.

[18] C. Udagani, "Dependence of gamma ray attenuation on concentration of manganese (II) chloride solution," International Journal of Scientific&Technology Research, vol. 2, no. 7, pp. 55-59, 2013.

[19] L. Chaudhari and M. Teli, "Linear attenuation (or absorption) coefficient of gamma radiation for dilute solutions of potassium chloride," Applied Radiation and Isotopes, vol. 47, no. 3, pp. 365-367, 1996.

[20] S. Dongarge, P. Wadkar and M. Teli, "Measurement of linear attenuation coefficients of gamma rays for ammonium sulfate salt by aqueous solution method," International Journal of Physics and Applications, vol. 2, no. 1, pp. 1-8, 2010.

[21] L. Gerward, "On the attenuation of X-rays and gamma-rays in dilute solutions," Radiation Physics and Chemistry, vol. 48, no. 6, pp. 697-699, 1996.

[22] M. Dumpala and A. Nageswara Rao, "Mass attenuation coefficients of lead nitrate dilute solutions for 13.5 cm thickness at 1173 and 1333 keV," International Journal of Innovative Research in Science, Engineering and Technology, vol. 5, no. 5, pp. 8266-8271, 2016.

[23] M. Teli, "On the attenuation of X-rays and γ-rays for aqueous solutions of salts," Radiation Physics and Chemistry, vol. 53, pp. 593-595, 1998.

[24] M. Teli, C. Mahajan and R. Nathuram, "Measurement of mass and linear attenuation coefficients of gamma-rays for various elements through aqueous solution of salts," Indian Journal of Pure & Applied Physics, vol. 39, pp. 816-824, 2001.

[25] D. Gaikwada, P. Pawar and T. Selvam, "Mass attenuation coefficients and effective atomic numbers of biological compounds for gamma ray interactions," Radiation Physics and Chemistry, vol. 138, pp. 75-80, 2017.

[26] P. Kore and P. Pawar, "Measurements of mass attenuation coefficient, effective atomic number and electron density of some amino acids," Radiation Physics and Chemistry, vol. 98, pp. 86-91, 2014.

[27] S. Dongarge and S. Mitkar, "Measurement of linear and mass attenuation coefficient of alcohol soluable compound for gamma-rays at energy 0.36 MeV," Journal of

Chemical and Pharmaceutical Research, vol. 4, no. 6, pp. 3116-3120, 2012.

[28] S. Mitkar and S. Dongarge, "Measurement of linear and mass attenuation coefficient of alcohol soluble compound for gamma rays at energy 0.511 MeV," Archives of Applied Science Research, vol. 4, no. 4, pp. 1748-1752, 2012.

[29] R. Morabad and B. Kerur, "Mass attenuation coefficients of X-rays in different medicinal plants," Applied Radiation and Isotopes, vol. 68, pp. 271-274, 2010.

[30] S. Teerthe and B. Kerur, "X-Ray mass attenuation coefficient of medicinal plant using different energies 32.890 keV to 13.596 keV," Materials Today: Proceedings, vol. 3, pp. 3925-3929, 2016.

[31] B. Saritha and A. Nageswara, "A study on photon attenuation coefficients of different wood materials with different densities," Journal of Physics: Conference Series, vol. 662, p. 012030, 2015.

[32] K. Satoh, N. Ohashi, H. Higuchi and M. Noguchi, "Determination of attenuation coefficient for self-absorption correction in routine gamma ray spectrometry of environmental bulk sample," Journal of Radioanalytical and Nuclear Chemistry, vol. 84, no. 2, pp. 431-440, 1984.

[33] V. Trunova, A. Sidorina and V. Kriventsov, "Measurement of X-ray mass attenuation coefficients in biological and geological samples in the energy range of 7-12 keV," Applied Radiation and Isotopes, vol. 95, pp. 48-52, 2015.

[34] Maestro-32: Multi-channel analyser software, A65-B32 model, Ortec, 2008. [Online].Available: https://www.ortec-online.com/-/media/ametekortec/manuals/a65-mnl.pdf [Accessed 01 Feb 2018].

[35] E. San Miguel, J. Perez-Moreno, J. Bolivar, R. Garcia-Tenorio and J. Martin, "^{210}Pb determination by gamma spectrometry in voluminal samples (cylindrical geometry)," Nuclear Instruments and Methods in Physics Research Section A: Accelerators, Spectrometers, Detectors and Associated Equipment, vol. 493, pp. 111-120, 2002.

[36] Wolfram Research, Inc., Mathematica, Version 8, Champaign, IL, 2010.

[37] M.T. Teli, L.M. Chaudhari, S.S. Malode, "Attenuation Coefficient of 123 keV γ-radiation by dilute solutions of sodium chloride," Applied Radiation and Isotopes, vol.45 (10), pp. 987-990, 1994.

[38] L. Gerward, "Comments on attenuation coefficient of 123 keV γ-radiation by dilute solutions of sodium chloride," Applied Radiation and Isotopes, vol. 47, pp.1149-1150, 1996.

[39] H. Duggal, A. Bhalla, S. Kumar, J.S. Shani, D. Mehta, "Elemental analysis of condiments, food additives and edible salts using X-ray fluorescence technique," International Journal of Pharmaceutical Sciences Review and Research, vol.35, no,2, pp.126-133, 2015.

[40] L. Gerward, N. Guilbert, K.B. Jenden, H. Levring, "WinXCom—a program for calculating X-ray attenuation coefficients, "Radiation Physics and Chemistry, vol.71, pp.653-654, 2004.

[41] M.E. Medhat, V.P. Singh, "Mass attenuation coefficients of composite materials by Geant4, XCOM and experimental data: comparative study," Radiation Effects and Defects in Solids, vol. 169, no. 9, pp. 800-807, 2014.

JOURNAL OF SCIENCE
SAKARYA UNIVERSITY

Sakarya University Journal of Science

ISSN 1301-4048 | e-ISSN 2147-835X | Period Bimonthly | Founded: 1997 | Publisher Sakarya University
http://www.saujs.sakarya.edu.tr/en/

Title: Artificial Neural Networks Based Decision Support System for the Detection of Diabetic Retinopathy

Authors: Zehra Karapınar Şentürk
Recieved: 2019-10-07 15:58:55

Accepted: 2020-03-11 12:11:14

Article Type: Research Article
Volume: 24
Issue: 2
Month: April
Year: 2020
Pages: 424-431

How to cite
Zehra Karapınar Şentürk; (2020), Artificial Neural Networks Based Decision Support System for the Detection of Diabetic Retinopathy . Sakarya University Journal of Science, 24(2), 424-431, DOI:
https://doi.org/10.16984/saufenbilder.630482
Access link
http://www.saujs.sakarya.edu.tr/tr/issue/52471/630482

Sakarya University Journal of Science 24(2), 424-431, 2020

Artificial Neural Networks Based Decision Support System for the Detection of Diabetic Retinopathy

Zehra KARAPINAR ŞENTÜRK*[1]

Abstract

Machine learning methods have been frequently used for the diagnosis of several diseases recently because of its reliability and convenience. In this paper, a comprehensive overview of the literature related to diabetes and diabetic retinopathy has been done and diagnosis of diabetic retinopathy disease is investigated. Artificial Neural Networks (ANN) method has been applied to the problem using Rapid Miner, a data mining tool. Some other methods have also adapted to the problem, but ANN based detection approach gave the best results. 88.52% sensitivity has been obtained using the features of Messidor dataset. Besides showing the success of ANN in diabetic retinopathy detection, this study also proved that Rapid Miner can be used effectively for the analysis of diabetic retinopathy.

Keywords: diabetic retinopathy, artificial neural networks, Rapid Miner.

1. INTRODUCTION

Diabetes is a critical and protracted disease which occurs depending on the insufficient releasing of insulin or the inability of human body to use insulin [1]. Main types of diabetes are type 1 and type 2 diabetes. Type 1 diabetes is the primary cause of childhood diabetes but can be seen at any age and it cannot be prevented [1]. 90% of diabetes worldwide has type 2 diabetes and it can be controlled and even get rid of it [1]. To defer farther problems caused by type 2 diabetes may be possible via regularizations in eating and work out habits when an early diagnosis is achieved, but early diagnosis is not always possible and it takes seven years on the average to diagnose this disease [2]. Diabetic retinopathy (DR) is one of the diabetic eye diseases and early diagnosis and timely treatment of DR can prevent vision disorders and blindness [1]. 21% of type 2 diabetes patients also have retinopathy once the disease is diagnosed and it is a progressive disease [3]. More than 60% of type 2 patients have retinopathy and a very often reason of recent occurrences of blindness between the ages 20 and 74 is because of diabetic retinopathy [3]. Therefore, early diagnosis of diabetes and diabetic retinopathy is crucial. Medical diagnosis of diseases is accurate, but may take a long time, costly, and psychologically disturbing for possible patients. So, computer aided decision support mechanisms which perform fast and

*Corresponding Author. zehrakarapinar@duzce.edu.tr
[1]Düzce University, Faculty of Engineering, Computer Engineering Department, 81620, Düzce, Turkey
ORCID: https://orcid.org/0000-0003-3116-1985

almost accurate diagnosis help significantly both to the doctors and the patients.

There are many studies related to the diagnosis of diabetes in the literature. In [4], the researchers applied multi-layer perceptron, radial basis function and general regression neural networks to Pima Indian Diabetes (PID) dataset and showed that general regression neural networks perform the best with 80.21% accuracy for the diagnosis of diabetes. ID3 and Decision Tree algorithms are used for diabetes detection in [5] and their accuracies were found as 80% and 72% respectively. Classification of whether a patient has diabetes or not was achieved 80.72% by AdaBoost algorithm and four base classifiers which are Support Vector Machine, Naïve Bayes, Decision Tree and Decision Stump were considered in [6]. Experimental results of the study indicate that Decision Stump supported AdaBoost classifies better than the other three base classifiers. A new distance metric, Lorentzian Distance is proposed in [7] for classification purposes and they applied this metric with k-nearest neighbor method to classification problem of diabetes. They achieved 76% success with k=10 neighbors. In [8], multi-layer perceptron (MLP) and different versions of Support Vector Machines (SVM) were used. Different kernel functions (linear, polynomial, radial) were used for diagnosis and SVM with linear kernel is decided as the most successful classifier with 77.47% accuracy.

Another machine learning based diabetes diagnosis was realized by Naïve Bayes in [9]. The authors also used Genetic Algorithm to select affective four attributes among eight and applied NB together with these selected four attributes. The performance of NB was improved to 78.69%. As a prevalent and easy to apply method, an artificial neural network was used for the classification of diabetes in [10]. Four-layer neural network with eight input neurons, 10 hidden neurons for each of two hidden layers and one neuron for output layer is trained and 92% accuracy was obtained. Different from the others, a mobile application was realized in [11] for diabetes diagnosis. Type of diabetes and the possibility of developing diabetes in the future were determined by the developed system using blood glucose level data. They developed a decision tree like algorithm based on the guidance of the health professional not a machine learning method. Random forests algorithm was used in [12] for diabetes diagnosis and they achieved 89.63% accuracy. Decision Tree, SVM, and Naïve Bayes were used for the same purpose in [13] and they showed that Naïve Bayes has the best diagnostic performance when compared to others with 76.3% accuracy. In [14], an auto encoder neural network with 24 hidden layers was proposed for classification. Average accuracy of the study after twenty trials was found as 97.3%, which is the highest classification performance related to the classification of diabetes. As seen from the above mentioned studies diabetes are diagnosed using machine learning methods satisfactorily accurate with 97.3% at most.

Although there are many studies on machine learning based diagnosis of diabetes, there is a few study related to the classification of diabetic retinopathy (DR) which affects many diabetics as mentioned above. A computer aided diagnostic system was proposed in [15]. Using a graph kernel, they proposed a multi-kernel multi-instance learning method. They first detected hemorrhages and micro aneurisms (HMA) from fundus images and extracted some features related to color, shape, texture and gradient. An IOT based diagnosis of diabetic retinopathy (DR) was studied in [16] and they determined the blood glucose level of diabetics via Dexcom G4Plantinum sensors. Readings of the sensor were send to DRapp device and the patient's diabetes type was determined as type 1 or type 2. If it was determined as type 1, then the patient was directed for some treatments and a doctor appointment is set. If the patient had type 2 diabetes, then the patient's fundus image was caught by fundus camera and retinal blood vessels were detected by the proposed image segmentation method. Accuracy of this method is 99.58% and its sensitivity is 72.51%. Face recognition methods were used for fundus images in [17] to detect exudates and their features were extracted very recently. Four classifiers were implemented by the extracted features. These classifiers are k-NN, ANN, Random Forests, and

SVM. The best classification was achieved by SVM with 80.4% accuracy.

Deep learning (DL) has been used in the solution of many medical problems. Some of them are as follows. As explained in [18], DL models have been used in many medical imaging applications. In [19], the researchers developed a tool for the ophthalmologists to help them for grading DR via DL. Retinal fundus images were graded using this tool with the support of image magnification and contrast adjustment. They obtained very high performance metrics, but their approach is not a fully machine learning based decision system. An interpretable classifier was proposed in [20] for DR via DL. The proposed approach classifies retina images indicating the severity level. They developed a method and generated visual maps to be easily interpreted by the ophthalmologists to help the diagnosis of DR.

In this study, different from the previously mentioned papers, the features of retinal fundus images of Messidor dataset [21] and artificial neural networks (ANN) model of Rapid Miner are used for the classification of possible diabetic patients whether having retinopathy since ANN provides solution to not only linear classification problems but also non-linear, multi-class problems with low computational cost. Our method provides a cheap, fast and accurate decision support system for DR classification. Contributions of the paper can be summarized as the followings:

- Features of retinal fundus images of Messidor dataset is used for diagnosis.
- Detailed tables are provided for machine learning based diagnosis of diabetes and diabetic retinopathy.
- Rapid Miner Studio is used for the first time as a tool for classification of DR so far.
- Independent Component Analysis is used to reduce the dimension of the problem.
- Sensitivity is respected as a performance metric and high sensitivity is achieved in diagnosis.

Rest of the paper is organized as follows: Section 2 gives the details of the method and the application, Section 3 provides the experimental results of the application and Section 4 concludes the paper and mentions about the future works.

2. METHODOLOGY

Early detection of DR is quite important since it is one of the main causes of blindness among the people between the ages 20 and 74 [3]. In this study, we intend to detect this serious disease by a popular and an easy approach. The details are given in the following subsections.

2.1. Dataset Description

In this study we used the dataset which includes the extracted features of Messidor dataset provided by Dr. Antal and Dr. Hajdu via UCI Machine Learning Repository [22]. For details of the features in this dataset, the explanations given in [21] can be examined. They are also summarized in Table 3. Number of samples are 1151 and 540 of them belong to the healthy people and are labeled as zero. 611 of the features are of DR patients and they are labeled as 1. The dataset contains twenty columns which represent the lesions, describe an anatomical part or is an image-level descriptor. The last column of the dataset defines the diagnostic class whether 1 in case the patient has DR or 0 if he is healthy.

2.2. Performance Assessment

Accuracy of detection of true positives, i.e. number of samples with DR and diagnosed as having DR, must especially be satisfactory for a proper decision support system. Misdetection of samples with DR by an automatic machine learning based system may mislead their users and may cause to lose the chance of coming around by early treatment. This affects the rest of the life of people with DR. That is, misclassification of healthy people and advising them to see doctor when they are not DR patient in real are not much important than misclassification of DR patients and telling them that they are healthy. In general, the performance

of a classification method is measured as given in equation (1)

$$\text{Accuracy} = \frac{\text{TP+TN}}{\text{TP+TN+FP+FN}} \quad (1)$$

where TP = True positive, FP = False positive, TN = True negative, FN = False negative. But, in health-based vital classification problems using true positive ratio, given in equation (2), is more convenient than other performance metrics**.**

$$\text{TPR} = \frac{\text{TP}}{\text{TP+FN}} \quad (2)$$

True positive ratio (TPR) is known as sensitivity or recall in the literature. Therefore, TPR will be used in this study as most of other health based classification studies instead of considering accuracy as a performance metric since our method is also a health-based application. In the experiments we will try to minimize FN and try to maximize sensitivity of the current classification problem even if it leads to a lower accuracy.

2.3. Artificial Neural Networks (ANN) Based Diabetic Retinopathy Detection

ANN is a part of machine learning (ML) methods and it is frequently used in wide range of applications nowadays such as computer vision, bioinformatics, medical image analysis, computer networks, etc. It has multiple layers: input layer, hidden layer(s) and output layer. It learns in a supervised fashion. ML based disease diagnosis is becoming more prevalent day by day since these methods provide faster and cheaper solutions to real life problems. There are many papers related to ML based detection of diseases in the literature. Machine learning based detection of diabetes as a subset of ML based diagnosis is summarized in Table I. Although there are many studies related to the diagnosis of diabetes, there are few papers related to the detection of diabetic retinopathy which seriously affects many type 2 diabetics. The details of the papers related to the diagnosis of diabetic retinopathy are given in Table II.

Table 1. Studies related to ML based detection of diabetes

Ref. No.	Method	Compared Methods	Accuracy
[4]	General regression neural networks	Multi-layer perceptron, radial basis function and general regression neural networks	80.21%
[5]	ID3	ID3 and Decision Tree	80%
[6]	AdaBoost with Decision Stump	Support Vector Machine, Naïve Bayes, Decision Tree and Decision Stump	80.72%
[7]	k-nearest neighbor with Lorentzian Distance	-	76%
[8]	SVM with linear kernel	MLP, SVM with polynomial and radial kernels	77.47%
[9]	Naïve Bayes and GA	Naïve Bayes	78.69%
[10]	Artificial Neural Networks	-	92%
[12]	Random Forests	Binary Tree, SVM, Adaptive Boosting Model, Generalized Linear Models, Neural Network Model	89.63%
[14]	Auto Encoder Neural Networks	-	97.3%

Table 2. Studies related to the detection of ML based diabetic retinopathy

Ref. No.	Method	Compared Methods	Accuracy
[15]	Multi-kernel multi-instance learning	-	91.6%
[16]	Fuzzy c-means clustering	-	99.58%
[17]	SVM	k-NN, ANN, Random Forests	80.4%
[19]	Deep learning	-	90% (TPR)
[20]	Deep learning	-	91.1% (TPR)

As seen from the tables, DR is not studied properly by ML approaches. ANN method as a compatible ML approach can be adapted to the problem of the detection of DR and may help ophthalmologists and patients. There are very few studies related to the diagnosis of DR via ANN and their results are not satisfactory enough. In this study, ANN will be adapted to the classification of DR patients using the features of an open dataset. In addition, this application will be realized using a very popular data mining tool to make an easy analysis. To further improve the performance of ANN based classification, Independent Component Analysis (ICA) has also been applied for dimensionality reduction. Details of the tool based classification are given in below section.

3. EXPERIMENTAL RESULTS

In this study, an ANN model has been created using Rapid Miner Studio, a free software for data analysis [23] . This tool has not been used yet for the detection of diabetic retinopathy so far. It provides easy and various solutions for the problem. Dimensionality reduction has also been performed to improve the performance of ANN. More number of features mean more number of input nodes in ANN model and this may complicate the learning process. Therefore, feature reduction is used. ICA method has been used for the purpose. ICA is a frequently used statistical technique and it estimates independent components by maximizing the non-Gaussianity of them, or maximizing the likelihood, or minimizing mutual information between them [24]. Weights of the attributes after ICA was applied are given in Table 3. There are 19 attributes in Messidor dataset and 14 most independent attributes have been used in the input set. Bold-written attributes in Table 3 are the top 14 attributes. These inputs were then given to ANN. 1151 samples in the dataset were divided into two as 0.8 and 0.2 splitting ratio for training and testing respectively. 920 samples were used in training the model and 230 unseen and unlabeled sample were used for testing.

Table 3. Weights of the attributes determined by ICA

Attribute No.	Weight of Attribute	Information about Attribute
1	0.003	Result of quality assessment
2	0.090	Result of pre-screening
3	10.299	Number of MAs (Micro Aneurysm) found at the confidence levels α=0.5,…,1 respectively
4	9.891	
5	9.570	
6	9.133	
7	8.166	
8	5.456	
9	-10.996	Number of exudates at the confidence levels α=0.5,…,1 respectively.
10	-2.143	
11	-1.522	
12	-0.658	
13	-0.589	
14	-0.155	
15	-0.016	
16	0.002	
17	0.001	Euclidean distance of the center of the macula and the center of the optic disc
18	0.001	Diameter of the optic disc
19	-0.384	Result of the AM/FM-based classification

Different topologies have been tried to determine the best topology of the ANN model for the problem. The highest- performance ANN model has one hidden

layer with 8 neurons, 0.01 learning rate, and 0.9 momentum coefficient. Proposed ANN model is given in Figure 1. According to the confusion matrix given in Table 4, TPR (or sensitivity) and accuracy of the established model can be calculated as given in equation (3) and (4).

$$\text{TPR} = \frac{108}{108+14} = 0.8852 \quad (3)$$

$$\text{Accuracy} = \frac{108+67}{108+67+14+41} = 0.7609 \quad (4)$$

Table 4. Confusion matrix of Diabetic Retinopathy detection model

		Actual	
		Has DR	Does not have DR
Predicted	Has DR	108	67
	Does not have DR	14	41

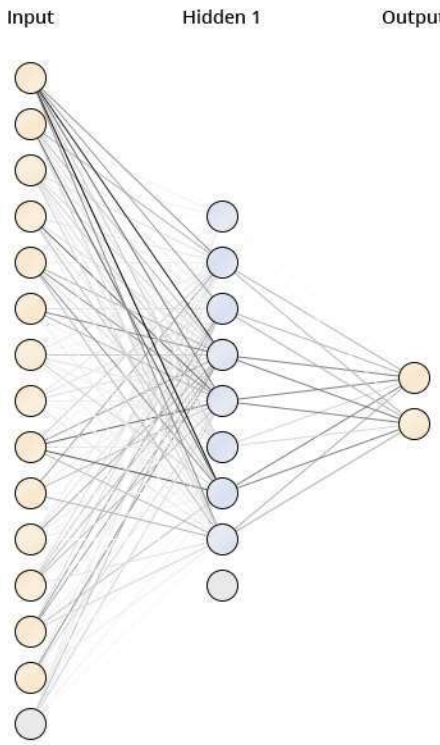

Figure 1. Proposed ANN topology

Although the accuracy of the method proposed in [16] is 99.58%, its sensitivity is low, i.e. 72.51%. This means this method classifies 72 of DR patients among 100 of them. About 28% of DR patients are predicted as normal, not having DR. That is, the method misdiagnoses DR patients considerably. Sensitivity becomes more of an issue in such health related problems. Therefore, one must regard sensitivity as a performance metric. [19] and [20] have good sensitivities but their methods are computationally harder. 88.52% sensitivity by an easy application is well enough to assist doctors for classifying their patients.

4. CONCLUSIONS AND FUTURE WORK

In this paper, ANN based DR detection method is proposed. The features of Messidor dataset have been used for the classification and quite sensitive results were obtained. Although there are many detection methods for diabetes, there is a few paper for diabetic retinopathy detection. ANN method have been frequently and easily used in many different applications and provided successful results. Applying this approach to DR classification simplifies the ML based diagnosis. Making analysis in an easier and faster way is very important for a research topic in health based problems. Rapid Miner is also introduced in this paper for the diagnosis of DR. It is proved by this research that Rapid Miner and ANN can efficiently be used in the analysis of DR data.

Early detection of DR is quite important for diabetic patients and high-sensitive and low-complexity methods must be developed for them. ML based methods proved their superior performance in many medical classification issues and DR classification can be one of these. The proposed method can be improved in the future studies. Parameter selection process can be optimized. DL can be adapted to the problem.

5. REFERENCES

[1] International Diabetes Federation, *IDF Diabetes Atlas 9th edition*. 2019.

[2] B. E. R. Gaillard and D. K. Karumanchi, "Trends in early diabetes diagnosis," *Ophthalmol. Manag.*, vol. 18, no. November 2015, pp. 28–30, 2015.

[3] M. Dansinger, "Types of Diabetes Mellitus," *WebMD Medical Reference*, 2017. [Online]. Available: https://www.webmd.com/diabetes/guide/types-of-diabetes-mellitus#3. [Accessed: 15-Jan-2019].

[4] K. Kayaer and T. Yildirim, "Medical diagnosis on Pima Indian diabetes using general regression neural networks," in *Proceedings of the international conference on artificial neural networks and neural information processing (ICANN/ICONIP)*, 2003, pp. 181–184.

[5] J. Han, J. C. Rodriguze, and M. Beheshti, "Diabetes data analysis and prediction model discovery using RapidMiner," in *2nd International Conference on Future Generation Communication and Networking*, 2008, vol. 3, pp. 96–99.

[6] V. V. Vijayan and C. Anjali, "Prediction and diagnosis of diabetes mellitus - A machine learning approach," in *IEEE Recent Advances in Intelligent Computational Systems, RAICS 2015*, 2015, no. December, pp. 122–127.

[7] H. S. Bilge and Y. Kerimbekov, "Classification with Lorentzian distance metric," in *23rd Signal Processing and Communications Applications Conference*, 2015, pp. 1–4.

[8] M. S. Kurt and T. Ensari, "Diabet diagnosis with support vector machines and multi layer perceptron," in *Electric Electronics, Computer Science, Biomedical Engineerings' Meeting (EBBT)*, 2017, pp. 1–4.

[9] D. Choubey, S. Paul, S. Kumar, and S. Kumar, "Classification of Pima indian diabetes dataset using naive bayes with genetic algorithm as an attribute selection," *Commun. Comput. Syst.*, pp. 451–455, 2017.

[10] O. Y. Okuboyejo, S. Misra, R. Maskeliunas, and R. Damasevicius, "A Neural Network Based Expert System for the Diagnosis of Diabetes Mellitus," in *International Conference on Information Technology Science*, 2018, vol. 724, no. February.

[11] I. Arikpo *et al.*, "Development of a Mobile Software Tool for Diabetes Diagnosis," vol. 5, no. 3, pp. 1–8, 2018.

[12] P. Samant and R. Agarwal, "Machine learning techniques for medical diagnosis of diabetes using iris images," *Comput. Methods Programs Biomed.*, vol. 157, pp. 121–128, 2018.

[13] D. Sisodia and D. S. Sisodia, "Prediction of Diabetes using Classification Algorithms," *Procedia Comput. Sci.*, vol. 132, no. Iccids, pp. 1578–1585, 2018.

[14] Ö. Deperlıoglu and U. Kose, "Diagnosis of Diabetes by Using Deep Neural Network," in *2nd International Symposium on Multidisciplinary Studies and Innovative Technologies*, 2018.

[15] P. Cao, F. Ren, C. Wan, J. Yang, and O. Zaiane, "Efficient multi-kernel multi-instance learning using weakly supervised and imbalanced data for diabetic retinopathy diagnosis," *Comput. Med. Imaging Graph.*, vol. 69, pp. 112–124, 2018.

[16] T. Jemima Jebaseeli, C. Anand Deva Durai, and J. Dinesh Peter, "IOT based sustainable diabetic retinopathy diagnosis system," *Sustain. Comput. Informatics Syst.*, 2018.

[17] L. B. Frazao, N. Theera-Umpon, and S. Auephanwiriyakul, "Diagnosis of diabetic retinopathy based on holistic texture and local retinal features," *Inf. Sci. (Ny).*, vol. 475, pp. 44–66, 2019.

[18] A. S. Lundervold and A. Lundervold, "An overview of deep learning in medical imaging focusing on MRI," *Z. Med. Phys.*, vol. 29, no. 2, pp. 102–127, May 2019.

[19] V. Gulshan *et al.*, "Development and Validation of a Deep Learning Algorithm for Detection of Diabetic Retinopathy in Retinal Fundus Photographs," *JAMA*, vol. 316, no. 22, p. 2402, Dec. 2016.

[20] J. de la Torre, A. Valls, and D. Puig, "A deep learning interpretable classifier for diabetic retinopathy disease grading," *Neurocomputing*, 2019.

[21] B. Antal and A. Hajdu, "An ensemble-based system for automatic screening of diabetic retinopathy," *Knowledge-Based Syst.*, vol. 60, pp. 20–27, Apr. 2014.

[22] "UCI Machine Learning Repository: Diabetic Retinopathy Debrecen Data Set Data Set." [Online]. Available: https://archive.ics.uci.edu/ml/datasets/Diabetic+Retinopathy+Debrecen+Data+Set. [Accessed: 25-Jan-2020].

[23] "RapidMiner©." [Online]. Available: https://rapidminer.com/. [Accessed: 04-Mar-2019].

[24] A. Tharwat, "Independent component analysis: An introduction," *Appl. Comput. Informatics*, Aug. 2018.